INFORMATION TO USERS

This manuscript has been reproduced from the microfilm master. UMI films the text directly from the original or copy submitted. Thus, some thesis and dissertation copies are in typewriter face, while others may be from any type of computer printer.

The quality of this reproduction is dependent upon the quality of the copy submitted. Broken or indistinct print, colored or poor quality illustrations and photographs, print bleedthrough, substandard margins, and improper alignment can adversely affect reproduction.

In the unlikely event that the author did not send UMI a complete manuscript and there are missing pages, these will be noted. Also, if unauthorized copyright material had to be removed, a note will indicate the deletion.

Oversize materials (e.g., maps, drawings, charts) are reproduced by sectioning the original, beginning at the upper left-hand corner and continuing from left to right in equal sections with small overlaps. Each original is also photographed in one exposure and is included in reduced form at the back of the book.

Photographs included in the original manuscript have been reproduced xerographically in this copy. Higher quality 6" x 9" black and white photographic prints are available for any photographs or illustrations appearing in this copy for an additional charge. Contact UMI directly to order.

UMI

A Bell & Howell Information Company
300 North Zeeb Road, Ann Arbor MI 48106-1346 USA
313/761-4700 800/521-0600

Downloaded from SHAREOK. Persistent Handle URL: https://hdl.handle.net/11244/5426

UNIVERSITY OF OKLAHOMA

GRADUATE COLLEGE

THE THERMODYNAMICS AND KINETICS OF PRECIPITATION OF ANIONIC SURFACTANTS AND SURFACTANT MIXTURES

A Dissertation

SUBMITTED TO THE GRADUATE FACULTY

in partial fulfillment of the requirements for the

degree of

Doctor of Philosophy

By

CHERYL HASKINS RODRIGUEZ

Norman, Oklahoma

1997

UMI Number: 9719901

Copyright 1997 by
Rodriguez, Cheryl Haskins

All rights reserved.

UMI Microform 9719901
Copyright 1997, by UMI Company. All rights reserved.

This microform edition is protected against unauthorized
copying under Title 17, United States Code.

UMI
300 North Zeeb Road
Ann Arbor, MI 48103

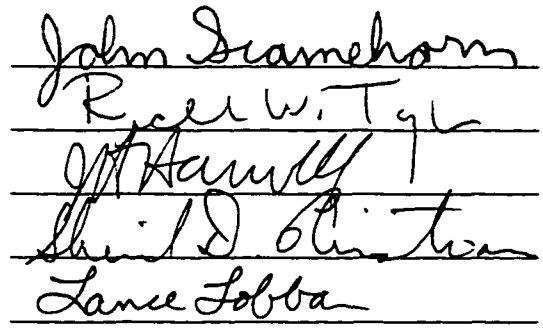
© Copyright by CHERYL HASKINS RODRIGUEZ 1997

All Rights Reserved.

THE THERMODYNAMICS AND KINETICS OF PRECIPITATION OF ANIONIC SURFACTANTS AND SURFACTANT MIXTURES

A Dissertation APPROVED FOR THE
SCHOOL OF CHEMICAL ENGINEERING AND MATERIALS SCIENCE

BY



Dedicated to

My husband, Carlos

And my parents

For their understanding, support, and love

ACKNOWLEDGEMENTS

First, I would like to thank Dr. John Scamehorn for his guidance, enthusiasm, and encouragement. His belief in me helped make this accomplishment possible. I would also like to thank Dr. Sherril Christian and Dr. Richard Taylor for their guidance during my studies and for being a part of my committe, and Dr. Jeff Harwell and Dr. Lance Lobban for being on my committe and their support throughout my education. I would like to give special thanks to all of the Surfactant group, especially: Bruce Roberts for all of his research advice, Bita Young, Lle Riviello, Hatice Gecol, Laura Wesson, Ahmadali Tabatabi, and Jerry Newman for all of those lab discussions where so much learning takes place. All have been great lab mates and friends. Also, Wei Li Yuan was very giving of his time in helping me obtain the AFM graphs. I would like to thank the remaining faculty and staff, includig Rick, Donna, Sherry, and Shirley for their never-ending willingness to help.

Financial support for this work was provided by the industrial sponsors of the Institute for Applied Surfactant Research including Akzo Nobel, Amway Corporation, Colgate-Palmolive, Dow Chemical Company, DowElanco, E.I. DuPont de Nemours & Co., Henkel Corporation, ICI Surfactants, Kerr-McGee Corporation, Lever Brothers, Lubrizol Corporation, Nikko Chemicals, Phillips Petroleum Company, Pilot Chemical Company, Reckitt and Coleman, Shell Development Company, Sun Chemical Corporation, and Witco Corporation.

Finally, I would like to thank my family, including my sister, Laura, and my good friend, Shannon, for their encouragement and support. Without them this accomplishment would not have been possible.

TABLE OF CONTENTS

Page

ACKNOWLEDGEMENTS v

LIST OF TABLES ix

LIST OF FIGURES xi

ABSTRACT xix

CHAPTER

1 Modification of Krafft Temperature or Solubility of Surfactants Using Surfactant Mixtures 1
1.1 Introduction 2
1.2 Experimental 3
1.2.1 Materials 3
1.2.2 Methods 3
1.2.2.1 Krafft Temperatures 3
1.2.2.2 CMC Determination 4
1.2.2.3 Determination of Solubility Product 4
1.2.2.4 Crystal Composition 5
1.3 Results and Discussion 6
1.3.1 Prediction of Mixture Krafft Temperatures 6
1.3.2 Obtaining Parameters Used in Model 15
1.3.3 Precipitate Composition 17
1.3.4 Experimental and Theoretical Krafft Temperatures 18
1.4 References 25

2 Precipitation in Solutions Containing Mixtures of Synthetic Anionic Surfactant and Soap 46
2.1 Introduction 47
2.2 Experimental Procedures 48
2.2.1 Materials 48
2.2.2 Methods 48
2.2.2.1 Precipitation Phase Boundaries 48
2.2.2.2 Titration Curves 49
2.2.2.3 Critical Micelle Concentrations 49

TABLE OF CONTENTS (Continued)

Page

CHAPTER

2.3 Results and Discussion 50
2.4 References 60

3 Kinetics of Precipitation of Anionic Surfactant Mixtures and Physical Interactions Affecting This Rate 80
3.1 Introduction 82
3.2 Experimental Procedures 82
3.2.1 Materials 82
3.2.2 Methods 83
3.2.2.1 Precipitation Phase Boundaries 83
3.2.2.2 Calorimeter Studies 84
3.2.2.3 Heats of Reaction 85
3.2.2.4 Determination of Factors Affecting Rate . . . 86
3.3 Theory 89
3.3.1 Precipitation Phase Boundaries 89
3.3.2 Theory of Crystallization 95
3.3.3 Effect of Impurities 98
3.4 Results and Discussion 99
3.4.1 Precipitation Phase Boundaries 99
3.4.2 Adsorption Studies 101
3.4.3 Determination of Reaction Pathways 102
3.4.4 Precipitation Rates for SDS with Calcium 103
3.4.5 Precipitation Rates for SDS/SOBS Mixtures with Calcium 104
3.4.6 Nonequilibrium Crystal Compositions 106
3.4.7 Head Group Arrangements in $Ca(DS)_2$ and $Ca(OBS)_2$ Crystal Lattices 107
3.4.8 Effect of Seeds on Overall Precipitation Rate 108
3.4.9 Atomic Force Microscopy of Crystal Surfaces 108
3.4.10 Image Analysis 111
3.5 Conclusions 112
3.6 References 115

APPENDIX A 172

APPENDIX B 199

TABLE OF CONTENTS (Continued)

Page

APPENDIX C. 202

APPENDIX D. 209

LIST OF TABLES

TABLE		Page
I.1	Summary of Parameters Used in Model to Predict Mixture Krafft Temperatures	30
I.2	Binary Interaction Parameters of SDS and SOBS with $NP(EO)_{10}$	31
I.3	Precipitate Compositions from Solutions 0.5, 1.0, and 1.5 °C Below the Krafft Temperature	32
II.1	Solubility Limit of the Fatty Acid, HO, at 30 °C	62
II.2	K_{SP} Values for SDS and SO with Calcium at Several pH Levels and 30 °C	63
III.1	Comparison of Initial Supersaturation Ratios with Precipitate SDS/SOBS Molar Ratios for Various 0.075 M SDS/SOBS Mixtures Precipitated with 0.01 M $CaCl_2$ at 30 °C	118
III.2	Comparison of Initial Supersaturation Ratios with Precipitate SDS/SOBS Molar Ratios for Various 0.0288 M SDS/SOBS Mixtures Precipitated with 0.01 M $CaCl_2$ at 30 °C	119
III.3	Comparison of Initial Supersaturation Ratios for Various 0.0192 M SDS/SOBS Mixtures Precipitated with 0.01 M $CaCl_2$ at 30 °C	120
III.4	Comparison of Initial Supersaturation Ratios with Precipitate SDS/SOBS Molar Ratios for Various 0.0096 M SDS/SOBS Mixtures Precipitated with 0.01 M $CaCl_2$ at 30 °C	121
III.5	Comparison of Initial Supersaturation Ratios with Precipitate SDS/SOBS Molar Ratios for Various 0.0025 M SDS/SOBS Mixtures Precipitated with 0.01 M $CaCl_2$ at 30 °C	122
III.6	Nonequilibrium Crystal Compositions, Precipitated From Various Supersaturated Concentrations of SDS and SOBS in the Presence of Dilute Surfactant	123

LIST OF TABLES (Continued)

TABLE Page

III.7 Comparison of Initial Supersaturation Ratios of SDS and SOBS in 0.0096 M Surfactant Solutions at Various Mixtures For Unfiltered Water and Water Filtered Through a 10,000 MWCO Membrane . . . 124

LIST OF FIGURES

FIGURE		Page
I.1	Micelle-Monomer-Precipitate Equilibrium for a Ternary Anionic/Anionic/Nonionic Surfactant System Just Below the Krafft Temperature	33
I.2	CMC as a Function of Temperature for SDS, SOBS, and $NP(EO)_{10}$	34
I.3	CMC as a Function of Sodium Concentration for SDS, SOBS, and $NP(EO)_{10}$	35
I.4	Activity-based Solubility Product as a Function of Inverse Temperature	36
I.5	Krafft Temperatures for SDS/SOBS System at 0.04 M Total Surfactant Concentration and 0, 0.1, and 0.2 M NaCl Compared with Theory; No Adjustable Parameter	37
I.6	Krafft Temperatures for SDS/SOBS System at 0.04 M Total Surfactant Concentration and 0, 0.1, and 0.2 M NaCl Compared with Theory; K_{SP} Adjusted for Pure SDS and Pure SOBS at 0 M NaCl	38
I.7	Krafft Temperatures for SDS/SOBS Dystem at 0.04 M Total Surfactant Concentration and 0, 0.1, and 0.2 M NaCl Compared with Theory; K_{SP} Adjusted for Pure SDS and Pure SOBS at Each NaCl Concentration	39
I.8	Krafft Temperatures for SDS/SOBS System at 0.04 M and 0.02 M Total Surfactant Concentrations at Various NaCl Concentrations	40
I.9	Krafft Temperatures for 0.04 M SDS/$NP(EO)_{10}$ at 0, 0.1, and 0.2 M NaCl	41
I.10	Krafft Temperatures for 0.04 M SOBS/$NP(EO)_{10}$ at 0, 0.1, and 0.2 M NaCl	42
I.11	Ternary SDS/SOBS/$NP(EO)_{10}$ Krafft Temperatures at 0.04 M Total Surfactant Concentration at 0 M NaCl	43

LIST OF FIGURES (Continued)

FIGURE Page

I.12 The Effect of Increasing SOBS Concentration on Krafft Temperatures of 0.04 M SDS/SOBS/NP(EO)$_{10}$ Mixtures at 0 M NaCl 44

I.13 Predicted Monomer Concentrations for the 0.04 M SDS/SOBS/NP(EO)$_{10}$ Systems at 0 M Added NaCl 45

II.1 Micelle-Monomer-Precipitate Equilibrium Diagram for SDS in the Presence of Calcium Ions. 64

II.2 Precipitation Phase Boundaries (Hardness Tolerance) for SDS at pH Levels of 5.0, 7.0, and 9.0 and 30 °C 65

II.3 Rate of Hydrolysis of SDS as a Function of pH at 50.4 °C Calculated from Rate Constants from Motsavage and Kostenbauder (10) 66

II.4 Rate of Hydrolysis of SDS as a Function of pH at 60.2 °C Calculated from Rate Constants from Motsavage and Kostenbauder (10) 67

II.5 Rate of Hydrolysis of SDS as a Function of Temperature at a pH Level of 5.0 Calculated by Extrapolation Using Best Fit Curves in Figures II.3 and II.4. 68

II.6 Micelle-Monomer-Precipitate Equilibrium Diagram for SO in the Presence of Calcium Ions. 69

II.7 Precipitation Phase Boundaries (Hardness Tolerance) for SO at pH Levels of 6.0, 7.0, and 9.0 and 30 °C 70

II.8 Micelle-Monomer-Precipitate Equilibrium Diagram for an SDS/SO Mixture in the Presence of Calcium Ions with Ca(DS)$_2$ Precipitating. 71

II.9 CMC as a Function of Mole Fraction SO in SDS/SO Mixtures for pH Levels of 6.0, 7.0, and 9.0 and 30 °C 72

LIST OF FIGURES (Continued)

FIGURE		Page
II.10	Precipitation Phase Boundaries (Hardness Tolerance) for 80/20 SDS/SO at pH Levels of 5.0, 7.0, and 9.0 and 30 °C	73
II.11	Precipitation Phase Boundaries (Hardness Tolerance) for 60/40 SDS/SO at pH Levels of 5.0, 7.0, and 9.0 and 30 °C	74
II.12	Precipitation Phase Boundaries (Hardness Tolerance) for 40/60 SDS/SO at pH Levels of 5.0, 7.0, and 9.0 and 30 °C	75
II.13	Precipitation Phase Boundaries (Hardness Tolerance) for 20/80 SDS/SO at pH Levels of 6.0, 7.0, and 9.0 and 30 °C	76
II.14	Comparison of Precipitation Phase Boundaries (Hardness Tolerance) for 100/0, 80/20, 60/40, and 40/60 SDS/SO Mixtures at a pH Level of 5.0 and 30 °C	77
II.15	Comparison of Precipitation Phase Boundaries (Hardness Tolerance) for 100/0, 80/20, 60/40, 40/60 and 20/80 SDS/SO Mixtures at a pH Level of 7.0 and 30 °C	78
II.16	Comparison of Precipitation Phase Boundaries (Hardness Tolerance) for 100/0, 80/20, 60/40, 40/60, and 20/80 SDS/SO Mixtures at a pH Level of 9.0 and 30 °C	79
III.1	Schematic of Isoperibol Calorimeter Set-Up	125
III.2	Micelle-Monomer-Precipitate Equilibrium Diagram for Two Anionic Surfactants in the Presence of Calcium	126
III.3	Theoretical Precipitation Phase Boundaries for SDS in Various SDS/SOBS Mixtures; Comparison with Experimental Hardness Tolerance Points; 30 °C	127
III.4	Theoretical Precipitation Phase Boundaries for SOBS in Various SDS/SOBS Mixtures; Comparison with Experimental Hardness Tolerance Points; 30 °C	128

LIST OF FIGURES (Continued)

FIGURE Page

III.5 Comparison Between SDS-$CaCl_2$ Precipitation Reaction Pathways for Various Total Surfactant Concentrations and 100/0 SDS/SOBS Solution and the Precipitation Phase Boundary for SDS for the 100/0 SDS/SOBS System at 30 °C 129

III.6 Comparison Between SDS-$CaCl_2$ Precipitation Reaction Pathways for Various Total Surfactant Concentrations and 80/20 SDS/SOBS Solution and the Precipitation Phase Boundary for SDS for the 80/20 SDS/SOBS System at 30 °C 130

III.7 Comparison Between SDS-$CaCl_2$ Precipitation Reaction Pathways for Various Total Surfactant Concentrations and 60/40 SDS/SOBS Solution and the Precipitation Phase Boundary for SDS for the 60/40 SDS/SOBS System at 30 °C 131

III.8 Comparison Between SDS-$CaCl_2$ Precipitation Reaction Pathways for Various Total Surfactant Concentrations and 40/60 SDS/SOBS Solution and the Precipitation Phase Boundary for SDS for the 40/60 SDS/SOBS System at 30 °C. 132

III.9 Comparison Between SDS-$CaCl_2$ Precipitation Reaction Pathways for Various Total Surfactant Concentrations and 20/80 SDS/SOBS Solution and the Precipitation Phase Boundary for SDS for the 20/80 SDS/SOBS System at 30 °C. 133

III.10 Comparison Between SOBS-$CaCl_2$ Precipitation Reaction Pathways for Various Total Surfactant Concentrations and 0/100 SDS/SOBS Solution and the Precipitation Phase Boundary for SOBS for the 0/100 SDS/SOBS System at 30 °C. 134

III.11 Comparison Between SOBS-$CaCl_2$ Precipitation Reaction Pathways for Various Total Surfactant Concentrations and 20/80 SDS/SOBS Solution and the Precipitation Phase Boundary for SOBS for the 20/80 SDS/SOBS System at 30 °C. 135

LIST OF FIGURES (Continued)

FIGURE Page

III.12 Comparison Between SOBS-$CaCl_2$ Precipitation Reaction Pathways for Various Total Surfactant Concentrations and 40/60 SDS/SOBS Solution and the Precipitation Phase Boundary for SOBS for the 40/60 SDS/SOBS System at 30 °C. 136

III.13 Comparison Between SOBS-$CaCl_2$ Precipitation Reaction Pathways for Various Total Surfactant Concentrations and 60/40 SDS/SOBS Solution and the Precipitation Phase Boundary for SOBS for the 60/40 SDS/SOBS System at 30 °C. 137

III.14 Comparison Between SOBS-$CaCl_2$ Precipitation Reaction Pathways for Various Total Surfactant Concentrations and 80/20 SDS/SOBS Solution and the Precipitation Phase Boundary for SOBS for the 80/20 SDS/SOBS System at 30 °C. 138

III.15 Precipitation Rate Curves for SDS with Calcium for Various Supersaturation Ratios Below the CMC and at 30 °C 139

III.16 Precipitation Rate Curves for SDS with Calcium for Various Supersaturation Ratios Above the CMC and at 30 °C 140

III.17 Precipitation Rate Curves for SDS with Calcium for Various Supersaturation Ratios at 30 °C 141

III.18 Precipitation Rate Curves for 0.075 M Total Surfactant Concentration and Varying SDS/SOBS Mole Fractions with 0.01 M $CaCl_2$ at 30 °C. 142

III.19 Precipitation Rate Curves for 0.0288 M Total Surfactant Concentration and Varying SDS/SOBS Mole Fractions with 0.01 M $CaCl_2$ at 30 °C. 143

III.20 Precipitation Rate Curves for 0.0192 M Total Surfactant Concentration and Varying SDS/SOBS Mole Fractions with 0.01 M $CaCl_2$ at 30 °C. 144

LIST OF FIGURES (Continued)

FIGURE Page

III.21 Precipitation Rate Curves for 0.0096 M Total Surfactant Concentration and Varying SDS/SOBS Mole Fractions with 0.01 M $CaCl_2$ at 30 °C. 145

III.22 Precipitation Rate Curves for 0.0025 M Total Surfactant Concentration and Varying SDS/SOBS Mole Fractions with 0.01 M $CaCl_2$ at 30 °C. 146

III.23 Concentration Versus Time at 30 °C For 0.0092 M Surfactant, 40/60 SDS/SOBS and 0.01 M $CaCl_2$ Related to the Extent of Precipitation During Each Time Segment. 147

III.24 Atomic Force Microscope Graph of $Ca(DS)_2$ Head Groups in Crystal Lattice. 148

III.25 Atomic Force Microscope Graph of $Ca(OBS)_2$ Head Groups in Crystal Lattice. 149

III.26 Precipitation Rate Curves for Various 0.0096 M SDS/SOBS Surfactant Solutions at 30 °C; Comparing Solutions in which the Water Used Was Unfiltered and Filtered with a 10,000 MWCO Ultrafiltration Membrane. 150

III.27 3-D Atomic Force Microscope Graph of $CaDS_2$ Crystals Precipitated from a 0.020 M SDS/0.010 M $CaCl_2$ Solution at 30 °C; 50 μm x 50 μm. 151

III.28 3-D Atomic Force Microscope Graph of $CaOBS_2$ Crystals Precipitated from a 0.020 M SOBS/0.010 M $CaCl_2$ Solution at 30 °C; 50 μm x 50 μm. 152

III.29 3-D Atomic Force Microscope Graph of Crystals Precipitated from 0.020 M Total Surfactant and 60/40 SDS/SOBS Mole Ratio Containing 0.010 M $CaCl_2$ at 30 °C; 50 μm x 50 μm 153

LIST OF FIGURES (Continued)

FIGURE Page

III.30 3-D Atomic Force Microscope Graph of Crystals Precipitated from 0.020 M Total Surfactant and 40/60 SDS/SOBS Mole Ratio Containing 0.010 M $CaCl_2$ at 30 °C; 50 μm x 50 μm 154

III.31 Top View of $CaDS_2$ Crystals Precipitated from a 0.020 M SDS/0.010 M $CaCl_2$ Solution at 30 °C; Taken with Atomic Force Microscope; 50 μm x 50 μm 155

III.32 Top View of $CaOBS_2$ Crystals Precipitated from a 0.020 M SOBS/0.010 M $CaCl_2$ Solution at 30 °C; Taken with Atomic Force Microscope; 50 μm x 50 μm 156

III.33 Top View of Crystals Precipitated from a 0.020 M Surfactant Solution Containing 60/40 SDS/SOBS and 0.010 M $CaCl_2$ at 30 °C; Taken with Atomic Force Microscope; 50 μm x 50 μm 157

III.34 Top View of Crystals Precipitated from a 0.020 M Surfactant Solution Containing 40/60 SDS/SOBS and 0.010 M $CaCl_2$ at 30 °C; Taken with Atomic Force Microscope; 50 μm x 50 μm 158

III.35 3-D Atomic Force Microscope Graph of $CaDS_2$ Crystals Precipitated from a 0.020 M SDS/0.010 M $CaCl_2$ Solution at 30 °C; 8 μm x 8 μm 159

III.36 3-D Atomic Force Microscope Graph of $CaOBS_2$ Crystals Precipitated from a 0.020 M SOBS/0.010 M $CaCl_2$ Solution at 30 °C; 10 μm x 10 μm 160

III.37 3-D Atomic Force Microscope Graph of Crystals Precipitated from a 0.020 M Surfactant Solution Containing 60/40 SDS/SOBS and 0.010 M $CaCl_2$ at 30 °C; 10 μm x 10 μm 161

III.38 3-D Atomic Force Microscope Graph of Crystals Precipitated from a 0.020 M Surfactant Solution Containing 40/60 SDS/SOBS and 0.010 M $CaCl_2$ at 30 °C; 8 μm x 8 μm 162

LIST OF FIGURES (Continued)

FIGURE Page

III.39 Top View Atomic Force Microscope Graph of Crystals Precipitated from a 0.020 M Surfactant Solution Containing 40/60 SDS/SOBS and 0.010 M $CaCl_2$ at 30 °C; 5 μm x 5 μm 163

III.40 40X Image Analysis Picture of $CaOBS_2$ Crystals Precipitated from a 0.075 M SOBS/0.010 M $CaCl_2$ Solution; Taken 4 Minutes After Mixing at 30 °C. 164

III.41 40X Image Analysis Picture of $CaDS_2$ Crystals Precipitated from a 0.010 M SDS/0.008 M $CaCl_2$ Solution; Taken 4 Minutes After Mixing at 30 °C. 165

III.42 40X Image Analysis Picture of Crystals Precipitated from a 0.012 M Surfactant Solution Containing 83/17 SDS/SOBS and 0.008 M $CaCl_2$; Taken 4 Minutes After Mixing at 30 °C. 166

III.43 40X Image Analysis Picture of Crystals Precipitated from a 0.014 M Surfactant Solution Containing 71/29 SDS/SOBS and 0.008 M $CaCl_2$; Taken 4 Minutes After Mixing at 30 °C. 167

III.44 40X Image Analysis Picture of $CaOBS_2$ Crystals Precipitated from a 0.075 M SOBS/0.010 M $CaCl_2$ Solution, After 1 Week at 30 °C 168

III.45 40X Image Analysis Picture of $CaDS_2$ Crystals Precipitated from a 0.010 M SDS/0.008 M $CaCl_2$ Solution, After 1 Week at 30 °C. 169

III.46 40X Image Analysis Picture of Crystals Precipitated from a 0.012 M Surfactant Solution Containing 83/17 SDS/SOBS and 0.008 M $CaCl_2$, After 1 Week at 30 °C. 170

III.47 40X Image Analysis Picture of Crystals Precipitated from a 0.014 M Surfactant Solution Containing 71/29 SDS/SOBS and 0.008 M $CaCl_2$, After 1 Week at 30 °C. 171

ABSTRACT

An important characteristic of ionic surfactants is their tendency to precipitate from aqueous solution. Both the thermodynamics and kinetics of surfactant precipitation are important when determining formulation compositions for a surfactant application. In this study, Krafft temperatures of surfactant mixtures, hardness tolerances of synthetic anionic surfactant solutions in the presence of soap, and the kinetics of precipitation of anionic surfactants and anionic surfactant mixtures are studied. A eutectic-type behavior is seen when surfactants are mixed. A Krafft temperature depression occurs when surfactants are mixed due to mixed micelle formation, even if the surfactants form ideal mixed micelles. The addition of a nonionic surfactant to an anionic surfactant can cause an even further Krafft temperature depression. A pseudo-phase separation model can successfully predict mixture Krafft temperatures based on pure surfactant behavior and the interactions in the mixed micelles, using an adjustable parameter to fit the pure component Krafft temperatures. The effect of soap on the hardness tolerance of a synthetic anionic surfactant is to raise the hardness tolerance above the CMC due to enhanced micelle formation. Adjusting the pH changes the ratio of fatty acid to octanoate ion in solution. The molar ratio in the micelles is driven by a lower pH level in the region of the surfactant head groups which synergizes micelle formation. Isoperibol calorimetry is used to investigate the kinetics of precipitation of anionic surfactants and anionic surfactant mixtures. When two anionic surfactants are mixed, the time required for precipitation of a supersaturated solution dramatically increases. Part of the increase in time can be attributed to micelle formation which lowers the initial supersaturation

of each anionic surfactant. However, there are also physical interactions during crystallization which greatly affect the kinetics of precipitation.

CHAPTER 1

Modification of Krafft Temperature or Solubility of Surfactants Using Surfactant Mixtures

Krafft temperatures of anionic/anionic, anionic/nonionic, and anionic/anionic/nonionic surfactant mixtures were studied at various surfactant compositions and salt concentrations. The Krafft temperature of a binary mixture of anionic surfactants can be less than that of either single surfactant. The addition of a nonionic surfactant to an anionic surfactant can cause an even further Krafft temperature depression. The addition of a monovalent counterion to each system decreases the CMC, but increases the Krafft temperature of anionic surfactants or their mixtures. A pseudo-phase separation model can successfully predict the mixture Krafft temperatures based on pure surfactant behavior and the interactions in the mixed micelles. Predictions from the model are very sensitive to the solubility products and CMC parameters.

Key words: Krafft temperature, precipitation, surfactant, surfactant mixture, surfactant solubility, synergism

1.1 Introduction

An important characteristic of ionic surfactants is their tendency to precipitate from aqueous solutions. Precipitation of anionic surfactants can inhibit their use in many applications and can affect formulation compositions substantially. Some applications where precipitation can be detrimental are detergency (1,2), where builder is commonly added to prevent precipitation, surfactant based separations (3), and enhanced oil recovery (4). Surfactant precipitation is desirable in some applications such as surfactant recovery by crystallization (5,6). In processes where precipitation is detrimental, the use of surfactant mixtures generally can have synergistic advantages over the use of a single surfactant (4,7).

The highest temperature at which precipitate forms above the CMC is called the Krafft temperature of the system (4). Studies have found that in binary systems where the two surfactants have like charge, very similar structures, and contain the same counterion, the mixture Krafft temperature is between the pure surfactant Krafft temperatures (or results in only a very shallow depression) (8). In these systems the precipitate contains both surfactants (8). A greater depression in the mixture Krafft temperature results for mixtures where the surfactants are of like charge but their structures are more dissimilar or they contain different counterions (8-13). In these systems, only one surfactant precipitates in any substantial amount at the Krafft temperature (on a phase boundary) (8-11). The addition of a nonionic surfactant to an anionic surfactant can decrease the Krafft temperature of the anionic surfactant by an even larger extent (7). Previous investigations of surfactant mixture precipitation behavior which include mixtures at the Krafft temperature have been thoroughly discussed in a recent review (4). In this paper, the Krafft temperature is measured and

modeled for anionic/anionic, anionic/nonionic, and anionic/anionic/nonionic surfactant mixtures with and without added NaCl.

1.2 Experimental

1.2.1 Materials

The two anionic surfactants studied were sodium dodecyl sulfate (SDS) and sodium octyl benzene sulfonate (SOBS). The nonionic surfactant used was nonylphenol polyethoxylate with an average degree of polymerization of ten ($NP(EO)_{10}$). Electrophoresis/HPLC grade SDS was at least 99 % pure and was obtained from Fisher Scientific. It was further purified by recrystallization from water and then from methanol, followed by drying under a vacuum at 30 °C. The SOBS was obtained from Aldrich with a purity of 97 %. The SOBS was recrystallized first from methanol, and then from water. It was then rinsed with cold methanol and dried under a vacuum at 30 °C. The polydisperse nonionic surfactant, $NP(EO)_{10}$ (trade name Igepal CO-660 from Rhone-Poulenc) was used as received. The NaCl was ACS reagent grade from Fisher Scientific. The water was double deionized and the methanol was HPLC grade from either Baker or Fisher Scientific.

1.2.2 Methods

1.2.2.1 Krafft Temperatures. A series of 25 mL solutions at varying mole fractions of each surfactant was made for every system. Krafft temperatures were obtained for surfactant total concentrations of 0.02 and 0.04 M, at NaCl concentrations varying from 0 to 0.2 M. Surfactant solutions can stay supersaturated for long periods of time (14,15) resulting in non-equilibrium apparent Krafft

temperatures. Therefore, the solutions were first cooled to approximately 0 °C for at least 24 hours to force precipitation to occur (16-19). The temperature was then raised by 3 °C/hour. The solutions were gently shaken every 10 minutes and the presence or absence of precipitate noted. The Krafft temperature was recorded as the temperature of the solution where the last crystal became invisible in a high intensity beam of light.

1.2.2.2 CMC Determination. The critical micelle concentrations (CMC) for each individual surfactant at 0, 0.1, and 0.15 M NaCl were found over a range of temperatures above the mixture Krafft temperatures. The CMC was recorded as the surfactant concentration where a sharp change in slope occurred in a plot of the surface tension versus the log of surfactant concentration. A Sensadyne 6000 maximum bubble pressure tensiometer was used to determine the surface tension of each anionic surfactant solution. The bubble rate that was used was determined by setting a rate of 20 seconds/bubble for water and keeping the valve setting the same for all surfactant solutions studied. It is difficult to achieve an equilibrium surface tension using the maximum bubble pressure method for $NP(EO)_{10}$ due to its low CMC and heterogeneity. Therefore the CMC for $NP(EO)_{10}$ was measured using a Central Scientific Du Nouy Ring tensiometer with a platinum/iridium ring. The Du Nouy ring tensiometer was also used for some of the anionic surfactant solutions with added salt.

1.2.2.3 Determination of Solubility Product. The solubility products of dodecyl sulfate and octylbenzene sulfonate anions with sodium cations were found at 6, 10, 12.5, and 15 °C for SDS and 3, 6, 10, 15, 20, 25, and 30 °C for SOBS. A series of 25 mL solutions was made for both SDS and SOBS at surfactant concentrations of 1, 2, 3, 4, and 5 mM. The NaCl was added at concentrations just

above that required for precipitation at the temperature of interest. The solutions were first placed in a water bath at a temperature just above freezing for at least 24 hours to force precipitate to form (16-19). The desired temperature was then held constant for four days while gently shaking the samples daily to insure equilibrium (17). The supernatant was filtered with a B-D Multifit 50 CC syringe filter apparatus with a Whatman 3.0 micrometer pore size cellulose nitrate membrane filter. The filtering was done quickly so that the solution remained isothermal. The absence of solids in the filtered supernatant was immediately confirmed with a high intensity beam of light. The sodium concentration in the supernatant was measured using a Varian SpectrAA atomic absorption spectrometer and the SDS concentration was determined using a Wescan conductivity detector via HPLC with a reverse phase silica column. A multiple wavelength Hewlett Packard diode array spectrophotometer at a wavelength of 224 nm was used to determine the SOBS concentration. Since these supernatant solutions were always below the CMC, these measured concentrations could be combined with activity coefficients to calculate the activity-based solubility product.

1.2.2.4 Crystal Composition. The precipitated surfactant crystal composition in equilibrium with solutions containing various mixtures of SDS and SOBS was analyzed for surfactant composition. The precipitate was formed at 0.5, 1.0, and 1.5 °C below the Krafft temperature. The solutions were filtered through a Whatman 3.0 micrometer pore size cellulose membrane filter via a B-D Multifit 50 CC syringe filter. The SDS and SOBS levels in the dissolved, washed crystals were measured by either a Wescan or Alltech 320 conductivity detector using HPLC with a reverse phase silica column.

1.3 Results and Discussion

1.3.1 Prediction of Mixture Krafft Temperatures

By definition, the Krafft temperature applies at or above the CMC. Therefore, at the Krafft temperature, a simultaneous equilibrium exists between the precipitating surfactant in the micelles, as monomers, and in the precipitate. Figure I.1 shows this equilibrium for a ternary surfactant system containing two anionic surfactants and one nonionic surfactant. For such a multicomponent system, exactly at the Krafft temperature, an infinitesimal amount of surfactant is present as precipitate at equilibrium. This precipitate normally consists of only one anionic surfactant and is formed when the monomeric concentration of the least soluble surfactant satisfies the surfactant's solubility product (4,8,9). The activity based solubility product, $K_{SP,i}$, for a monovalent anionic surfactant being precipitated by sodium cations is defined by (9):

$$K_{SP,i} = [surf_i^-]_{mon} [Na^+]_u \gamma_i \gamma_{Na} \qquad (I.1)$$

where $[surf_i^-]_{mon}$ is the surfactant monomer concentration of the precipitating surfactant, $[Na^+]_u$ is the unbound sodium concentration (the sodium not bound to micelles), and γ_i and γ_{Na} are the activity coefficients of the precipitating surfactant anion and the unbound sodium cation, respectively. The other surfactants are present as monomer and in the micelles, as shown in Figure I.1. There is also an equilibrium between the unbound counterion, counterion bound to the micelles, and counterion in the precipitate.

The Krafft temperature of an anionic surfactant can be decreased as the heterogeneity of the system is increased by adding other surfactants, even if those surfactants all have similar properties. This is due to a decrease in the monomer concentration of the precipitating surfactant caused by the formation of mixed micelles (4,7). The result is that the solution temperature must be lowered for precipitation to occur at equilibrium. As two anionic surfactants are mixed above the CMC, dilution of the least soluble surfactant in the micelles occurs. This dilution effect results in a shift of the equilibrium toward the micelles. As a nonionic surfactant is added to this system, the absolute electrical potential on the micelle surface is reduced due to insertion of the nonionic surfactant between the charged head groups of the anionic surfactants. The more favorable formation of micelles shifts the equilibrium even further toward the micelles.

A model has been developed to predict the effect of mixed micelles on Krafft temperatures using information obtained from the pure surfactant component behavior only (9). The following assumptions were made in the model used here.

1. The pseudo-phase separation model was used to describe the monomer-micelle equilibrium (7,20,21). The pseudo-phase separation model treats the micelle as a thermodynamic phase in equilibrium with the monomer.

2. Equations resulting from regular solution theory or ideal solution theory were used to model the thermodynamics of mixed micelle formation. Systems containing only anionic surfactants were assumed to form micelles behaving as ideal solutions (7,22,23), while systems containing mixtures of anionic and nonionic surfactants

formed micelles described by regular solution theory (sometimes referred to as Rubingh solution theory or nonideal solution theory) (7,16,18,21,23-28).

3. The CMC is assumed to be independent of temperature over the temperature range studied here. The effect of temperature on the CMC is secondary to the effect of mixture composition (22,29,30). However, equations describing the temperature dependence of CMC values (31,32) could easily be incorporated if required.

4. The heat of precipitation is assumed to be independent of temperature (8).

5. It is assumed that single component pure crystals form when precipitation occurs. This assumption was checked experimentally, as discussed later.

6. The nonionic surfactant CMC is assumed to be independent of ionic strength of the solution (33), an assumption which has been verified for the system studied here within experimental error.

7. The surfactant ion activity coefficients are calculated assuming that the surfactant is a simple, strong electrolyte (34,35).

At any temperature, the solubility of a surfactant anion in the presence of sodium can be described by the solubility product (Equation I.1). Below the CMC, the surfactant monomer can be treated as a simple, strong electrolyte. However, there is no universally accepted practice for the calculation of activity coefficients in a micellar solution. In this study, the anionic surfactants and the NaCl in the micellar solutions

are treated as simple, strong electrolytes, as our group has done previously (34). Several other methods have been proposed. One proposed method considers the micelles as a separate species in solution contributing only a portion of the actual micelle valence (a shielded micelle) (35). Another method treats the micelles as a separate phase which therefore does not contribute to the ionic strength of the aqueous solution (36). Burchfield and Woolley (35) also discuss the work by other researchers who treat the surfactant in solution as a simple, strong electrolyte as we have done here. The activity coefficients in Equation I.1 are from an extended Debye-Huckel expression (37).

$$\log \gamma_{Na}, \log \gamma_i = \frac{-A (z_i)^2 I^{1/2}}{(1 + B a_i I^{1/2})} - 0.3 I \qquad (I.2)$$

The constants A and B are dependent on the solvent and the temperature of solution. The parameter z_i is the ion valence and a_i is an empirical value based on the diameter of the ion. Values for A and B are tabulated (38), as well as a_i (38,39). The parameter I is the ionic strength of the solution. For this study, the ionic strength is given as:

$$I = \Sigma 0.5 c_i (z_i)^2 = [NaDS] + [NaOBS] + [NaCl] \qquad (I.3)$$

where c_i is the total concentration of ion i in solution, [NaDS] and [NaOBS] are the total concentrations of SDS and SOBS in solution, and [NaCl] is the total NaCl concentration in solution.

Since the solubility product relationship requires the monomeric surfactant concentration and unbound counterion concentration, material balances are required to determine these values. The sum of the surfactant-only mole fractions of all surfactants in the micellar phase and those in the monomer phase equal unity.

$$\Sigma x_i = x_{SDS} + x_{SOBS} + x_{NP} = 1 \qquad (I.4)$$

$$\Sigma y_i = y_{SDS} + y_{SOBS} + y_{NP} = 1 \qquad (I.5)$$

where x_i is the concentration of surfactant i in the micelles/total surfactant concentration in the micelles, and y_i is the concentration of surfactant i in the monomer phase/total surfactant concentration in the monomer phase. The subscripts SDS, SOBS, and NP refer to the two anionic surfactants and $NP(EO)_{10}$, respectively. Only an infinitesimal amount of surfactant is present as precipitate at the Krafft temperature. Therefore, material balances on each component need only to consider the monomer and micelle phases:

$$[NaDS] = [DS^-]_{mon} + [DS^-]_{mic} = [DS^-]_{mon} + x_{SDS}\, C_{mic} \qquad (I.6)$$

$$[NaOBS] = [OBS^-]_{mon} + [OBS^-]_{mic} = [OBS^-]_{mon} + x_{SOBS}\, C_{mic} \qquad (I.7)$$

$$[NP(EO)_{10}] = [NP(EO)_{10}]_{mon} + [NP(EO)_{10}]_{mic} = [NP(EO)_{10}]_{mon} + x_{NP}\, C_{mic} \qquad (I.8)$$

$$[Na^+]_{total} = [NaDS] + [NaOBS] + [NaCl] \qquad (I.9)$$
$$= [Na^+]_u + [Na^+]_b$$
$$= [Na^+]_u + \xi_{Na} C_{mic} (1 - x_{NP})$$

where $[NP(EO)_{10}]$ is the total $NP(EO)_{10}$ concentration, $[Na^+]_b$ is the sodium bound to the micelles, $[Na^+]_u$ is the unbound sodium ion concentration, and $[Na^+]_{total}$ is the total sodium ion concentration. The subscript (mon) refers to a component in the monomeric phase and the subscript (mic) refers to a component in the micellar phase. The parameter C_{mic} is the total micellar surfactant concentration and the parameter, ξ_{Na}, is the fractional counterion binding in the system. The fractional counterion binding in a pure SDS or SOBS surfactant solution is defined as the ratio of the number of counterions bound to the micelles to the number of surfactant molecules in the micelles. The fractional counterion binding of a mixed anionic system has been shown to be a weighted average of the values obtained for the pure surfactants (40,41), so for the binary SDS/SOBS system:

$$\xi_{Na,\,ideal} = X_{SDS}\, \xi_{Na,SDS} + X_{SOBS}\, \xi_{Na,SOBS} \qquad (I.10)$$

where X_{SDS} and X_{SOBS} are the mole fractions of the anionic surfactants in the micellar phase, such that

$$X_{SDS} = x_{SDS}\, C_{mic} / \{(x_{SDS} + x_{SOBS})\, C_{mic}\} \qquad (I.11)$$

$$X_{SOBS} = x_{SOBS}\, C_{mic} / \{(x_{SDS} + x_{SOBS})\, C_{mic}\} \qquad (I.12)$$

For the anionic/nonionic mixed surfactant systems, Equation I.10 is used in an empirical correlation from Hall and Price (42), as we have done previously (41,43):

$$\xi_{Na,nonideal} = \frac{(1 - x_{NP})\,\xi_{Na,ideal}}{1 - x_{NP}\,\xi_{Na,ideal}} \qquad (I.13)$$

At the CMC, the surfactant monomeric concentration is equal to the CMC. Using the Corrin-Harkins equation, the change in surfactant monomer concentration due to unbound counterion concentration can be calculated (20,44,45).

$$\ln (CMC_{SDS}) = -K_{g,SDS} \ln [Na^+]_u + K_{SDS} \qquad (I.14)$$

$$\ln (CMC_{SOBS}) = -K_{g,SOBS} \ln [Na^+]_u + K_{SOBS} \qquad (I.15)$$

where CMC_{SDS} and CMC_{SOBS} are the CMC values for pure SDS and pure SOBS at the solution temperature and salinity, respectively. The parameters K_g and K in both equations are constants that can be found experimentally from a plot of ln (CMC) versus $\ln [Na^+]_u$ for the appropriate surfactant. At the CMC, the bound sodium is negligible, so the unbound sodium concentration equals the total sodium concentration.

In a surfactant mixture, the monomer concentration of each surfactant is related to the mixture CMC, which is a function of the individual CMC values (23):

$$y_{SDS}\, CMC_{mix} = x_{SDS}\, CMC_{SDS}\, f_{SDS} \qquad (I.16)$$

$$y_{SOBS}\, CMC_{mix} = x_{SOBS}\, CMC_{SOBS}\, f_{SOBS} \quad (I.17)$$

$$y_{NP}\, CMC_{mix} = x_{NP}\, CMC_{NP}\, f_{NP} \quad (I.18)$$

$$[DS^-]_{mon} = y_{SDS}\, CMC_{mix} \quad (I.19)$$

$$[OBS^-]_{mon} = y_{SOBS}\, CMC_{mix} \quad (I.20)$$

$$[NP(EO)_{10}]_{mon} = y_{NP}\, CMC_{mix} \quad (I.21)$$

where CMC_{mix} is the mixture CMC and each parameter, f, is the activity coefficient of the relevant surfactant in the micellar phase. For an ideal system, all f values equal one.

Regular solution theory is used to describe mixed micelle formation in the anionic/nonionic and anionic/anionic/nonionic surfactant mixtures (7,16,18,21,23-28). The micellar phase activity coefficients for the ternary system are given by the equations (21,27,28):

$$f_{SDS} = \exp\{(x_{NP})^2\, \beta_{SDS\text{-}NP} + (\beta_{SDS\text{-}NP} - \beta_{SOBS\text{-}NP})\, x_{SOBS}\, x_{NP}\} \quad (I.22)$$

$$f_{SOBS} = \exp\{(x_{NP})^2\, \beta_{SOBS\text{-}NP} + (\beta_{SOBS\text{-}NP} - \beta_{SDS\text{-}NP})\, x_{SDS}\, x_{NP}\} \quad (I.23)$$

$$f_{NP} = \exp\{(x_{SOBS})^2\, \beta_{SOBS\text{-}NP} + (x_{SDS})^2\, \beta_{SDS\text{-}NP} + (\beta_{SOBS\text{-}NP} + \beta_{SDS\text{-}NP})\, x_{SOBS}\, x_{SDS}\} \quad (I.24)$$

Each parameter β is a dimensionless interaction parameter for the binary system indicated by the subscripts. The interaction parameter between two similar surfactants is approximately zero (ideal solution), and the non-zero interaction parameters present in these equations can be found from mixture CMC data.

The last equation needed to predict the Krafft temperature of a mixture from pure surfactant data is a relation between the heat of precipitation, $\Delta H_{p,i}$, solubility products, and temperature (21,34):

$$\frac{R\, d\,(\ln [K_{SP,i}])}{d\,(1/T)} = \Delta H_{p,i} \qquad \text{(I.25)}$$

If it is assumed that the heat of precipitation is independent of temperature, Equation I.25 can be integrated to yield:

$$\ln \frac{[K_{SP,i}]_{T2}}{[K_{SP,i}]_{T1}} = \frac{\Delta H_{p,i}\left(\left[1/T2\right] - \left[1/T1\right]\right)}{R} \qquad \text{(I.26)}$$

where $[K_{SP,i}]_{T1}$ is the K_{SP} at temperature T1 for precipitating surfactant i and $[K_{SP,i}]_{T2}$ is the K_{SP} at temperature T2 for precipitating surfactant i. The $\Delta H_{p,i}$ can be obtained by plotting Equation I.26, or from calorimetric measurements.

The independently obtained or defined variables in this model are K_{gSDS}, K_{gSOBS}, K_{SDS}, K_{SOBS}, CMC_{NP}, [NaDS], [NaOBS], $[NP(EO)_{10}]$, $[Na^+]_{total}$, K_{SP} of the precipitating surfactant at temperature T1, $\Delta H_{p,i}$, $\xi_{Na,SDS}$, $\xi_{Na,SOBS}$,

$\beta_{SDS\text{-}NP}$, and $\beta_{SOBS\text{-}NP}$. This leaves the unknowns; $[OBS^-]_{mon}$, $[DS^-]_{mon}$, $[NP(EO)_{10}]_{mon}$, C_{mic}, x_{SDS}, x_{SOBS}, x_{NP}, y_{SDS}, y_{SOBS}, y_{NP}, $[Na^+]_u$, $\xi_{Na,ideal}$, $\xi_{Na,nonideal}$, X_{SDS}, X_{SOBS}, CMC_{mix}, CMC_{SDS}, CMC_{SOBS}, γ_i, γ_{Na}, I, f_{SDS}, f_{SOBS}, f_{NP}, K_{SP} at the mixture Krafft temperature T2, and the mixture Krafft temperature T2, which can be found by solving Equations I.1-I.24, and I.26 simultaneously (with Equation I.2 being used once for the precipitating surfactant, and once for sodium), resulting in 26 equations and 26 unknowns. The model calculations are repeated for each anionic surfactant component in the system. The highest temperature, T2, obtained from these calculations for any anionic surfactant is the Krafft temperature of the solution.

1.3.2 Obtaining Parameters Used in Model

The CMC of each single surfactant system was obtained from surface tension measurements over a 10 to 15 °C temperature range above the pure component Krafft temperature (46). The CMC was observed to not have a substantial dependence on temperature in the region of interest for this paper (maximum percent change from the lowest to highest value is 14 %, found for SDS), as shown in Figure I.2, and could not be measured at some mixture Krafft temperatures due to precipitation. Therefore, for use in the calculation of K_g and K, the CMC values that were found for the various temperatures were averaged. The CMC's were determined at six NaCl concentrations for SDS and at three NaCl concentrations for SOBS to find the constants K_{gi} and K_i for Equations I.14and I.15 as shown in Figure I.3. The average K_{gi} and K_i values are shown in Table I.1. The CMC for $NP(EO)_{10}$ is relatively constant with respect to NaCl concentration as shown in Figure I.3. The average CMC values for $NP(EO)_{10}$, SDS, and SOBS are shown in Table I.1. The parameters K_{gi} and K_i for SDS have

been found previously (0.698 and -8.5134, respectively (19)), and are in good agreement with this study. The CMC obtained for $NP(EO)_{10}$ is consistent with other CMC values found previously (18,43). The values of ξ_{Na} for SDS and SOBS at 30 ° C from Rathman and Scamehorn (43) were used here since this parameter also has only a small temperature dependence (41,47). These values were calculated from emf data using specific ion electrodes (41) and are shown in Table I.1.

The activity based solubility products were found for SDS for a range of temperatures between 6 and 15 °C, and for SOBS for a range between 3 and 30 °C. The solubility product for SDS could not be found at higher temperatures because the amount of sodium required for precipitation to occur also lowered the CMC so that the solutions contained micelles. The activity based heats of precipitation for SDS and SOBS were found from the average solubility products for the surfactant concentrations of 2, 3, 4, and 5 mM. Figure I.4 shows the resulting solubility product averages as a function of inverse temperature for SDS and SOBS. From Equation I.26, the slope of each line yields the $\Delta H_{p,i}$ for that surfactant. The K_{SP} at the Krafft temperature can be found from the data in Figure I.4. The K_{SP} values for SDS and SOBS at their respective Krafft temperatures, as well as the heats of precipitation are listed in Table I.1. The heat of precipitation for SDS with NaCl has previously been used by Scamehorn (21) as an adjustable parameter in a model used to describe mixture Krafft temperatures. The resulting value was -5710 cal/mol, lower than the much more carefully determined value of -9000 cal/mol in this work. The Krafft temperatures for SDS and SOBS without added NaCl were used in the model to predict all of the mixture Krafft temperatures, and are given in Table I.1.

The binary interaction parameters used for this study were obtained from the literature (16,43) as shown in Table I.2. The interaction parameter is a mild function

of temperature (7,21). However, the predicted Krafft temperatures are relatively insensitive to the value of the interaction parameters, so ignoring temperature effects on β values is justified.

1.3.3 Precipitate Composition

The precipitate compositions for 0.04 M SDS/SOBS mixtures from 0/100 to 100/0 SDS/SOBS and 0.5, 1.0, and 1.5 °C below each solution's Krafft temperature are given in Table I.3. The precipitate compositions were studied to determine whether the precipitate at the Krafft temperature consists of only one anionic surfactant, which is the assumption used in the modelling of the mixture Krafft temperatures. In the SOBS rich side (solution compositions from which SOBS precipitates at a higher temperature than SDS), only SOBS is precipitating near the Krafft temperature, with SDS beginning to precipitate at 0.4 SDS solution mole fraction as the temperature is lowered more than 1 °C below the Krafft temperature. This result agrees with the assumption used in the model that only one surfactant precipitates at the mixture Krafft temperature. On the SDS rich side, SOBS is present in the precipitate in decreasing amounts as one moves towards pure SDS and closer to the Krafft temperature. As the temperature is reduced below the Krafft temperature enough, precipitation of both surfactants is expected as the solubility product of each is reached. At 0.°5 C below the Krafft temperature, at mole fractions of SDS greater than 0.7, no detectable amount of SOBS was present in the precipitate. It may be concluded that at the Krafft temperature, coprecipitation of surfactant components is negligible and for this system the assumption of single component surfactant precipitate on a phase boundary is justified. SOBS may also be adsorbing onto the SDS crystals, resulting in the presence of SOBS near the Krafft temperature.

$NP(EO)_{10}$ has already been shown to not incorporate itself onto anionic precipitate similar to the ones used here (18).

1.3.4 Experimental and Theoretical Krafft Temperatures

Figure I.5 represents the Krafft temperature as a function of surfactant composition for 0.04 M SDS/SOBS mixtures at several NaCl concentrations. The systems exhibit eutectic-type behavior as has been qualitatively seen in other work on similar systems (8-11). Mixture Krafft temperature depressions as much as 24.7 °C (relative to the most easily precipitating pure surfactant) are seen in Figure I.5, indicative of the synergisms of these mixtures in avoiding precipitation. This eutectic-type behavior is due to the formation of ideal mixed micelles which lower the precipitating surfactant's monomer concentration.

Both single anionic surfactant and binary anionic/anionic surfactant mixtures exhibit higher Krafft temperatures with increasing NaCl concentration as seen in Figure I.5. There are two opposing phenomena which occur when counterion is added to these systems. Increasing the counterion concentration tends to decrease the surfactant monomer concentration required to satisfy the solubility product (Equation 1). However, adding NaCl lowers the CMC. This decreases the anionic surfactant monomer concentration, causing precipitation to be more difficult. For this system, the former effect dominates the latter and the Krafft temperature increases with added NaCl.

The solid lines shown in Figure I.5 are the predicted phase boundaries. The eutectic type of behavior of the anionic/anionic surfactant mixtures is predicted by the model which only utilizes properties of each pure component. This, therefore, is an

a priori predictive model for mixture Krafft temperatures. Also, the change in the precipitation phase boundary of the anionic surfactants as NaCl is added to the system is predicted by the model. The Krafft temperatures on the left side of Figure I.5 are predicted well (where SOBS is the precipitating species) with no added NaCl. However, the prediction of the Krafft temperatures on the right side (where SDS is precipitating) or at high salinities is not as good. Figure I.6 shows the result of adjusting the solubility product for SDS and SOBS so that the pure component Krafft temperatures for the no added salt case is exactly predicted. This was done because the pure SDS Krafft temperature was not well predicted by the model. The mixture data are then still being predicted only from pure component data. Similar results could also be achieved by adjusting the Corrin-Harkins parameter, K_g, for the pure components. The value of K_{SP} was adjusted here instead of K_g just to show ability of the model to predict the mixture Krafft temperatures using an adjustable parameter. For SOBS, the exact value of the pure component Krafft temperature can be found if K_{SP} is changed to 1.31×10^{-4} M^2. This is a -1.5 % change which results in a -0.06 % correction to the experimentally determined Krafft temperature from 28.2 °C to the experimentally determined value of 28.0 °C. The adjusted K_{SP} value for SDS is 4.86×10^{-5} M^2, which is a -50.2 % change. This results in a 4.5 % change in the Krafft temperature of SDS from 6.0 °C to the experimental value of 18.4 °C. This shows how sensitive the pure component predicted Krafft temperature is to the K_{SP}. The model is able to predict that adding sodium increases the Krafft temperature. However, it does not predict the extent of the increase, and actually predicts a slight decrease at a sodium concentration of 0.2 M on the SDS rich side of the phase boundary. At this higher NaCl concentration, the model predicts that the effect of sodium on the CMC outweighs the effect of sodium on the solubility product.

Adjusting the other parameters in the model in addition to K_{SP} did not improve the prediction. Deviations between the model predictions of precipitation phase boundaries (hardness tolerance) and experimental data have been seen before when NaCl concentrations were increased to 0.1 M (17). The assumptions used in calculating the activity coefficients in these micellar solutions may be a cause for this discrepancy. Above the CMC, the micelles do not contribute to the ionic strength to the same degree as free, strong electrolytes. A model has been developed to account for the difference (35), and could be used for a more accurate calculation. However, the number of parameters in that model does not allow for simple calculations of Krafft temperatures which is the goal of this paper. If an adjustable K_{SP} is used for the pure components at each NaCl concentration, the mixture precipitation phase boundaries can be predicted more accurately, even at high NaCl concentrations as shown in Figure I.7. This same result can be achieved by adjusting K_g. Therefore, we may conclude that the Krafft temperature of binary anionic surfactants can be predicted from pure component properties well, although prediction of pure surfactant Krafft temperatures from solubility product and micelle formation parameters is more difficult.

Changing the overall concentration of the surfactants in the anionic/anionic system does not significantly change the experimental Krafft temperature as seen in Figure I.8. This figure compares Krafft temperatures at 0.04 M and 0.02 M total surfactant concentrations and predictions from the model used in Figure I.7. Above the CMC, as the anionic surfactant concentration is increased, most of the additional surfactant added to the system above the CMC goes into the micellar phase and is therefore not available for precipitation (4). However, a small increase in the

monomer concentration usually occurs and is predicted by the model. The result is a slight increase in the Krafft temperature as the surfactant concentration is increased.

Nonionic surfactants not only dilute the anionic surfactant in the micelle, but enhance, or synergize, micelle formation. The nonideal mixture CMC can be well below that of the pure components' CMC's due to the insertion of the nonionic hydrophilic groups between the anionic hydrophilic groups. This insertion of the nonionic surfactant reduces electrostatic head group repulsions between the anionic hydrophilic groups, lowering the absolute value of the electrical potential at the micelle surface. Therefore, the addition of a nonionic surfactant to an anionic surfactant system can cause an even more substantial depression of the Krafft temperature than the addition of another anionic surfactant. The effect of the addition of a nonionic surfactant to an anionic surfactant on the micelle-monomer equilibrium has been studied previously by Stellner and Scamehorn (16-18). The resulting Krafft temperature reduction is illustrated in Figures I.9 and I.10, where SDS/NP(EO)$_{10}$ and SOBS/NP(EO)$_{10}$ Krafft temperatures, respectively, are shown for various NaCl concentrations at a total surfactant concentration of 0.04 M. The solid lines represent the predicted Krafft temperatures using regular solution theory to model the nonideal mixed micelles and a K_{SP} for the anionic surfactant to force-fit the pure component Krafft temperature at each salinity. Krafft temperatures of anionic surfactants with added alcohols at various electrolyte concentrations have been studied with similar results and have been described using an empirical model (48). The larger Krafft temperature depression for each anionic surfactant in the presence of the nonionic surfactant when compared to the addition of a second anionic surfactant (by comparing Figures I.9 and I.10 with Figure I.6) is evident. For example, when the mole fraction of SDS in solution decreases from 1 to 0.7, the Krafft temperature

depression is - 4.7 °C for an anionic cosurfactant and - 12.0 °C for a nonionic cosurfactant. There is a stronger dependence of the Krafft temperature on [NaCl] in the anionic/nonionic systems than in the anionic/anionic system. The binding of Na^+ to the micelles and the insertion of the nonionic surfactant into the micelles both reduce the absolute value of the electrical potential on the micelle surface. The presence of the nonionic surfactant in the micelles reduces the fraction of bound Na^+, leaving a higher concentration of unbound Na^+ available for precipitation with the anionic surfactant monomer. The model used here is still predictive (employs only single component Krafft temperatures and mixed micelle parameters) and provides excellent fit to the data, considering the lack of adjustable parameters.

Figure I.11 shows the Krafft temperatures for the ternary SDS/SOBS/$NP(EO)_{10}$ system with $NP(EO)_{10}$ varying from 0 to 0.25 mole fraction of the total surfactant for either pure anionic surfactant or with both anionic surfactants present. As the $NP(EO)_{10}$ concentration increases, a greater Krafft temperature depression occurs. The solid line shows the model which describes the effect of nonideal mixed micelles on the precipitation. The depression of the experimental data at higher $NP(EO)_{10}$ concentrations as the two anionic surfactants are mixed is much greater than the model predicts. The addition of a nonionic component to an anionic surfactant was observed to increase the time required for precipitation to occur. Therefore, not only does increased heterogeneity depress the Krafft temperature, it also increases the amount of time required for precipitation to occur. A study of the effect of mixing two anionic surfactants on the rate of precipitation has been done in Chapter 3 and a preliminary study of the effect of adding a nonionic surfactant to an anionic surfactant on the rate of precipitation has also been done (49). In both cases, it was found that mixing surfactants increased the

amount of time required for precipitation. At 0.25 mole fraction $NP(EO)_{10}$, none of the systems containing both anionic surfactants precipitated after being held at -1.6 °C for 16 days. However, the model predicts Krafft temperatures above 0 °C. The kinetics of precipitation for these solutions may be very slow so that even though the solutions could have a Krafft temperature, the slow kinetics could make this unimportant in most practical situations. It has been seen previously by another group that certain compositions of anionic/nonionic mixtures took two weeks for precipitation to occur when attempting to force precipitation close to 0 °C (14). However, this does not explain the much larger drops in the Krafft temperature data on the SDS rich side for 0.15 and 0.20 mole fraction $NP(EO)_{10}$ than is predicted. Also, coprecipitation (possibly due to adsorption of the cosurfactant onto the surfactant crystal surface) could be occurring, which the model does not incorporate. Adsorption of nonionic surfactant on anionic/cationic surfactant precipitate has been considered to be the cause of deviation between theory and experiment in that ternary system (28).

Figure I.12 shows the effect of adding SOBS to SDS on the Krafft temperatures of SDS/SOBS/$NP(EO)_{10}$. From this figure, it is evident that increasing the heterogeneity of the surfactant mixture reduces the Krafft temperature. As the SOBS mole fraction is increased, the Krafft temperature is lowered. Also, as the mole fraction of total anionic surfactant is decreased, the Krafft temperature is reduced, the effect being more pronounced at a SOBS mole fraction of 0.5, close to the minimum in the eutectic Krafft temperature plot.

An understanding of the synergistic effect of mixing two anionic surfactants in a ternary system with a nonionic surfactant can be obtained from monomer concentrations of the surfactants as they are mixed. Figure I.13 shows the predicted

monomer concentrations of SDS and SOBS as they are mixed in solutions containing various mole fractions of $NP(EO)_{10}$. For each system, as SDS is added to SOBS, the monomer concentration of SOBS decreases and SDS increases. As a result, a reduced temperature is necessary to meet the requirements for precipitation of SOBS as dictated by the K_{SP}. As the SDS mole fraction is increased further, a point is reached where enough SDS is present that the solubility product of SDS is satisfied at a higher temperature than that of SOBS, resulting in SDS precipitating at the mixture Krafft temperature. Therefore, at the Krafft temperatures (on the phase boundary) to the left of the minimum in Figure I.5, SOBS precipitates and to the right of the minimum, SDS crystals form. The effect of adding a nonionic surfactant is to decrease the monomeric concentrations of the anionic surfactants as can be seen in Figure I.13.

In this study, precipitation characteristics of ideal and nonideal surfactant mixtures have been elucidated. Increasing surfactant heterogeneity or the number of components in a system tends to depress the Krafft temperature of the system. The degree of depression observed in the Krafft temperature upon mixing surfactants, however, is not significantly affected by added NaCl. Changing the overall surfactant concentration when well above the CMC only slightly lowers the Krafft temperature. The addition of a nonionic surfactant can increase the Krafft temperature depression substantially due to nonideal mixed micelle formation.

Krafft temperatures of binary anionic/anionic surfactant mixtures can be successfully predicted from a simple thermodynamic model by using an adjustable parameter (K_{SP} or K_g). Only properties of the individual surfactant components are required. Greater than predicted Krafft temperature depressions were observed for the ternary surfactant mixtures. Factors such as slow kinetics of precipitation or surfactant adsorption on precipitate crystals are possible causes for this discrepancy.

1.4 References

1. Coons, D., M. Dankowski, M. Diehl, G. Jakobi, P. Kuzel, E. Sung, and U. Trabitizsch, Performance in detergents, cleaning agents, and personal care products 5.1 Detergents, in *Surfactants in Consumer Products, Theory, Technology, and Applications*, edited by J. Falbe, Springer-Verlag, Berlin, 1987, pp 197-305.

2. Lynn, J.L., Jr., Detergency, in *Kirk-Othmer Encyclopedia of Chemical Technology*, 4th ed., Vol. 7, Wiley, New York, 1991, pp 1072-1117.

3. Dunn, R.O., J.F. Scamehorn, and S.D. Christian, Use of micellar-enhanced ultrafiltration to remove dissolved organics from aqueous streams, *Sep. Sci. Technol., 20:*257-284 (1985).

4. Scamehorn, J.F., and J.H. Harwell, Precipitation of surfactant mixtures, in *Mixed Surfactant Systems*, edited by K. Ogino and M. Abe, Marcel Dekker, New York, 1993, pp 283-312.

5. Brant, L.W., K.L. Stellner, and J.F. Scamehorn, Recovery of surfactant from surfactant-based separations using a precipitation process, in *Surfactant-Based Separation Processes*, edited by J.F. Scamehorn and J.H. Harwell, Marcel Dekker, New York, 1989, Vol. 33, pp 323-338.

6. Yin Y., J.F. Scamehorn, and S.D. Christian, Recovery of a dialkyl diphenyl ether disulfonate surfactant from surfactant flush solutions by Precipitation, *ACS Symp. Ser., 594:*231-248 (1995).

7. Scamehorn, J.F., An overview of phenomena involving surfactant mixtures, in *Phenomena in Mixed Surfactant Systems*, edited by J.F. Scamehorn, ACS Symp. Ser., Vol. 311, American Chemical Society, Washington, 1986, pp 1-27.

8. Tsujii, K., N. Saito, and T. Takeuchi, Krafft points of anionic surfactants and their mixtures with special attention to their applicability in hard water, *J. Phys. Chem., 84:*2287-2291 (1980).

9. Scamehorn, J.F., Precipitation of mixtures of anionic surfactants, in *Mixed Surfactant Systems*, edited by P.M. Holland and D.N. Rubingh, ACS Symp. Ser., Vol. 501, American Chemical Society, Washington, 1992, pp 392-401.

10. Hato, M., and K. Shinoda, Krafft points of calcium and sodium dodecylpoly(oxyethylene) sulfates and their mixtures, *J. Phys. Chem.*, *77:*378-381 (1973).

11. Moroi, Y., T. Oyama, and R. Matuura, Phase equilibria of anionic surfactant mixtures in aqueous solution, *J. Colloid Interface Sci.*, *60:*103-111 (1977).

12. Rosen, M.J., *Surfactants and Interfacial Phenomena*, 2nd ed., Wiley, New York, 1989, p 215.

13. Ogino, K., K. Kato, and M. Abe, Effect of inorganic electrolytes on dissolution behavior of mixed anionic-amphoteric surfactant systems, *J. Amer. Oil Chem. Soc.*, *65:*272-276 (1988).

14. Fan, X.J., P. Stenius, N. Kallay, and E. Matijevic, Precipitation of surfactant salts II. the effect of nonionic surfactants on precipitation of calcium dodecyl sulfate, *J. Colloid Interface Sci.*, *121:*571-578 (1988).

15. Peacock, J.M., and E. Matijevic, Precipitation of alkylbenzene sulfonates with metal ions, *J. Colloid Interface Sci.*, *77:*548-554 (1980).

16. Stellner, K.L. and J.F. Scamehorn, Surfactant precipitation in aqueous solutions containing mixtures of anionic and nonionic surfactants, *J. Amer. Oil Chem. Soc.*, *63:*566-574 (1986).

17. Stellner, K.L. and J.F. Scamehorn, Hardness tolerance of anionic surfactant solutions: 1. anionic surfactant with added monovalent electrolyte, *Langmuir*, *5:*70-77 (1989).

18. Stellner, K.L. and J.F. Scamehorn, Hardness tolerance of anionic surfactant solutions: 2. effect of added nonionic surfactant, *Langmuir*, *5:*77-84 (1989).

19. Stellner, K.L., J.C. Amante, J.F. Scamehorn, and J.H. Harwell, Precipitation phenomena in mixtures of anionic and cationic surfactants in aqueous solutions, *J. Colloid Interface Sci.*, *123:*186-200 (1988).

20. Shinoda, K., The formation of micelles, in *Colloidal Surfactants*, edited by K. Shinoda, T. Tamamushi, T. Nakagawa, and T. Isemura, Acad. Press., NY, 1963, pp1-96.

21. Holland, P.M., Nonideal mixed micellar solutions, *Adv. Colloid Interface Sci.*, *26:*111-129 (1986).

22. Rosen, M.J., *Surfactants and Interfacial Phenomena*, 2nd ed., Wiley, NY, 1989, pp108-169.

23. Scamehorn, J.F., R.S. Schechter, and W.H. Wade, Micelle formation in mixtures of anionic and nonionic surfactants, *J. Dispersion Sci. Technol., 3:*261-278 (1982).

24. Balzhizer, R.E., M.R. Samuels, and J.D. Eliassen, *Chemical Engineering Thermodynamics*, Prentice Hall, Englewood Cliffs, 1972, pp 403-405.

25. Rosen, M.J., *Surfactants and Interfacial Phenomena*, 2nd ed., Wiley, NY, 1989, pp 393-419.

26. Rubingh, D.N., Mixed micelle solutions, in *Solution Chemistry of Surfactants*, edited by K.L. Mittal, Plenum Press, NY, 1979, pp 337-354.

27. Holland, P.M. and D.N. Rubingh, Nonideal multicomponent mixed micelle model, *J. Phys. Chem., 87:*1984-1990 (1983).

28. Shiau, B., J.H. Harwell, and J.F. Scamehorn, Precipitation of mixtures of anionic and cationic surfactant: III. effect of added nonionic surfactant, *J. Colloid Interface Sci., 167:*332-345 (1994).

29. Musbally, G.M., G. Perron, and J.E. Desnoyers, Apparent molal volumes and heat capacities of ionic surfactants in water at 25 °C, *J. Colloid Interface Sci., 48:*494-501 (1974).

30. Mukerjee, P., K.J. Mysels, *Critical Micelle Concentrations of Aqueous Surfactant Systems; National Bureau of Standards*, Washington, 1971.

31. Muller, N., Temperature dependence of critical micelle concentrations and heat capacities of micellization for ionic surfactants, *Langmuir 9:*96-100 (1993).

32. Stasiuk, E.N.B., and L.L. Schramm, The temperature dependence of the critical micelle concentrations of foam-forming surfactants, *J. Colloid Interface Sci., 178:*324-333 (1996).

33. Shinoda K., T. Yamaguchi, and R. Hori, The surface tension and the critical micelle concentration in aqueous solution of β-*D*-alkyl glucosides and their mixtures, *Bull. Chem. Soc. Jpn., 34:*237-241 (1961).

34. Amante, J.C., J.F. Scamehorn, and J.H. Harwell, Precipitation of mixtures of anionic and cationic surfactants: II. effect of surfactant structure, temperature, and pH, *J. Colloid Interface Sci., 144:*243-253 (1991).

35. Burchfield, T.E., and E.M. Woolley, Model for thermodynamics of ionic surfactant solutions: 1. osmotic and activity coefficients *J. Phys. Chem., 88:*2149-2155 (1984).

36. Dharmawardana, U.R., S.D. Christian, E.E. Tucker, R.W. Taylor, and J.F. Scamehorn, A surface tension method for determining binding constants for cyclodextrin inclusion complexes of ionic surfactants, *Langmuir, 9:*2258-2263 (1993).

37. Davies, C.W., *Ion Association*, Butterworths, London, 1962, p 41.

38. Klotz, I.R. and R.M. Rosenberg, *Chemical Thermodynamics: Basic Theory and Methods*, 4th ed., Krieger Publishing Co., Malabar, 1991, pp 440-442.

39. Robinson, R.A. and R.H. Stokes, *Electrolyte Solutions*, 2nd ed., Butterworths, London, 1959, pp 174-252.

40. Shedlovsky, L., C.W. Jakob, and M.B. Epstein, Study of pNa of aqueous solutions of sodium decyl, dodecyl, and tetradecyl sulfates by e.m.f. measurements, *J. Phys. Chem., 67:*2075-2079 (1963).

41. Rathman, J.F. and J.F. Scamehorn, Counterion binding on mixed micelles, *J. Phys. Chem., 88:*5807-5816 (1984).

42. Hall, D.G., and T.J. Price, Electrochemical studies of micelle-counterion interactions in mixtures of ionic and non-ionic surfactants, *J. Chem. Soc. Faraday Trans., 80:*1193-1199 (1984).

43. Rathman, J.F. and J.F. Scamehorn, Counterion binding on mixed micelles: effect of surfactant structure, *Langmuir 3:*372-377 (1987).

44. Corrin, M.L. and W.D. Harkins, The effect of salts on the critical concentration for the formation of micelles in colloidal electrolytes, *J. Amer. Chem. Soc., 69:*683-688 (1947).

45. Sowada, R., The effect of electrolytes on the critical micelle concentration of ionic surfactants; The Corrin-Harkins Equation, *de Surf. Det., 31:*195-199 (1994).

46. Rodriguez, C.H., Ph.D. Dissertation, The University of Oklahoma, 1997.

47. Zana, R., Effect of alcohols on the equilibrium properties and dynamics of micellar solutions, in *Surface Phenomena in Enhanced Oil Recovery*, edited by D.O. Shah, Plenum Press, New York, 1981, pp 521-533.

48. Gendy, T.S., S.A. El-Mergawy, Y. Barakat, and A.I. Mead, Quantitative evaluation of the effect of alkyl chain length, added alcohols and/or electrolyte on Krafft point of linear 1-phenylalkane sodium sulphonates, *Hungarian J. Ind. Chem.*, *22*:219-225 (1994).

49. Lee, R.S., and I.D. Robb, Precipitation of calcium surfactants, *J. Chem. Soc. Faraday Trans. 1*, *75*:2126-2136 (1979).

Table I.1. Summary of Parameters Used in Model to Predict Mixture Krafft Temperatures

	Units	SDS	SOBS	$NP(EO)_{10}$
CMC (0 M NaCl)	M	0.0072	0.012	7.5×10^{-5}
K_g	unitless	0.704	0.627	0
K	ln(M)	-8.317	-7.082	-
ξ_{Na}	unitless	0.67	0.65	-
ΔH_p	cal/mol	-9000	-6950	-
K_{SP} at Krafft Temperature	M^2	9.77×10^{-5}	1.33×10^{-4}	-
Krafft Temperature	°C	18.4	28.0	-

Table I.2. Binary Interaction Paramaters of SDS and SOBS with $NP(EO)_{10}$

NaCl concentration, M	$\beta_{SDS\text{-}NP(EO)_{10}}$	$\beta_{SOBS\text{-}NP(EO)_{10}}$
0.0	-2.72	-2.73
0.1	-2.70	-2.71
0.2	-2.32	-2.33

Table I.3. Precipitate Compositions from Solutions 0.5, 1.0, and 1.5 °C Below the Krafft Temperature

	0.5 °C Below	1.0 °C Below	1.5 °C Below
SDS/SOBS in Solution	SDS/SOBS in Precipitate	SDS/SOBS in Precipitate	SDS/SOBS in Precipitate
0/100	0/100	0/100	0/100
10/90	0/100	0/100	0/100
20/80	0/100	0/100	0/100
30/70	0/100	0/100	0/100
40/60	0/100	3/97	6/94
50/50	46/54	9/91	6/94
60/40	87/13	63/37	24/76
70/30	100/0	97/3	84/16
80/20	100/0	99/1	90/10
90/10	100/0	100/0	100/0
100/0	100/0	100/0	100/0

Figure I.1 Micelle-Monomer-Precipitate Equlibrium for a Ternary Anionic/Anionic/Nonionic Surfactant System Just Below the Krafft Temperature

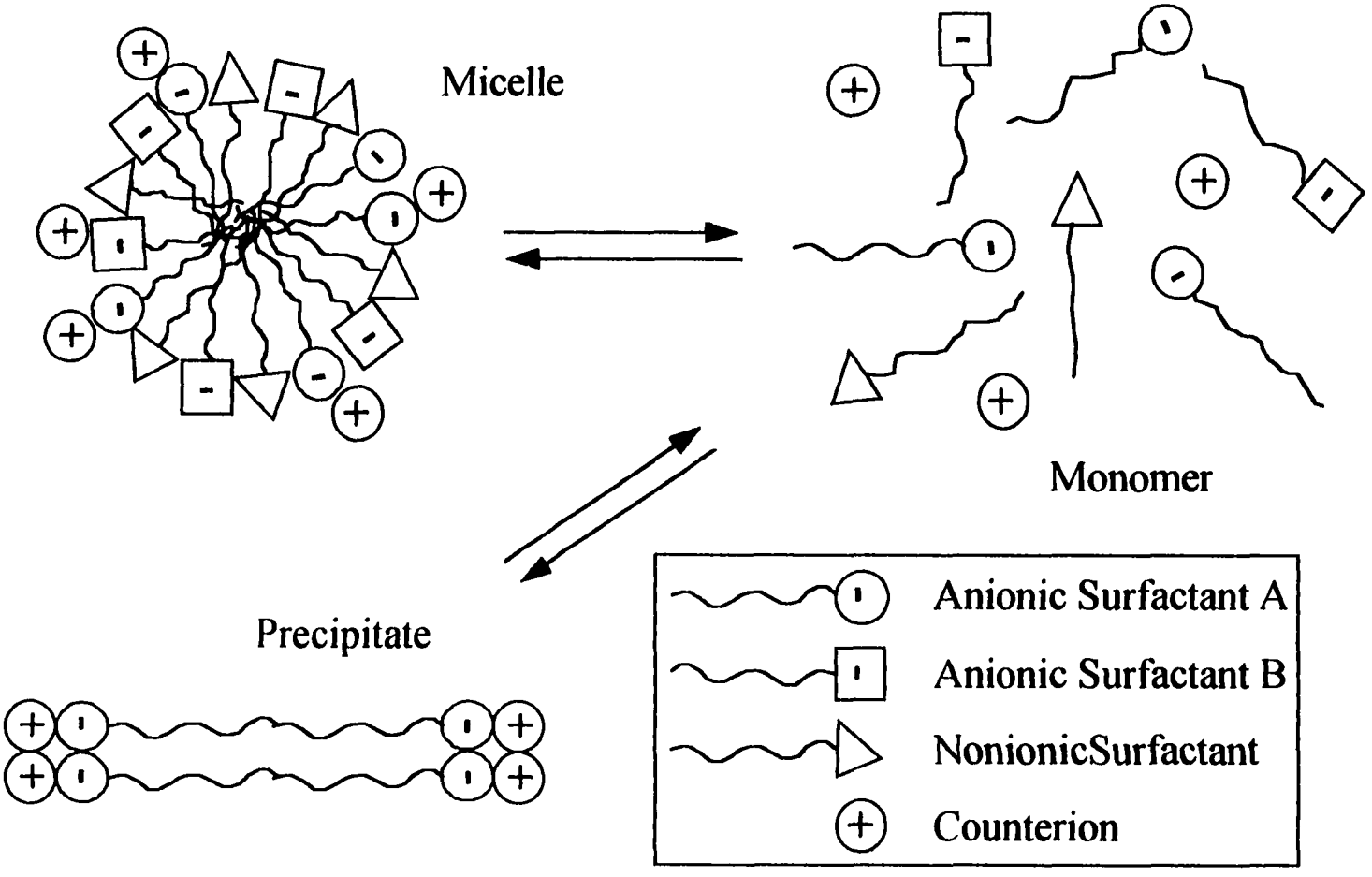


Figure I.2 CMC as a Function of Temperature for SDS, SOBS, and $NP(EO)_{10}$

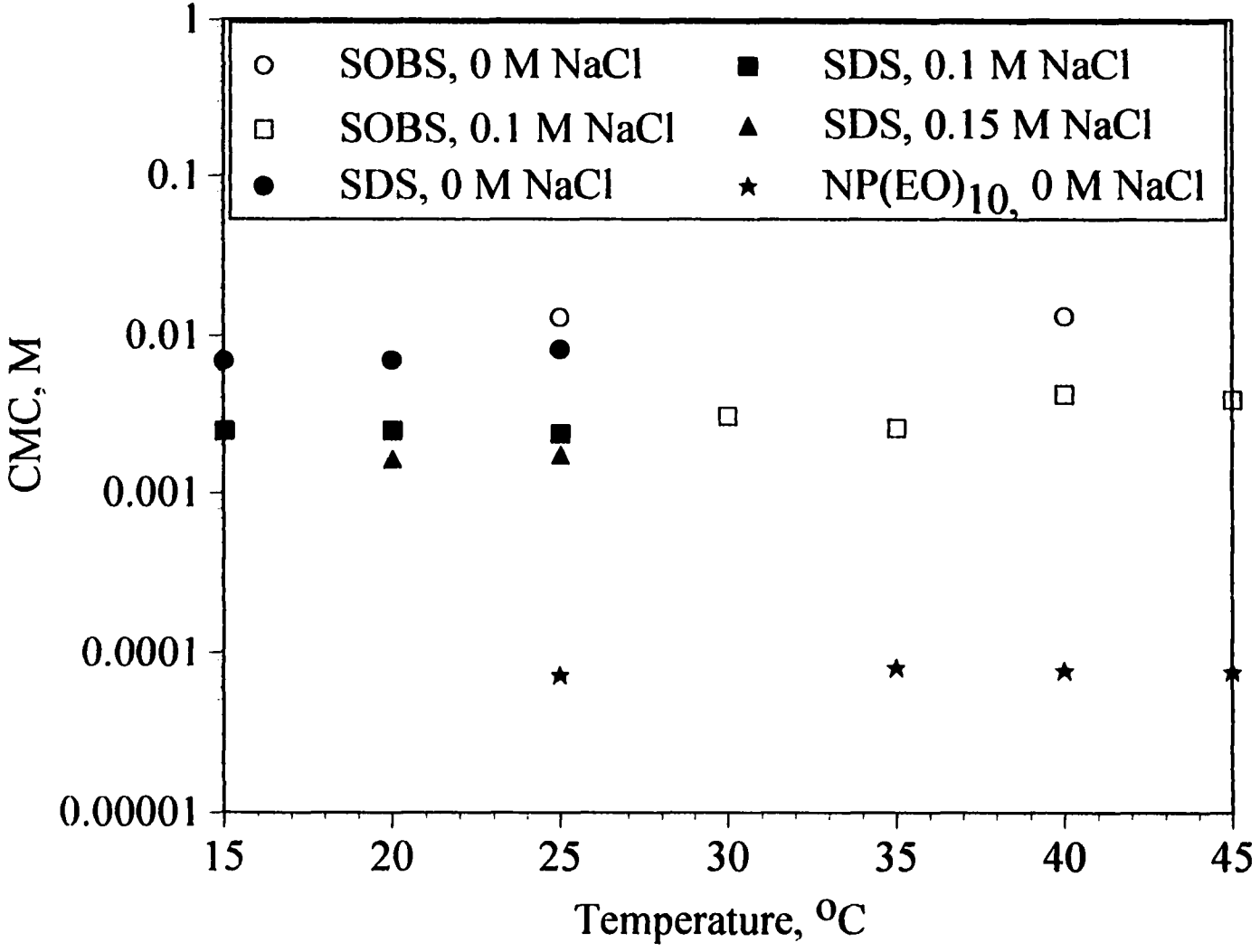


Figure I.3 CMC as a Function of Sodium Concentration for SDS, SOBS and $NP(EO)_{10}$

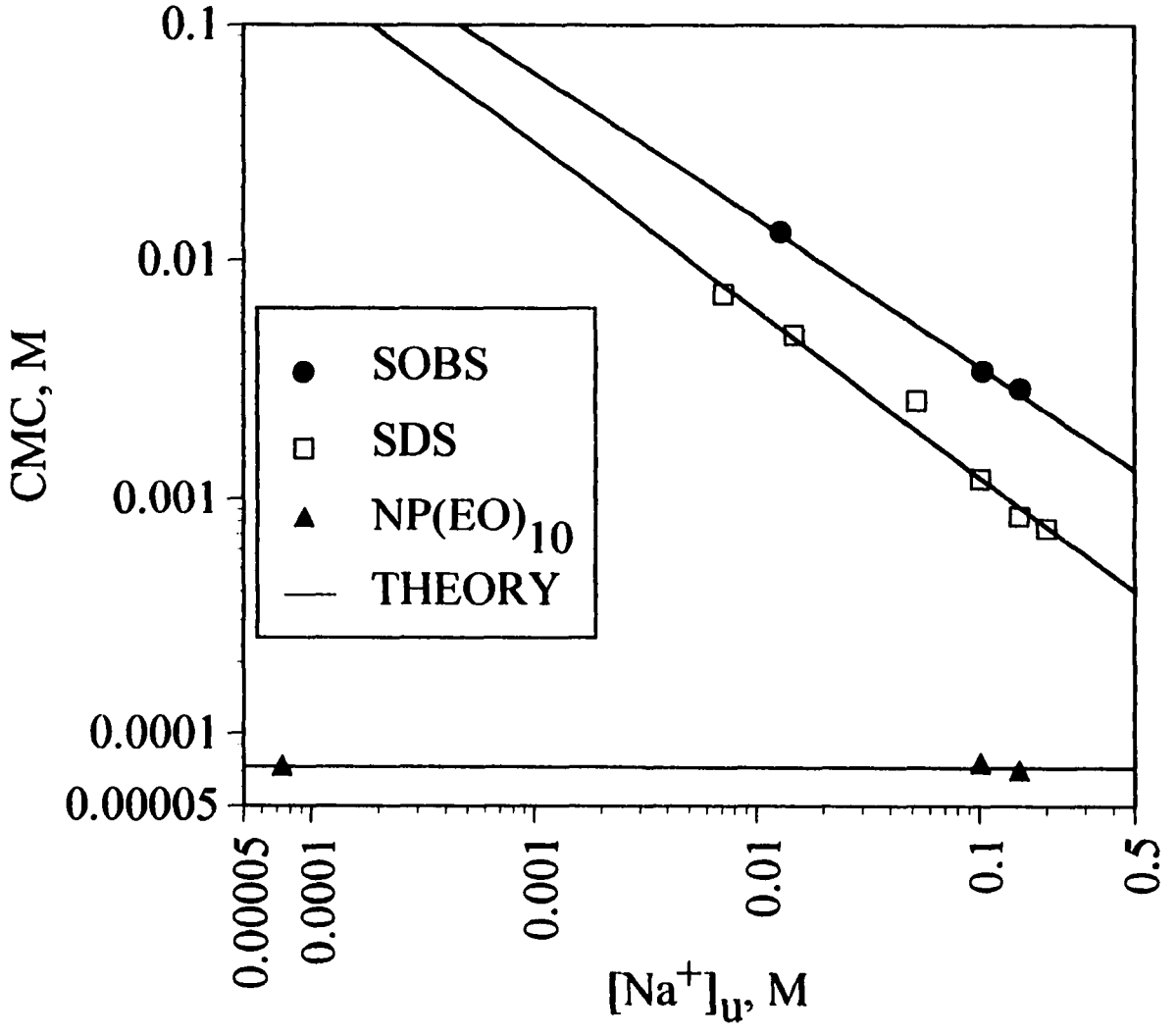


Figure I.4 Activity-Based Solubility Product as a Function of Inverse Temperature

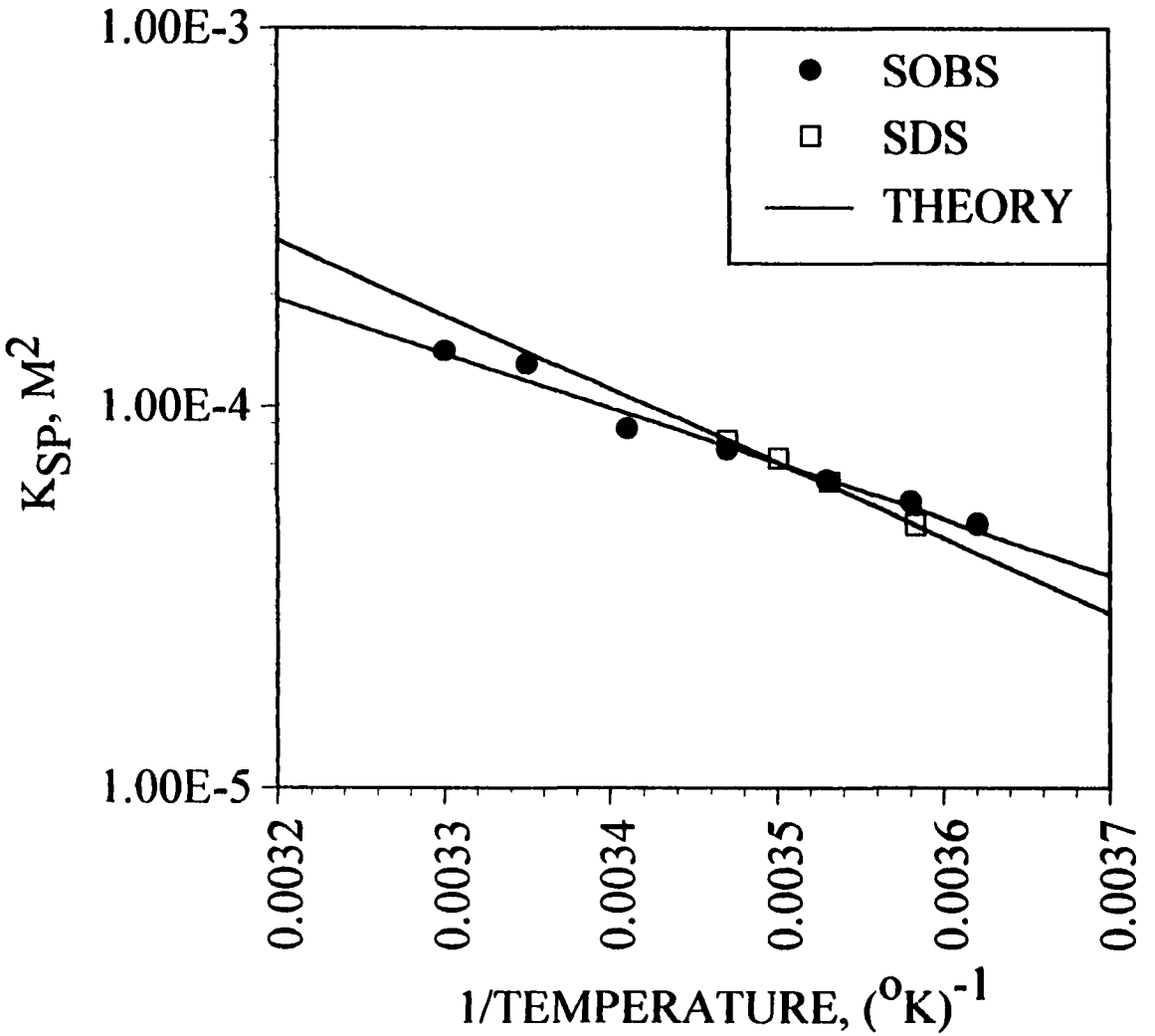


Figure I.5 Krafft Temperatures for SDS/SOBS System at 0.04 M Total Surfactant Concentration and 0, 0.1, and 0.2 M NaCl Compared with Theory; No Adjustable Parameter

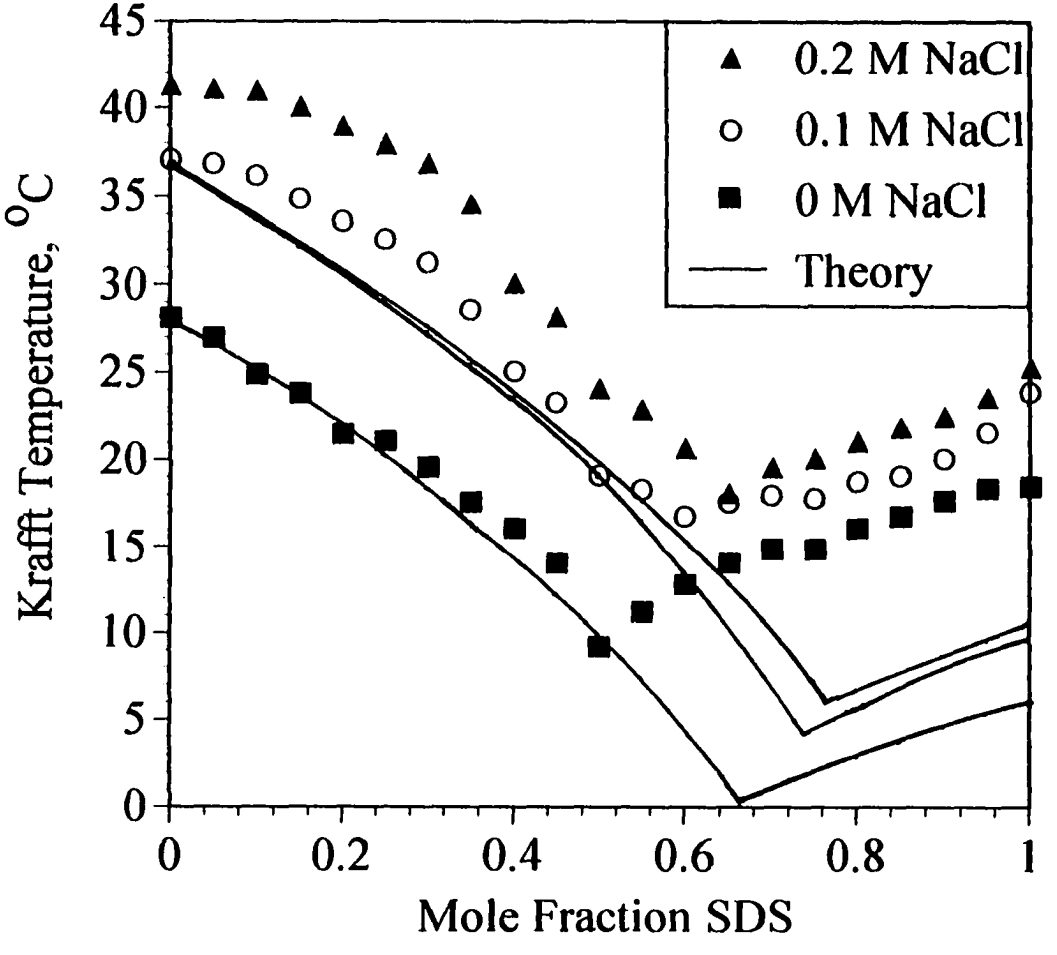


Figure I.6 Krafft Temperatures for SDS/SOBS System at 0.04 M Total Surfactant Concentration and 0, 0.1, and 0.2 M NaCl Compared with Theory; K_{SP} Adjusted for Pure SDS and Pure SOBS at 0 M NaCl

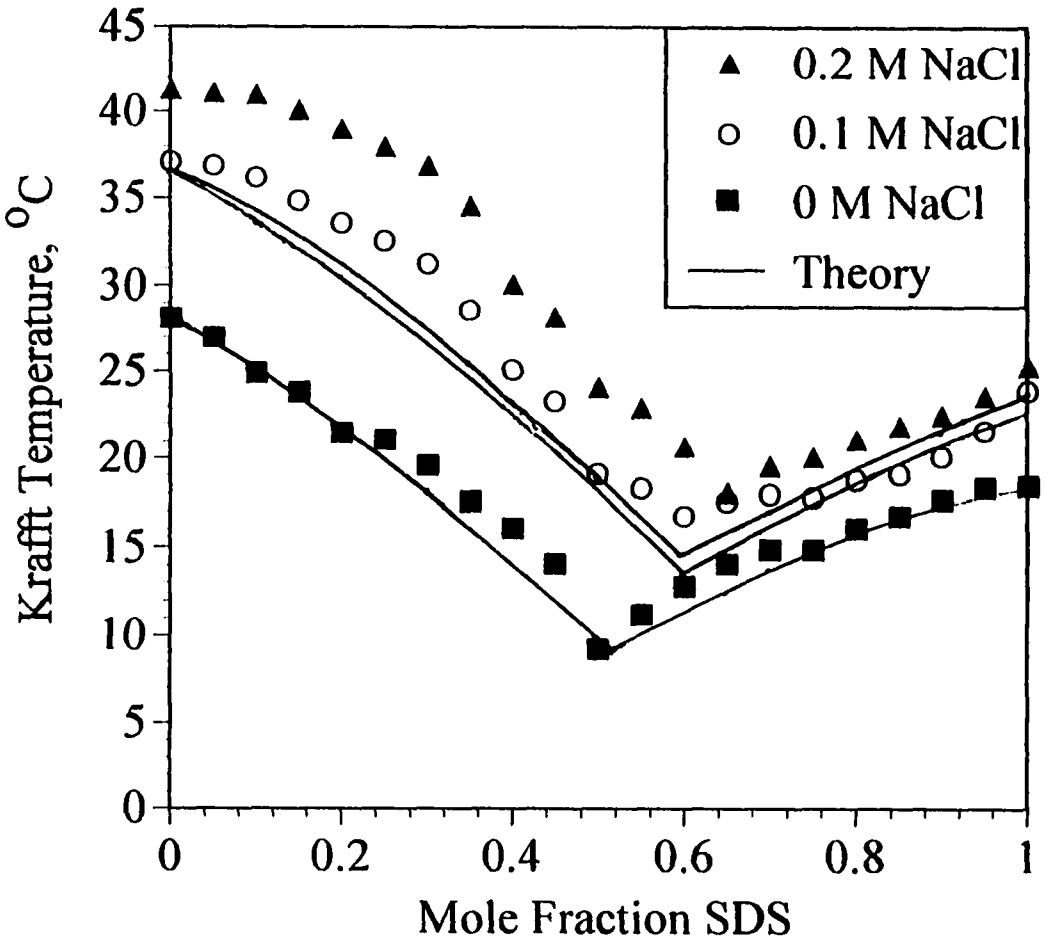


Figure I.7 Krafft Temperatures for SDS/SOBS System at 0.04 M Total Surfactant Concentration and 0, 0.1, and 0.2 M NaCl Compared with Theory; K_{SP} Adjusted for Pure SDS and Pure SOBS at Each NaCl Concentration

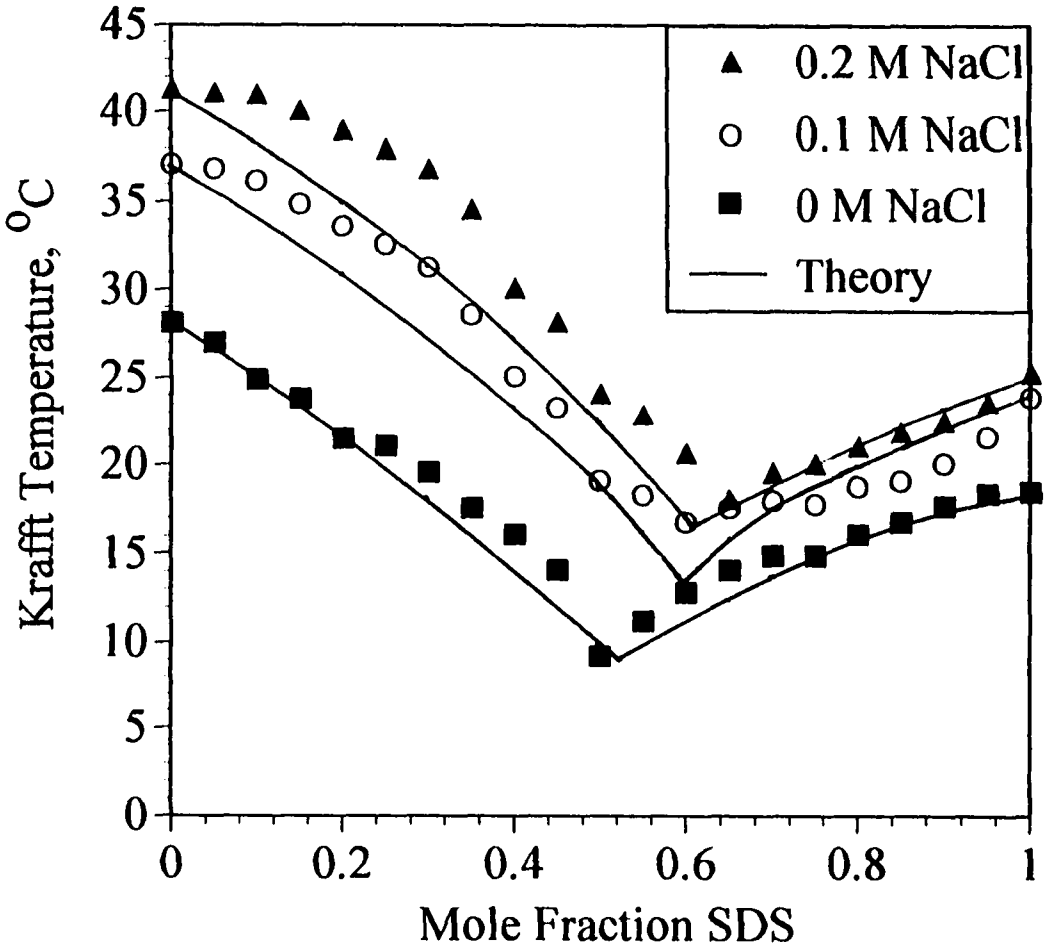


Figure I.8 Krafft Temperatures for SDS/SOBS System at 0.04 M and 0.02 M Total Surfactant Concentrations at Various NaCl Concentrations

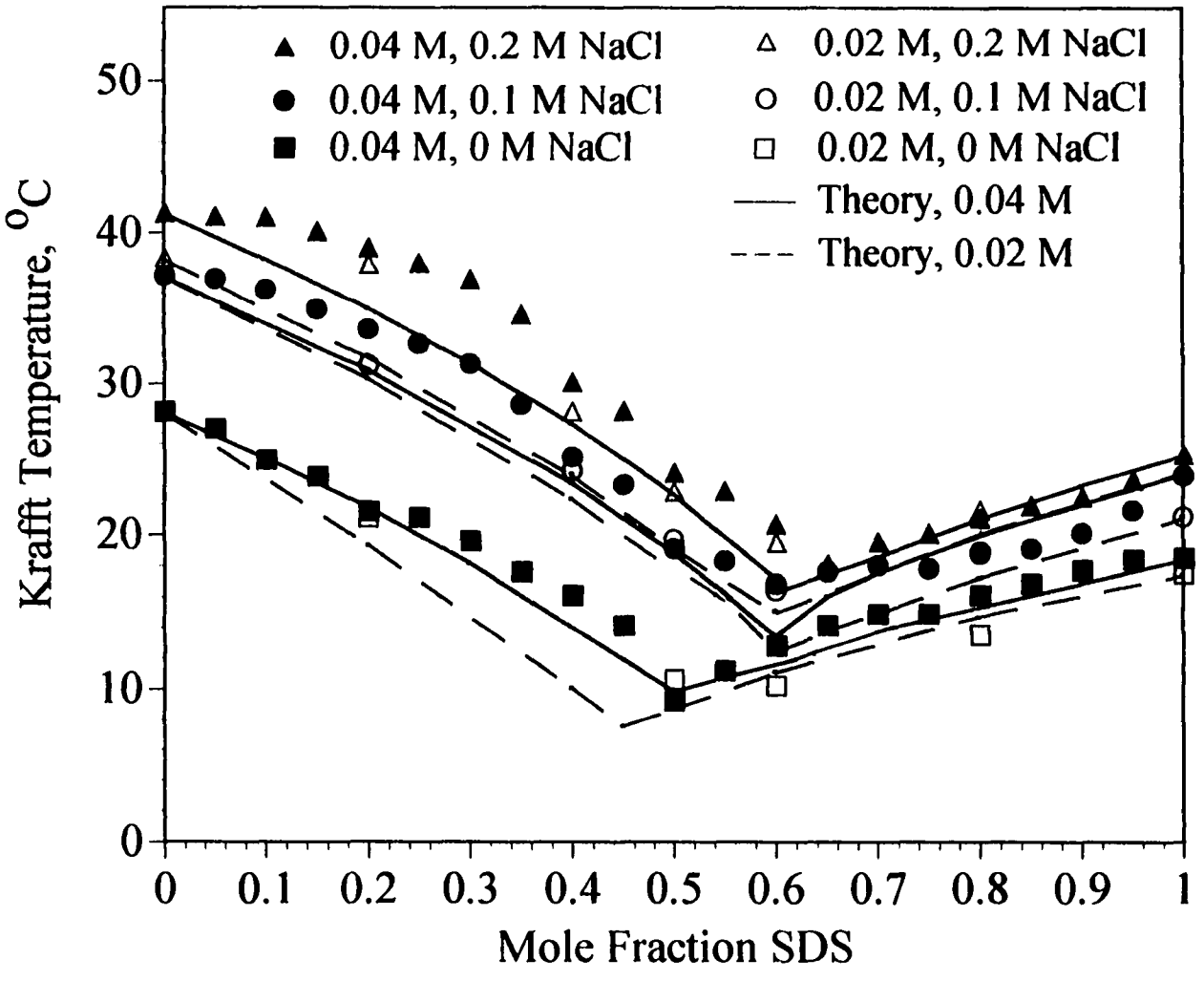


Figure I.9 Krafft Temperatures for 0.04 M SDS/NP(EO)$_{10}$ at 0, 0.1, and 0.2 M NaCl

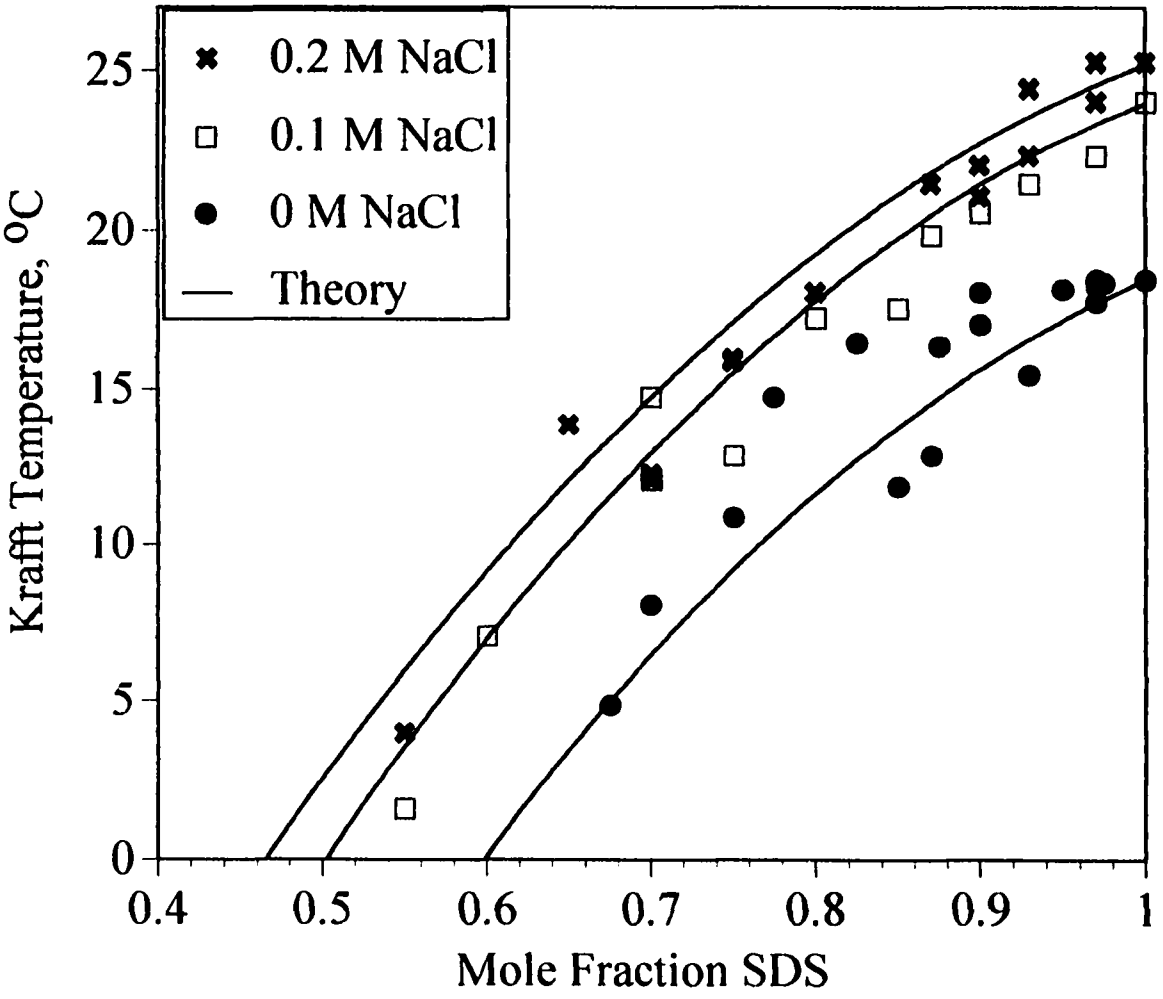


Figure I.10 Krafft Temperatures for 0.04 M SOBS/NP(EO)$_{10}$ at 0, 0.1, and 0.2 M NaCl

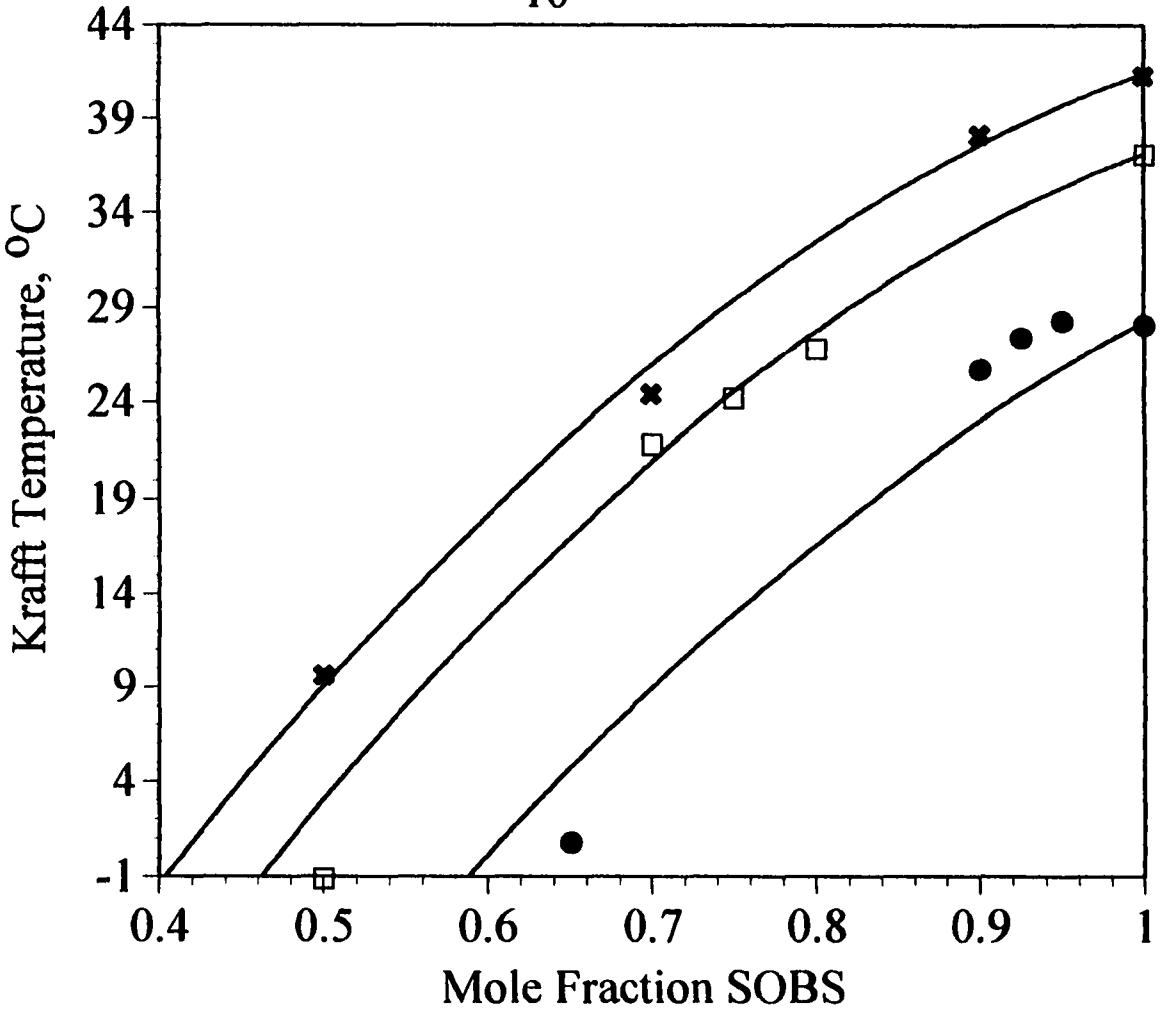


Figure I.11 Ternary SDS/SOBS/NP(EO)$_{10}$ Krafft Temperatures at 0.04 M Total Surfactant Concentration at 0 M NaCl

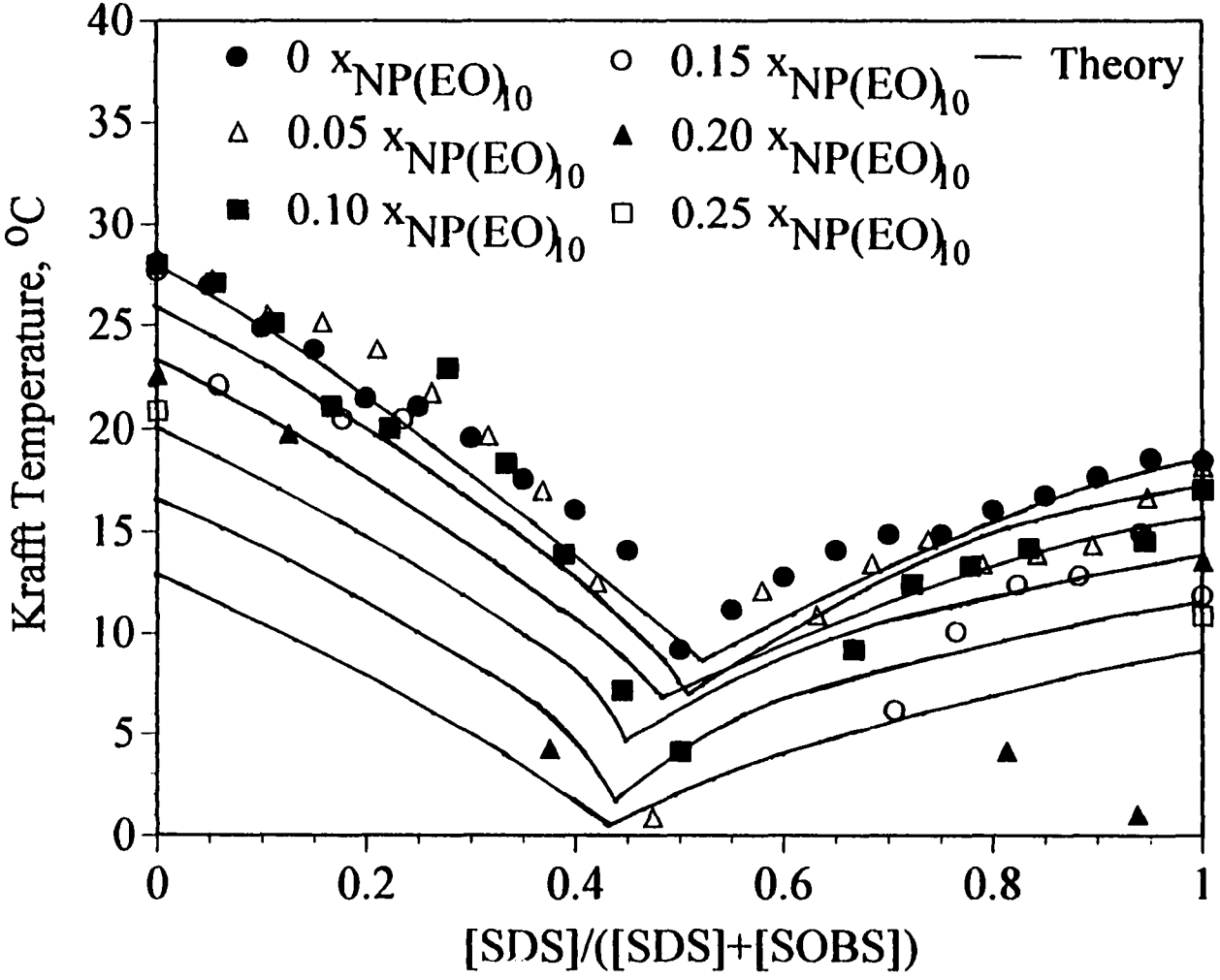


Figure I.12 The Effect of Increasing SOBS Concentration on Krafft Temperatures of 0.04 M SDS/SOBS/$NP(EO)_{10}$ Mixtures at 0 M NaCl

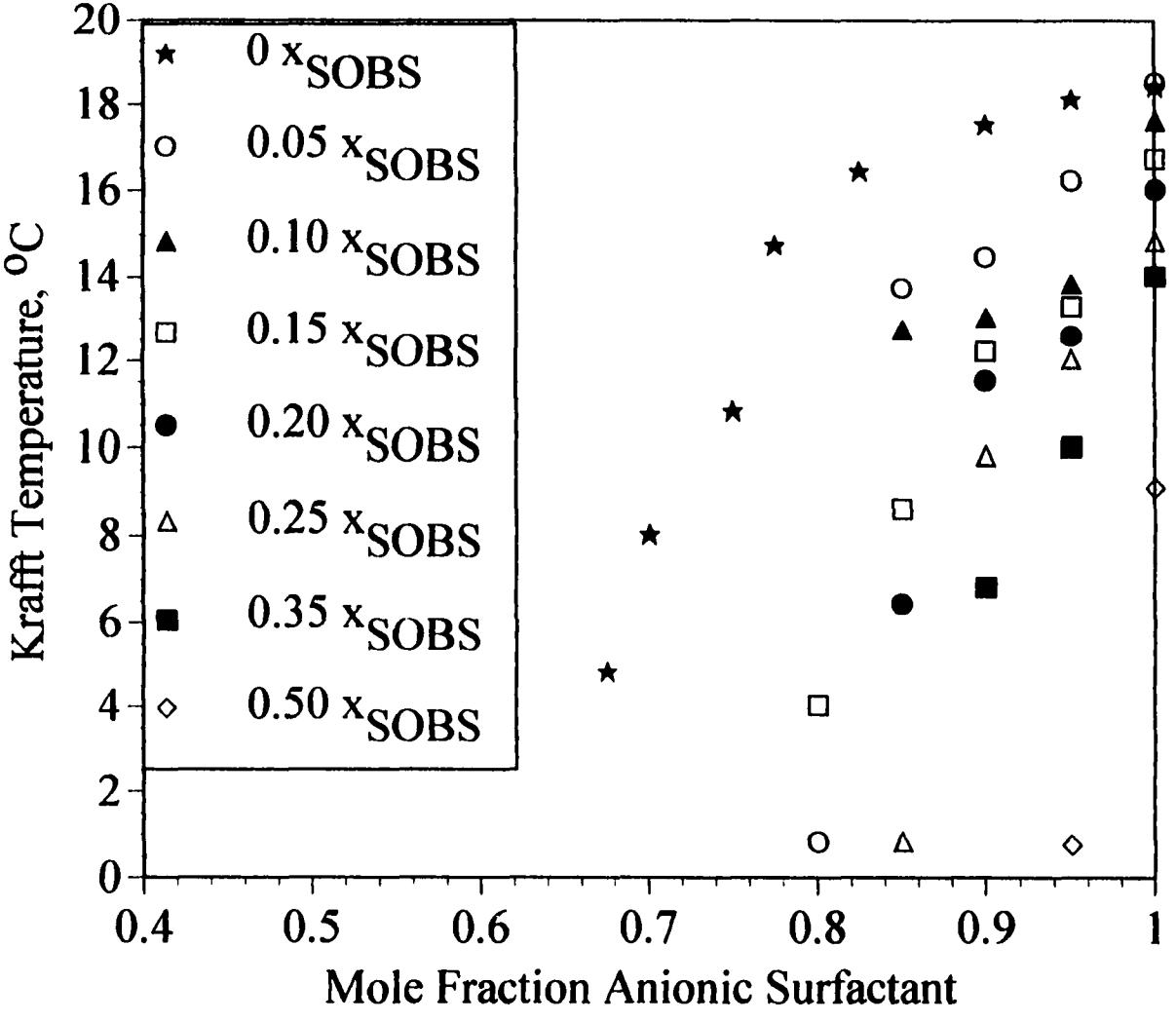
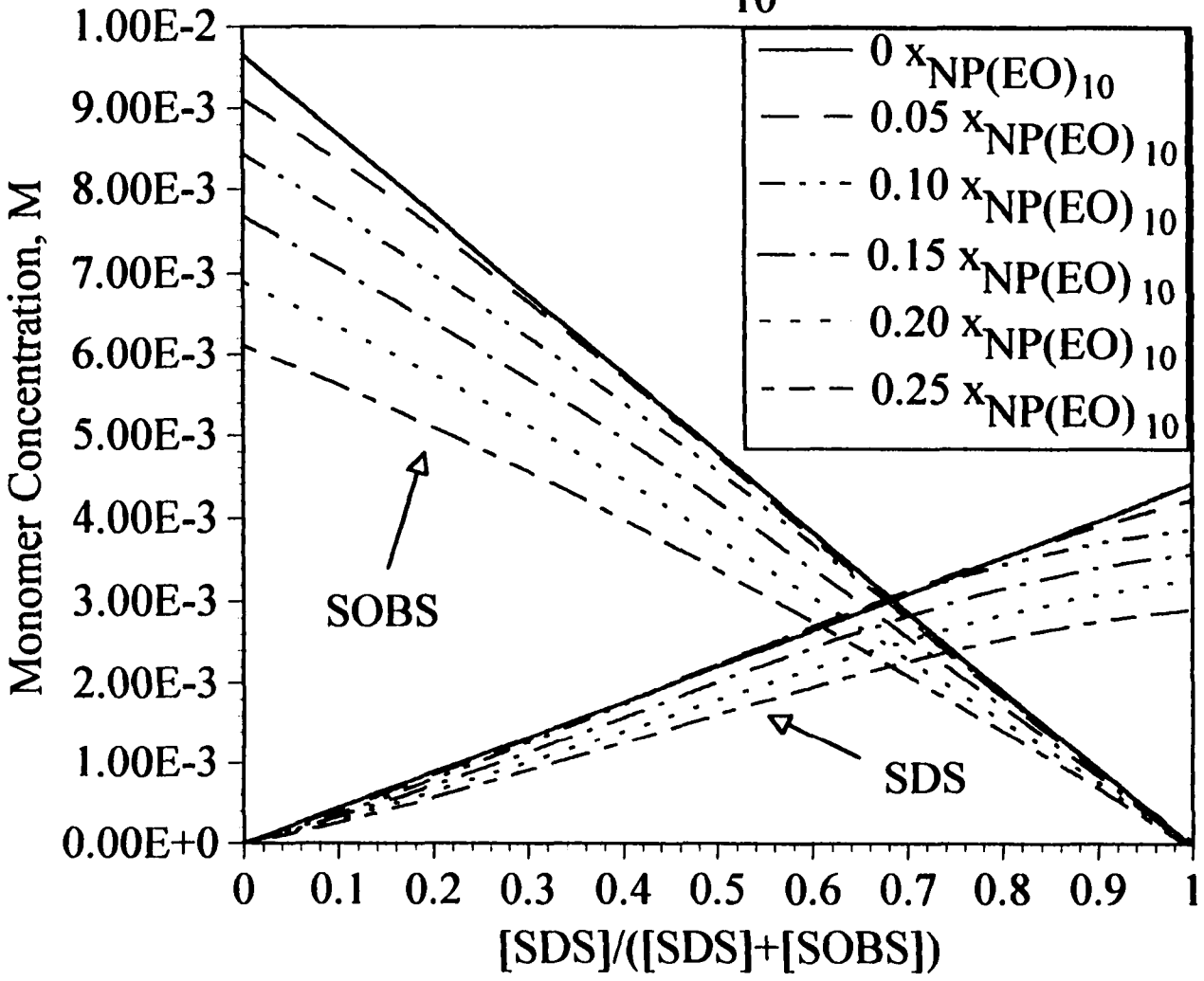


Figure I.13 Predicted Monomer Concentrations for the 0.04 M SDS/SOBS/$NP(EO)_{10}$ Systems at 0 M NaCl



Chapter 2

PRECIPITATION IN SOLUTIONS CONTAINING MIXTURES OF SYNTHETIC ANIONIC SURFACTANT AND SOAP

I. EFFECT OF SODIUM OCTANOATE ON HARDNESS TOLERANCE OF SODIUM DODECYL SULFATE

The effect of sodium octanoate (SO) and pH on the precipitation of sodium dodecyl sulfate (SDS) with calcium (hardness tolerance) was investigated. Adjusting the pH changes the ratio of fatty acid (HO) to octanoate ion (O^-) in solution. Titrations were done for SDS/SO mixtures and it was found that the HO/O^- molar ratio in the micelles is driven by the synergism of mixed anionic/nonionic micelle formation. Critical micelle concentrations (CMC) of the mixtures at various pH levels showed synergistic behavior typically found in nonideal systems. The hardness tolerance for mixtures of SDS and SO were determined at various pH levels. It was found that lowering the pH slightly increased the hardness tolerance of SDS in the SDS/SO mixtures above the CMC and that the addition of SO to SDS also increased the hardness tolerance of SDS above the CMC. Due to nonideal mixed micelle formation, the most synergistic system studied was 80/20 SDS/SO at a pH level of 5.0.

Key Words: hardness tolerance, nonideal mixed micelles, pH dependence of surfactant behavior, precipitation, soap, sodium carboxylate, surfactant, synergistic behavior

2.1 Introduction

Soaps and synthetic anionic surfactants have traditionally been major constituents in many cleaning agents (1). An important characteristic of anionic surfactants is their tendency to precipitate from hard water. Precipitation of anionic surfactants can inhibit their use in many applications and can affect formulation compositions substantially. The use of surfactant mixtures can have synergistic advantages over the use of a single surfactant in cases such as detergency where surfactant precipitation is detrimental (2,3).

The hardness tolerance enhancement of synthetic anionic surfactants due to the addition of monovalent counterions (4) or nonionic surfactant (5) has been studied by our group. The effect of soap (salt of fatty acid) as a cosurfactant on the hardness tolerance of a synthetic anionic surfactant is investigated in this paper at various pH levels. The hardness tolerance is the minimum concentration of multivalent counterion which causes precipitation of an anionic surfactant; in this study, calcium is the counterion used. The CMC of these surfactant mixtures is also studied here at various pH levels, and mixed micelle formation is shown to greatly affect precipitation behavior. Sodium dodecyl sulfate (SDS) is used as a model synthetic anionic surfactant. Sodium octanoate, SO, was used rather than a longer chain length soap even though longer chain lengths are used in most applications. In general, the solubility of a fatty acid decreases as the soap chain length increases. The object of this study was to understand the precipitation of the SDS due to calcium, and so a more soluble fatty acid (hence, a shorter chain length) was required.

2.2 Experimental Procedures

2.2.1 Materials

Sodium dodecyl sulfate, SDS, was obtained from Henkel Co. with a purity no less than 96.5%. The SDS was purified by first dissolving the SDS powder into distilled water and filtering through a fritted glass filter to eliminate large particles. The filtrate was then left overnight at about 10 °C to allow the surfactant to recrystallize. The precipitated solution was filtered through a fritted glass filter to obtain the crystals, which were dissolved in 100% HPLC grade methanol. This solution was heated slightly to help dissolve the SDS and was then cooled overnight at about 0 °C to force precipitation. The precipitated SDS was again filtered and dried under vacuum overnight at about 30 °C. The purity of the recrystallized SDS was verified by the lack of formerly present impurity peaks using HPLC. The sodium octanoate, SO, was obtained from Sigma Chemical Co. at a purity of at least 99% and was used without further purification. The calcium chloride was analytical reagent grade from J.T. Baker Chemicals B.V.-Deventer-Holland and was used as received. The water was distilled and had a conductivity of 2 μmho/cm.

2.2.2 Methods

2.2.2.1 Precipitation Phase Boundaries. All experiments in this study were performed at a constant temperature of 30 °C maintained using a temperature controlled water bath. The precipitation phase boundaries for the SDS/SO mixtures were determined for varying SO concentrations and pH levels of 5.0, 7.0, and 9.0. Precipitation phase boundaries were also determined for pure SDS and pure SO at pH levels of 5.0, 7.0, and 9.0. For each point on a precipitation phase boundary, a series

of solutions was prepared with varying $CaCl_2$ concentration at constant SO concentration and pH. Sodium hydroxide and hydrochloric acid were used to adjust the pH. A Benchtop pH/ISE meter with a Triode pH electrode was used for all pH measurements. A surfactant solution can remain supersaturated for long periods of time (6,7) resulting in a non-equilibrium apparent hardness tolerance. Therefore, the solutions were first cooled to 5 °C for at least 24 hours to force precipitation (4,5,8,9). The solutions were then heated to 30 °C and were shaken daily for four days to insure equilibrium (4). After four days, a high intensity beam of light was used to check each solution for crystals, which glisten against a dark background in the light. If a solution was outside of the precipitation region, crystals would redissolve so that the solution became clear. If crystals remained in the solution after equilibration, the initial solution composition was considered to be inside the precipitation region. The hardness tolerance is taken as the average $CaCl_2$ concentration of the lowest concentration resulting in precipitate and the highest concentration for which precipitate is absent.

2.2.2.2 Titration Curves. In order to determine the fraction of the SO which is protonated, titration curves for 80/20 and 60/40 SDS/SO mixtures above the CMC were measured using a Metrohm 665 Dosimat automatic titrator with a Fisher Scientific Accumet pH meter model 825 MP interfaced with a Zenith computer using Titration Station software. The solutions were either titrated with HCl or NaOH.

2.2.2.3 Critical Micelle Concentrations. The CMC of each SDS/SO mixture and of pure SDS and pure SO at pH levels of 5.0, 7.0, and 9.0 were determined at 30 °C. A Kruss digital Du Nuoy ring tensiometer with a platinum/iridium ring was used to measure the surface tension of each solution. Each CMC was determined at the surfactant concentration where there was a sharp change in the slope in a plot of the surface tension versus the log of the surfactant concentration.

2.3 Results and Discussion

The possible precipitation reactions occurring in these systems are represented by the following equations:

$$Ca^{2+}(aq) + DS^{-}(aq) \leftrightarrow Ca(DS)_2(s) \qquad (II.1)$$

$$Ca^{2+}(aq) + O^{-}(aq) \leftrightarrow Ca(O)_2(s) \qquad (II.2)$$

$$HO(aq) \leftrightarrow HO(s) \qquad (II.3)$$

where DS^- is the dodecyl sulfate ion, Ca^{2+} is the calcium ion, and $Ca(DS)_2$ is the calcium dodecyl sulfate precipitate. The symbol, O^-, represents the deprotonated octanoate ion, $Ca(O)_2$ is the calcium octanoate precipitate, and HO is the fatty acid (protonated octanoate ion). The material balances to describe these SDS/SO mixtures are:

$$[NaDS] = [DS^-]_{mon} + [DS^-]_{mic} \qquad (II.4)$$

$$[O^-] = [O^-]_{mon} + [O^-]_{mic} \qquad (II.5)$$

$$[HO] = [HO]_{mon} + [HO]_{mic} \qquad (II.6)$$

$$[Na^+] = [NaDS] + [NaO] + [NaOH] = [Na^+]_u + [Na^+]_b \qquad (II.7)$$

$$[Ca^{2+}] = [CaCl_2] = [Ca^{2+}]_u + [Ca^{2+}]_b \qquad (II.8)$$

where [NaDS], $[DS^-]_{mon}$, and $[DS^-]_{mic}$ are the total SDS, monomeric SDS, and micellar SDS concentrations, respectively. The parameters $[O^-]$, $[O^-]_{mon}$, and $[O^-]_{mic}$ are the total, monomer, and micellar deprotonated SO concentrations, and [HO], $[HO]_{mon}$, and $[HO]_{mic}$ are the total, monomer, and micellar concentrations of protonated SO in the system. The parameters $[Na^+]$, $[Na^+]_u$, and $[Na^+]_b$ are the total, unbound (not bound onto the micelles), and bound sodium concentrations, respectively, and [NaOH] is the added sodium hydroxide concentration. Finally, $[Ca^{2+}]$, $[Ca^{2+}]_u$, and $[Ca^{2+}]_b$ are the total, unbound, and bound calcium concentrations, where the total calcium concentration is equal to the total calcium chloride concentration in solution ($[CaCl_2]$). The total SO concentration in the solution is equal to the sum of $[O^-]$ and [HO]. The relative concentrations of each form can be adjusted by controlling the solution pH (lowering the pH increases the fraction of protonated SO). In these equations, the precipitate is neglected since along the precipitation phase boundary there is an infinitesimal amount of solid phase. There is assumed to be no added salt (e.g., NaCl) in these systems, but inclusion of these effects in the modeling is straightforward (4,5).

Below the CMC, all of the surfactant in the system is present as monomer, and precipitation depends on the total surfactant and total calcium concentrations. Therefore, as the surfactant concentration is increased in the solution, the amount of calcium required to cause precipitation decreases as described by the solubility product relationship:

$$K_{SP} = [Ca^{2+}]\,[DS^-]^2\,\gamma_{Ca}\,\gamma_{DS}^2 \qquad (II.9)$$

where K_{SP} is the activity based solubility product, $[DS^-]$ is equal to the total SDS concentration, and γ_{Ca} and γ_{DS} are the activity coefficients of calcium and SDS, respectively. Precipitation above the CMC depends on the monomeric surfactant concentration and the unbound calcium concentration:

$$K_{SP} = [Ca^{2+}]_u [DS^-]_{mon}^2 \gamma_{Ca} \gamma_{DS}^2 \qquad \text{(II.10)}$$

The behavior above the CMC can be understood by examining the micelle-monomer-precipitate equilibria. These equilibria are shown in Figure II.1 for SDS in the presence of calcium. Above the CMC, as the SDS concentration is increased, the additional surfactant tends to form micelles. A larger concentration of unbound calcium ions will then bind to the micelles, reducing the amount of unbound calcium available for precipitation of the surfactant monomers. The total calcium concentration must then be increased to meet the conditions required by the monomeric solubility product relationship (Equation II.10) for precipitation to occur (4). There are also unbound and bound sodium ions in solution due to dissociation of the surfactant salt and from any added NaOH, which are not shown in Figure II.1 for clarity. Sodium was found to not precipitate the anionic surfactants studied at the concentration levels present in this paper due to a much larger K_{SP} with the surfactant ion (on the order of 10^{-4} M^2) than that of calcium (8).

Figure II.2 shows the precipitation phase boundaries for SDS at pH levels of 5.0, 7.0, and 9.0. For each SDS concentration, as the calcium concentration is increased, precipitation first occurs when the precipitation phase boundary is reached. Below the precipitation phase boundary the solution is isotropic. Above the

precipitation phase boundary, crystals are present. The eutectic point in each precipitation phase boundary corresponds to the surfactant concentration being at the CMC. Below the CMC, as the SDS concentration is increased, the concentration of calcium required to cause precipitation decreases as predicted by the solubility product relationship given in Equation II.9. Above the CMC, a drastic change is seen in the precipitation phase boundary. Due to calcium binding on the micelles, the total calcium concentration must be increased to precipitate the SDS monomers. No significant effect of adjusting the pH is seen in Figure II.2 as is expected for SDS, which does not significantly protonate at these pH levels.

The rate of hydrolysis of SDS has been shown to increase as the pH is lowered and the temperature is raised (10). This behavior was found to be more than 30 times more pronounced above the CMC than below it (10). In daylight at room temperature, negligible hydrolysis was found to occur in an aqueous 0.001 M SDS solution (below the CMC) after a period of more than 3 years (11). In this study, the pH is never below 5, and the age of the surfactant solutions are never more than 6 days old when the data is collected. Also, the solution temperature is near 0 °C for at least 24 hours of this time, and only at 30 °C for the succeeding 4 days. Above the CMC, the rate of hydrolysis has been found to be first order with pH and temperature (10). Rate constants from Motsavage and Kostenbauder (10) were used here in a first order rate equation for 0.1 M SDS (the largest concentration of SDS used in these experiments) to obtain the rate of hydrolysis for pH levels of 1.10, 2.10, and 3.28 at 50.4 and 60.2 °C (Figures II.3 and II.4, respectively). The most severe conditions for hydrolysis in the paper are 30 °C and a pH level of 5.0. Therefore, the rates of hydrolysis shown in Figures II.3 and II.4 were extrapolated to a pH level of 5.0 to obtain a new rate of hydrolysis for each temperature at this pH. Figure II.5 shows the

rates of hydrolysis at a pH level of II.5 plotted as a function of temperature, so that the final estimated rate of hydrolysis for 0.1 M SDS at a pH of 5 and temperature of 30 °C was found to be 2.32×10^{-6} M/day. After 4 days, the maximum lost SDS concentration would be approximately 9.28×10^{-6} M. The effect of additives able to lower the CMC of the solution has been found to increase the rate of hydrolysis of SDS (10). Therefore, it is possible that the rate of hydrolysis of SDS in solution with SO could be higher than found here, since the rate constants used are for pure SDS. However, an SDS concentration of 0.1 M was used in the calculations of the rate and in the SDS/SO mixtures, SDS concentrations no greater than 0.01 M were used. Therefore, the rate of 3.22×10^{-6} M/day is very likely a good approximation of the maximum rate of hydrolysis occurring in this study, and is not expected to alter the results given in this paper.

The micelle-monomer-precipitate equilibrium diagram for SO is shown in Figure II.6. There is an anionic, deprotonated form of SO (O^-) which is precipitating with calcium in this figure. The deprotonated form is also present as monomer and in the micelles. There is also an uncharged, protonated form of SO (HO) which is present in the micelles and as monomer. Due to the presence of these two forms, SO is able to form nonideal mixed micelles without the presence of any other components. Precipitation of HO is also possible in these systems if the solubility limit is reached, but the precipitation of SO with calcium is the focus of this study.

The effect of pH on the hardness tolerance of SO is shown in Figure II.7, where the precipitation phase boundaries were obtained for pH levels of 6.0, 7.0, and 9.0. Above the CMC, an increase in calcium concentration is required to precipitate a given amount of SO as the pH is lowered. When an anionic surfactant forms micelles, there is an electrostatic repulsion between the negatively charged surfactant head

groups. If an uncharged head group is inserted between the charged head groups, the electrostatic repulsions decrease and the micelles are easier to form (lower CMC). For the SO system, as the pH is decreased, a larger fraction of SO is present in the uncharged, protonated form. These HO monomers are inserted into the micelle between the negatively charged O^- ions, creating a more nonideal mixed micelle. As the micelles become more nonideal, the SO monomer concentration decreases, resulting in a higher hardness tolerance. The effect of adjusting the pH on the hardness tolerance below the CMC is not as strong as the effect when micelles are present as shown in Figure II.7.

As the SO concentration increases and the pH decreases, the monomeric fatty acid concentration reaches its solubility limit. At a pH level of 5, a majority of the precipitation phase boundary was not obtainable for SO due to precipitation of the fatty acid at low concentrations. At a pH level of 6, the precipitation phase boundary is truncated slightly above the eutectic point. At a pH level of 6, the solubility limit of the fatty acid is reached at 0.15 M SO. Table II.1 shows the solubility limit of the fatty acid for SO at pH levels of 5, 6, 7, and 9. The K_{SP} values for SDS and SO with calcium are shown in Table II.2. These values agree well with the literature. The K_{SP} value for SDS with calcium at 30 °C was found to be 5.02×10^{-3} M^3 by Stellner and Scamehorn (4). The K_{SP} value for SO with calcium at 25 °C and a pH of 12 was determined as 3.98×10^{-7} M^3 by Irani and Callis (12).

Figure II.8 illustrates the micelle-monomer-precipitate equilibrium for an SDS/SO mixture. The hardness tolerance of a mixture containing more than one anionic surfactant is obtained when the solubility product of the least soluble surfactant is reached (2,13). Mixed precipitate is usually not seen along the precipitation phase boundary of mixed anionic surfactants unless the K_{SP} values of the two surfactants are

very similar (14). For the conditions studied in this paper, SDS is always the precipitating species for the mixed SDS/SO system, as shown in Figure II.8. Hence, this study documents the effect of SO on SDS precipitation. The effect of SDS on SO precipitation will be the focus of a future study. The SO in Figure II.8 is present in both its protonated and deprotonated forms as monomers and in the micelles. The SDS is present in the micelles, as monomer, and as precipitate.

Above the CMC, the HO/O^- mole ratio is not the same in the micelles as for the monomer phase. Titration curves were obtained for SDS/SO mixtures above the CMC and compared with the pKa for SO to determine the change in the observed pKa as the two surfactants are mixed above the CMC. The pKa of pure SO below the CMC is 5.0 (15). Above the CMC, for 80/20 SDS/SO, the pKa increases to 5.6. For 60/40 SDS/SO, the pKa is equal to 5.3. Both the 80/20 and 60/40 SDS/SO mixtures above the CMC show a greater pKa than the pKa for pure SO below the CMC. Titrations above the CMC for mixtures containing higher fractions of SO are not included here because precipitation inhibited our ability to obtain accurate titration curves. Since the pKa is a thermodynamic constant (and therefore the true pKa of the surfactant monomers must remain constant) the higher, observed pKa values seen above the CMC are a result of a higher degree of protonation in the micelles due to a lower pH in the region of the micellar head groups. Above the CMC, the pKa decreases as the SDS/SO mole ratios change from 80/20 to 60/40. This shows that more SO in the micelles is in the protonated form for 80/20 SDS/SO than for 60/40 SDS/SO. For the 80/20 SDS/SO mixture, there is a higher fraction of the negatively charged DS^- head groups in the micellar phase than for the 60/40 SDS/SO mixture. This higher concentration of negative charges results in a higher concentration of

hydrogen around the head groups and, therefore, a larger HO/O^- mole ratio in the micelles.

Figure II.9 shows the CMC curves for the SDS/SO mixtures at pH levels of 6.0, 7.0, and 9.0. The CMC curves display the synergism typically seen in systems forming nonideal mixed micelles. The CMC curves also show that for pure SO, as the pH is lowered, the CMC drastically reduces. However, for the SDS/SO mixtures, the effect is negligable. In the SDS/SO mixtures, it seems that the presence of SDS in the micelles results in a higher fraction of protonated SO in the micelles, even at a pH of 9.0. The decrease in CMC with decrease in pH for fatty acid/soap mixtures has been seen previously and shown to be correlated to the effect of mixed micelles (15). A study of the effect of pH on the Krafft point of DDAHCl has also been done and the same type of behavior seen, although opposite, due to the difference in the charge for the protonated and deprotonated forms (16).

A general model has been developed which can predict the hardness tolerance of an anionic surfactant (4,5). This model uses pseudo-phase separation theory (3,17) to describe the micelle-monomer equilibrium. Regular solution theory (sometimes called Rubingh theory) (3,8,18-21) must be used with the pseudo-phase separation theory (rather than ideal solution theory) to describe the thermodynamics of mixed micelle formation between the protonated SO and the anionic components in the solution (SDS and deprotonated SO). In theory, the systems studied here can be modeled using this theory combined with a model to describe the degree of protonation of SO in the micelles and monomer phases. The model for the degree of protonation of SO treats the protonated and deprotonated forms as separate surfactants (22). Titration curves above the CMC for each SDS/SO mole ratio studied are required to model these systems. Also, the CMC value for the fatty acid is needed.

However, due to the low solubility of the fatty acid, much of this information was not experimentally available Therefore, modeling of this system was not achieved. One can see that similar, more soluble, systems could be modeled by combining hardness tolerance modeling with the degree of protonation modeling.

The precipitation phase boundaries (hardness tolerance) of mixtures of SDS and SO are shown in Figures II.10, II.11, II.12, and II.13 for 80/20, 60/40, 40/60, and 20/80 SDS/SO, respectively, at various pH levels. Every mixture studied shows a slight increase in the hardness tolerance above the CMC as the pH is lowered. The increase in the hardness tolerance is not as great as was seen in Figure II.4 for pure SO. In the SDS/SO mixtures, as was seen for the pure SO precipitation phase boundaries, pH does not have a significant effect on the hardness tolerance below the CMC.

Figures II.14, II.15, and II.16 show the hardness tolerance of SDS/SO mixtures at pH levels of 5.0, 7.0, and 9.0, respectively. Each figure compares precipitation phase boundaries for 100/0, 80/20, 60/40, 40/60, and 20/80 SDS/SO. In every case, when SO is added to the system, the hardness tolerance of SDS above the CMC is increased, due to the formation of mixed micelles. There is a large jump in the hardness tolerance of SDS from the 100/0 SDS/SO system to the 80/20 SDS/SO system. As the mole ratio, SDS/SO, is decreased from 80/20 to 60/40, 40/60, and 20/80, a slight decline in the hardness tolerance is seen. Due to the increased nonideality of the mixed micelles at 80/20 SDS/SO, compared with the other mixtures, precipitation for this mixture with calcium is the most difficult. This occurs because there is a larger concentration of negatively charged head groups in the micelles due to the presence of a larger concentration of SDS. Therefore, the pH surrounding the

micelles in the region of the head groups decreases, resulting in a higher fraction of protonated SO.

In this study, it has been found that the general effect of SO on the precipitation of SDS with calcium is to increase the hardness tolerance above the CMC. The driving force for increased protonation of SO in the micelles is the reduction in the free energy of the micelles associated with the formation of nonideal mixed micelles. The largest amount of synergism for the mixtures studied here is for 80/20 SDS/SO and a pH level of 5.0.

2.4 References

1. Lynn, J.L, Jr., Detergency, in *Kirk-Othmer Encyclopedia of Chemical Technology*, 4th ed., Vol. 7, Wiley, New York, 1991, pp1072-1117.

2. Scamehorn J.F. and J.H. Harwell, Precipitation of surfactant mixtures, in *Mixed Surfactant Systems*, edited by K. Ogino and M. Abe, Marcel Dekker, New York, 1993, pp 283-312.

3. Scamehorn, J.F., An overview of phenomena involving surfactant mixtures, in *Phenomena in Mixed Surfactant Systems*, edited by J.F. Scamehorn, ACS Symp. Ser., Vol. 311, American Chemical Society, Washington, 1986, pp 1-27.

4. Stellner, K.L. and J.F. Scamehorn, Hardness tolerance of anionic surfactant solutions: 1. Anionic surfactant with added monovalent electrolyte, *Langmuir, 5:*70-77 (1989).

5. Stellner, K.L. and J.F. Scamehorn, Hardness tolerance of anionic surfactant solutions: 2. Effect of added nonionic surfactant, *Langmuir, 5:*77-84 (1989).

6. Peacock, J.M., and E. Matijevic, Precipitation of alkylbenzene sulfonates with metal ions, *J. Colloid Interface Sci., 77:*548-554 (1980).

7. Fan, X.J., P. Stenius, N. Kallay, and E. Matijevic, Precipitation of surfactant salts II. The effect of nonionic surfactants on precipitation of calcium dodecyl sulfate, *J. Colloid Interface Sci., 121:*571-578 (1988).

8. Stellner, K.L. and J.F. Scamehorn, Surfactant precipitation in aqueous solutions containing mixtures of anionic and nonionic surfactants, *J. Amer. Oil Chem. Soc., 63:*566-574 (1986).

9. Stellner, K.L., J.C. Amante, J.F. Scamehorn, and J.H. Harwell, Precipitation phenomena in mixtures of anionic and cationic surfactants in aqueous solutions, *J. Colloid Interface Sci., 123:*186-200 (1988).

10. Motsavage V.A., and H.B. Kostenbauder, The influence of the state of aggregation on the specific acid-catalyzed hydrolysis of sodium dodecyl sulfate, *J. Colloid Sci., 18:*603-615 (1963).

11. Lunkenheimer, K., and B. Czichocki, On the stability of aqueous sodium dodecyl sulfate solutions, *J. Colloid Interface Sci., 160:*509-510 (1993).

12. Irani, R.R., and C.F. Callis, Metal complexing by phosphorus compounds: II. Solubilities of calcium soaps of linear carboxylic acids, *J. Phys. Chem., 64:*1741-1743 (1960).

13. Scamehorn, J.F., Precipitation of mixtures of anionic surfactants, in *Mixed Surfactant Systems*, edited by P.M. Holland and D.N. Rubingh, ACS Symp. Ser., Vol.501, American Chemical Society, Washington, 1992, pp 392-401.

14. Tsujii, K., N. Saito, and T. Takeuchi, Krafft points of anionic surfactants and their mixtures with special attention to their applicability in hard water, *J. Phys. Chem., 84:*2287-2291 (1980).

15. Klevins, H.B., and M.M. Raison, The effect of pH on micelle formation, *1er Congr. mondial de'tergence et prods. tensio-actifs, Paris, 1:*66-71 (1954).

16. Dai, Q., and J.S. Laskowski, The Krafft point of dodecylammonium chloride: pH effect, *Langmuir, 7:*1361-1364 (1991).

17. Shinoda K., The formation of micelles, in *Colloidal Surfactants*, edited by K. Shinoda, T. Tamamushi, T. Nakagawa, and T. Isemura, Acad. Press., New York, 1963, pp 1-96.

18. Holland, P.M. and D.N. Rubingh, Nonideal multicomponent mixed micelle model, *J. Phys. Chem., 87:*1984-1990 (1983).

19. Rubingh, D.N., Mixed micelle solutions, in *Solution Chemistry of Surfactants*, Vol. 1, edited by K.L. Mittal, Plenum Press, New York, 1979, pp 337-354.

20. Scamehorn, J.F., R.S. Schechter, and W.H. Wade, Micelle formation in mixtures of anionic and nonionic surfactants, *J. Dispersion Sci. Technol., 3:*261-278 (1982).

21. Shiau, B., J.H. Harwell, and J.F. Scamehorn, Precipitation of mixtures of anionic and cationic surfactant: III. Effect of added nonionic surfactant, *J. Colloid Interface Sci., 167:*332-345 (1994).

22. Rathman, J.F., and S.D. Christian, Determination of surfactant activities in micellar solutions of dimethyldodecylamine oxide, *Langmuir, 6:*391-395 (1990).

Table II.1 Solubility Limit of the Fatty Acid, HO, at 30 °C

pH	Solubility Limit
5.0	0.03 M
6.0	0.15 M
7.0	0.5 M
9.0	1.0 M

Table II.2. K_{SP} Values for SDS and SO with Calcium at Several pH Levels and 30 °C

Surfactant	pH = 6.0	pH = 7.0	pH = 9.0
SDS	5.79×10^{-10} M^3	5.99×10^{-10} M^3	4.37×10^{-10} M^3
SO	3.29×10^{-7} M^3	3.65×10^{-7} M^3	4.08×10^{-7} M^3

Figure II.1 Micelle-Monomer-Precipitate Equilibrium Diagram for SDS in the Presence of Calcium

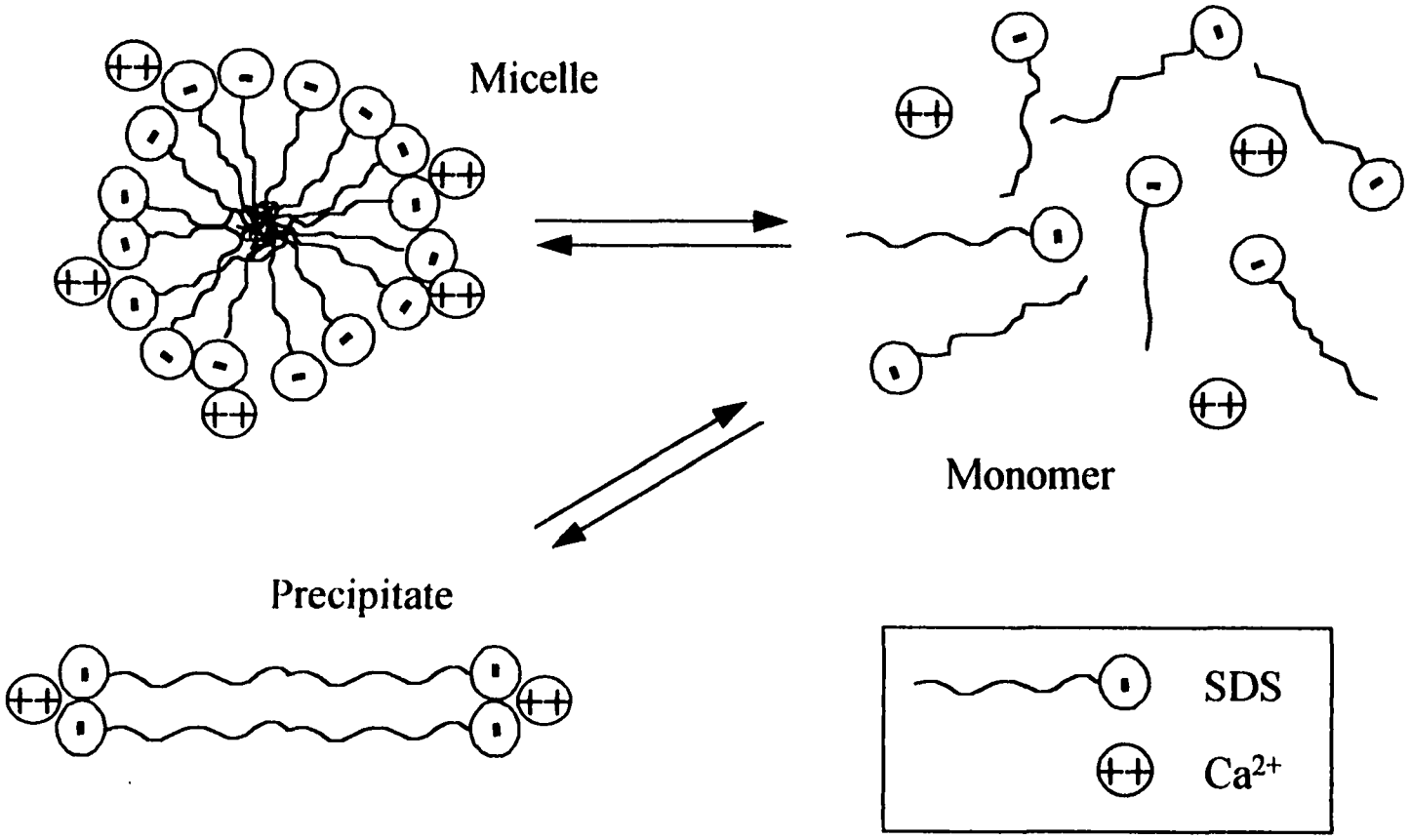


Figure II.2 Precipitation Phase Boundaries (Hardness Tolerance) for SDS at pH Levels of 5.0, 7.0, and 9.0 and 30 ^{o}C

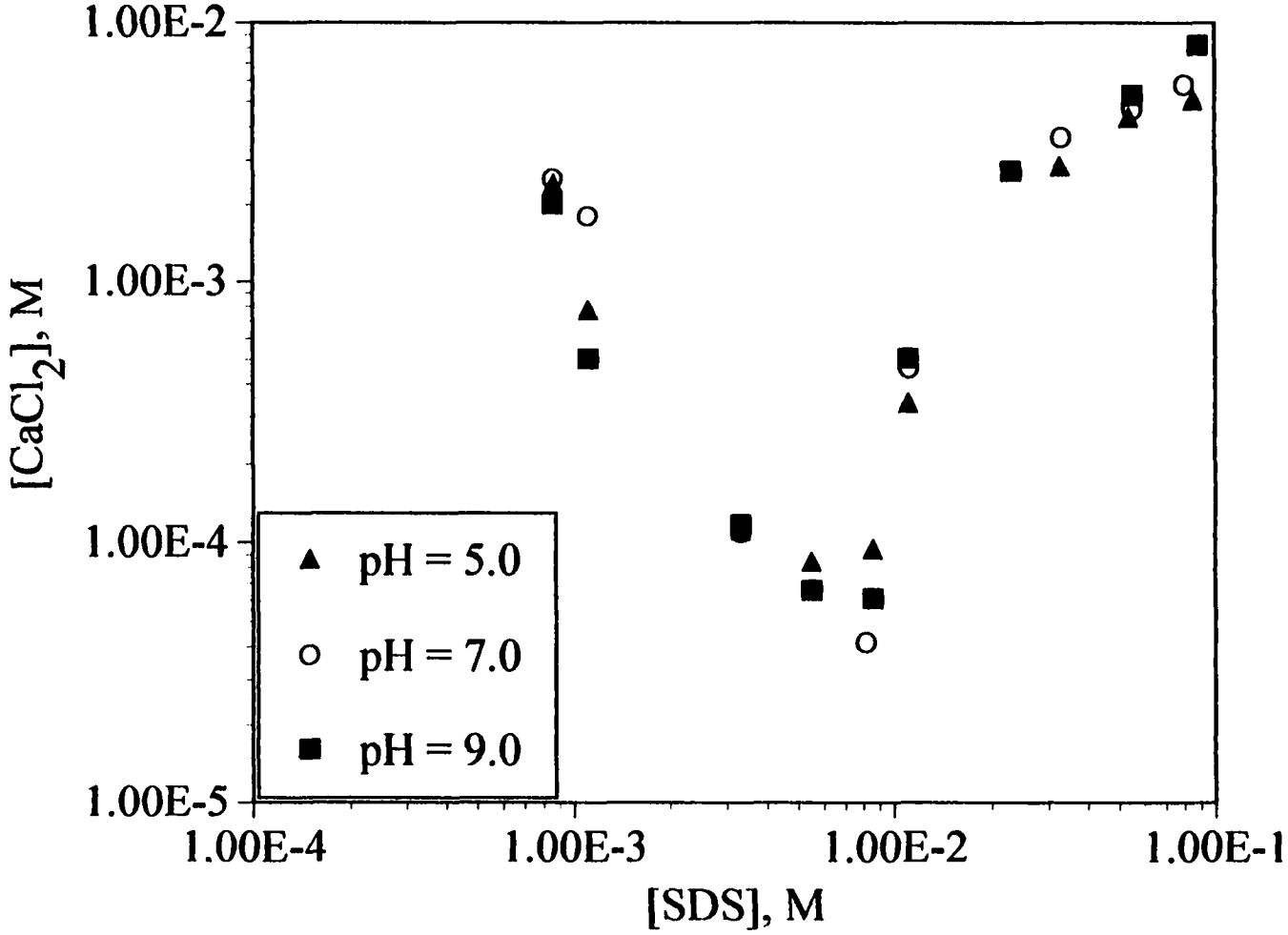


Figure II.3 Rate of Hydrolysis of SDS as a Function of pH at 50.4 °C Calculated from Rate Constants from Motsavage and Kostenbauder (10)

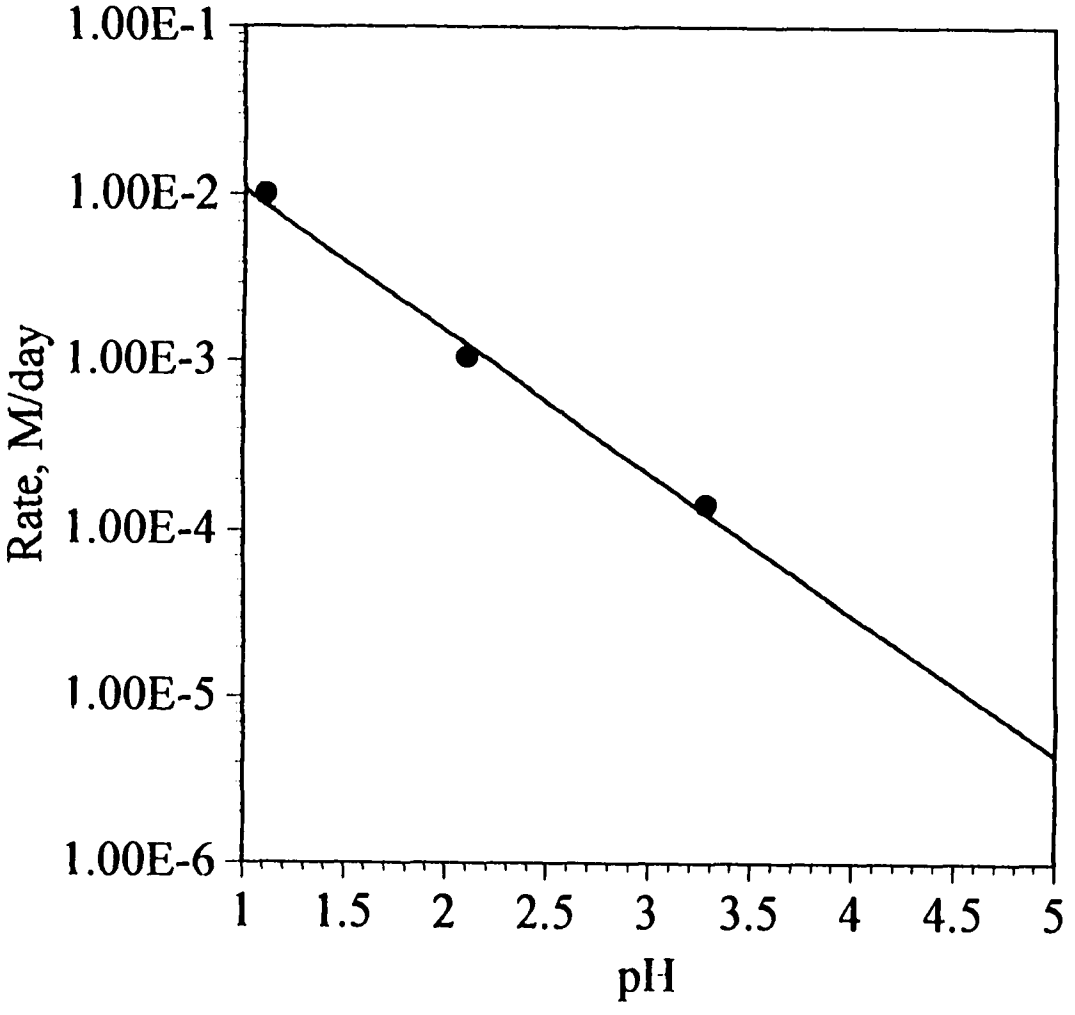


Figure II.4 Rate of Hydrolysis of SDS as a Function of pH at 60.4 °C Calculated from Rate Constants from Motsavage and Kostenbauder (10)

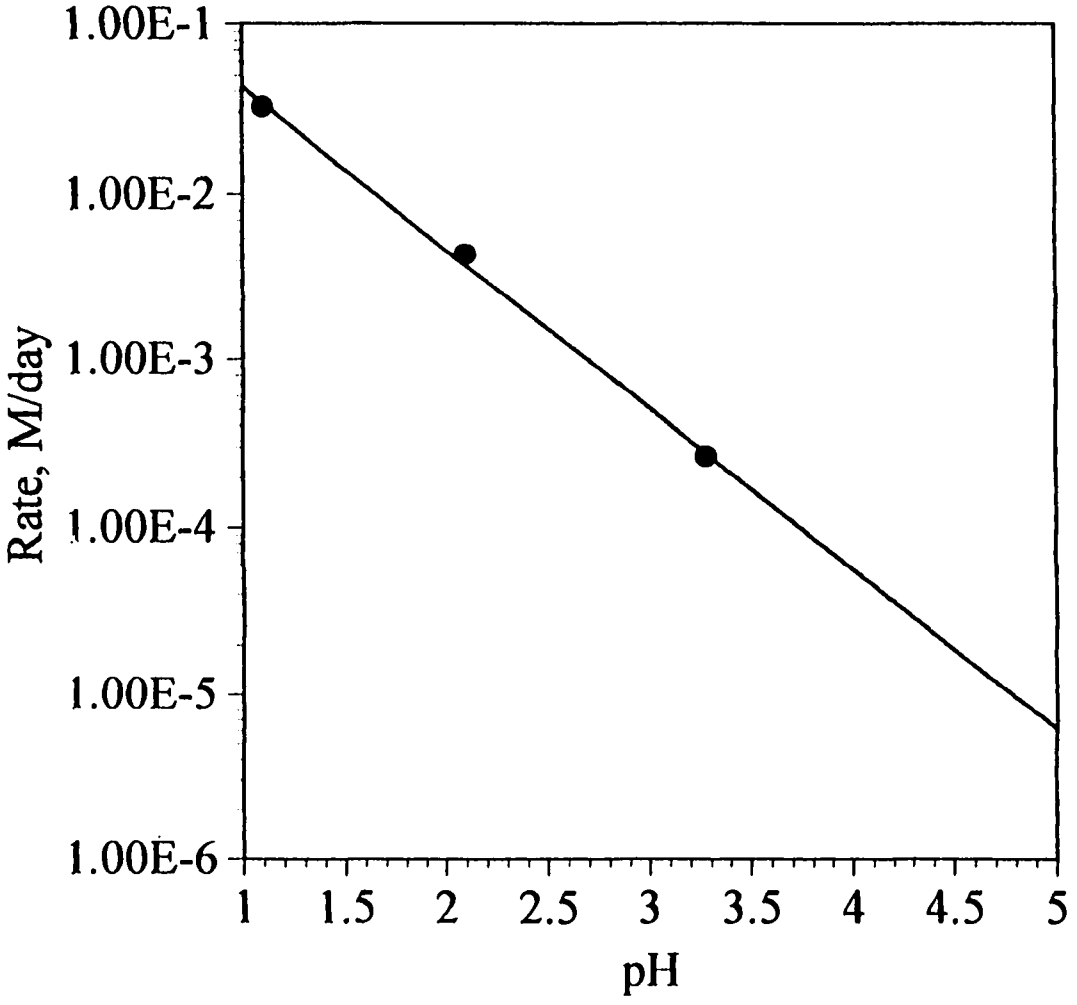


Figure II.5 Rate of Hydrolysis of SDS as a Function of Temperature at a pH Level of 5.0 Calculated by Extrapolation Using Best Fit Curves in Figures II.3 and II.4

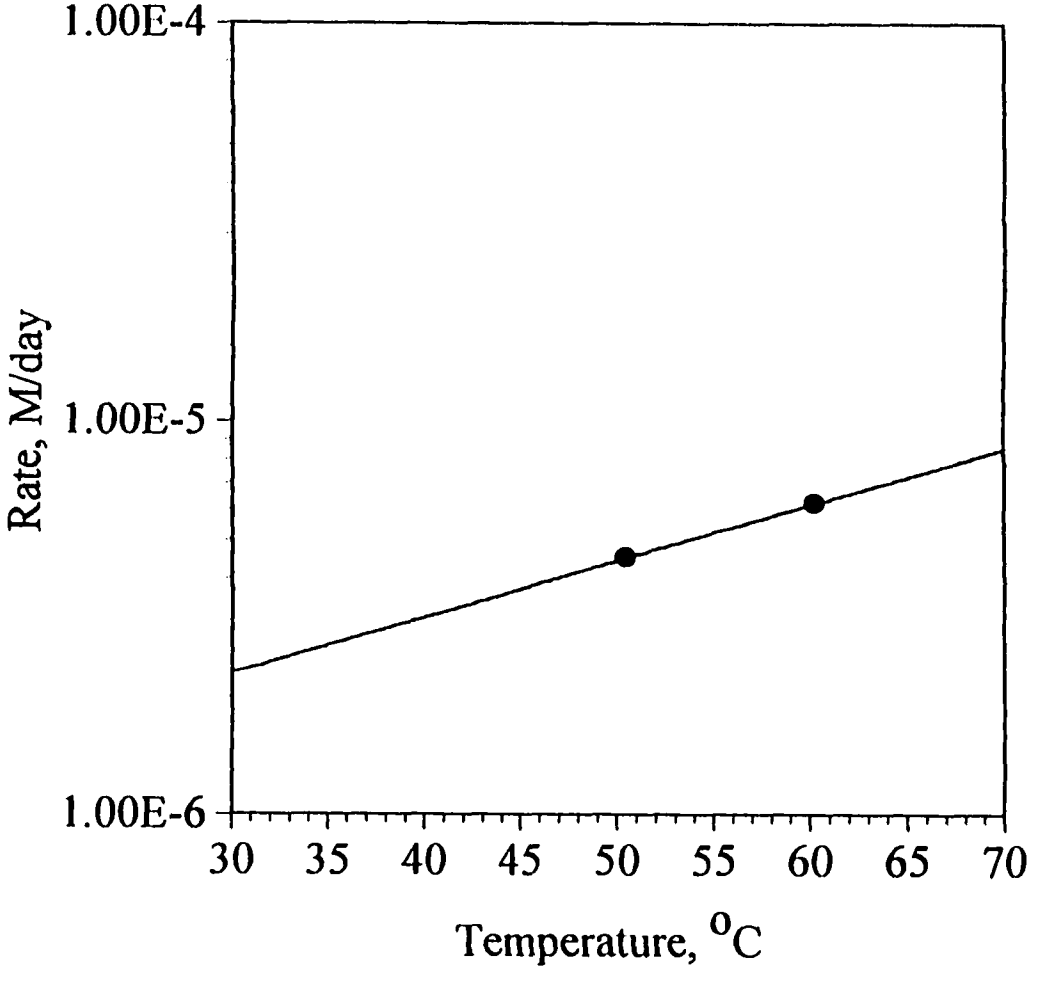


Figure II.6 Micelle-Monomer-Precipitate Equilibrium Diagram for SO in the Presence of Calcium Ions

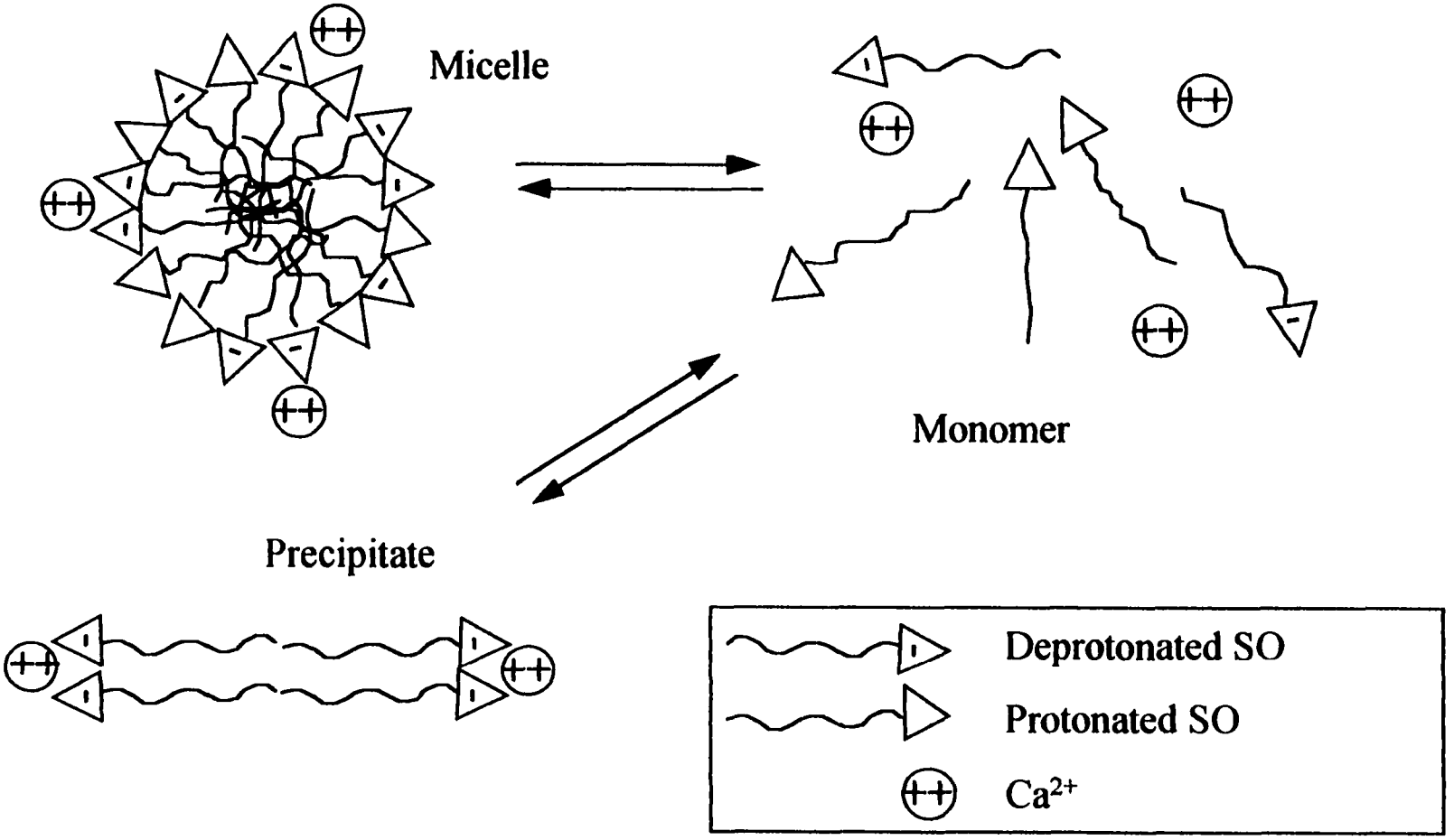


Figure II.7 Precipitation Phase Boundaries (Hardness Tolerance) for SO at pH Levels of 6.0, 7.0, and 9.0 and 30 ^{o}C

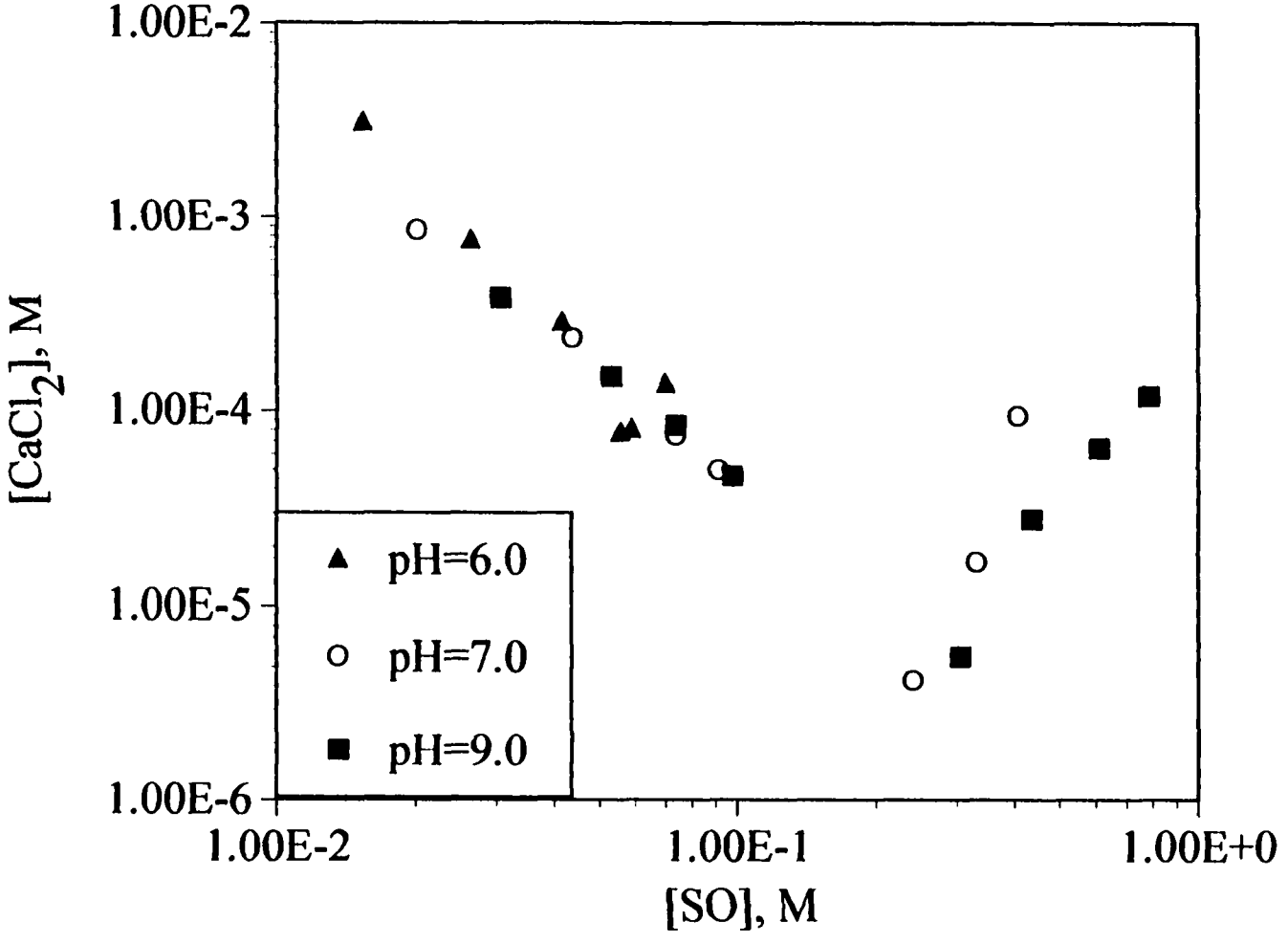


Figure II.8 Micelle-Monomer-Precipitate Equilibrium Diagram for an SDS/SO Mixture in the Presence of Calcium Ions with $Ca(DS)_2$ Precipitating

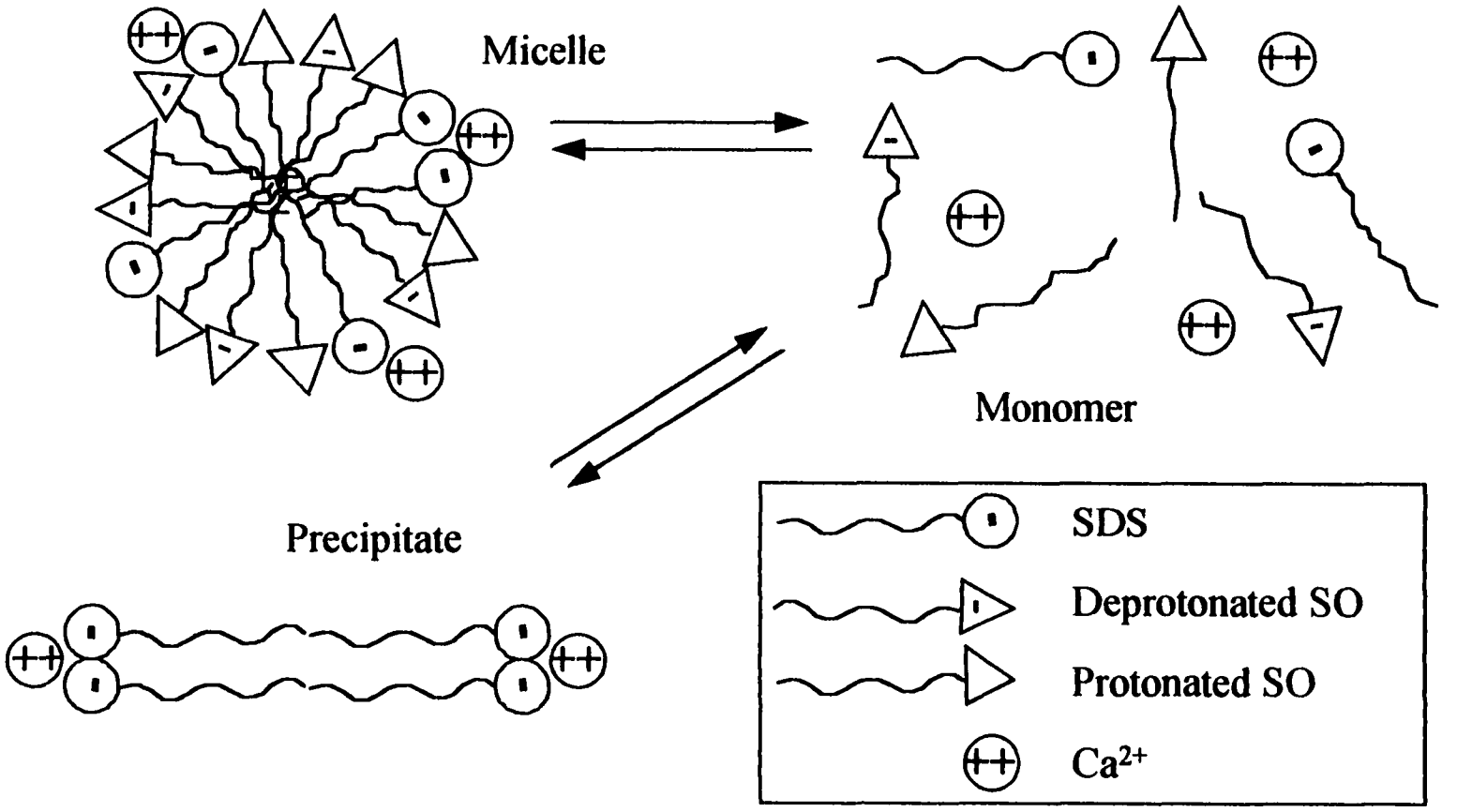


Figure II.9 CMC as a Function of Mole Fraction SO in SDS/SO Mixtures for pH Levels of 6.0, 7.0, and 9.0 and 30 °C

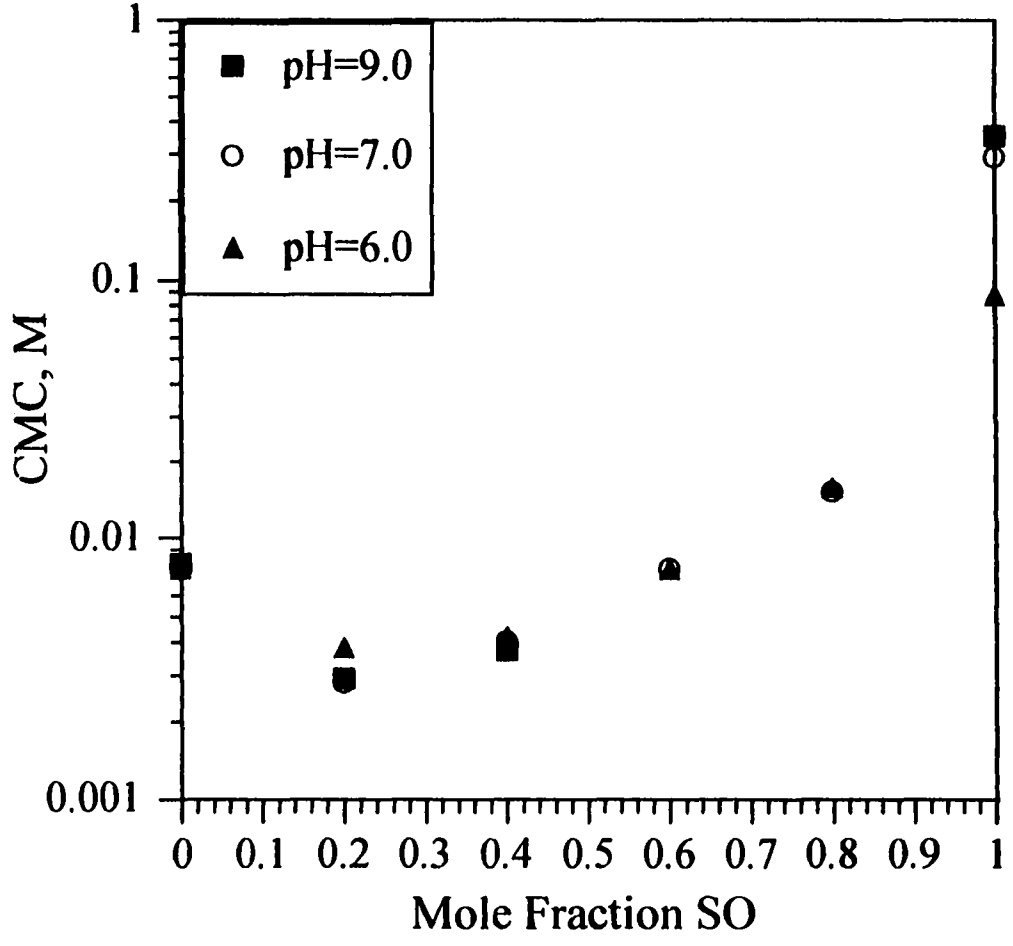


Figure II.10 Precipitation Phase Boundaries (Hardness Tolerance) for 80/20 SDS/SO at pH Levels of 5.0, 7.0, and 9.0 and 30 ^{o}C

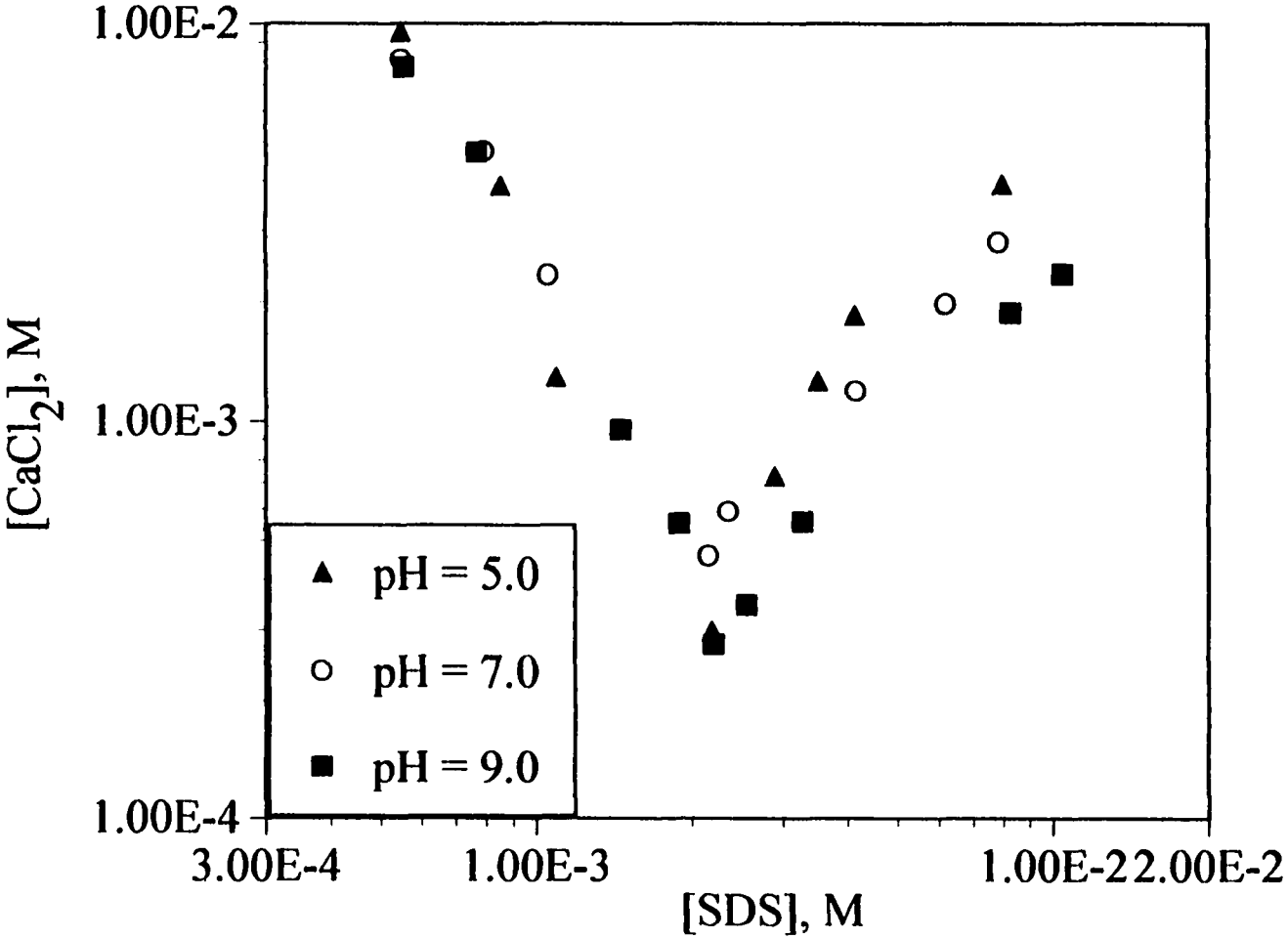


Figure II.11 Precipitation Phase Boundaries (Hardness Tolerance) for 60/40 SDS/SO at pH Levels of 5.0, 7.0, and 9.0 and 30 ^{o}C

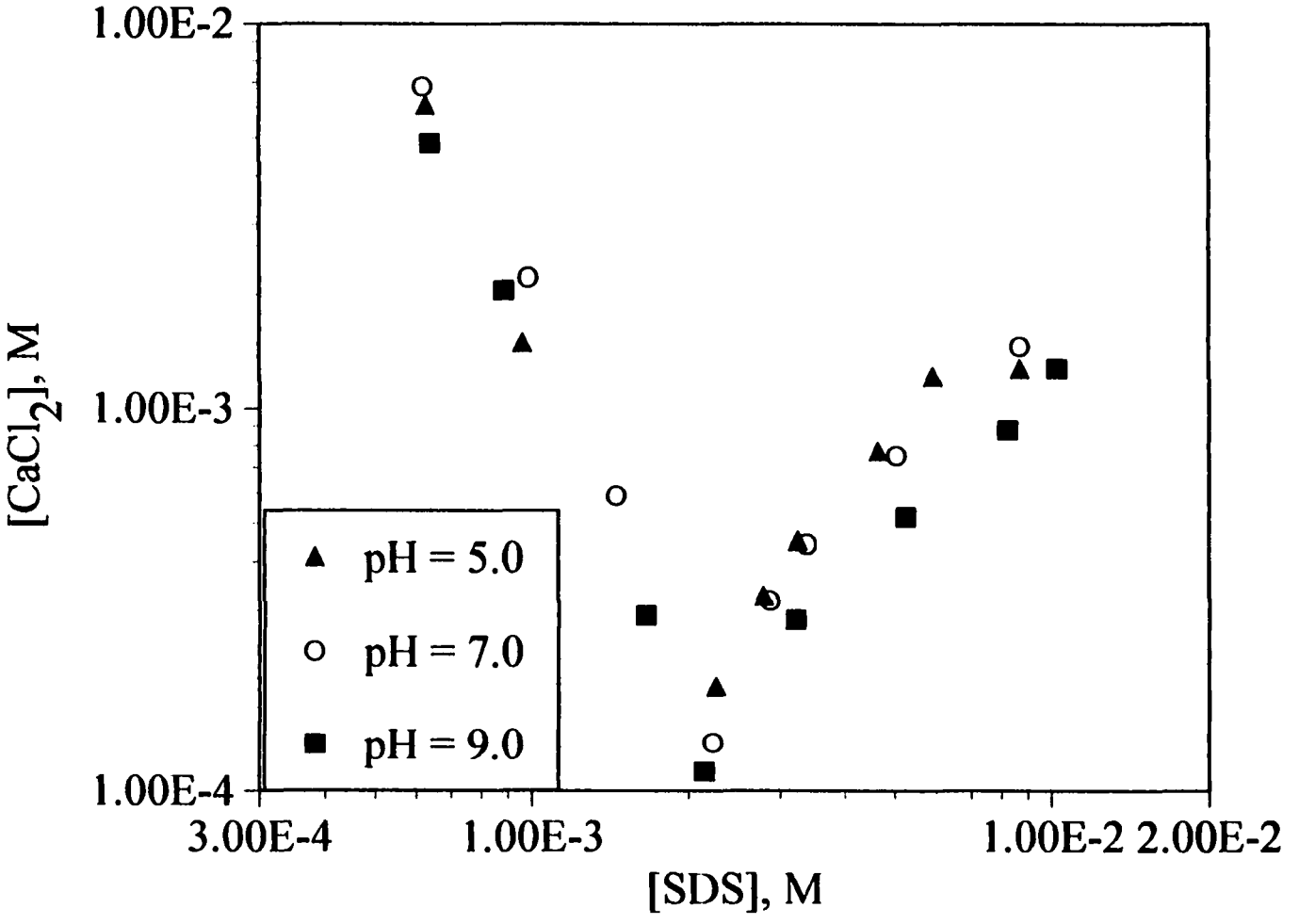


Figure II.12 Precipitation Phase Boundaries (Hardness Tolerance) for 40/60 SDS/SO at pH Levels of 5.0, 7.0, and 9.0 and 30 ^{o}C

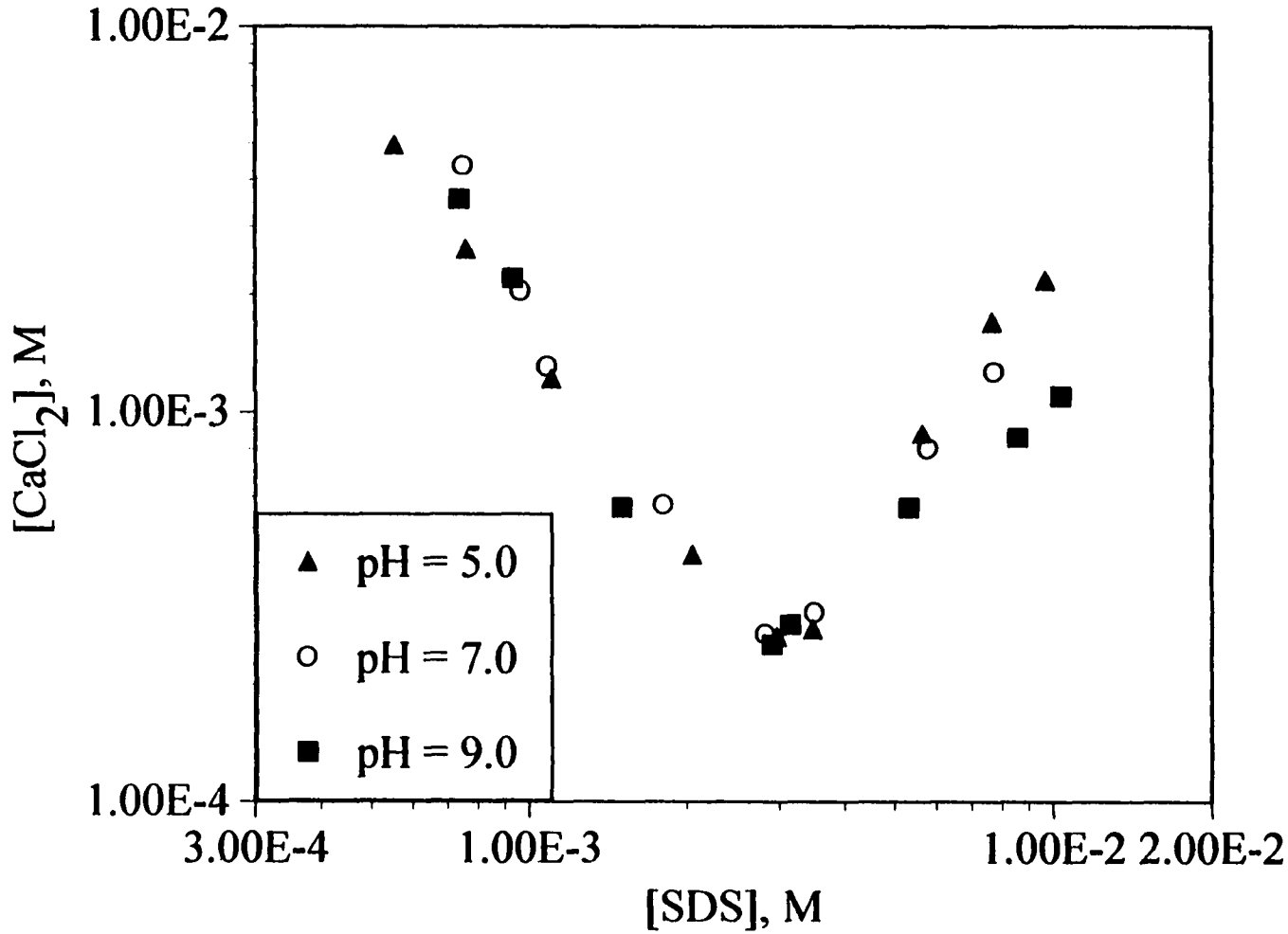


Figure II.13 Precipitation Phase Boundaries (Hardness Tolerance) for 20/80 SDS/SO at pH Levels of 6.0, 7.0, and 9.0 and 30 ^{o}C

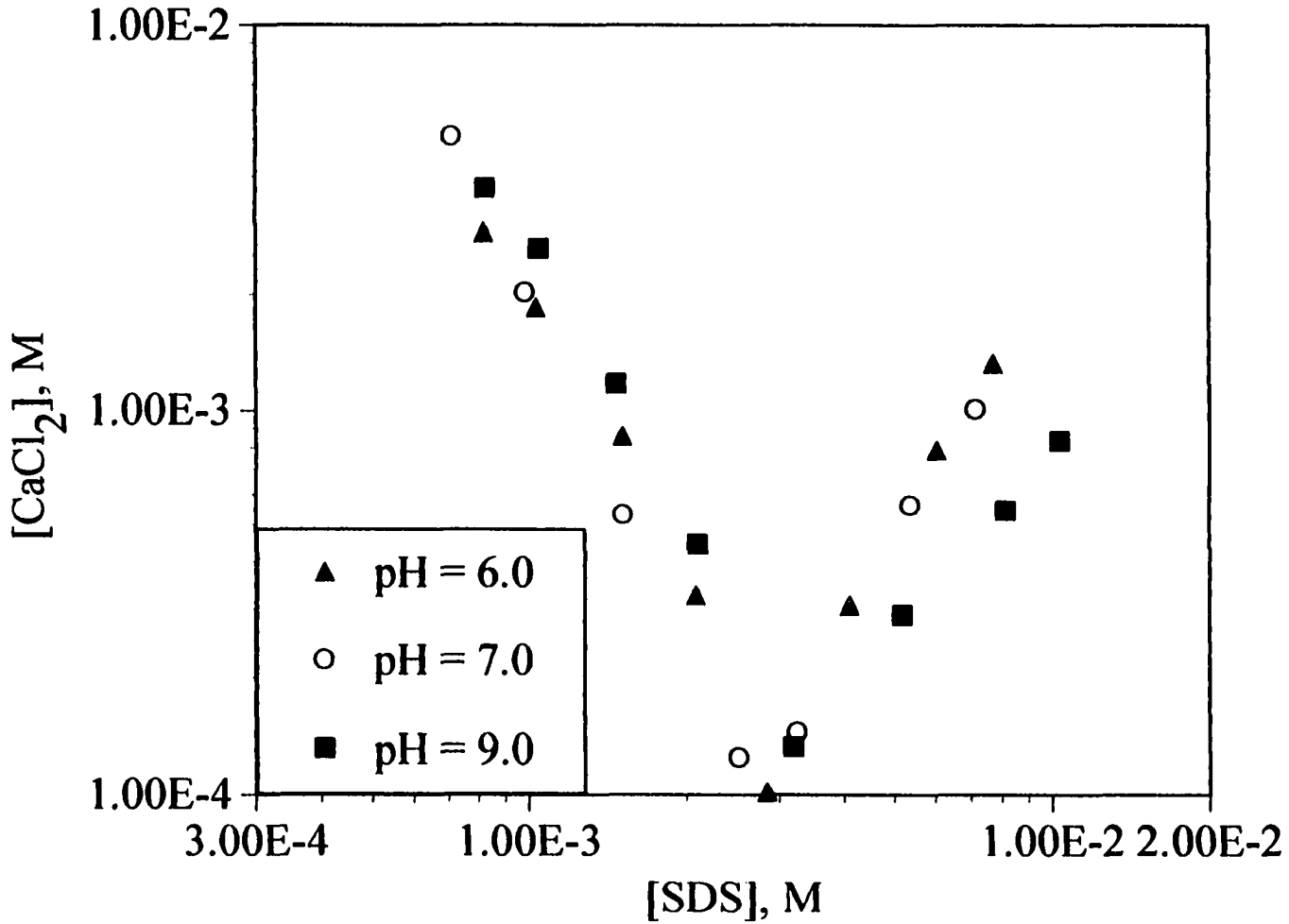


Figure II.14 Precipitation Phase Boundaries (Hardness Tolerance) for 100/0, 80/20, 60/40, and 40/60 SDS/SO Mixtures at a pH Level of 5.0 and 30 ^{o}C

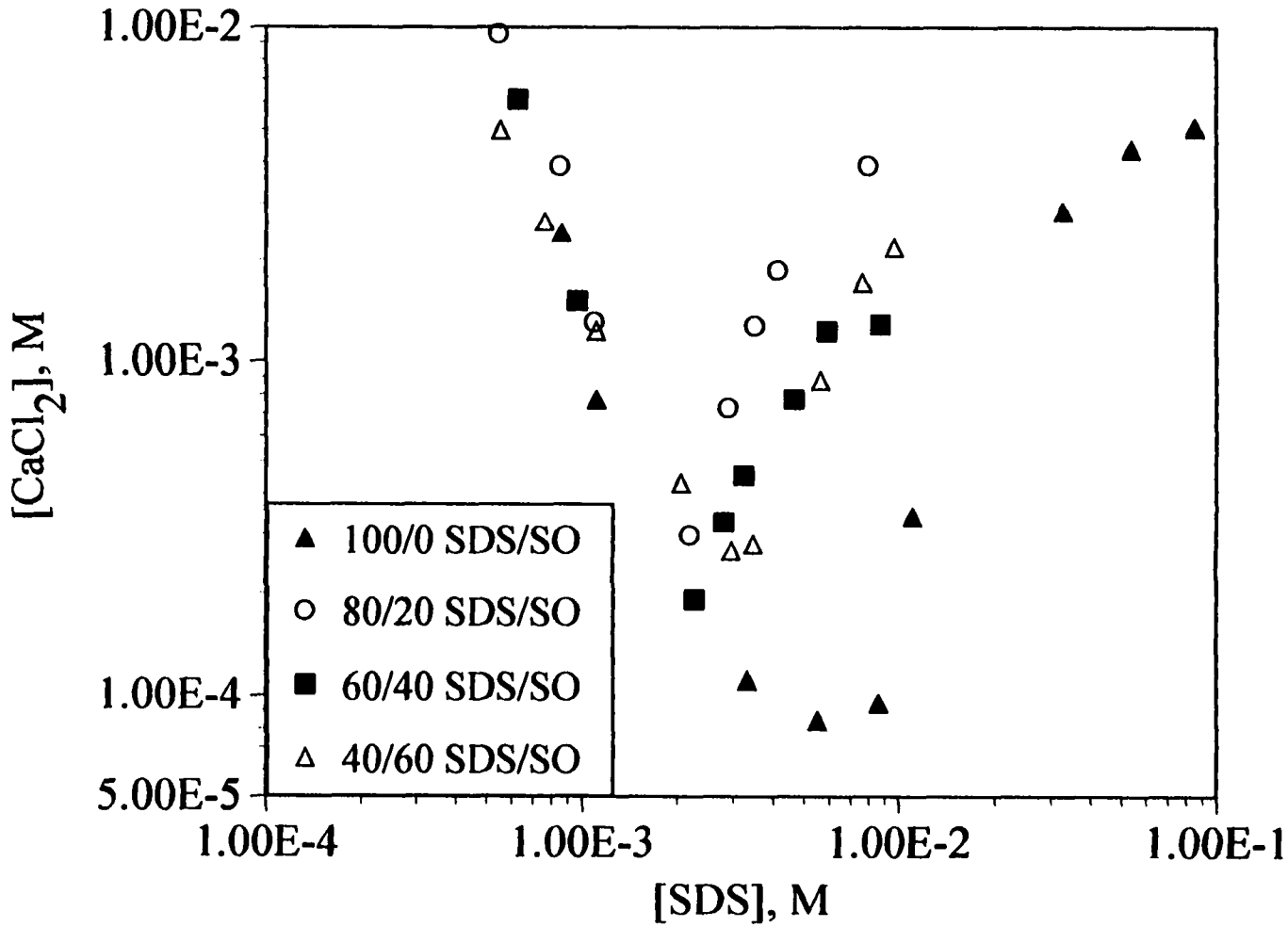


Figure II.15 Precipitation Phase Boundaries (Hardness Tolerance) for 100/0, 80/20, 60/40, 40/60, and 20/80 SDS/SO Mixtures at a pH Level of 7.0 and 30 ^{o}C

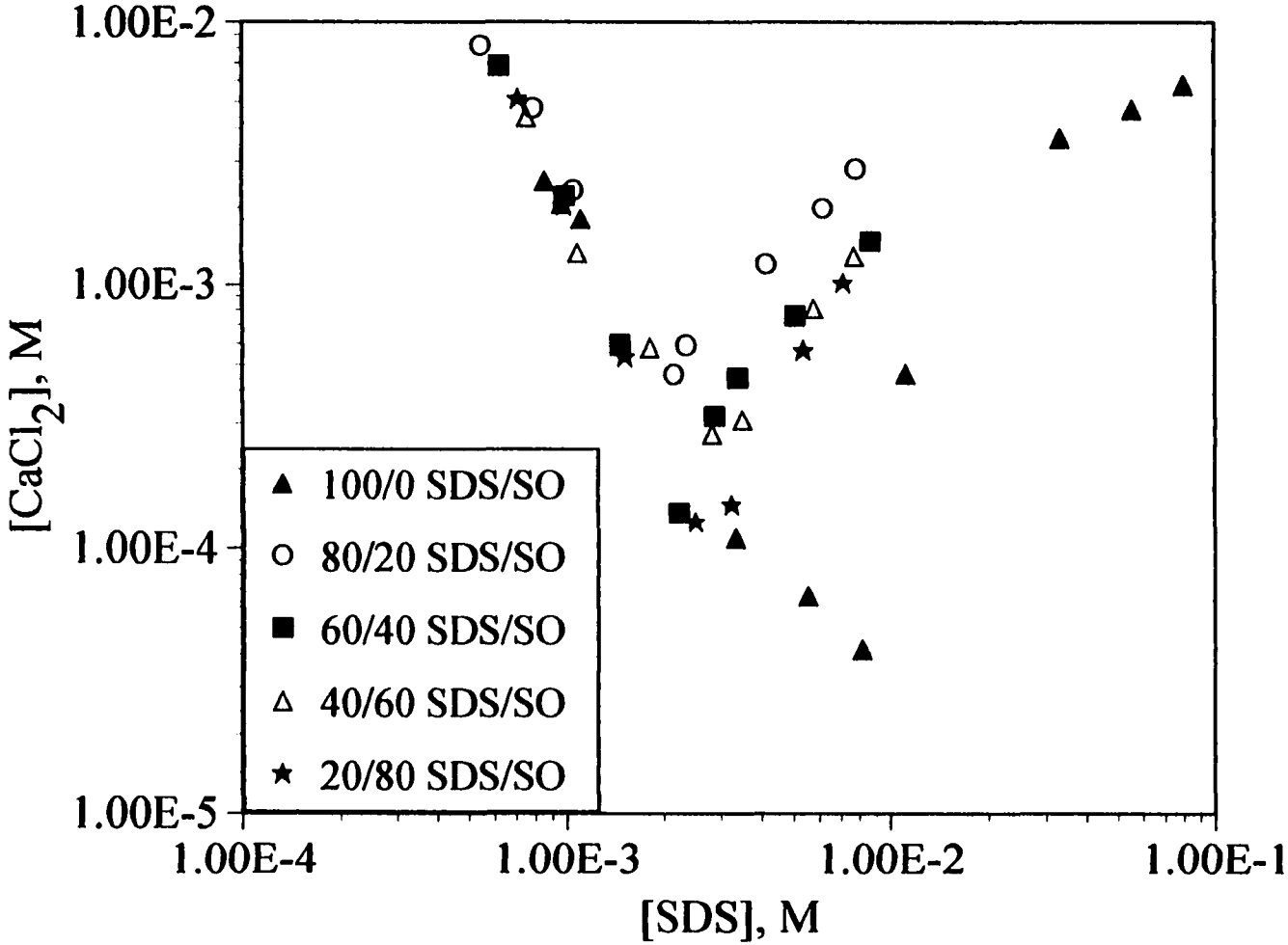
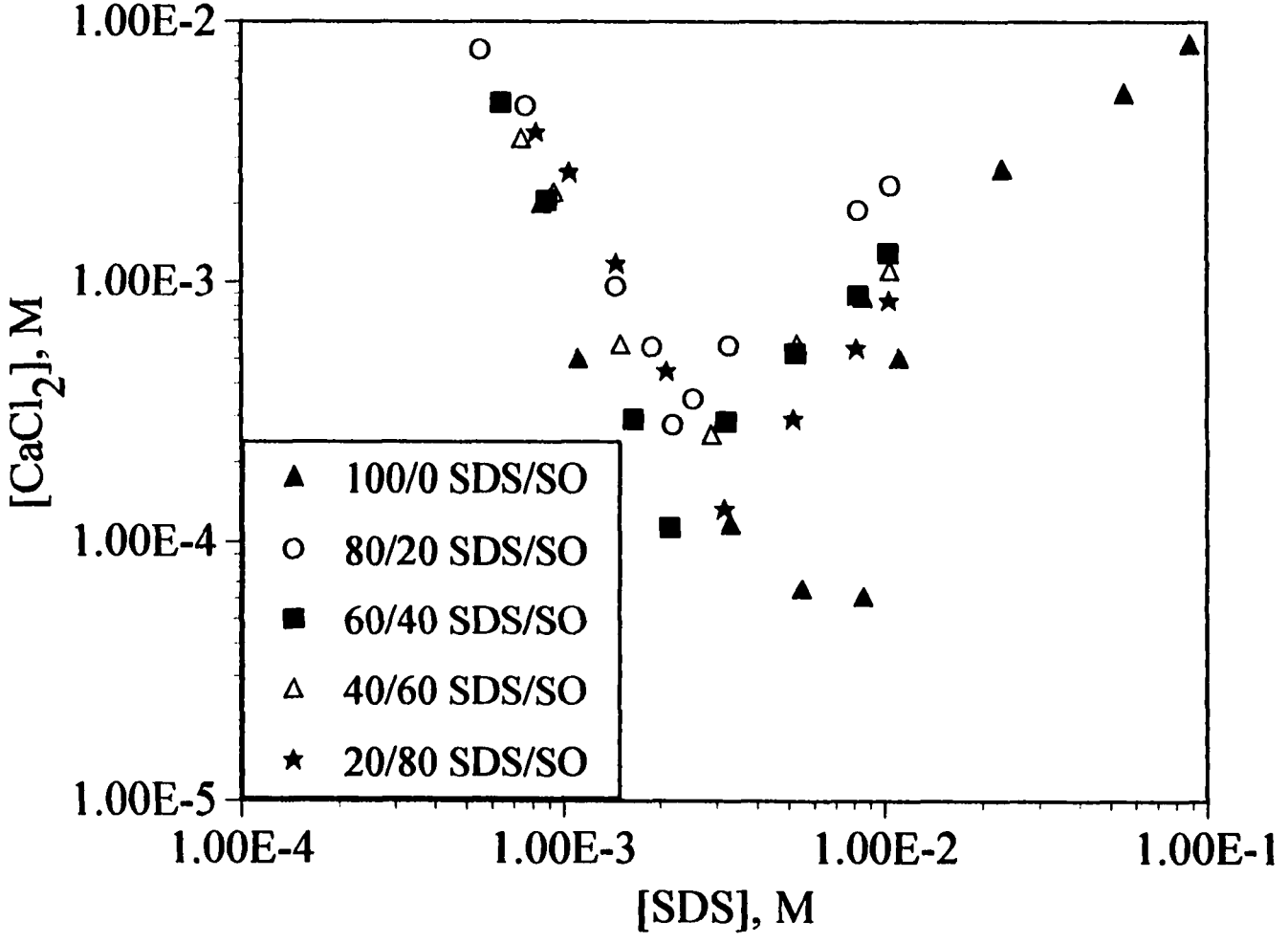


Figure II.16 Precipitation Phase Boundaries (Hardness Tolerance) for 100/0, 80/20, 60/40, 40/60, and 20/80 SDS/SO Mixtures at a pH Level of 9.0 and 30 ^{o}C



CHAPTER 3

KINETICS OF PRECIPITATION OF ANIONIC SURFACTANT MIXTURES

The precipitation kinetics were measured for calcium induced precipitation of mixtures of two anionic surfactants. The overall time required for precipitation to occur can increase dramatically in a range of compositions for the surfactant mixtures compared to single components. Adsorption of the nonprecipitating surfactant onto the precipitate surface was shown to be responsible for this remarkable synergism. The higher the supersaturation of surfactant monomers, the more rapidly precipitation occurs. The precipitation occurs in step-wise fashion under some conditions where crystals of different composition are formed with different induction times. Atomic force microscopy (AFM) was used to visually study the crystal surfaces. Graphs of what seems to be the surfactant head groups in the crystal lattice show a hexagonal arrangement of the head groups for the anionic surfactants studied. A comparison of AFM graphs between pure anionic surfactant crystals and crystals formed from anionic surfactant mixtures shows dramatic differences. Spiral crystal growth due to a screw dislocation was observed for one of the pure systems. For the mixtures, a crystalline phase growing on the surface of another crystal surface seemed to occur in one case and two types of crystals, with one type being stressed enough to result in incomplete layers and holes, was observed for a system which exhibited a step-wise rate curve. Image analysis was used in this study to obtain visual information about the effect of mixing two anionic surfactants on crystal habit. It was found that changes do occur when the two surfactants are mixed. This indicates that processes such as adsorption

and coprecipitation are occurring. The crystals were then allowed to age in solution for a period of one week and it was found that the crystalline phase from the mixed surfactant solutions separated into two types of crystals which resembled the week old pure crystals.

3.1 Introduction

An important characteristic of anionic surfactants which can inhibit their use in many applications is their tendency to precipitate from aqueous solutions. One condition which can cause anionic surfactants to precipitate easily is hard water (water containing multivalent cations). Precipitation of surfactants due to hard water can be detrimental in applications such as detergency, where precipitated surfactant is not available for participation in the cleaning process. There have been numerous studies of the thermodynamics of surfactant precipitation. However, there have been very few investigations of the kinetics or rate of surfactant precipitation despite the fact that many practical surfactant processes may be far from equilibrium. Since the vast majority of surfactants in industrial or consumer products are mixtures of surfactant molecular structures, the effect of mixture composition on precipitation kinetics has important consequences for applications.

In this study, the rate of anionic surfactant precipitation from anionic surfactant mixtures by calcium is studied both above and below the critical micelle concentration, or CMC. Precipitate crystal structure for single and mixed surfactant systems is also investigated and the correlation to precipitation kinetics discussed.

3.2 Experimental Procedures

3.2.1 *Materials*

The two anionic surfactants used in this study were sodium dodecyl sulfate (SDS) and sodium octyl benzene sulfonate (SOBS). Electrophoresis/HPLC grade SDS was at least 99% pure and was obtained from Fisher Scientific. It was further

purified by recrystallization from water and then from methanol, followed by drying under a vacuum at approximately 30 °C. The SOBS was obtained from Aldrich at a purity of 97%. The SOBS was recrystallized first from methanol, and then from water. It was then rinsed with cold methanol and dried under a vacuum at approximately 30 °C. The reagent grade calcium chloride was obtained from Fisher Scientific and was used as received. Water was double deionized.

3.2.2 Methods

3.2.2.1 Precipitation Phase Boundaries. Precipitation phase boundaries for each surfactant are important to kinetic studies in order to quantify supersaturation and whether micelles are present. For each surfactant concentration studied, a series of solutions was made with varying $CaCl_2$ concentrations. Surfactant solutions can stay supersaturated for long periods of time (1,2) resulting in non-equilibrium apparent hardness tolerances. Therefore, the temperature of these solutions was first lowered to near 0 °C for at least 24 hours to force precipitation. The temperature was then held constant at 30 °C for four days while gently shaking the samples daily to insure equilibrium (3). For each series of solutions, some samples still contained crystals, while others became clear. The clear solutions were recorded as being below the precipitation phase boundary, while the turbid solutions were above the precipitation phase boundary. The solutions on the precipitation phase boundary contained the first amount of precipitate seen using a high intensity beam of light.

The equilibrium supernatant concentrations for the individual surfactant components in the surfactant mixtures can be predicted at arbitrary initial conditions using a model by Stellner and Scamehorn (3,4). Experimental determination of a few points was done to verify the accuracy of the model for SDS/SOBS mixtures.

Experimental determination of points along the precipitation phase boundary of the least soluble surfactant in a mixture was found in the same way as for the pure surfactant hardness tolerance, using a high intensity beam of light to visually detect the crystalline phase. Experimental determination of a few points along the precipitation phase boundary for the more soluble surfactant was made by determining the point where the more soluble surfactant was initially present in the crystals via conductivity. Any solution still containing precipitate at equilibrium was filtered with a Whatman 3.0 μm pore size cellulose nitrate membrane filter and analyzed with a Wescan conductivity detector via HPLC, using a reverse phase silica column. The filtering was done quickly so that the solution remained isothermal. The absence of solids in the filtered supernatant was immediately confirmed with a high intensity beam of light. The precipitate was washed with cold water to remove the mother liquor, and dissolved in water. For the samples which contained the more soluble surfactant, the initial solution concentration was considered to be inside the precipitation region for that surfactant. For solutions in which the more soluble surfactant was not detected in the precipitate, the initial solution concentration was considered to be outside the surfactant's precipitation phase boundary.

3.2.2.2 Calorimeter Studies. A Tronac model 458/558 calorimeter was used in isoperibol mode to measure the heat of reaction (which can be related to the amount of surfactant precipitated) as a function of time. Isoperibol calorimetry is a nearly adiabatic process. However, there is a small amount of heat transferred from the reaction vessel to the water bath and added to the reaction vessel by the stirrer and thermistors. Over small lengths of time, this heat leak can be modeled as a linear function of the reaction vessel temperature. The temperature of the water bath at

30 °C can be maintained within ± 0.025 °C using a Tronac PTC-41 temperature controller. A diagram of the reaction vessel set-up is shown in Figure III.1. The rates of precipitation of SDS/SOBS mixtures with calcium were measured. Total concentrations of 0.0025, 0.0096, 0.0192, 0.0288, and 0.0750 M were studied with SDS/SOBS mole ratios of 0/1, 0.2/0.8, 0.4/0.6, 0.6/0.4, 0.8/0.2, and 1/0. Approximately 48 g of surfactant solution was placed in the reaction vessel, and approximately 2 g of 0.25 M calcium chloride solution was injected into a soft glass ampoule which was then sealed with a Microflame butane torch and placed in the ampoule holder/stirrer. The system was then allowed to equilibrate with the water bath temperature. The ampoule could then be broken with the hammer to allow "instantaneous" mixing of the reactants which are being stirred vigorously.

3.2.2.3 Heats of Reaction. When an anionic surfactant solution is mixed with a counterion, the apparent experimental heat of reaction is the total heat released from the precipitation reaction, dilution of the ampoule contents, dilution of the reaction vessel contents, breaking of the ampoule, and in some cases, micelle formation and dissociation. Additional experiments must be done to determine these extraneous heats. The heat of breaking the ampoule was measured by breaking an ampoule containing water into the reaction vessel containing water. Heat of dilution of the ampoule solution was measured by breaking an ampoule containing a solution of $CaCl_2$ into water, and heat of dilution of the reaction vessel solution was measured by breaking water into the appropriate reaction vessel solution. Heat of micellization was measured by breaking an ampoule containing a concentrated $CaCl_2$ solution into a surfactant solution that was above the CMC, but outside the precipitation region. This resulted in the formation of additional micelles without precipitation. The decrease in the CMC upon addition of a counterion was calculated using a model presented by

Stellner and Scamehorn (4). A Microscribe 450 chart recorder was used to plot the temperature difference between the reaction vessel and the water bath, in voltage, versus time. For each run, the average heat capacity, C_p, was obtained by adding a known amount of heat for a known amount of time before and after the reaction. Then, using this heat capacity, the overall heat produced during a reaction, Q_T, could be obtained:

$$Q_T = C_p \Delta T \qquad \text{(III.1)}$$

where ΔT is the total temperature change, in mV, during the reaction minus the heat leak discussed in the previous section.

For systems that start above the CMC, demicellization occurs as the precipitation reaction proceeds due to an equilibrium shift from the micelles to the monomers. The heat associated with this process should be subtracted from the heat of reaction as a function of time. The concentration of surfactant as micelles in solution can be found at each point during a reaction using the same model by Stellner and Scamehorn (4) along with a model of the precipitation reaction pathway (5-7). The heat due only to precipitation at each point along the reaction pathway can thus be separated from all of the extraneous heats associated with a calorimeter run.

3.2.2.4 Determination of Factors Affecting Precipitation. HPLC was used to determine if adsorption of one surfactant on the crystals of the other surfactant can occur in these systems. Solutions of 0.02 M SDS and 0.02 M SOBS were precipitated using 0.01 M $CaCl_2$. The precipitated solutions were then filtered, and the precipitate was dried and weighed. Solutions of each surfactant that were outside the precipitation phase boundary were made and placed in a constant temperature water

bath at 30 °C. Both SDS and SOBS solutions were made with surfactant concentrations of 1.0×10^{-5}, 5.0×10^{-5}, 1.0×10^{-4}, 1.5×10^{-4}, 2.0×10^{-4}, and 2.5×10^{-4} M in order to determine the presence of any adsorbing surfactant on the dissolved precipitate. Dried and weighed $Ca(DS)_2$ precipitate was added to each dilute solution of SOBS, and vice versa. The solutions were then held at 30 °C for four days to ensure equilibrium (8). The solutions were then filtered with a Whatman 3.0 μm pore size cellulose nitrate membrane filter. The filtering was done quickly so that the solution remained isothermal. The filter cake was rinsed with cold water to remove the mother liquor, and dissolved in water. A reverse phase silica column on an HPLC with a Wescan conductivity detector was then used to measure surfactant concentrations.

Calorimetry was used to determine the possibility of coprecipitation for mixtures of supersaturated SDS and 2.5×10^{-4} M SOBS with calcium. This same study was done for supersaturated SOBS and 2.5×10^{-4} M SDS. The supersaturated solutions contained 0.020, 0.010, 0.0025, 0.0010, and 0.0006 M surfactant with 0.010 M $CaCl_2$. The solutions were filtered immediately after the calorimeter run with a Whatman 3.0 μm pore size cellulose nitrate membrane filter, and concentrations were measured with a Wescan conductivity detector via HPLC using a reverse phase silica column. Solutions containing 2.5×10^{-4} M SDS and 2.5×10^{-4} M SOBS with 0.010 M $CaCl_2$ were stirred for over 30 minutes at 30 °C to ensure that no precipitation would occur in these solutions.

A series of solutions containing 48 g of 0.0196 M surfactant was precipitated with 2 mL of 0.25 M $CaCl_2$. The solution being precipitated was stirred vigorously by a submergible stir plate in a 30 °C water bath. Each reaction was stopped at different times by quickly filtering via a Whatman 1.0 μm pore size cellulose nitrate filter, and

throwing out the first portion of the filtered solution. The time required to obtain a filtered sample was noted. The filtered solutions were diluted and the concentrations measured with an Alltech 320 conductivity detector via a Shimadzu LC-10AD HPLC using a reverse phase silica column.

Atomic force microscopy (AFM) was used to determine any changes in surface characteristics as SDS and SOBS were mixed in supersaturated solutions. Crystals from solutions containing 0.020 M total surfactant concentration and 0/100, 40/60, 60/40, and 100/0 SDS/SOBS were analyzed with a Digital Instruments and Co. Nanoscope III scanning probe microscope in contact mode. The surfactant solution being studied and a 0.25 M $CaCl_2$ solution were placed in a constant temperature water bath at 30 °C. The 48 g surfactant solution was vigorously stirred on a submergible stir plate and allowed to come to equilibrium with the water bath temperature. A 2 mL quantity of $CaCl_2$ was added quickly using a 5000 μL pipette after equilibrium was reached. The precipitated solution was gently poured over a mica plate 4 minutes after the visual onset of precipitation. The mica plate was then rinsed with cold water and dried. This procedure left dispersed crystals over the entire mica surface. The samples were analyzed using AFM for a range of sizes from 50 x 50 μm to 10 x 10 μm.

Image analysis was used to determine any change in crystal habit as SDS and SOBS were mixed in supersaturated solutions. Bottles containing 48 mL of different surfactant mixtures were placed on a submergible stirrer in a constant temperature water bath. As the surfactant solution was being vigorously stirred, 2 mL of $CaCl_2$ was quickly pipetted into the surfactant solution. Each experiment was allowed to continue for either 4 minutes or 1 week so that the crystals could be analyzed just after precipitation and after ripening. At the end of the time allotment, a sample was

removed, placed on a slide, and a 40X picture was saved through the image analysis via Optimas software. The solutions studied were 0.075 M SOBS with 0.010 M $CaCl_2$, 0.010 M SDS with 0.008 M $CaCl_2$, and the mixtures 0.010 M SDS/0.002 M SOBS, and 0.01 M SDS/0.004 M SOBS each with 0.008 M $CaCl_2$.

3.3 Theory

3.3.1 Precipitation Phase Boundaries

Along a precipitation phase boundary, an infinitesimal amount of precipitate is present which normally consists of only one ionic surfactant. Precipitation occurs below the CMC when the solubility product relationship for the least soluble surfactant is reached. The solubility product relationship for a surfactant anion with calcium below the CMC is shown below:

$$K_{SP} = [S^-]^2 [Ca^{2+}] f_S^2 f_{Ca} \qquad \text{(III.2)}$$

where K_{SP} is the activity based solubility product, $[S^-]$ is the total surfactant concentration of the precipitating anionic surfactant, and $[Ca^{2+}]$ is the total calcium concentration in solution. Total concentrations are used below the CMC since all of the surfactant is in its monomer form. The parameters f_S and f_{Ca} are the activity coefficients of the surfactant and calcium, respectively. Along the precipitation phase boundary and above the CMC, a simultaneous equilibrium exists between the precipitating surfactant as monomer, in micelles, and in precipitate. Precipitation occurs above the CMC when the monomeric concentration of the least soluble ionic surfactant, along with the unbound counterion concentration, equals the surfactant's

solubility product (10). The solubility product relationship which describes surfactant precipitation above the CMC is shown below:

$$K_{SP} = ([S^-]_{mon})^2 [Ca^{2+}]_{un} f_S^2 f_{Ca} \qquad \text{(III.3)}$$

where $[S^-]_{mon}$ is the monomeric concentration of the precipitating surfactant and $[Ca^{2+}]_{un}$ is the unbound calcium concentration (calcium not bound to the micelles). The activity coefficients for insertion into equations III.2 and III.3 are found using an extended Debye-Huckel expression (11).

$$\log f_i = -A (z_i)^2 I^{0.5} / (1+B a_i I^{0.5}) - 0.3 I \qquad \text{(III.4)}$$

The constants A and B are dependent on the solvent and the temperature of solution. At 30 °C, A has a value of 0.5139 and B has a value of 0.3297×10^8 (9). The parameter z_i is the ion valence and is equal to one for either anionic surfactant and two for calcium. The parameter a_i is an empirical value based on the diameter of the ion, and is equal to 6×10^{-8} cm^{-1} for calcium (9) and is estimated as 7×10^{-8} cm^{-1} for SDS and SOBS (3,9,12). The parameter I is the ionic strength of the solution. For this study, the ionic strength is given as:

$$I = \Sigma\, 0.5\, c_i (z_i)^2 = [NaDS] + [NaOBS] + 3[CaCl_2] \qquad \text{(III.5)}$$

where c_i is the total concentration of ion i in solution, [NaDS] and [NaOBS] are the total concentrations of SDS and SOBS in solution, and $[CaCl_2]$ is the total $CaCl_2$ concentration in solution.

Below the CMC, the surfactant monomer can be treated as a simple, strong electrolyte. However, there is no universally accepted practice for the calculation of activity coefficients in a micellar solution. In this study, the anionic surfactants and the $CaCl_2$ in the micellar solutions are treated as simple, strong electrolytes, as has been done previously (13). Several other methods have been proposed. One proposed method considers the micelles as a separate species in solution contributing only a portion of the actual micelle valence (a shielded micelle) (14). Another method that has been proposed treats the micelles as a separate phase which therefore does not contribute to the ionic strength of the aqueous solution (15). Burchfield and Woolley (14) also discuss the work by other researchers who treat the surfactant in solution as a simple, strong electrolyte as we have done here.

Below the CMC, as the anionic surfactant concentration increases, the amount of calcium required for precipitation to occur decreases, as dictated by Equation III.2. The effect of micelle formation on surfactant precipitation is an increase in the concentration of calcium required for precipitation to occur. When micelles form, calcium ions bind to the micelles, reducing the amount of unbound calcium available for precipitation. As more surfactant is added to the system, the additional surfactant tends to form more micelles. The formation of more micelles reduces $[Ca^{2+}]_{un}$ even further. Therefore, a minimum in the precipitation phase boundary occurs at the CMC. When two surfactants of similar structure and charge are mixed together, ideal mixed micelles form, which results in a further lowering of the unbound calcium ion concentration (10,16).

Figure III.2 shows a micelle-monomer-precipitate equilibrium diagram for a mixture of two anionic surfactants in the presence of calcium. There are also sodium ions in solution due to the dissociation of the surfactant salt, which are not shown in

Figure III.2 for clarity. Sodium does not precipitate the anionic surfactants studied at the concentration levels present in this paper due to a much larger K_{SP} with these surfactants than the calcium salt. The hardness tolerance of a mixture containing more than one anionic surfactant is obtained when the solubility product of the least soluble surfactant is reached (10,16). Mixed precipitate is usually not seen along the precipitation phase boundary of mixed anionic surfactants unless the K_{SP} values of the two surfactants are very similar (17). The result of this type of behavior is that as the precipitating surfactant is mixed with another anionic surfactant, the precipitating surfactant is diluted in the micellar phase. This shifts the equilibrium toward the micelles, and causes precipitation of that surfactant to be more difficult.

A general model has been developed which can predict the hardness tolerance of an anionic surfactant (3,4) using pseudo-phase separation theory (18,19) to describe the micelle-monomer equilibrium which occurs in micellar solutions. This model can be used to predict the hardness tolerance of a mixture as well as the monomer and micellar concentrations of each component in the system. If the precipitating component of interest is the least soluble, its hardness tolerance is equal to the hardness tolerance of the surfactant mixture. If this surfactant is the more soluble, an iterative approach must be taken in which the amount of the least soluble surfactant precipitated is initially guessed. Using the solubility product relationship, the hardness tolerance model, and material balances, the amount of calcium required initially in the solution to precipitate out the more soluble component can be calculated. The total amount of calcium that is needed in the system to precipitate the more soluble surfactant equals the following:

$$[CaCl_2] = [Ca^{2+}]_b + [Ca^{2+}]_{un} + [Ca^{2+}]_{ppt} \qquad \text{(III.6)}$$

where $[CaCl_2]$ is the total $CaCl_2$ concentration, $[Ca^{2+}]_b$ is the calcium bound to the micelles, and $[Ca^{2+}]_{ppt}$ is the total amount of calcium which has precipitated with the least soluble surfactant.

A solution which contains surfactant and calcium concentrations that lie inside the precipitation phase boundary is supersaturated. Supersaturation is a measure of the excess concentration of the reactants above the equilibrium solubility concentrations (20-22). A supersaturated solution will precipitate after some measurable amount of time so that the equilibrium concentration of the solution will lie on the precipitation phase boundary. In this paper, the degree of supersaturation, or supersaturation ratio (S_o) for an anionic surfactant precipitating with Ca^{2+}, is defined as follows:

$$S_o = ([Ca^{2+}]_{un} ([S^-]_{mon})^2 f_{Ca} f_S^2 / K_{SP})^{1/3} \qquad \text{(III.7)}$$

Equation III.7 only takes into consideration the monomer surfactant concentration and the unbound calcium concentration. The initial presence of micelles in a supersaturated solution decreases the supersaturation ratio because the micelles remove the surfactant and calcium from the monomer phase.

In a solution containing two anionic surfactants, the supersaturation ratio for each surfactant can be calculated separately. Using a supersaturation ratio that considers only the monomer surfactant and unbound calcium concentrations allows the effect of micelles to be accounted for. Thus, above the CMC, as a surfactant is diluted due to mixing with another surfactant, the supersaturation ratio for that surfactant will generally decrease.

A reaction pathway theoretically predicts the supernatant concentration of each reacting component (calcium and surfactant anion) as the reaction proceeds from the initial supersaturated solution to the equilibrium composition (on the phase boundary). The reaction pathways for the precipitation of each surfactant in the mixture can be predicted theoretically (5-7). Modeling of the reaction pathways can be accomplished using material balances for each surfactant along with the knowledge that two surfactant ions precipitate with one calcium ion:

$$2[NaS] = 2[S^-]_{unr} + 2[S^-]_{ppt} \qquad \text{(III.8)}$$

$$[CaCl_2] = [Ca^{2+}]_{unr} + [Ca^{2+}]_{ppt} \qquad \text{(III.9)}$$

$$2[S^-]_{ppt} = [Ca^{2+}]_{ppt} \qquad \text{(III.10)}$$

where [NaS] is the total surfactant concentration, $[S^-]_{unr}$ is the unreacted (or unprecipitated) surfactant ion concentration, $[S^-]_{ppt}$ is the precipitated surfactant concentration, and $[Ca^{2+}]_{unr}$ is the unreacted calcium concentration. Combining these equations gives the reaction pathway constant, D:

$$D = 2[S^-]_{unr} + [Ca^{2+}]_{unr} \qquad \text{(III.11)}$$

For every $[Ca^{2+}]_{unr}$ during the precipitation reaction, $[S^-]_{unr}$ can be calculated using Equation III.11. The equilibrium condition for the reaction is found by the point

where the reaction pathway crosses the appropriate precipitation phase boundary. This information can be put into the pseudo-phase separation model to calculate the concentration of surfactant in the micelles and the concentration of calcium bound onto the micelles at each point along the reaction pathway. This information can then be related to the extent of reaction and, therefore, to any time during the precipitation reaction.

3.3.2 Theory of Crystallization

There is extensive literature in the area of crystallization theory. Most of this literature has been developed in relation to the precipitation of inorganic salts, but is being found to extrapolate to studies involving many other precipitation systems. The theory discussed in this section is a general discussion of the theory of crystallization and is believed to be applicable to the precipitation of surfactant salts.

The induction period is the period between the attainment of supersaturation and the onset of precipitation determined visually or by the measurement of some appropriate physical property. The steps in crystallization are nucleation, crystal growth, and secondary growth. Nucleation can either be homogeneous, heterogeneous, or secondary. Homogeneous, or spontaneous, nucleation occurs when the nuclei are made up of the precipitating components. Sub-nuclei, or embryos, are thought to form and dissipate constantly in supersaturated solutions. An energy barrier must be overcome in order for a sub-nucleus to form a critical nucleus, which is the smallest nucleus that can grow into a crystal. A critical nucleus can form as a result of random free energy or concentration fluctuations in local regions of a solution (20,23,24). The structure of a critical nucleus is thought to either be a tiny replica of the crystal it will form or a diffuse body of ions, not yet in the rigid lattice of a crystal.

Since very few ions are thought to form a critical nucleus, it is most likely that the critical nucleus does not have the characteristics of the bulk crystal (25). A solution can remain supersaturated for a long time, and metastable zones (regions beginning just above the precipitation phase boundary) have repeatedly been shown to exist where spontaneous nucleation does not occur. There are many factors such as thermal history, mechanical action, and presence of solid particulates which affect the metastable zone width (24). In usual situations, large supersaturation ratios are required for spontaneous nucleation to occur (25-27). Very few studies have been done on the kinetics of precipitation of surfactant salts. A study has been done, however, of the precipitation of calcium laurate below the CMC, in which it was found by observing particle numbers that a supersaturation ratio of 5 was required to precipitate via spontaneous nucleation (25).

Heterogeneous nucleation occurs when small particles are present in the system which act as nucleation sites for the deposition of the precipitating components. The most active nuclei are probably in the range of 0.1 to 1.0 μm (26). In this paper, the shattered glass of the ampoule could act as nucleation sites. Other possible nucleation sites are the stirring rod, thermistors, reaction vessel walls, as well as any particulates which might be present in the surfactant and calcium solutions.

Secondary nucleation occurs when nucleation sites are present due to the loss of weak outer layers or weak outgrowths of the crystals of the precipitating species due mostly to collisions with other crystals or the reaction vessel hardware (26,28). It has been shown by several groups that there is an adsorbed layer of solute on the surface of a growing crystal (28), which can be easily separated to form new nuclei. Thorough discussions of the thermodynamics of nucleation are given in reviews including Nývlt, et al. (24) and Adamson (29).

Crystal growth can either be diffusion controlled or surface reaction controlled. In diffusion controlled growth, the rate limiting step is the diffusion of the precipitating components from the bulk to the crystal surface. A model that describes the diffusion mechanism has been used to describe crystal growth of inorganic salt precipitation (30). This same model has been shown to apply to anionic surfactant precipitation with calcium (25). There are three possible mechanisms for surface reaction controlled growth. These are mononuclear growth, polynuclear growth, and growth due to a screw dislocation . A new layer of a crystal is started when the precipitating components nucleate onto the crystal surface. The first site that becomes occupied is a high energy site and is therefore difficult to fill. If the precipitating components nucleate onto the surface of a crystal very slowly compared to the growth of a layer, then each layer is completed before a new layer begins. This is called mononuclear growth and is the most constrained growth mechanism. If surface nucleation is fast, new layers begin before the old layers are complete. This is called polynuclear growth. A model that describes the surface reaction mechanism has been used to describe crystal growth of inorganic salt precipitation and can also be applied to surfactant precipitation with calcium (25,30).

A screw dislocation is a surface dislocation that forms when a slip in a crystal plane occurs, pushing up part of the surface layer. The Frank mechanism (31) describes a mechanism in which the crystal is formed from a single layer, spiraling upward as the precipitating species occupy the sites at the step of the screw dislocation. This removes the need for surface nucleation. Therefore, a crystal forming due to a screw dislocation can continue growing without inhibition until the supersaturation of the system is satiated. The Frank mechanism has been seen while occurring in a few systems (29,32). The spiral pattern which forms is many times

representative of the molecular pattern in the lattice (33) and the step heights have been found to be some multiple of the unit cell height (32,33). There are an exhausting number of theories in the literature attempting to describe crystal formation from a liquid solution. A portion of these theories are discussed in a review (34).

3.3.3 Effect of Impurities

Additional components in a solution can affect both the growth rate and crystal habit of a precipitating species (28,33). The supersaturation ratio can be changed due to the effect of impurities on the solubility of the precipitating species (28,35). Selective adsorption of a constituent can change the crystal habit by retarding the outward growth of certain planes (36). Adsorption can also affect surface nucleation as well as overgrowths, incomplete planes, steps, and dislocations (29,36).

Epitaxial growth is the oriented growth of a crystalline phase on the surface of another crystalline phase and depends on the lattice structure (27,29). If both species are supersaturated, epitaxial growth can affect the overall time for precipitation to eventuate. An increase in the overall time for precipitation to occur could take place if the epitaxial growth covered a screw dislocation.

Coprecipitation can occur when an impurity or microcomponent is present in solution, resulting in inclusion and/or the formation of a solid solution. A solid solution occurs when trace ions or molecules are incorporated into the host lattice during precipitation. The tendency for a solid solution to form depends on whether the macrocomponent and the microcomponent have similar ionic radii and the same charge (20). In surfactant systems, it would also be important that the two components have similar overall structures. Inclusion (35), sometimes called occlusion, is the entrapment of impurities during precipitation. This can occur due to

adsorption, chemical reaction, or entrapment of the mother liquor in pockets as imperfect layers are formed. In each of these cases (except when a chemical reaction has occurred), the impurity is free to diffuse through the solid phase and even to separate during ripening (20,37). In most situations where coprecipitation occurs, a combination of these phenomena exists (37).

3.4 Results and Discussion

3.4.1 Precipitation Phase Boundaries

The theoretical precipitation phase boundaries for the surfactant components in several SDS/SOBS mixtures are shown in Figures III.3 and III.4, along with some experimental results for confirmation of the model's accuracy. The model fits the data for pure SDS (3) and pure SOBS quite well as we have seen before (3). The minimum in the hardness tolerance in Figures 3 and 4 corresponds to the CMC values of SDS and SOBS, respectively; the minimum in the SDS hardness tolerance is 0.0067 M (3) and in the SOBS hardness tolerance is 0.012 M. These values are consistent with the CMC values obtained from surface tension measurements; 0.0072 M for SDS and 0.012 M for SOBS (38). On the left side of each precipitation phase boundary, the surfactant is present as monomer, and on the right side, the surfactant is present as monomer and in micelles. For each mixture, there is a precipitation phase boundary in Figure III.3 and in Figure III.4 which describes the minimum calcium concentration in solution at which that component would precipitate in the mixture. Above the minimum hardness tolerance, as SDS is mixed with SOBS from 100/0 to 60/40 SDS/SOBS, the precipitation phase boundary for SDS slightly increases. At 40/60 and then 20/80 SDS/SOBS, the right side of the precipitation phase boundary for SDS

dramatically increases. This same trend is seen for the 60/40 and 80/20 SDS/SOBS solutions at the SOBS precipitation phase boundaries. Below the mixture CMC, no significant change in the precipitation phase boundary is seen as the two surfactants are mixed. This shows that it is the effect of mixed micelles which causes the large increase in the precipitation phase boundaries for each surfactant. According to theory, SDS should precipitate at lower $CaCl_2$ concentrations at 80/20 and 60/40 SDS/SOBS and SOBS should precipitate at lower $CaCl_2$ concentrations at 20/80 and 40/60 SDS/SOBS. Hence, the hardness tolerance of the surfactant mixture corresponds to different surfactants precipitating at different mixture compositions. The individual surfactant component hardness tolerances can be obtained theoretically even when this surfactant is the least soluble (there is already precipitate in the system due to precipitation of another surfactant component with calcium). The hardness tolerances for SDS at 40/60 and 20/80 SDS/SOBS are the predicted hardness tolerances for SDS in the presence of $Ca(OBS)_2$ precipitate . The hardness tolerances for SOBS at 60/40 and 80/20 SDS/SOBS are the predicted hardness tolerances for SOBS in the presence of $Ca(DS)_2$ precipitate.

Several experimental hardness tolerance points above the CMC are plotted in Figures III.3 and III.4 to compare with the theoretical curve. For the precipitation of $Ca(OBS)_2$ from a 20/80 SDS/SOBS solution and 0.025 M and 0.1 M surfactant, the theory satisfactorily coincides with the experimental hardness tolerance points. The hardness tolerance of SDS from 20/80 SDS/SOBS and 0.025 M surfactant, also matches the predicted points. The onset of precipitation of $Ca(DS)_2$ from 20/80 SDS/SOBS and 0.1 M surfactant was not obtained due to SDS showing up on the HPLC chart as a shoulder peak to the much larger SOBS peak, making the exact determination of this point difficult. For the precipitation of SDS from 0.0125 M and

0.0625 M surfactant and 80/20 SDS/SOBS, the data matches the theory reasonably well. However, for the precipitation of SOBS with calcium from these same solutions, the experimental points lie below the theoretical line. The SOBS component was detected in the precipitate for these mixtures at the lowest calcium concentration where there was enough precipitate to separate and analyze practically. The presence of any $Ca(DS)_2$ precipitate results in the presence of OBS^- in the precipitate. However, the presence of $Ca(OBS)_2$ does not result in the presence of DS^- in the precipitate. In fact, DS^- does not show up in the precipitate until the solubility product of SDS and calcium has been reached. A possible explanation for this behavior is that OBS^- is adsorbing onto the $Ca(DS)_2$ crystals. Adsorption of OBS^- onto the crystal surfaces would result in the presence of OBS^- in the precipitate phase even outside of the SOBS/$CaCl_2$ precipitation phase boundary.

3.4.2 Adsorption Studies

In order to determine whether adsorption of OBS^- onto $Ca(DS)_2$ crystals is occurring, a separate measurement of adsorption onto preexisting crystals was performed. Experiments were carried out to determine the equilibrium composition of the crystalline phase for single component crystals mixed with a dilute surfactant solution. An adsorption isotherm was not possible since the phase boundary for the adsorbing species lies in the middle of where the majority of the isotherm concentrations would be (i.e., the adsorbing component would precipitate). In most adsorption studies, detailed knowledge of the surface area and/or a constant size distribution exists in each sample. Precipitation from direct mixing inherently results in wide size distributions. Also, during the experiments to measure equilibrium precipitate compositions, partial dissolution of the solid occurred when introduced into

solution. This dissolution changed the precipitate weight. Another problem is that the precipitate for each sample most likely had different size distributions due to agglomeration during the separation and drying procedures. Therefore, the question of whether it is possible for significant adsorption to occur was addressed, but the amount could not be quantified. The result was that the OBS^- component was detected in the $Ca(DS)_2$ crystals after four days for every sample studied. However, there was no evidence of any DS^- in the $Ca(OBS)_2$ crystals after the same time span. This result gives evidence to the ability of OBS^- to adsorb onto the $Ca(DS)_2$ crystals, and gives a possible explanation for the deviation of the experimental points on the SOBS precipitation phase boundary for the 80/20 SDS/SOBS system.

3.4.3 Determination of Reaction Pathways

Theoretical reaction pathways for each anionic surfactant are required in order to properly calculate the amount of the surfactants in the micellar phase at any point during the precipitation reaction. Figures III.5-III.9 show the reaction pathways of SDS with calcium compared with the SDS component precipitation phase boundaries for 100/0, 80/20, 60/40, 40/60, and 20/80 SDS/SOBS, respectively. The reaction pathways for the precipitation of $Ca(OBS)_2$ from 0/100, 20/80, 40/60, 60/40, and 80/20 SDS/SOBS solutions are shown in Figures III.10-III.14, respectively. The point where a reaction pathway crosses the precipitation phase boundary is the theoretical equilibrium supernatant concentration for that reaction. Any reaction pathway that begins outside of the precipitation phase boundary represents a solution where $Ca(DS)_2$ should not precipitate. As the precipitation region decreases for SDS as the SDS/SOBS ratio decreases (in the order 100/0, 80/20, 60/40, 40/60, and 20/80), the supersaturation ratio for SDS with calcium decreases. However, as the

supersaturation ration for SDS decreases, the supersaturation for SOBS increases. Due to this trade-off, large reductions in the precipitation rate as the two surfactants are mixed should not occur simply as a result of the effect of mixed micelles on the supersaturation ratio.

3.4.4 Precipitation Kinetics for SDS with Calcium

Before determining the kinetics of precipitation of SDS/SOBS mixtures with calcium, the effect of adjusting the supersaturation ratio on pure SDS both above and below the CMC is determined. Figure III.15 compares rates of precipitation of SDS with calcium for initial conditions which are below the CMC. Figure III.16 compares the extent of reaction for precipitation of SDS with calcium for initial conditions which are above the CMC. In both cases, as the supersaturation ratio is increased, the overall time for precipitation to occur decreases. Also, in both cases, an increase in the supersaturation ratio results in an increase in the induction time. Above the CMC, the supersaturation ratio is based on the monomer SDS concentration and unbound calcium concentration. Figure III.17 shows a comparison of the rates of precipitation for a range of supersaturation ratios both above and below the CMC. The general trend is a decrease in the time for precipitation to occur as the supersaturation ratio is increased, regardless of whether or not micelles are present. This trend is only true if the supersaturation ratio is calculated using the monomer surfactant concentration and unbound calcium concentration.

3.4.5 Precipitation Kinetics for SDS/SOBS Mixtures with Calcium

Figures III.18-III.22 depict the extent of precipitation curves for 0.075, 0.0288, 0.0192, 0.0096, and 0.0025 M total surfactant concentration. Each figure

compares the extent of precipitation curves for the entire range of SDS/SOBS mole ratios. Figure III.18 shows the extent of precipitation with time of solutions containing 0.075 M surfactant and 0.01 M $CaCl_2$. Even though 0.075 M SDS is inside the precipitation phase boundary, and a small amount of precipitate was seen at the end of the experiment, the heat released during the reaction was too small to measure with the technique used here. This result is most likely due to the SDS concentration being very close to the precipitation phase boundary. The 80/20, 60/40, and 40/60 SDS/SOBS solutions did not contain any visible precipitate at the end of the calorimeter runs. In general for the systems studied, as SDS and SOBS are mixed, the overall time for precipitation to occur is increased, with 60/40 SDS/SOBS requiring the longest time. In Figure III.19, the precipitation reaction for 60/40 SDS/SOBS takes approximately 35 minutes. This curve is not shown beyond 4.5 minutes to permit easier comparisons to the other data. The initial supersaturation ratios for each reaction are given in Tables III.1-III.5, corresponding with Figures III.18-III.22. Also, the percentage of SDS and SOBS in the precipitate at the end of the reaction, are given in Tables III.1, III.2, III.4, and III.5. In general, as a surfactant is diluted as it is mixed with another surfactant, the initial supersaturation ratio for that surfactant decreases and the final fraction of that surfactant in the precipitate decreases.

For each 80/20 SDS/SOBS precipitation reaction where the precipitation composition was determined, DS^- and OBS^- are both present in the precipitate. However, there are not individual extent of precipitation curves for the separate precipitation of the two surfactants. The time for precipitation to occur as the SDS/SOBS mole ratio changes from 100/0 to 80/20 and 60/40 increases along with the supersaturation ratio of SDS. For the change in SDS/SOBS mole ratios from 60/40 to 80/20, The supersaturation ratio for SOBS decreases, indicating that the

independent precipitation of SOBS with calcium should decrease. An explanation for this behavior is that OBS^- is being included into the $Ca(DS)_2$ crystal as it forms (by adsorption and possibly entrapment of the mother liquor). If the supersaturation of SOBS is satiated by this interaction, a separate reaction rate would not occur for the precipitation of $Ca(OBS)_2$.

The overall time for precipitation to occur for 60/40 SDS/SOBS in each case is much longer than would be expected from comparing the degree of decrease in supersaturation ratios as each surfactant is diluted to this point, with the degree of increase in time. For 0.0288, 0.0096, and 0.0025 M surfactant, both surfactants are present in the precipitate at the end of the calorimeter run, even though only a single extent of precipitation curve is seen. However, these interactions do not explain the drastic increase in time only seen for the precipitation of 60/40 SDS/SOBS.

An initial increase in the extent of reaction followed by a leveling off and a second increase is seen for 40/60 SDS/SOBS, and 0.0096, 0.0192, and 0.0025 M surfactant. This same behavior is also seen for 20/80 SDS/SOBS and 0.0096 M surfactant. Both surfactants are present in the precipitate at the end of the runs where the concentration was measured (Tables III.1, III.2, III.4, and III.5). In order to help explain the precipitation behavior of these solutions, the precipitate for 40/60 SDS/SOBS and 0.0092 M surfactant was analyzed at various times during the reaction to determine the relative precipitation of each surfactant component as the reaction progressed. The resulting concentrations related to the extent of reaction are shown in Figure III.23. The time spans for each measurement are the result of experimental restraints. During the first reaction step, the SOBS concentration drops dramatically. However, there is also a decrease in the SDS concentration. There is then an induction period during which both concentrations remain relatively constant. During

the second reaction step, the SDS concentration drops more drastically than does the SOBS concentration. Evidence has already been presented to show that both SDS and SOBS can become included into the precipitating surfactant. This seems to be occurring in this 40/60 SDS/SOBS reaction as well. During the first reaction step, $Ca(OBS)_2$ is the major precipitating component. The decrease in SDS concentration during this reaction step could likely be due to inclusion into the $Ca(OBS)_2$ crystals. The major precipitating component in the second reaction step is $Ca(DS)_2$. The induction time, then, can be considered the continuation of the total induction time required for the precipitation of $Ca(DS)_2$ from this solution.

3.4.6 Nonequilibrium Crystal Compositions

It is important to obtain the crystal compositions during crystallization before these compositions have reached equilibrium. Table III.6 shows the results of nonequilibrium studies. The precipitate compositions resulting from precipitation of an anionic surfactant in the presence of a different dilute anionic surfactant are shown. In this experiment, the crystals are filtered from the solution immediately at the end of the precipitation reaction. Since precipitation from direct mixing inherently results in broad crystal size distributions, and since the supersaturation ratio is being altered, it is not certain whether each sample contained the same crystal surface areas or morphologies. However, it can be unambiguously determined whether coprecipitation occurs. Table III.6 shows that DS^- is found in the precipitate of $Ca(OBS)_2$ and OBS^- is found in the precipitate of $Ca(DS)_2$. The presence of DS^- in the $Ca(OBS)_2$ crystals at equilibrium, however, was not found. Therefore, during a precipitation process, it is possible for DS^- to be included in the $Ca(OBS)_2$ crystals, possibly by entrapment of the mother liquor. As equilibrium is reached, the presence of DS^- decreases to either

near zero or zero. One can also intuitively realize that for slower precipitation rates, the precipitation reaction will begin to be influenced by the equilibrium conditions. For example, less DS^- will coprecipitate, influencing the precipitation reaction less. A solid solution is most likely not forming between these surfactants. The two surfactants have dissimilar structures; SOBS, has a benzene ring in an 8 carbon chain and a sulfonate head group, while SDS has a 12 carbon chain and a sulfate head group. Also, the two surfactants tend to separate with time, as will be shown in image analysis pictures later in this paper. It has already been shown that SDS does not remain in $Ca(OBS)_2$ crystals after equilibrium has been achieved. The SOBS adsorbs onto the $Ca(DS)_2$ crystal surfaces, and therefore the presence of SOBS in the $Ca(DS)_2$ crystalline phase can most likely be attributed to this adsorption.

3.4.7 Head Group Arrangements in $Ca(DS)_2$ and $Ca(OBS)_2$ Crystal Lattices

Atomic force microscopy graphs of crystals from 0.02 M SDS/0.01 M $CaCl_2$ and 0.020 M SOBS/0.01 M $CaCl_2$ solutions, respectively, are shown in Figures III.24 and III.25 over a 10 nm x 10 nm range. These figures show what seem to be surfactant head groups. The average distance from center to center of the head groups for SDS is 5.87 Å and for SOBS is 5.89 Å. The literature value for the head group diameter of SDS at a water/air interface and 25 °C is 8.21 Å and at a 0.1 M NaCl/air interface and 25 °C is 7.23 Å (29). Since the head groups here are arranged in the more compact form of a crystal lattice, the smaller values seem reasonable. The head groups for both surfactants are in hexagonal lattice arrangements.

3.4.8 Effect of Seeds on Overall Time for Precipitation

The presence of particulates in solution can affect the amount of time required for precipitation by acting as seeds for nucleation. Figure III.26 compares the extents of precipitation with time between unfiltered and filtered 0.0096 M SDS/SOBS mixtures. The water for solutions used to obtain the unfiltered data was double deionized. The water for solutions used to obtain the filtered data was further filtered through a 10,000 molecular weight cut-off (MWCO) membrane. The initial supersaturation ratios for SDS and SOBS in each solution studied are shown in Table III.7. The shapes of the curves are nearly identical, with small differences most likely being the result of slightly differing initial supersaturation ratios (compared in Table III.7). The largest difference between these solutions occurs in the induction period for the 60/40 SDS/SOBS case. The solution made from filtered water has a longer induction period than the unfiltered solution. There are also small increases in the induction times for each of the other SDS/SOBS mixtures, including the second induction period in the 40/60 SDS/SOBS case. Therefore, the presence of heterogeneous nucleation sites seems to affect the induction times but not the general shapes of the curves studied, which is an expected result.

3.4.9 Atomic Force Microscopy of Crystal Surfaces

Atomic force microscopy in contact mode was used to determine changes in the crystal surface structure as the two surfactants were mixed and to obtain further insight into the precipitation process of these systems. Figures III.27-III.30 compare 50 μm scale atomic force microscope three-dimensional graphs of pure $Ca(DS)_2$, pure $Ca(OBS)_2$, and crystals from 60/40 and 40/60 SDS/SOBS, respectively. The $Ca(DS)_2$ crystals in Figure III.27 show mounds as well as flat, stair-stepped planes,

with the tops of these crystals displaying spiraling growth due to screw dislocations. Several cases of crystal growth due to screw dislocations have been recorded, and some references for these cases can be found in reviews (29,32,35). The longest lengths are about 20 to 25 μm. The $Ca(OBS)_2$ crystals are about 10 μm for the longest length. The three-dimensional graph shows that there are many tall, jagged peaks, some flat regions, and overall uneven growth. The crystals from the 60/40 SDS/SOBS solution have some mounds as well as flat, planar crystals with jagged growths on top similar to the jagged peaks shown in Figure III.28. There are a few spiral patterns, as well. The jagged peak-type growth is not seen in the pure $Ca(DS)_2$ crystals and looks similar to the $Ca(OBS)_2$ crystals. The flat planes and spiraling growths look like crystals from the pure SDS solution. The flat, covered planes are possibly the beginning of a $Ca(DS)_2$ crystal in which the growth due to a screw dislocation has been halted by the jagged crystalline formation on this surface. This surface nucleation of one crystalline phase on another is possible if favorable sites exist on the original crystal substrate for nucleation of the second crystalline phase. Many cases of growth of one crystalline phase on another have been seen (27,29,39). The growth of the jagged crystals on the planar crystals can explain the much slower precipitation rate occurring in the 60/40 SDS/SOBS solutions. It has already been shown in this study that inclusion occurs in these systems, and it is very likely occurring in this case as well. The crystals from 40/60 SDS/SOBS are much smaller than for either of the pure component crystals. They range in size from less than 1 μm to about 7 μm. Many of the crystals throughout the sample are flat with holes in the center. This characteristic was not seen in the other samples. There are also many small, jagged peaks, and also a few tall, jagged peaks that look like the pure $Ca(OBS)_2$ crystals and the ones seen from the 60/40 SDS/SOBS solution. It may be

that the formation of the two very different appearing crystals relates to the different precipitate compositions forming during the step-wise precipitation process.

Differences in the crystal morphologies and habits can be seen by looking at these same AFM graphs in the "top view". These graphs are shown in Figures III.31-III.34 for $Ca(DS)_2$ crystals, $Ca(OBS)_2$ crystals, crystals from a 60/40 SDS/SOBS solution, and crystals from a 40/60 SDS/SOBS solution. Flat trapezoidal and hexagonal shaped $Ca(DS)_2$ crystals with rising spiral patterns can be seen in Figure III.31. The $Ca(OBS)_2$ crystals are shown in Figure III.32, with more elongated and amorphous-like shapes. In Figure III.33, the crystals from the 60/40 SDS/SOBS solution show some shapes that are similar to the crystal shapes formed from the pure SDS solution, but are less angular, and the rising of the spiral formation is not as evident. There are also smaller amorphous-like formations on the tops which correspond to the jagged peaks seen in the 3-D figure. The much smaller flat, crystals from the 40/60 SDS/SOBS solution shown in Figure III.34 have holes which are prevalent throughout the sample studied. Some elongated shapes and amorphous-like crystals are present as well. The taller, amorphous-like crystals look similar to the ones seen on the tops of the flat crystals in Figure III.33.

Figures III.35-III.38 compare flat portions of the crystals from the same solutions over an 8 to 10 μm scale. This allows a closer look at a portion of the surface structure of these crystals. These pictures are not an attempt to characterize the entire crystal sample, but are examples of some of the crystal surfaces present in each sample. Only flat portions of the crystals were scanned, so the more detailed structure of jagged areas cannot be extrapolated from the information obtained here. The crystals from a flat portion of a pure $Ca(DS)_2$ crystal shows that many smaller layers make up the flat surface. Several $Ca(OBS)_2$ crystals from a relatively flat area

show many steps and high walls. The crystal surface shown from the 60/40 SDS/SOBS solution displays many layers and steps as well as a peak growing from the flat surface. The crystal from the 40/60 SDS/SOBS solution shown here is one of the flat surfaces with a hole in the center. Steps are seen as well as very flat layers. Figure III.39 shows a closer view of the top of a crystal from the 40/60 SDS/SOBS solution. It is interesting to see several discontinuous planes at the far right of the picture, even far inside the crystal. This picture looks like a spiral formation is trying to form, but the stresses in the crystal may be keeping this from occurring.

3.4.10 Image Analysis

Image analysis at 40 X magnification was used to determine crystal habit for various crystals after 4 minutes elapsing upon mixing of the reactants. These pictures are shown in Figures III.40-III.43 for 0.075 M SOBS with 0.01 M $CaCl_2$, 0.01 M SDS with 0.008 M $CaCl_2$, and the mixtures 0.01 M SDS/0.002 M SOBS (83/17 SDS/SOBS) and 0.01 M SDS/0.004 M SOBS (71/29 SDS/SOBS), each with 0.008 M $CaCl_2$. Many $Ca(OBS)_2$ crystals are elongated flat plates with jagged edges. Some jagged-edged trapezoidal shapes are present in the samples as well. The $Ca(DS)_2$ crystals are mostly trapezoidal and rhombic in shape with a few hexagonal shapes. The crystals from the mixtures are much smaller at 4 minutes after mixing, with the crystals from the 83/17 SDS/SOBS solution mostly irregularly-shaped flat plates and the crystals from the 71/29 SDS/SOBS solution more needle-like. The crystals from the mixed solutions have different crystal habits from the pure crystals. A change in crystal habit in the presence of adsorbing components is a well-documented phenomenon in the crystallization literature. Adsorption of a surfactant onto certain

faces of the crystal will stunt the outward growth of that face, causing other faces to grow outward more quickly.

Image analysis was also used to view the crystals after aging for one week. The resulting scanned images are shown in Figures III.44-III.47 for 40 X magnification. These pictures were taken to view the crystals after ripening have occurred. The crystals from 0.075 M SOBS solution and 0.01 M $CaCl_2$ are long, clear, needle-like crystals, as shown in Figure III.44. The crystals from 0.01 M SDS solution and 0.008 M $CaCl_2$ are mostly clusters as shown in Figure III.45. The 83/17 and 71/29 SDS/SOBS mixtures seem to have both types of crystals present. There are long flat crystals similar to what is seen in the pure SOBS system along with clusters as seen in the pure SDS system. The crystals from the more concentrated SDS solution seems to have more clusters present than the crystals from the less concentrated solution. The long crystals, however, are not as well-shaped as seen in the pure $Ca(OBS)_2$ crystals. It appears that at least part of the surfactant components in the crystals are separating into more pure crystals.

3.5 Conclusions

For pure SDS, as the supersaturation ratio is increased, the rate of precipitation increases both below and above the CMC. A supersaturation ratio that only takes into account the monomer surfactant concentration and the unbound calcium concentration is able to describe the precipitation reaction above the CMC. An increase in the supersaturation ratio also resulted in a decrease in the induction time. For anionic surfactant mixtures, individual supersaturation ratios based on monomer concentrations describe the general trend in the precipitation rate as the SDS/SOBS

composition in solution is changed. It was found that the induction time for some solutions was increased by filtering the water from which the solutions are made, indicating heterogeneous nucleation occurred in these systems. From precipitate composition studies at equilibrium, it was found that OBS^- can adsorb onto $Ca(DS)_2$ crystals, which caused deviations of experimental hardness tolerances from the theory in solutions where $Ca(DS)_2$ was present. Image analysis showed differences in crystal habit as SOBS is added to an SDS solution, indicating that adsorption and coprecipitation (by inclusion) are most likely occurring. Adsorption and growth are thought to be responsible for the extremely large amounts of time for the occurrence of precipitation which was seen for the 60/40 SDS/SOBS systems. The growth of one crystalline phase on the screw dislocation of the other crystalline phase seen by AFM for the 60/40 SDS/SOBS system would stop the growth at the screw dislocation. This, combined with supersaturation being satiated by adsorption during crystal growth and possibly entrapment of the mother liquor, would drastically increase the amount of time for precipitation to occur. Nonequilibrium studies on crystal compositions of precipitate from SDS/SOBS mixtures have shown that either precipitating component is able to bring down the other surfactant component into the solid phase. In this system, it is thought that the mechanism for this behavior is inclusion due to adsorption and entrapment of the mother liquor in the crystalline phase. Since it has been shown that DS^- does not tend to adsorb onto the $Ca(OBS)_2$ crystal surfaces, the inclusion of DS^- into $Ca(OBS)_2$ crystals may be mostly or entirely due to entrapment of the mother liquor. The holes in the planes seen in the AFM graphs of some of the crystals for the 40/60 SDS/SOBS system show that entrapment of the mother liquor in these crystals is probable. It has been shown that the step-wise extent of precipitation curve is a result of two different compositions of crystals

forming, each with a separate induction time. The AFM graph taken for this mixture shows two types of crystal formations which may correlate with the two crystal compositions. However, an in situ visual study (such as with an AFM) would have to be done to confirm this conclusion. The AFM was also used to obtain graphs of what seem to be surfactant head groups in the crystalline lattices for the pure surfactants. The head groups for both surfactants are arranged in hexagonal patterns with sizes that seem reasonable for these surfactants in a crystal lattice.

3.6 References

(1) Peacock, J.M.; Matijevic, E. *J. Colloid Interface Sci.* **1980**, *77*, 548.

(2) Fan, X.J.; Stenius, P.; Kallay, N.; Matijevic, E. *J. Colloid Interface Sci.* **1988**, *121*, 571.

(3) Stellner, K.L.; Scamehorn, J.F. *Langmuir* **1989**, *5*, 70.

(4) Stellner, K.L.; Scamehorn, J.F. *Langmuir* **1989**, *5*, 77.

(5) Stellner, K.L.; Amante, J.C.; Scamehorn, J.F.; Harwell, J.H. *J. Colloid Interface Sci.* **1988**, *123*, 186.

(6) Matheson, K.L.; Cox, M.F.; Smith, D.L. *J. Amer. Oil Chem. Soc.* **1985**, *62*, 1391.

(7) Matheson, K.L. *J. Amer. Oil Chem. Soc.* **1985**, *62*, 1269.

(8) Scamehorn, J.F.; Schechter, R.S.; Wade, W.H. *J. Colloid Interface Sci.* **1982**, *85*, 463.

(9) Klotz, I.R.; Rosenberg, R.M. *Chemical Thermodynamics: Basic Theory and Methods*, 4th ed.; Krieger Publishing Co.: Malabar, 1991; pp 440-442.

(10) Scamehorn, J.F. In *Mixed Surfactant Systems*; Holland, P.M.; Rubingh, D.N., Eds.; American Chemical Society: Washington, 1992; ACS Symp. Ser., Vol. 501, pp 392-401.

(11) Davies, C.W. *Ion Association*; Butterworths: London, 1962; p 41.

(12) Robinson, R.A.; Stokes, R.H. *Electrolyte Solutions*, 2nd ed.; Butterworths: London, 1959; pp 174-252.

(13) Amante, J.C.; Scamehorn, J.F.; Harwell, J.H. *J. Colloid Interface Sci.* **1991**, *144*, 243.

(14) Burchfield, T.E.; Woolley, E.M. *J. Phys. Chem.* **1984**, *88*, 2149.

(15) Dharmawardana, U.R.; Christian, S.D.; Tucker, E.E.; Taylor, R.W.; Scamehorn, J.F. *Langmuir* **1993**, *9*, 2258.

(16) Scamehorn, J.F.; Harwell, J.H. In *Mixed Surfactant Systems*; Ogino, K.; Abe, M., Eds.; Marcel Dekker: New York, 1993; pp 283-312.

(17) Tsujii, K.; Saito, N.; Takeuchi, T. *J. Phys. Chem.* **1980**, *84*, 2287.

(18) Scamehorn, J.F. In *Phenomena in Mixed Surfactant Systems*; Scamehorn, J.F., Ed.; American Chemical Society: Washington, 1986; ACS Symp. Ser., Vol. 311, pp 1-27.

(19) Shinoda K. In *Colloidal Surfactants*; Shinoda, K.; Tamamushi, T.; Nakagawa, T.; Isemura, T., Eds.; Acad. Press: New York, 1963; pp 35-58.

(20) Lieser, K.H. *Angew. Chem. Internat. Edit.* **1969**, *8*, 188 .

(21) Konak, A.R. *Kristall. und Technik.* **1974**, *9*, 243.

(22) Johnson, R.A.; O'Rourke, J.D. *J. Amer. Chem. Soc.* **1954**, *76*, 2124.

(23) Mullin, J.W. *Crystallization*, 3rd ed.; Butterworth-Heinemann: Boston, 1993; pp 8-172.

(24) Nývlt, J.; Söhnel, O.; Matuchová, M.; Broul, M. *The Kinetics of Industrial Crystallization*; Elsevier: New York, 1985; pp 35-148.

(25) Clarke, D.E.; Lee, R.S.; Robb, I.D. *Faraday Disc. Chem. Soc.* **1976**, *61*, 165.

(26) Mullin, J.W. *Crystallization*, 3rd ed.; Butterworth-Heinemann: Boston, 1993; pp 180-186.

(27) Walton, A.G. *The Formation and Properties of Precipitates*; Wiley: New York, 1967; pp 1-43.

(28) Randolph, A.D.; Larson, M.A. *Theory of Particulate Processes*, 2nd ed.; Acad. Press: San Diego, 1988; pp 109-134.

(29) Adamson, A.W. *Physical Chemistry of Surfaces*, 5th ed.; Wiley: New York, 1990; pp 364-378.

(30) Nielsen, A.E., *Kinetics of Precipitation*; MacMillan: New York, 1964; pp 29-119.

(31) Frank, F.C. *Discuss. Faraday Soc.* **1949**, *5*, 48.

(32) Rawles, R. *C & E N* **1996**, *August 26*, 32.

(33) Walton, A.G. *The Formation and Properties of Precipitates*; Wiley: New York, 1967; pp 44-78.

(34) Nývlt, J.; Söhnel, O.; Matuchová, M.; Broul, M. *The Kinetics of Industrial Crystallization*; Elsevier: New York, 1985; pp 149-213.

(35) Mullin, J.W. *Crystallization*, 3rd ed.; Butterworth-Heinemann: Boston, 1993; pp 202-263.

(36) Adamson, A.W. *Physical Chemistry of Surfaces*, 5th ed.; Wiley: New York, 1990; pp 291-328.

(37) Walton, A.G. *The Formation and Properties of Precipitates*; Wiley: New York, 1967; pp 79-94.

(38) Rodriguez, C.H. *Ph.D. Dissertation*; The University of Oklahoma, 1997.

(39) Heughebaert, J.C.; Zawacki, S.J.; Nancollas, G.H. *J. Crystal Growth* **1983**, *63*, 83.

(40) Lowery, L., M.S. Thesis, The University of Oklahoma, 1994.

Table III.1 Comparison of Initial Supersaturation Ratios (S_o) with Precipitate SDS/SOBS Molar Ratios for Various 0.075 M SDS/SOBS Mixtures Precipitated with 0.01 M $CaCl_2$ at 30 °C

SDS/SOBS	S_o SDS	S_o SOBS	SDS/SOBS in Prec.
0/100	0.00	5.44	0.0/100.0
20/40	0.84	4.16	0.0/100.0
40/60	1.36	3.49	-
60/80	1.73	2.59	-
80/20	1.93	1.50	-
100/0	1.98	0.00	-

Table III.2 Comparison of Initial Supersaturation Ratios (S_o) with Precipitate SDS/SOBS Molar Ratios for Various 0.0288 M SDS/SOBS Mixtures Precipitated with 0.01 M $CaCl_2$ at 30 °C

SDS/SOBS	S_o SDS	S_o SOBS	SDS/SOBS in Prec.
0/100	0.00	8.90	0.0/100.0
20/80	1.76	7.42	0.0/100.0
40/60	2.64	5.84	0.0/100.0
60/40	3.38	4.37	1.8/98.2
80/20	3.91	2.65	96.1/3.9
100/0	4.31	0.00	100.0/0.0

Table III.3 Comparison of Initial Supersaturation Ratios (S_o) for Various 0.0192 M SDS/SOBS Mixtures Precipitated with 0.01 M $CaCl_2$ at 30 °C

SDS/SOBS	S_o SDS	S_o SOBS
0/100	0.00	10.11
20/80	2.20	8.17
40/60	3.22	6.48
60/40	4.29	4.96
80/20	4.76	2.89
100/0	5.42	0.00

Table III.4 Comparison of Initial Supersaturation Ratios (S_o) with Precipitate SDS/SOBS Molar Ratios for Various 0.0096 M SDS/SOBS Mixtures Precipitated with 0.01 M $CaCl_2$ at 30 °C

SDS/SOBS	S_o SDS	S_o SOBS	SDS/SOBS in Prec.
0/100	0.00	9.25	0.0/100.0
20/80	3.01	8.01	6.8/93.2
40/60	4.74	6.56	22.0/78.0
60/40	5.71	4.82	11.8/88.2
80/20	6.45	2.93	81.1/18.9
100/0	7.07	0.00	100.0/0.0

Table III.5 Comparison of Initial Supersaturation Ratios (S_0) with Precipitate SDS/SOBS Molar Ratios for Various 0.0025 M SDS/SOBS Mixtures Precipitated with 0.01 M $CaCl_2$ at 30 °C

SDS/SOBS	S_0 SDS	S_0 SOBS	SDS/SOBS in Prec.
0/100	0.00	3.86	0.0/100.0
20/80	1.25	3.33	0.0/100.0
40/60	1.97	2.73	21.8/78.2
60/40	2.57	2.07	64.8/35.2
80/20	3.12	1.31	95.9/4.1
100/0	3.65	0.00	100.0/0.0

Table III.6 Nonequilibrium Crystal Compositions, Precipitated from Various Supersaturated Concentrations of SDS and SOBS in the Presence of Dilute Surfactant

[SDS]	[SOBS]	SDS/SOBS in Prec.
2.5×10^{-4}	0.02	0.0/100.0
2.5×10^{-4}	0.01	18.7/81.3
2.5×10^{-4}	0.0025	9.5/90.5
2.5×10^{-4}	0.0006	8.7/91.3
2.5×10^{-4}	0.0	-
0.02	2.5×10^{-4}	97.7/2.2
0.01	2.5×10^{-4}	87.2/12.8
0.0025	2.5×10^{-4}	96.1/3.9
0.001	2.5×10^{-4}	97.9/2.1
0.0006	2.5×10^{-4}	98.1/1.9
0.0	2.5×10^{-4}	-

Table III.7 Comparison of Initial Supersaturation Ratios (So) of SDS and SOBS in 0.0096 M Surfactant SOlutions at Various Mixtures for Unfiltered Water and Water Filtered through a 10,000 MWCO Membrane

	Unfiltered Water		Filtered Water	
SDS/SOBS	S_o SDS	S_o SOBS	S_o SDS	S_o SOBS
0/100	0.00	9.25	0.00	8.87
40/60	4.74	6.56	4.81	6.65
60/40	5.71	4.82	5.63	4.76
100/0	7.07	0.00	7.10	0.00

Figure III.1 Isoperibol Calorimeter Set-Up

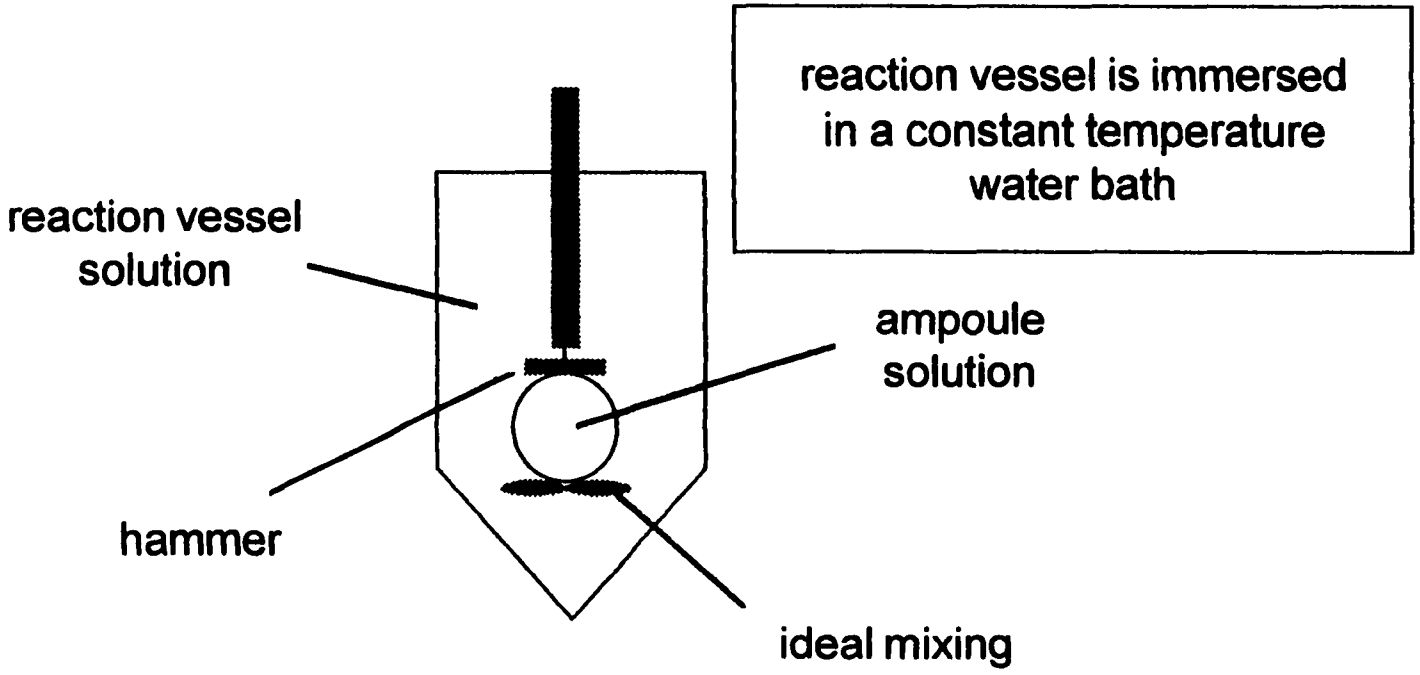


Figure III.2 Micelle-Monomer-Precipitate Equilibrium Diagram for Two Anionic Surfactants in the Presence of Calcium

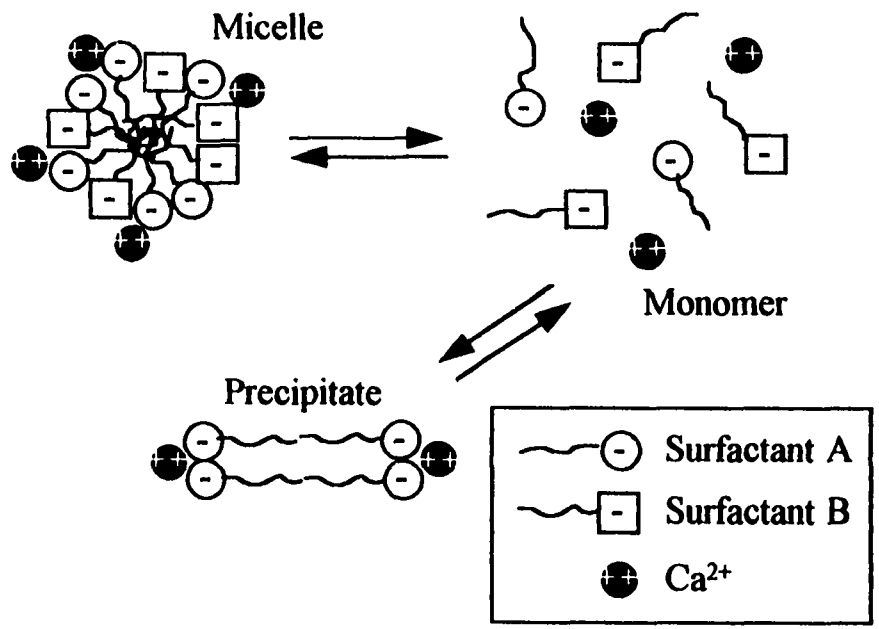


Figure III.3 Theoretical Precipitation Phase Boundaries for SDS in Various SDS/SOBS Mixtures; Comparison with Experimental Hardness Tolerance Points; 30 ^{o}C

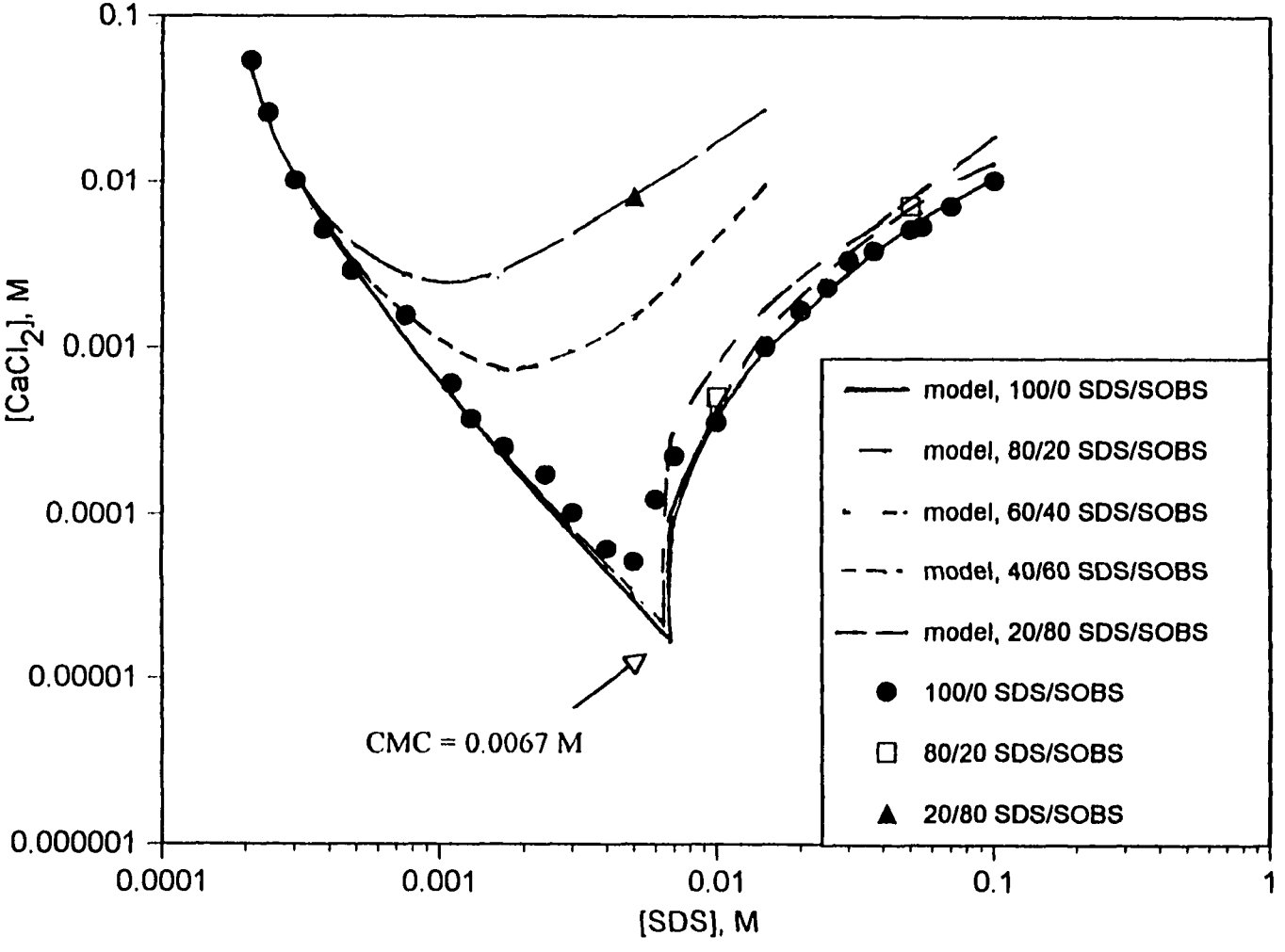


Figure III.4 Theoretical Precipitation Phase Boundaries for SOBS in Various SDS/SOBS Mixtures; Comparison with Experimental Hardness Tolerance Points; 30 ^{o}C

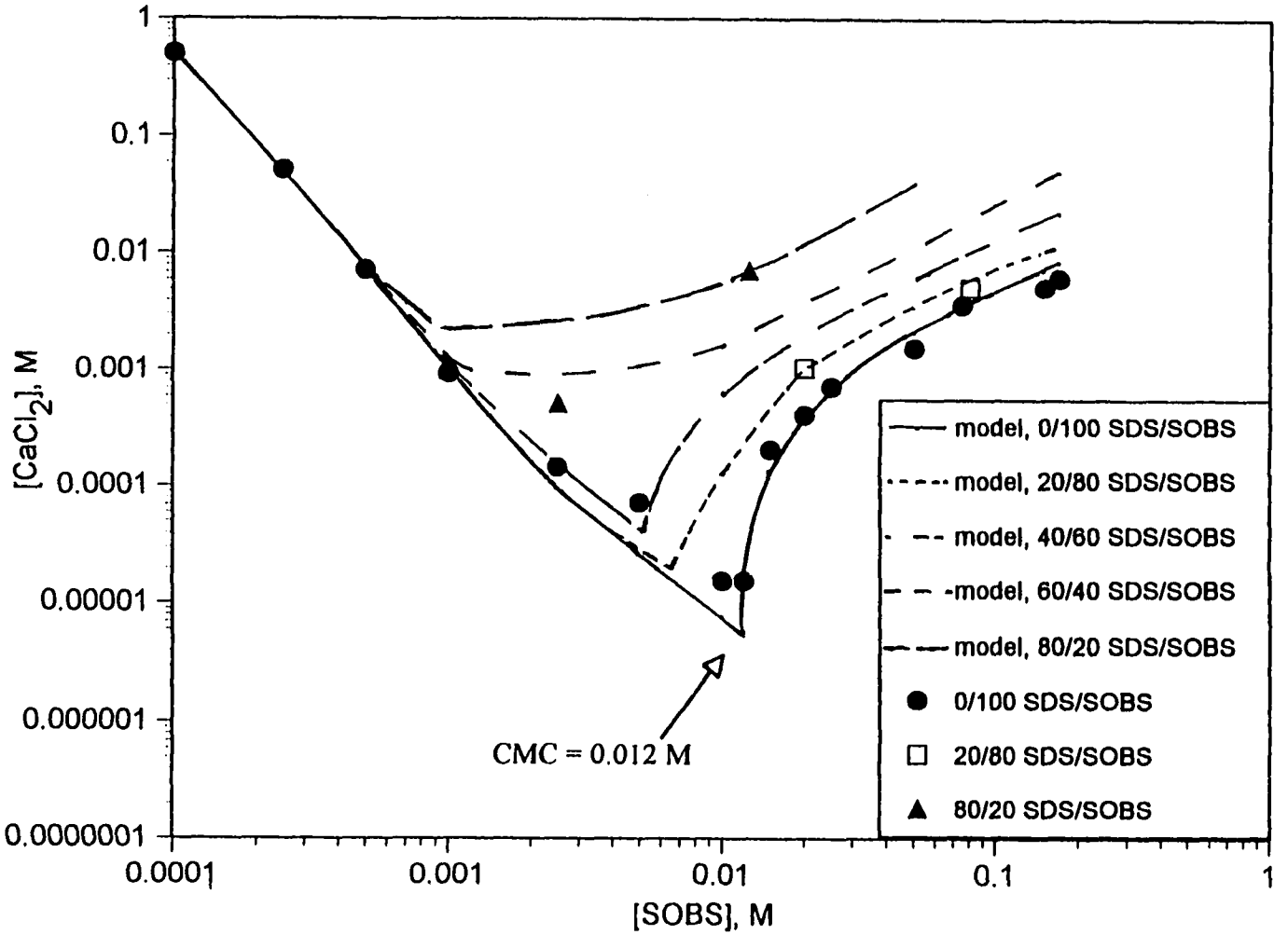


Figure III.5 Comparison Between SDS-$CaCl_2$ Precipitation Reaction Pathways for Various Total Surfactant Concentrations and 100/0 SDS/SOBS Solution, and the Precipitation Phase Boundary for SDS for the 100/0 SDS/SOBS System at 30 ^{o}C

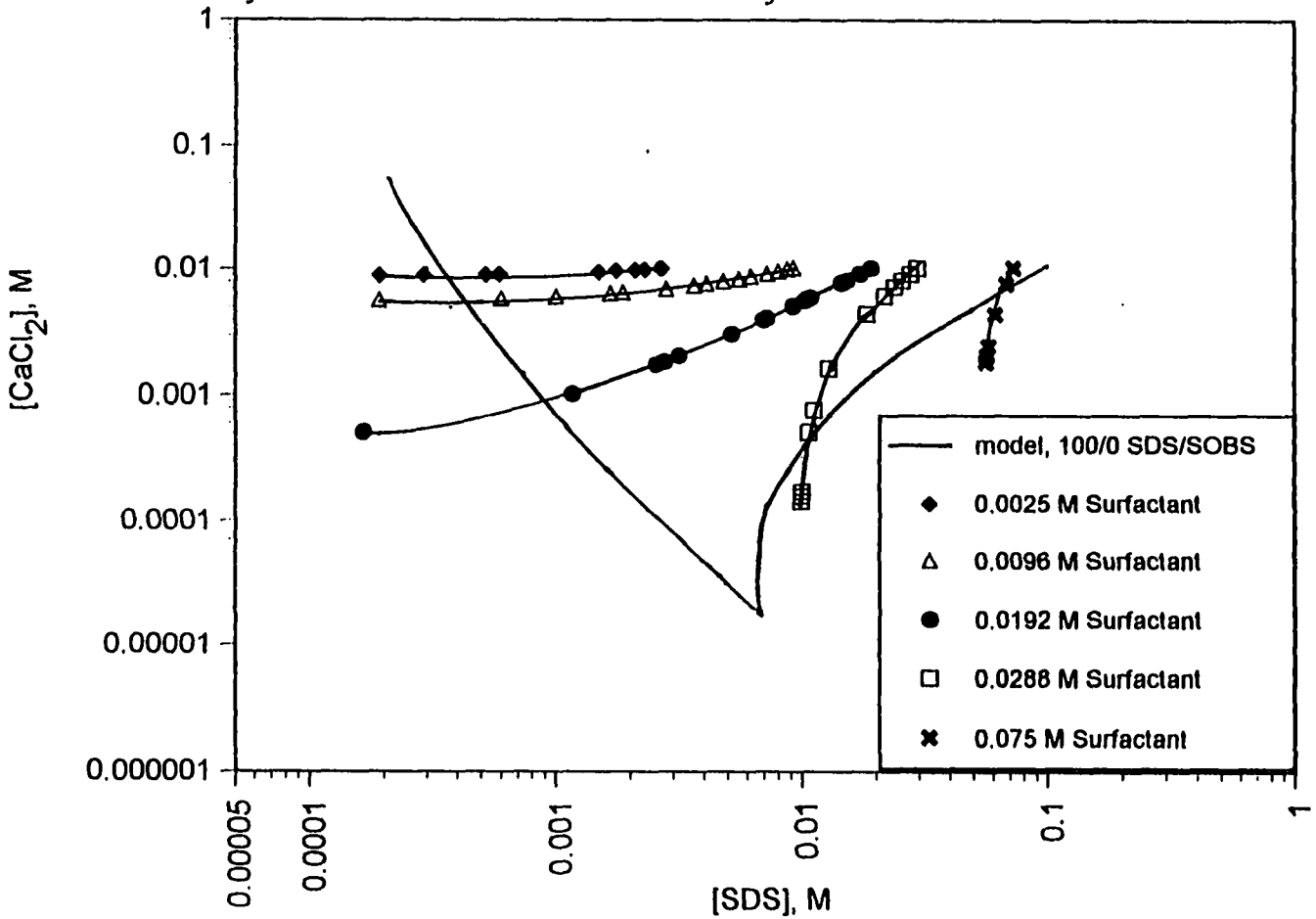


Figure III.6 Comparison Between SDS-$CaCl_2$ Precipitation Reaction Pathways for Various Total Surfactant Concentrations and 80/20 SDS/SOBS Solution, and the Precipitation Phase Boundary for SDS for the 80/20 SDS/SOBS System at 30 ^{o}C

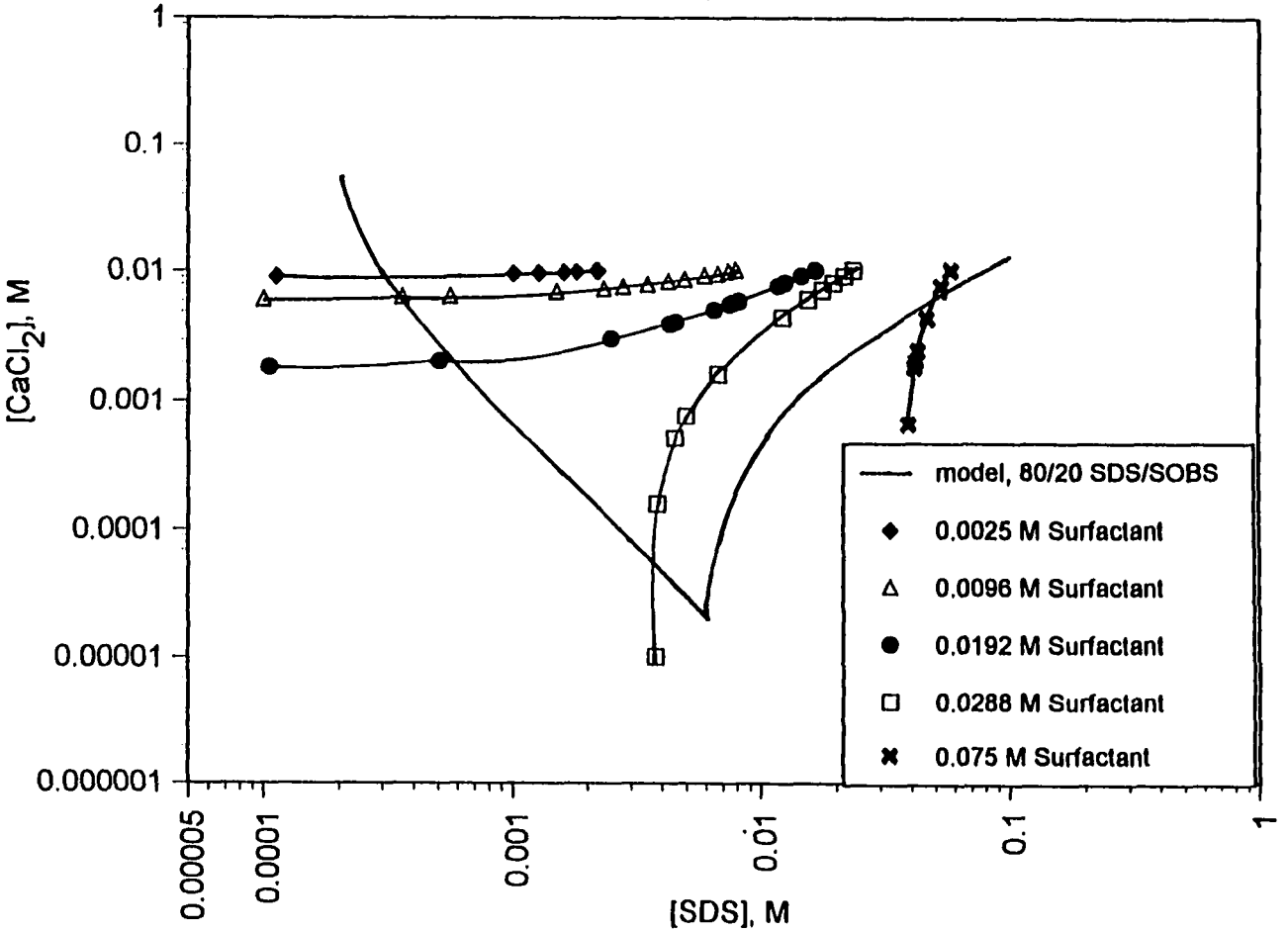


Figure III.7 Comparison Between SDS-$CaCl_2$ Precipitation Reaction Pathways for Various Total Surfactant Concentrations and 60/40 SDS/SOBS Solution, and the Precipitation Phase Boundary for SDS for the 60/40 SDS/SOBS System at 30 ^{o}C

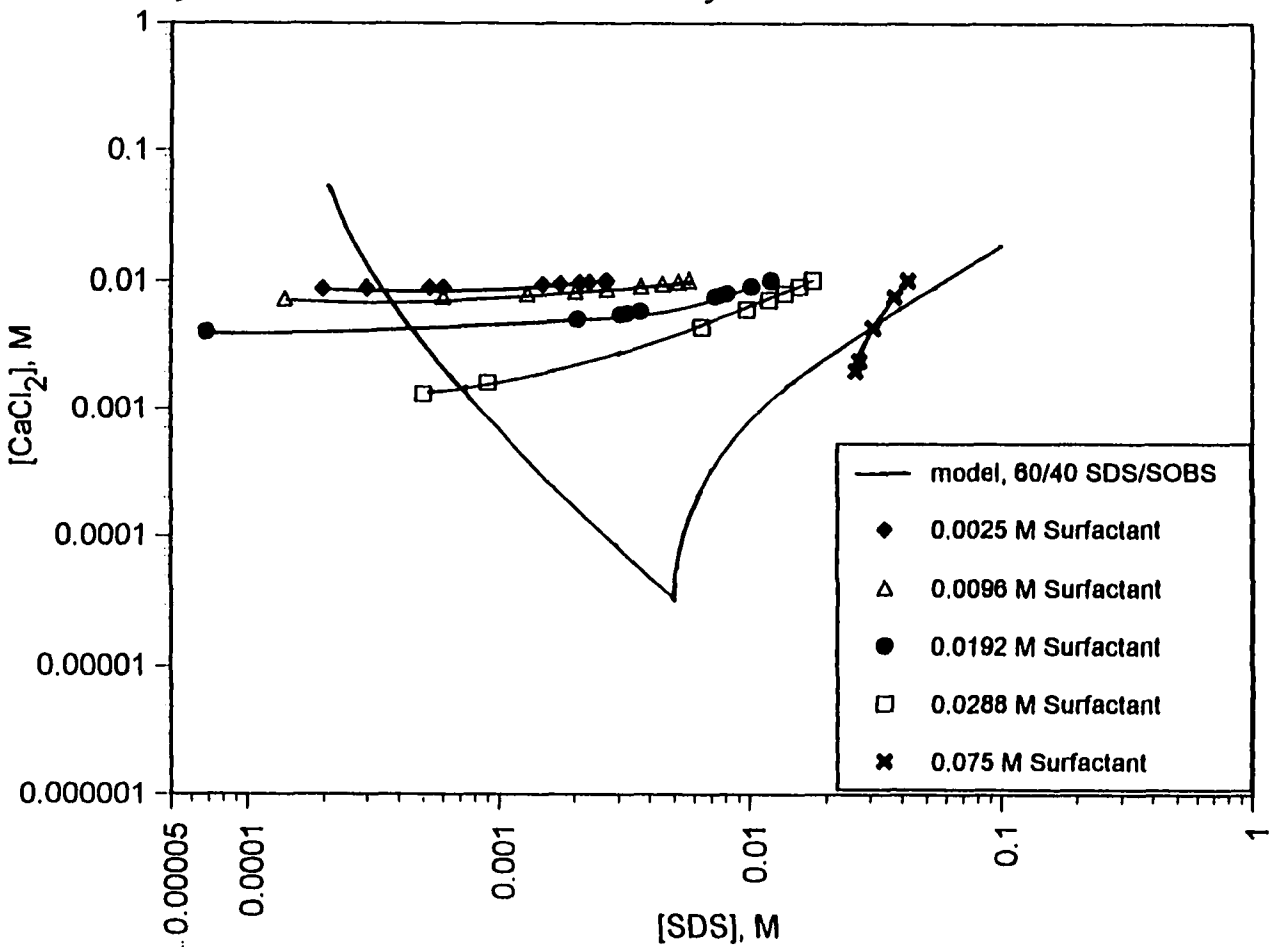


Figure III.8 Comparison Between SDS-$CaCl_2$ Precipitation Reaction Pathways for Various Total Surfactant Concentrations and 40/60 SDS/SOBS Solution, and the Precipitation Phase Boundary for SDS for the 40/60 SDS/SOBS System at 30 ^{o}C

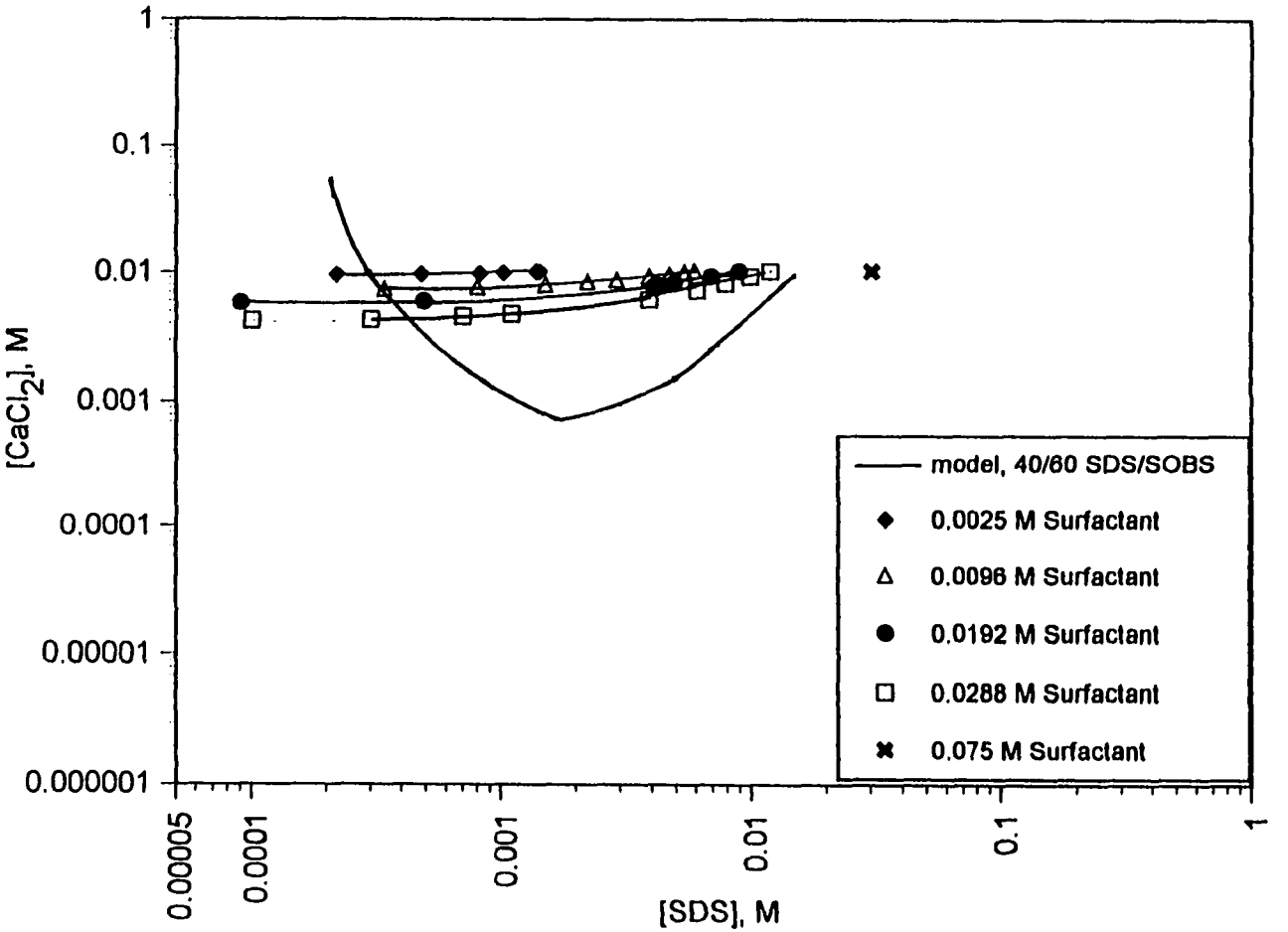


Figure III.9 Comparison Between SDS-$CaCl_2$ Precipitation Reaction Pathways for Various Total Surfactant Concentrations and 20/80 SDS/SOBS Solution, and the Precipitation Phase Boundary for SDS for the 20/80 SDS/SOBS System at 30 ^{o}C

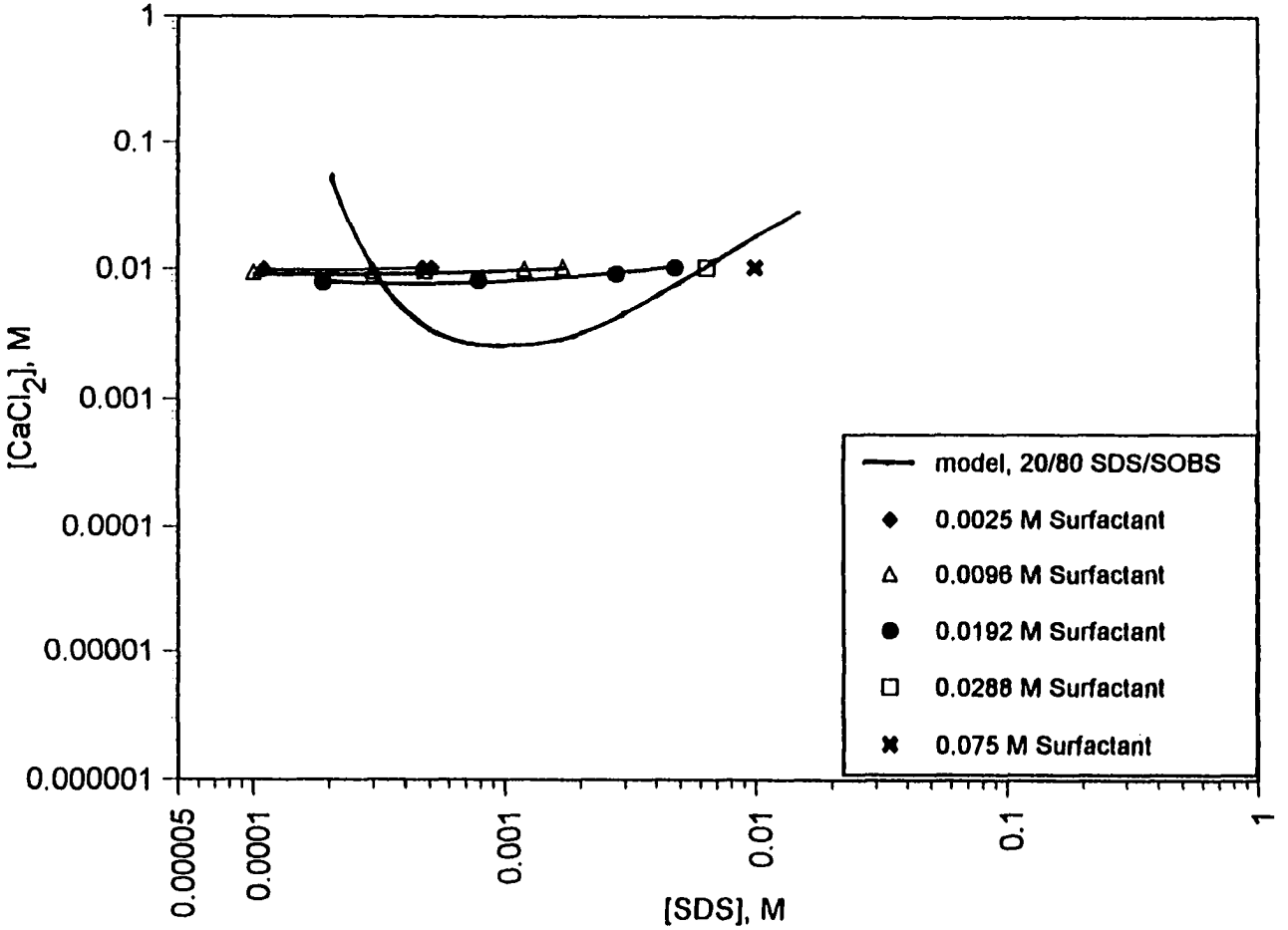


Figure III.10 Comparison Between SOBS-$CaCl_2$ Precipitation Reaction Pathways for Various Total Surfactant Concentrations and 0/100 SDS/SOBS Solution, and the Precipitation Phase Boundary for SOBS for the 0/100 SDS/SOBS System at 30 ^{o}C

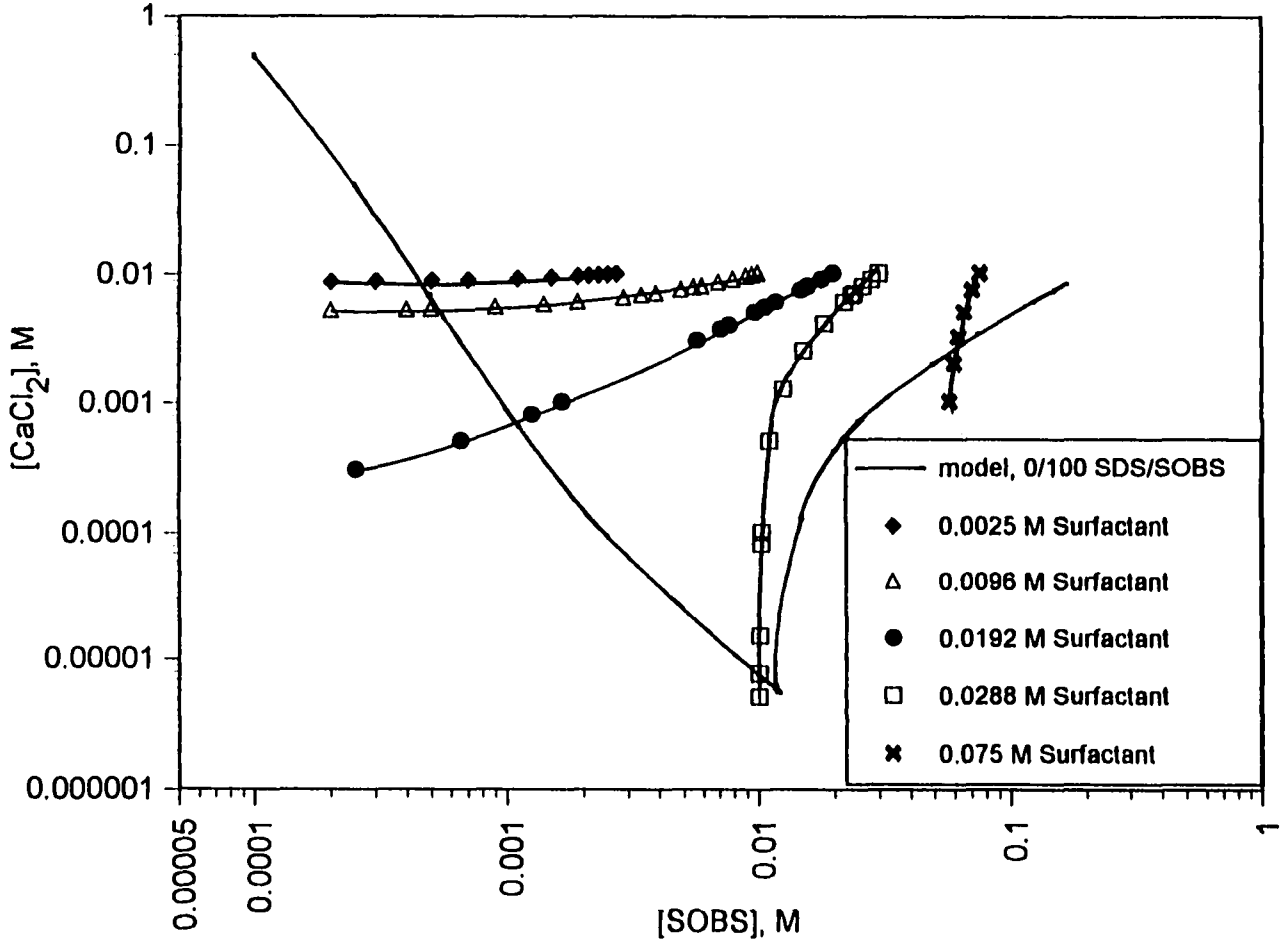


Figure III.11 Comparison Between SOBS-$CaCl_2$ Precipitation Reaction Pathways for Various Total Surfactant Concentrations and 20/80 SDS/SOBS Solution, and the Precipitation Phase Boundary for SOBS for the 20/80 SDS/SOBS System at 30 ^{o}C

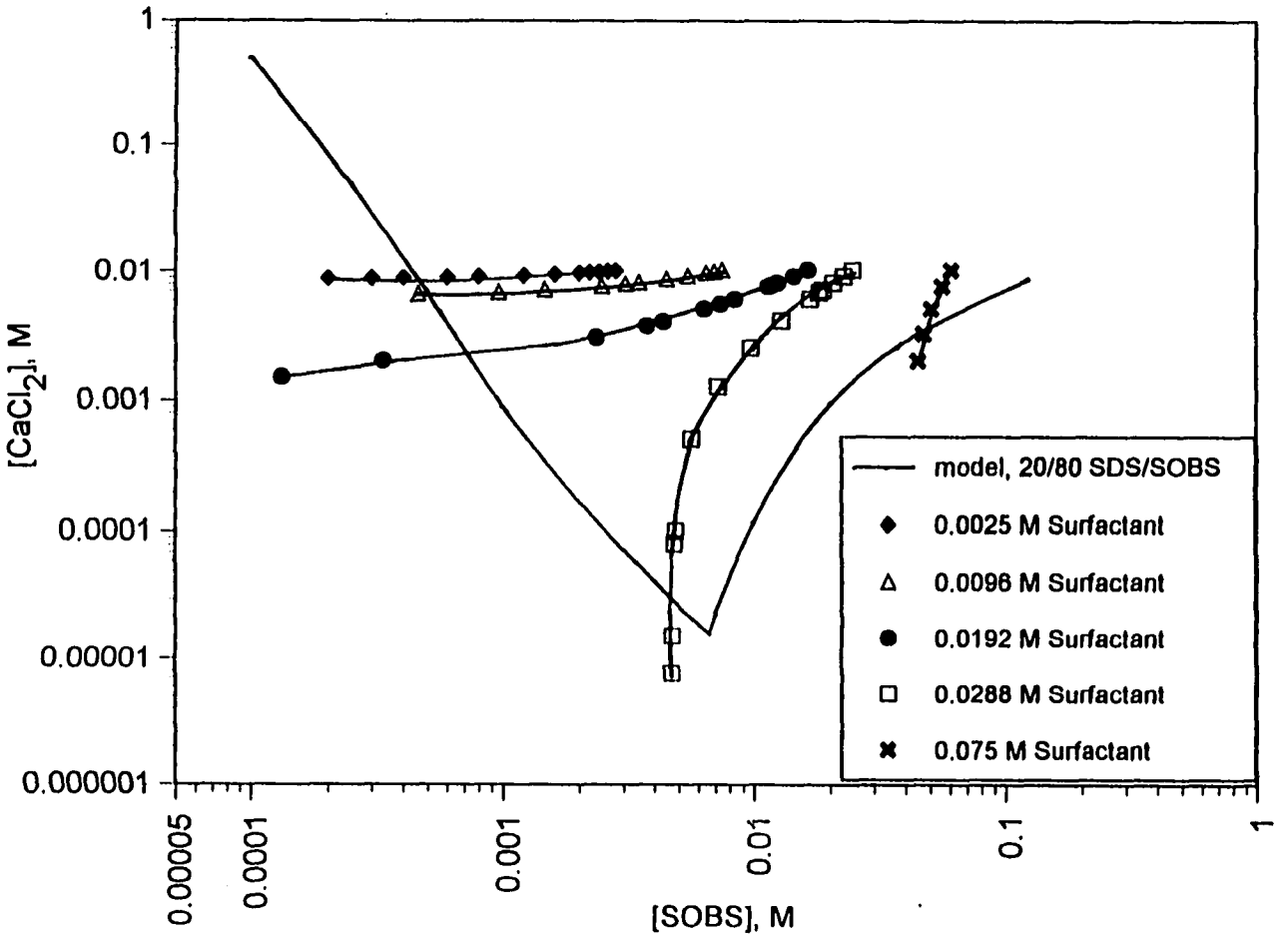


Figure III.12 Comparison Between SOBS-$CaCl_2$ Precipitation Reaction Pathways for Various Total Surfactant Concentrations and 40/60 SDS/SOBS Solution, and the Precipitation Phase Boundary for SOBS for the 40/60 SDS/SOBS System at 30 ^{o}C

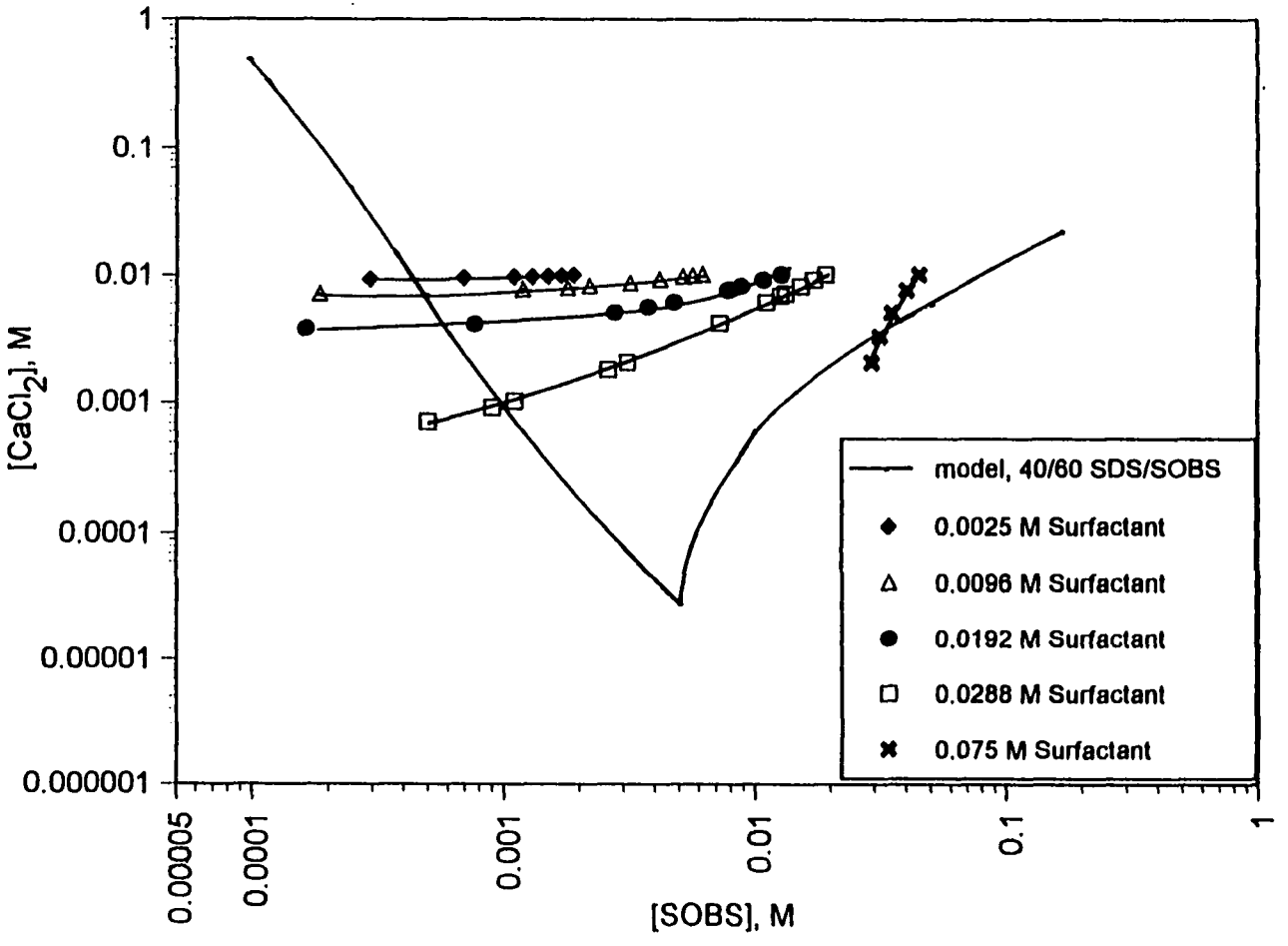


Figure III.13 Comparison Between SOBS-$CaCl_2$ Precipitation Reaction Pathways for Various Total Surfactant Concentrations and 60/40 SDS/SOBS Solution, and the Precipitation Phase Boundary for SOBS for the 60/40 SDS/SOBS System at 30 ^{o}C

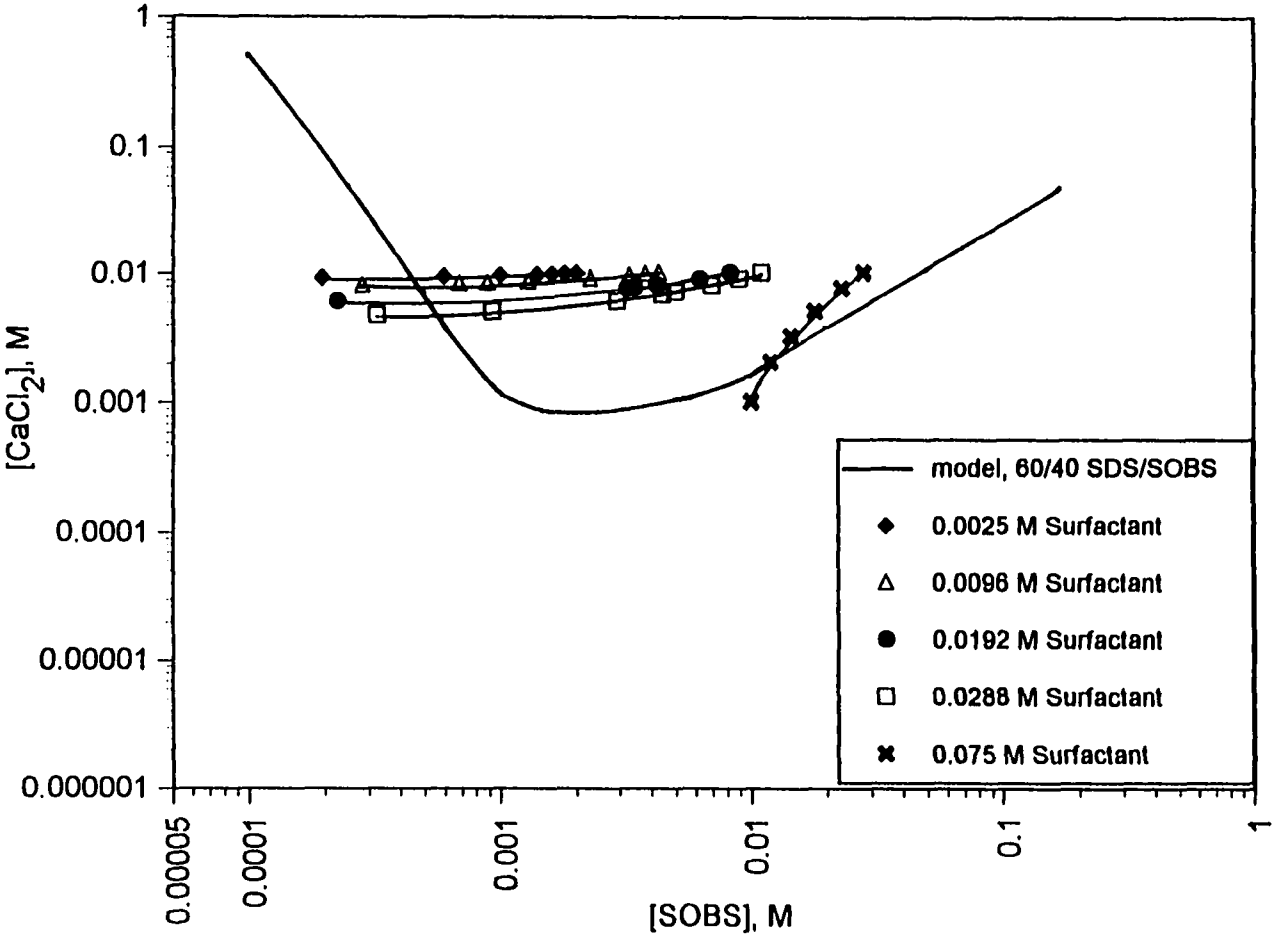


Figure III.14 Comparison Between SOBS-$CaCl_2$ Precipitation Reaction Pathways for Various Total Surfactant Concentrations and 80/20 SDS/SOBS Solution, and the Precipitation Phase Boundary for SOBS for the 80/20 SDS/SOBS System at 30 ^{o}C

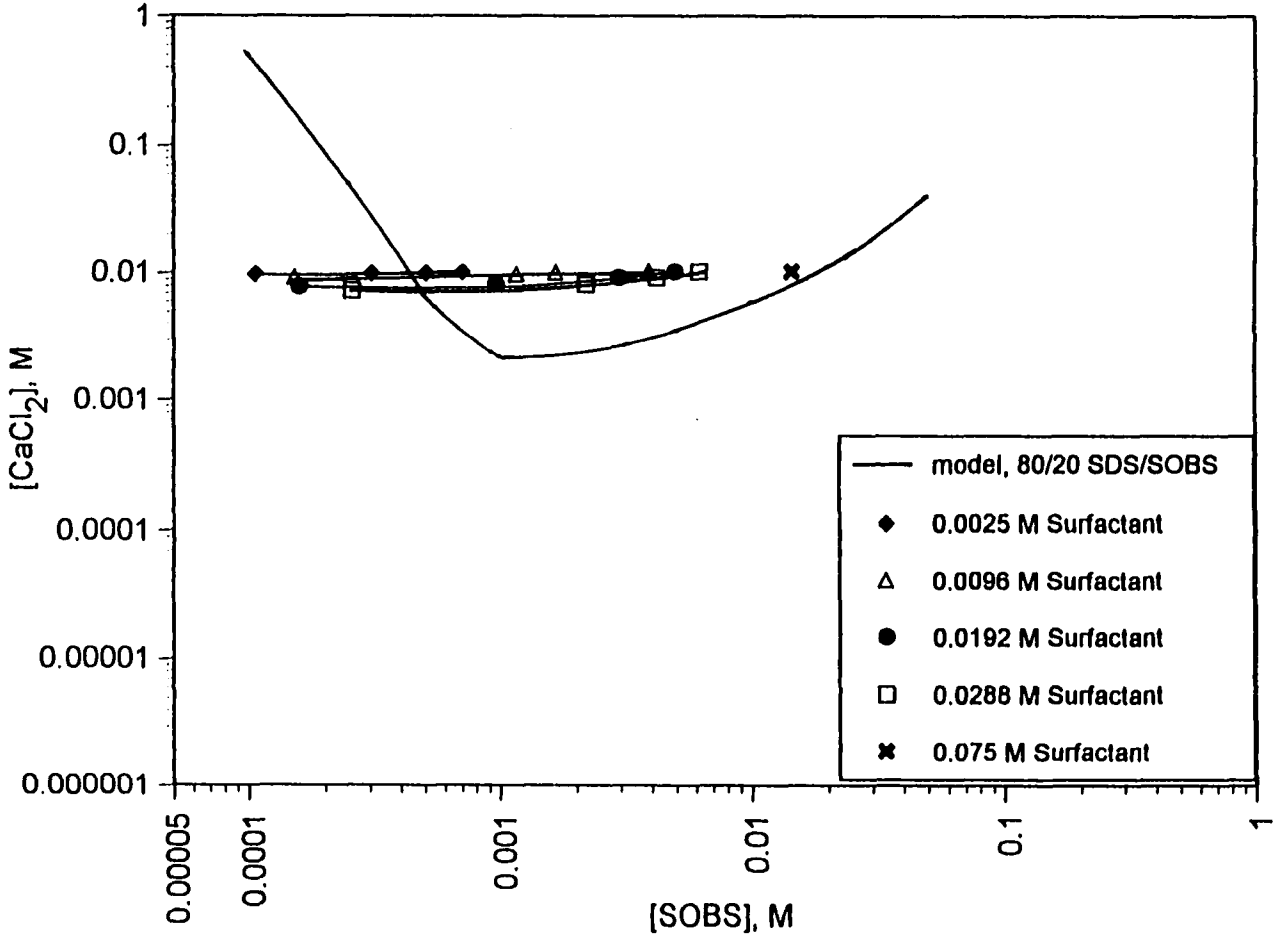
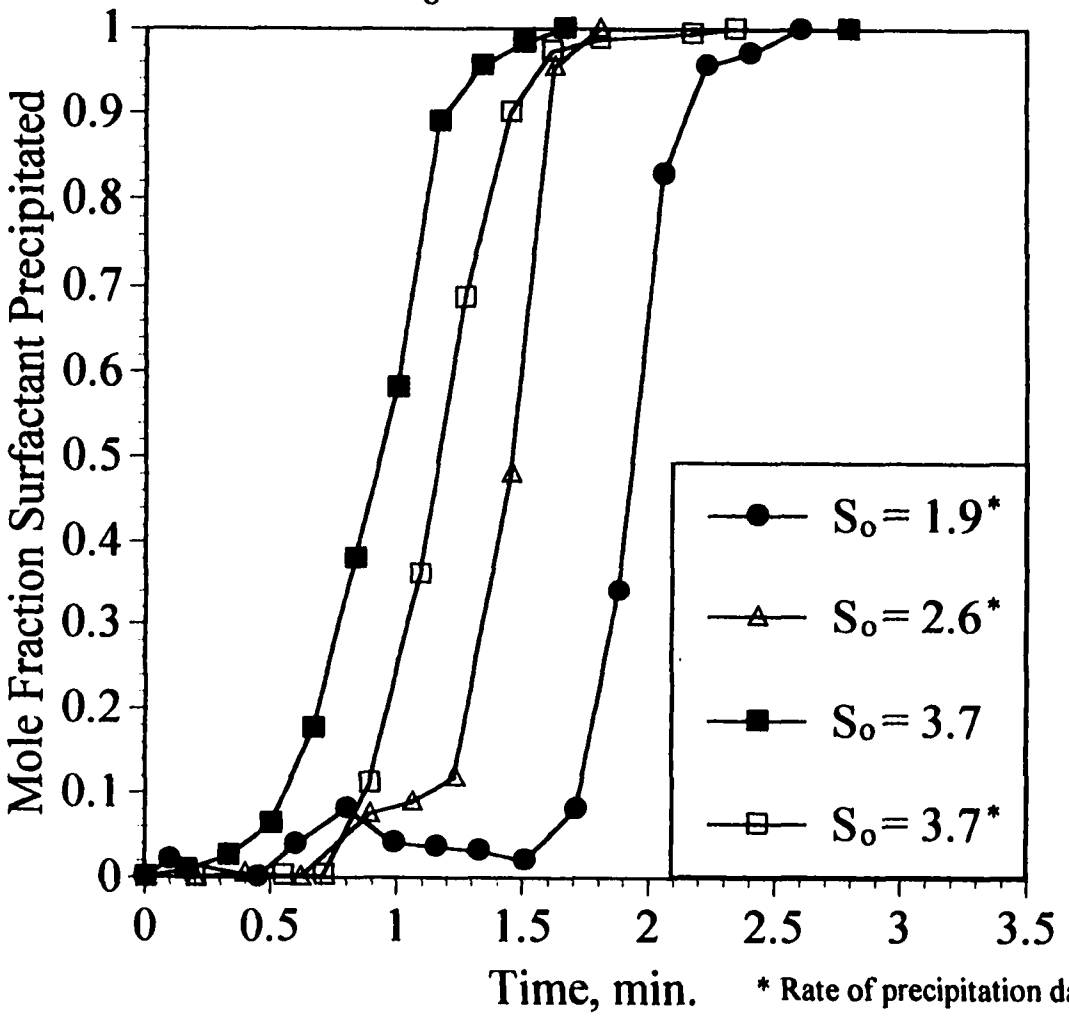
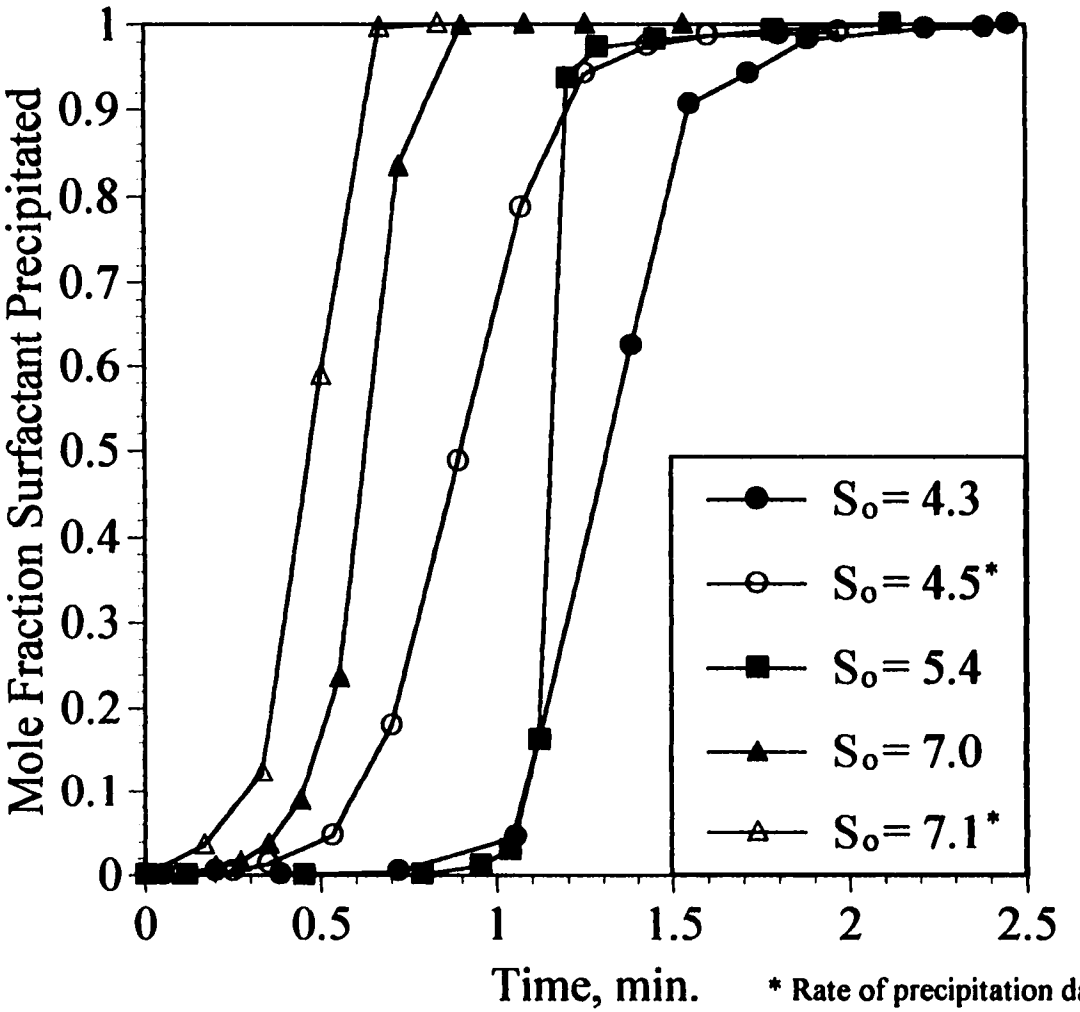


Figure III.15 Precipitation Rate Curves for SDS with Calcium for Various Supersaturation Ratios (S_o) Below the CMC and at 30 °C



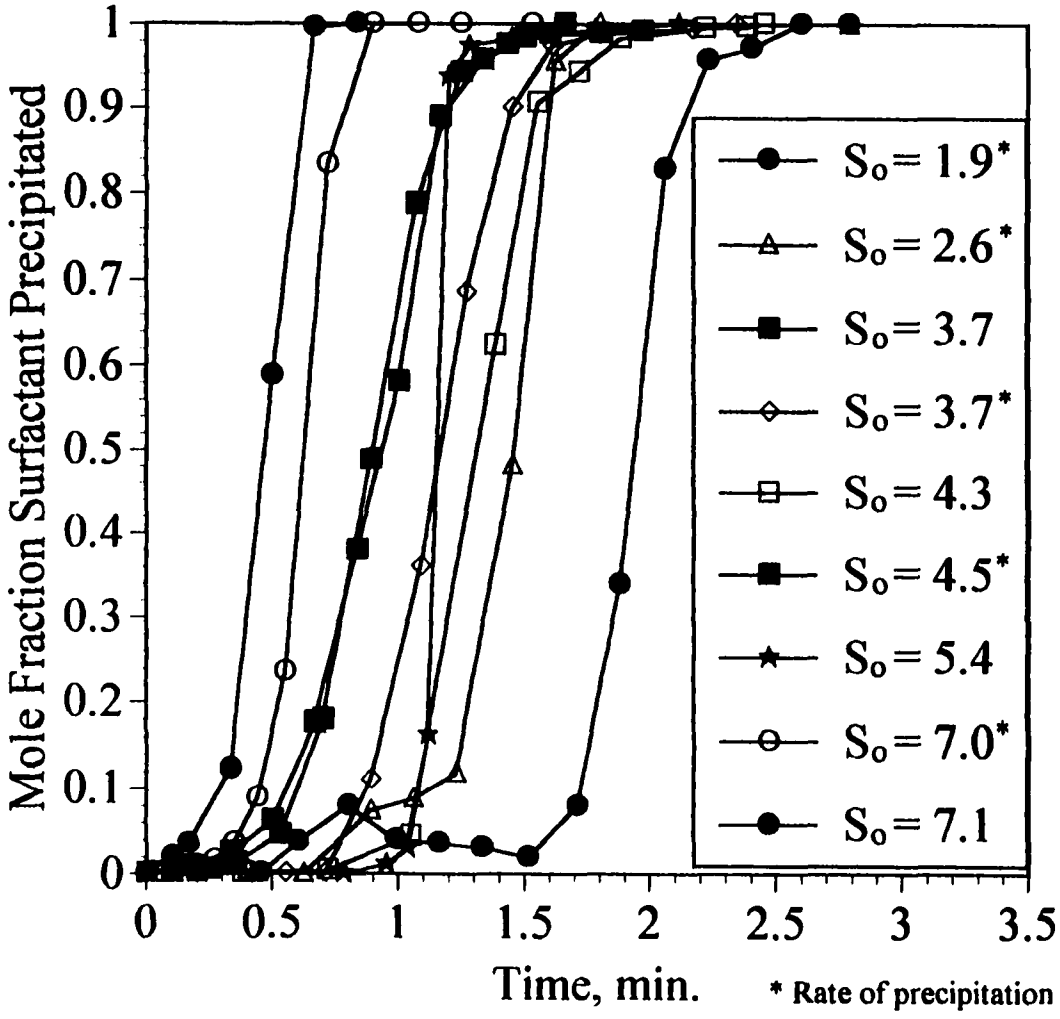
* Rate of precipitation data is from Lowery (40).

Figure III.16 Precipitation Rate Curves for SDS with Calcium for Various Supersaturation Ratios (S_o) Above the CMC and at 30 ^oC



* Rate of precipitation data is from Lowery (40).

Figure III.17 Precipitation Rate Curves for SDS with Calcium for Various Supersaturation Ratios (S_o) at 30 °C



* Rate of precipitation data is from Lowery (40).

Figure III.18 Precipitation Rate Curves for 0.075 M Total Surfactant Concentration and Varying SDS/SOBS Mole Fractions with 0.01 M $CaCl_2$ at 30 ^{o}C

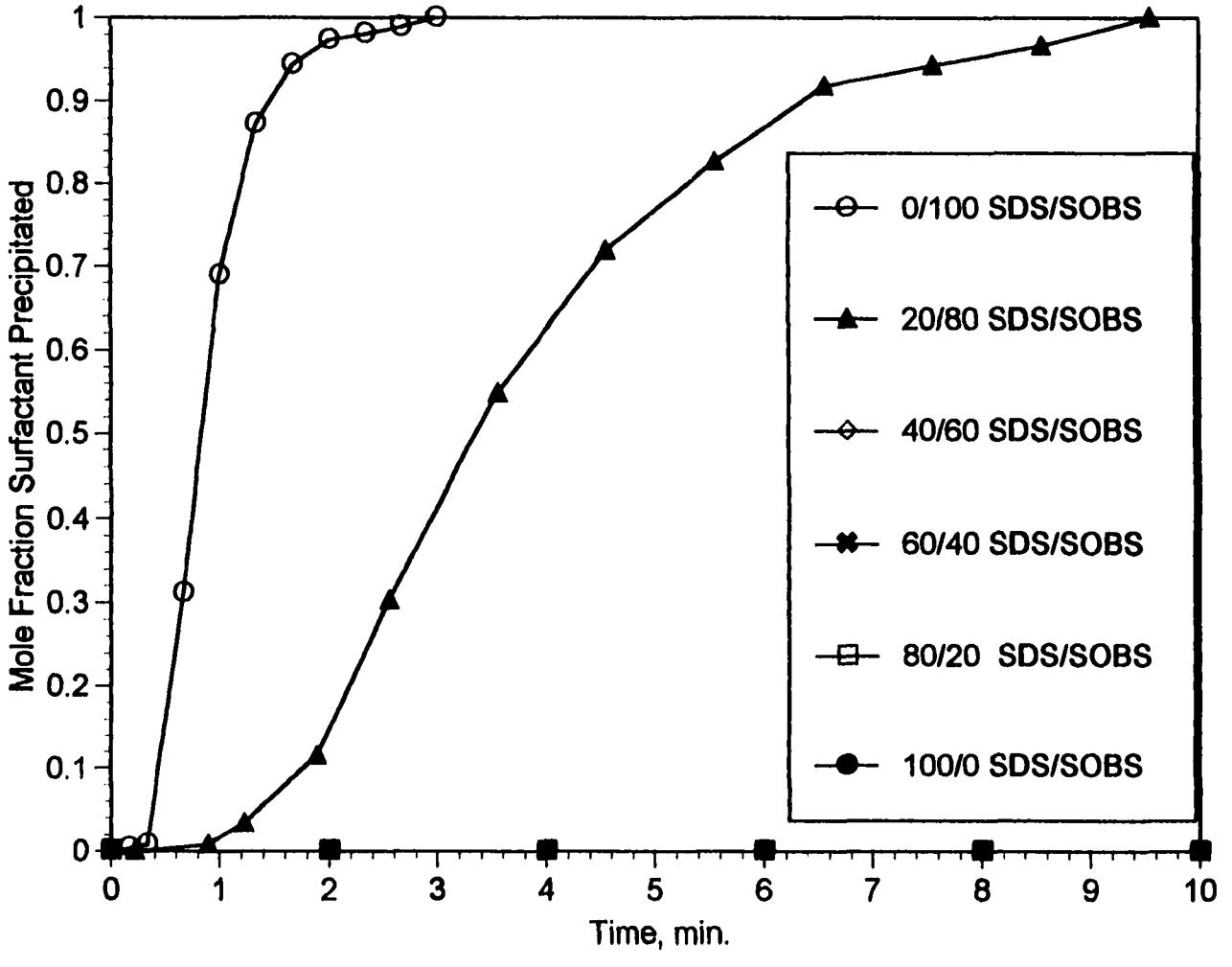


Figure III.19 Precipitation Rate Curves for 0.0288 M Total Surfactant Concentration and Varying SDS/SOBS Mole Fractions with 0.01 M $CaCl_2$ at 30 ^{o}C

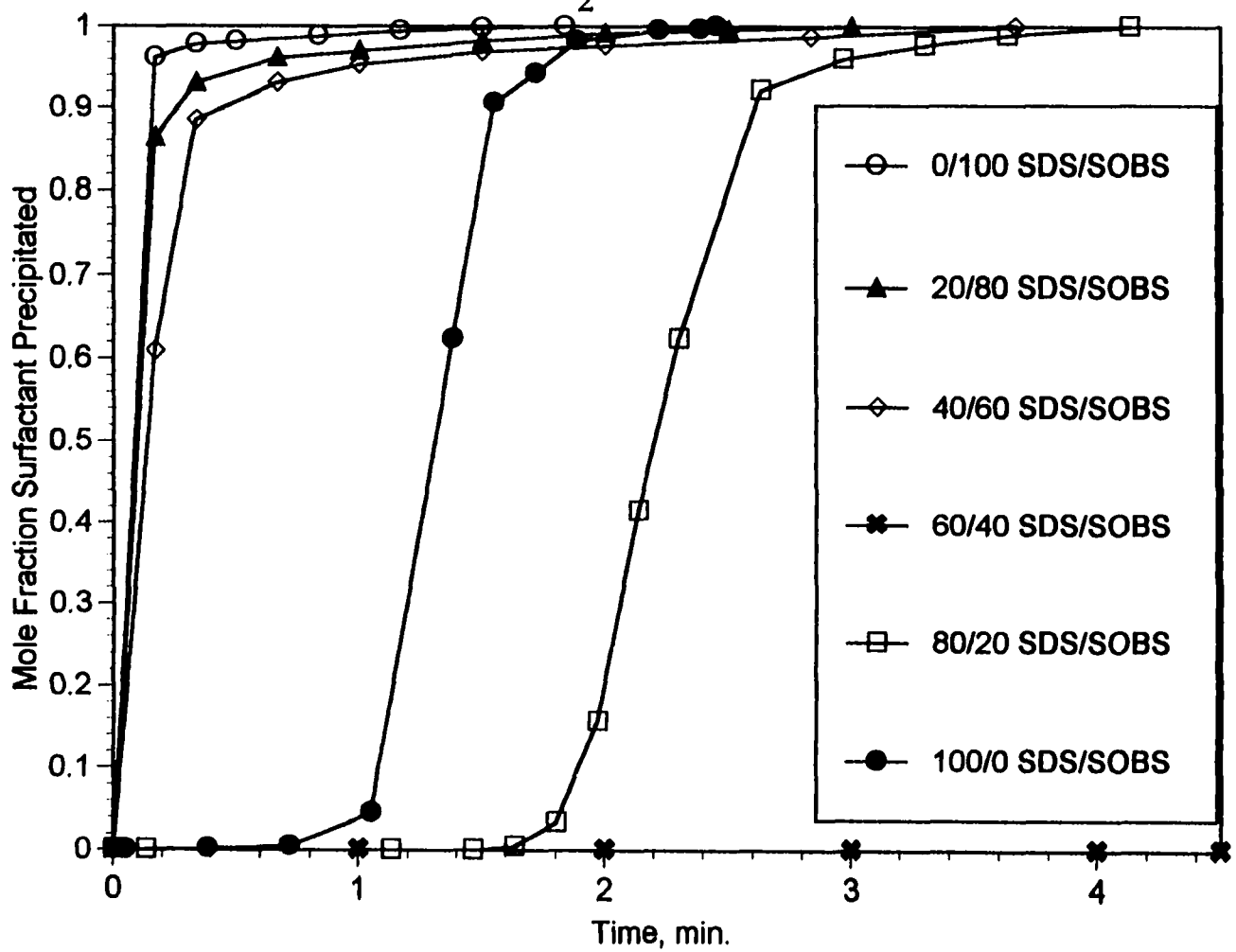


Figure III.20 Precipitation Rate Curves for 0.0192 M Total Surfactant Concentration and Varying SDS/SOBS Mole Fractions with 0.01 M $CaCl_2$ at 30 ^{o}C

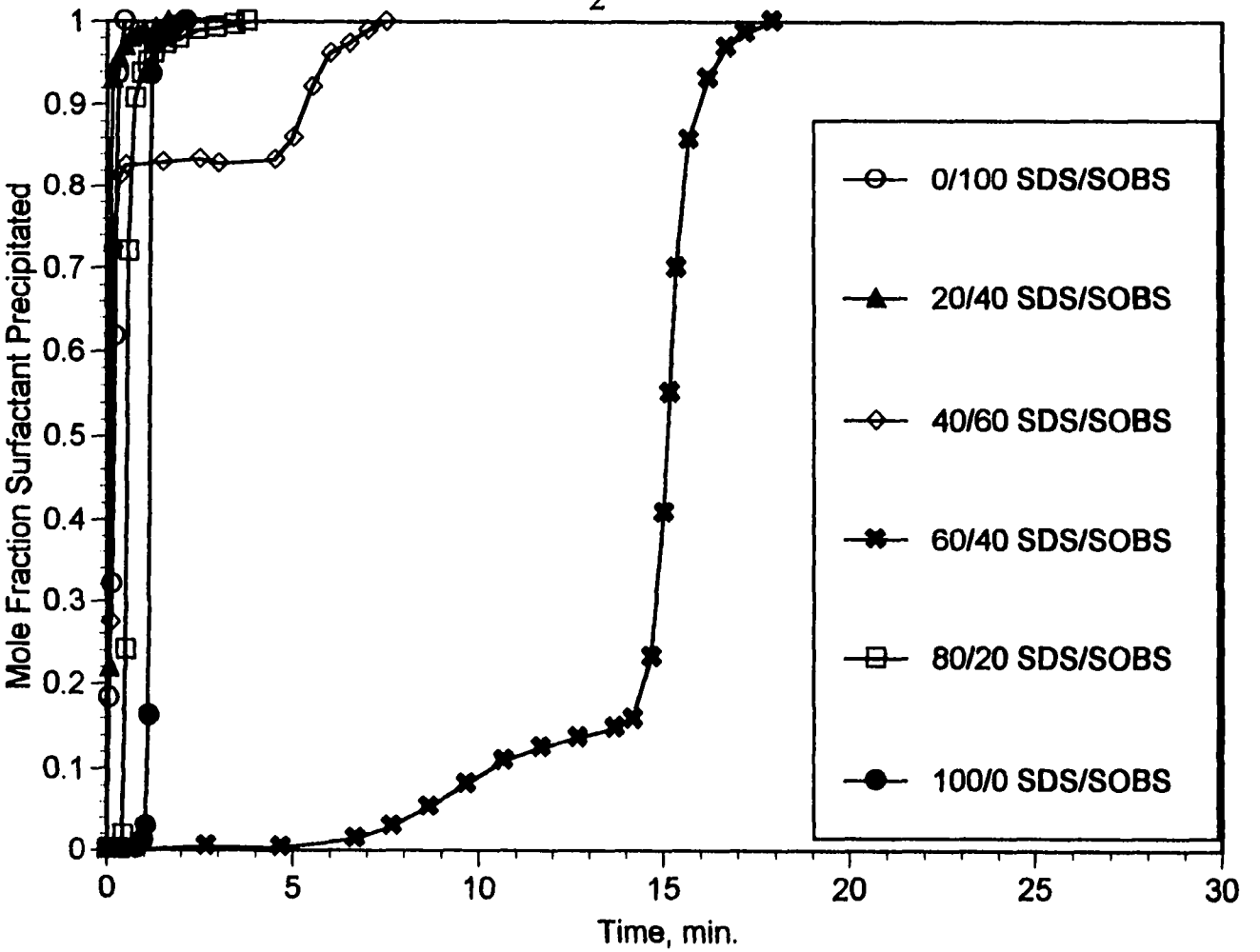


Figure III.21 Precipitation Rate Curves for 0.0096 M Total Surfactant Concentration and Varying SDS/SOBS Mole Fractions with 0.01 M $CaCl_2$ at 30 ^{o}C

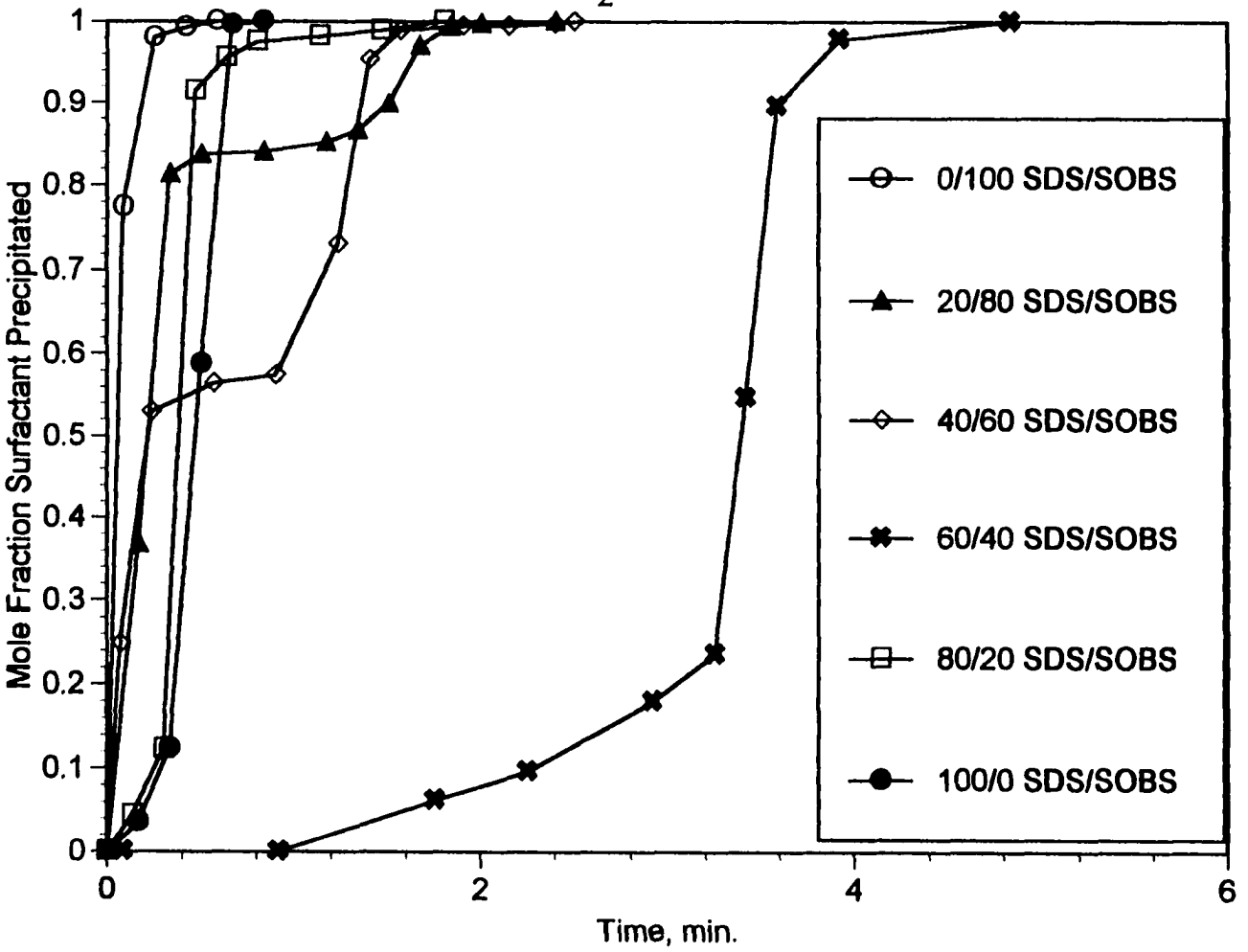


Figure III.22 Precipitation Rate Curves for 0.0025 M Total Surfactant Concentration and Varying SDS/SOBS Mole Fractions with 0.01 M $CaCl_2$ at 30 ^{o}C

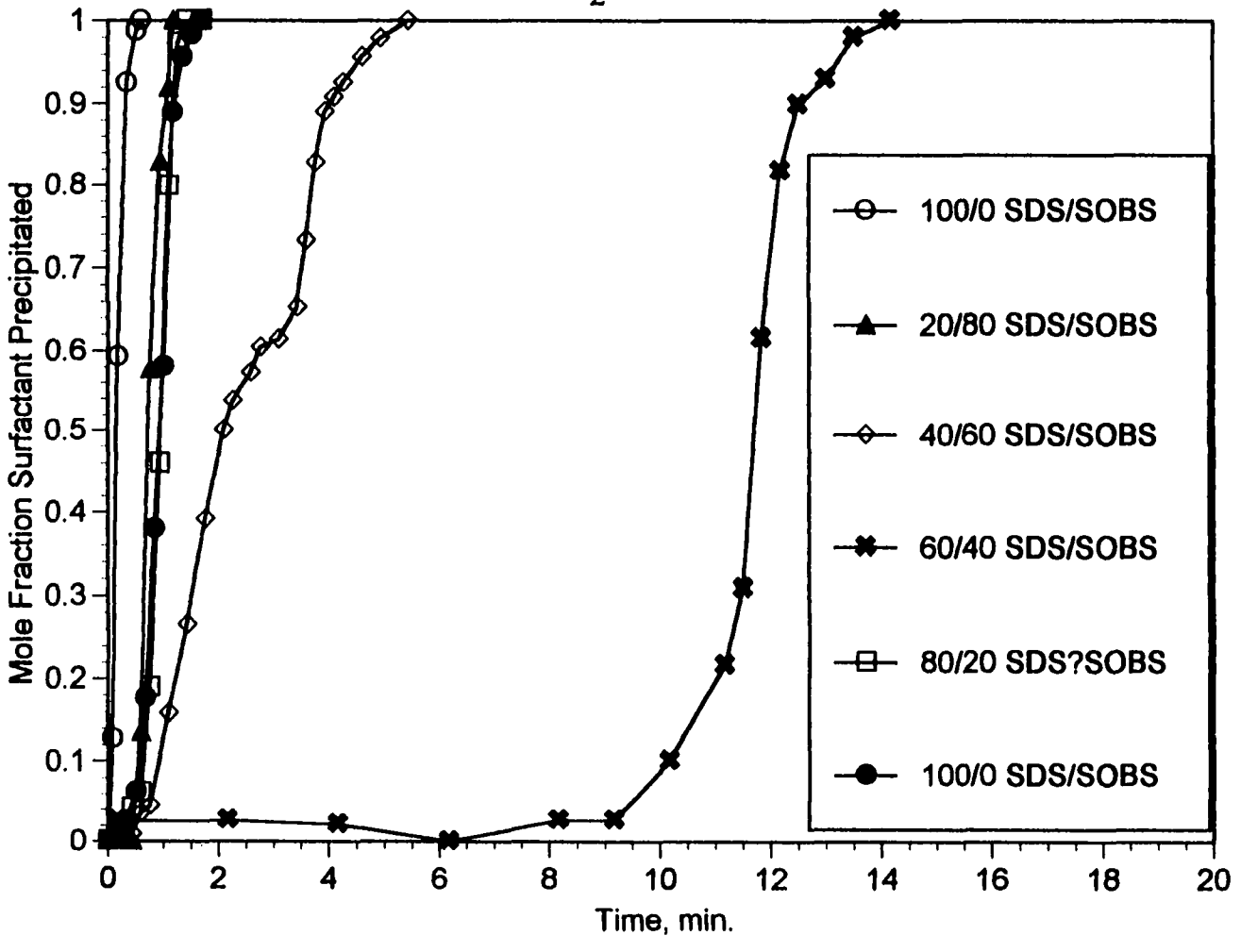


Figure III.23 Concentration Versus Time at 30 ^{o}C For 0.0092 M Surfactant, 40/60 SDS/SOBS and 0.01 M CaCl2 Related to the Extent of Precipitation

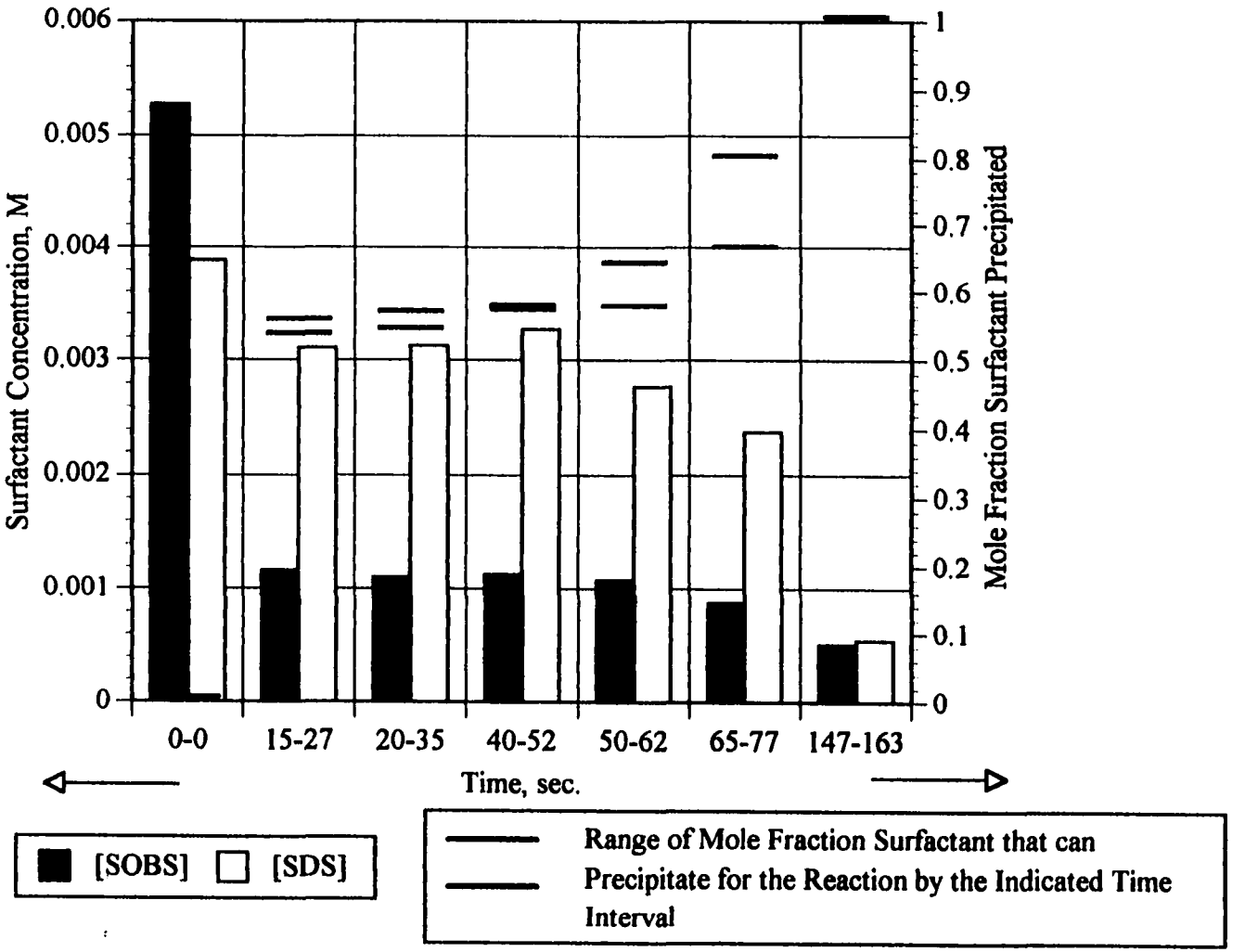


Figure III.24 Atomic Force Microscope Graph of $Ca(DS)_2$ Head Groups in Crystal Lattice

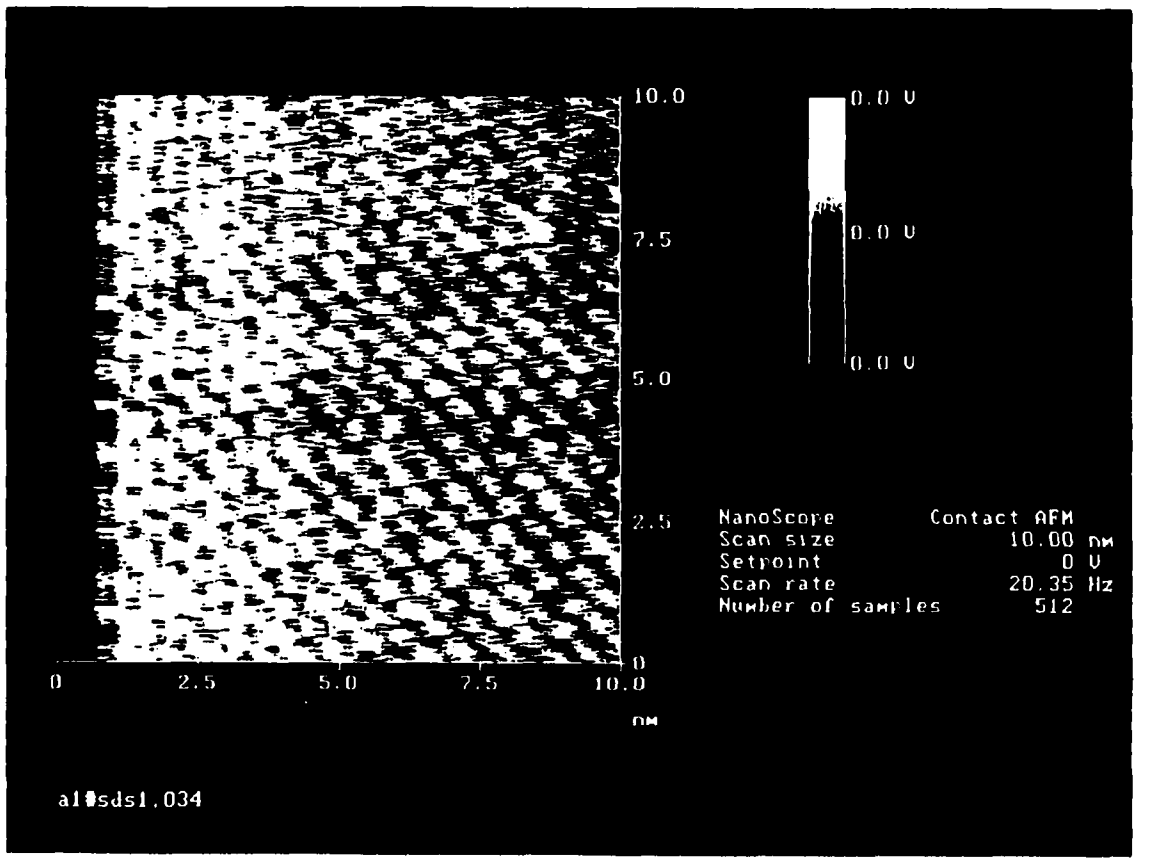


Figure III.25 Atomic Force Microscope Graph of $Ca(OBS)_2$ Head Groups in Crystal Lattice

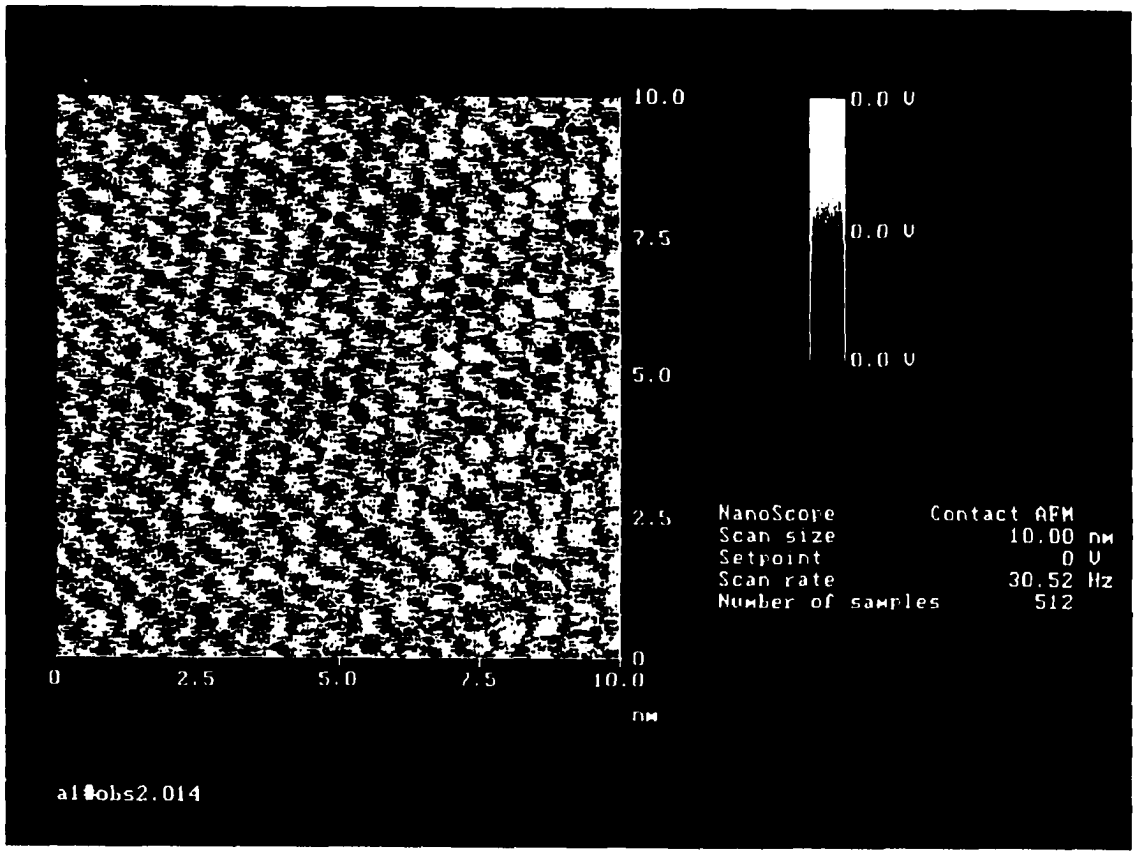


Figure III.26 Precipitation Rate Curves for Various 0.0096 M SDS/SOBS Surfactant Solutions at 30 ^{o}C; Comparing Solutions in which the Water Used Was Unfiltered and Filtered with a 10,000 MWCO Ultrafiltration Membrane

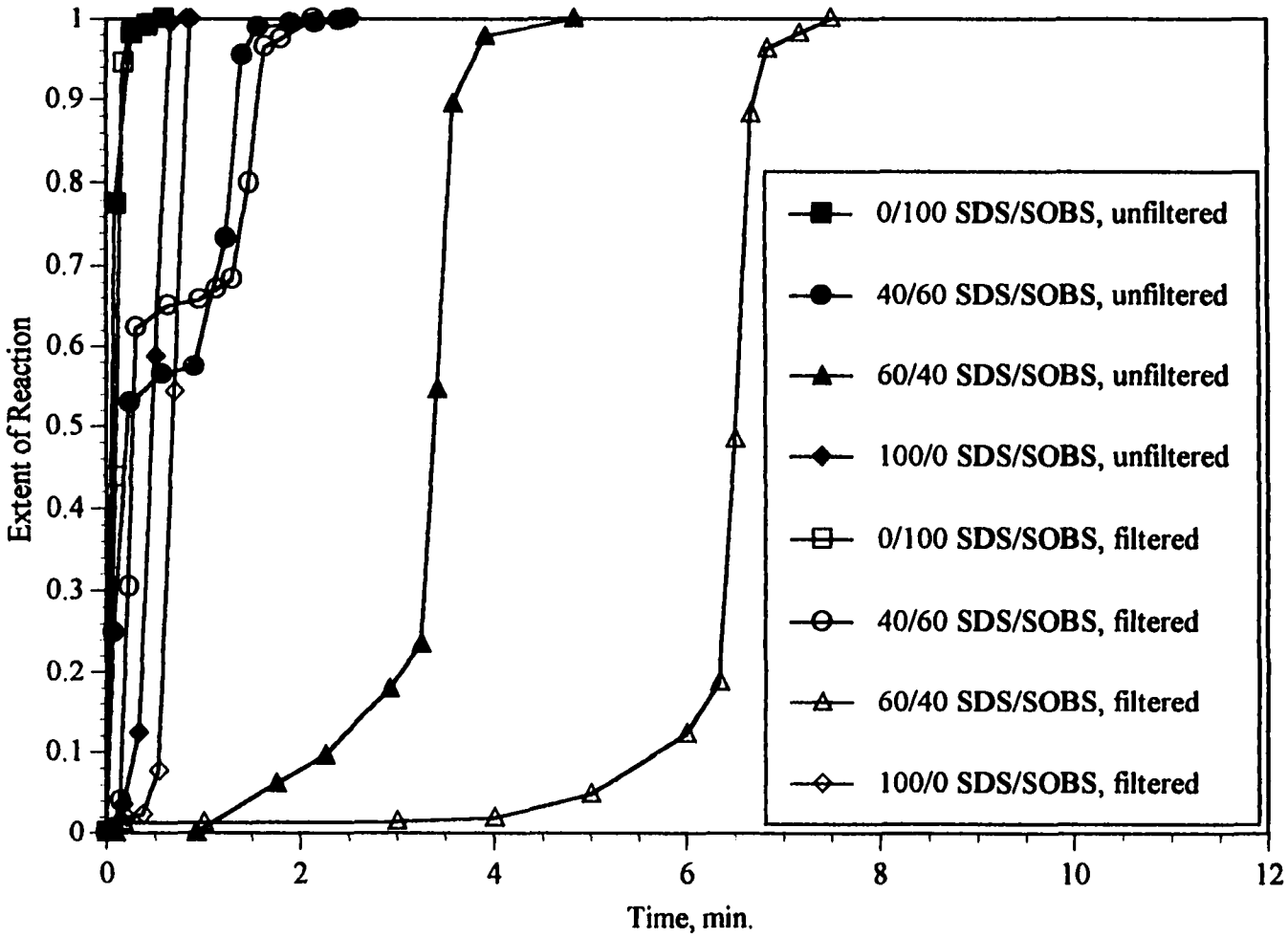


Figure III.27 3-D Atomic Force Microscope Graph of $Ca(DS)_2$ Crystals Precipitated from a 0.020 M SDS/0.010 M $CaCl_2$ Solution at 30 °C; 50 μm x 50 μm

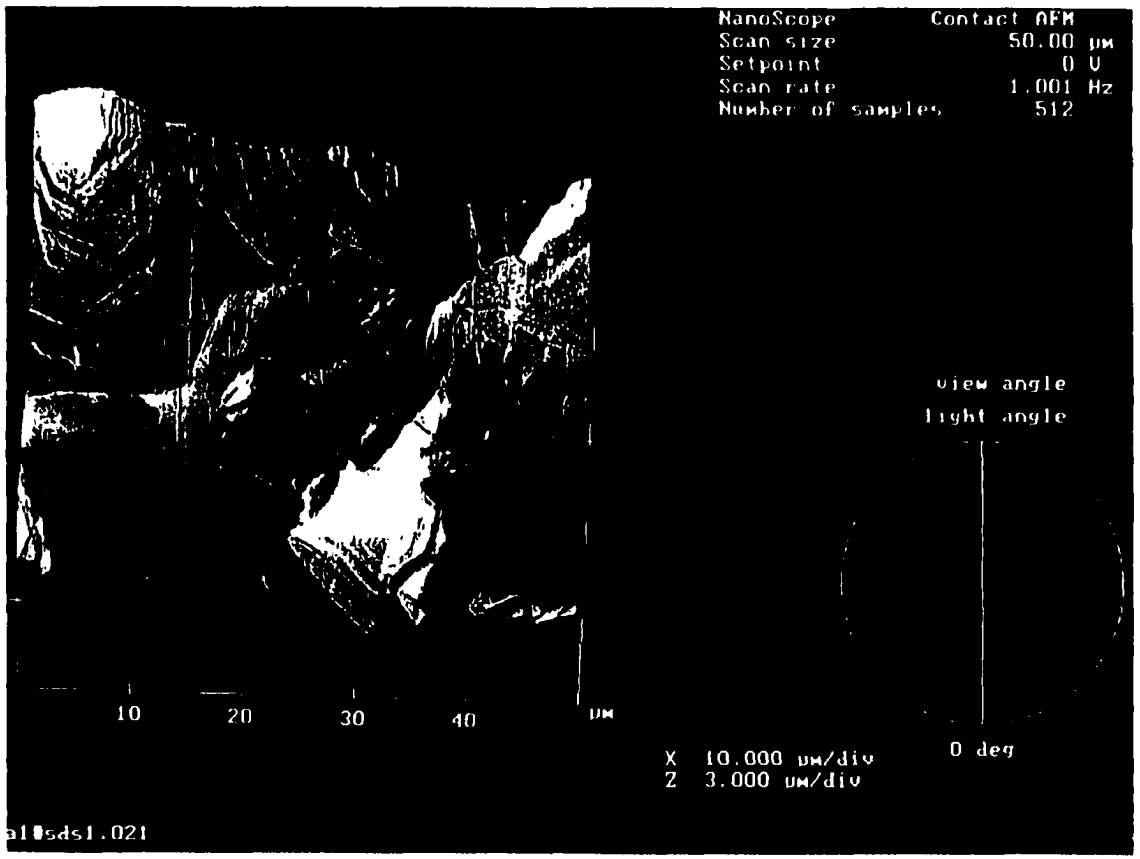


Figure III.28 3-D Atomic Force Microscope Graph of $Ca(OBS)_2$ Crystals Precipitatedfrom a 0.020 M SOBS/0.010 M $CaCl_2$ Solution at 30 °C; 50 μm x 50 μm



Figure III.29 3-D Atomic Force Microscope Graph of Crystals Precipitated from 0.020 M Total Surfactant and 60/40 SDS/SOBS Mole Ratio Containing 0.010 M $CaCl_2$ at 30 °C; 50 μm x 50 μm

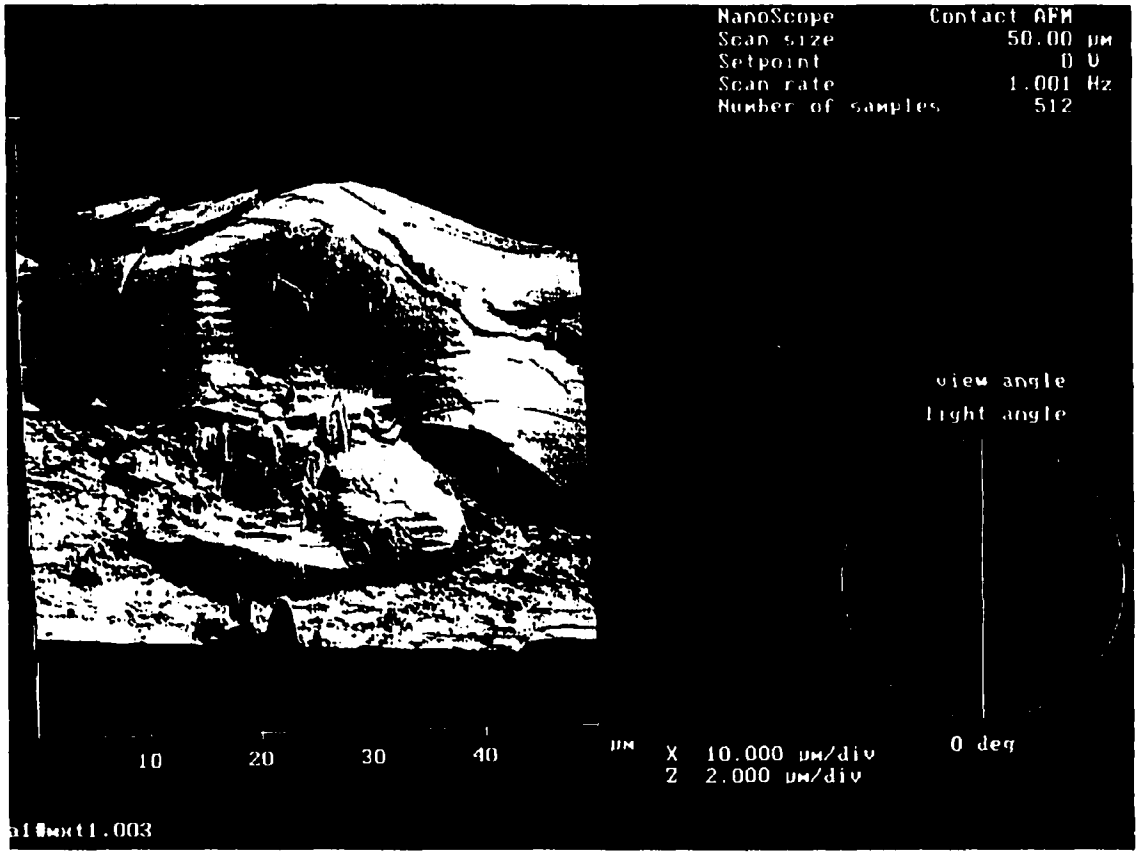


Figure III.30 3-D Atomic Force Microscope Graph of Crystals Precipitated from 0.020 M Total Surfactant and 40/60 SDS/SOBS Mole Ratio Containing 0.010 M $CaCl_2$ at 30 °C; 50 μm x 50 μm

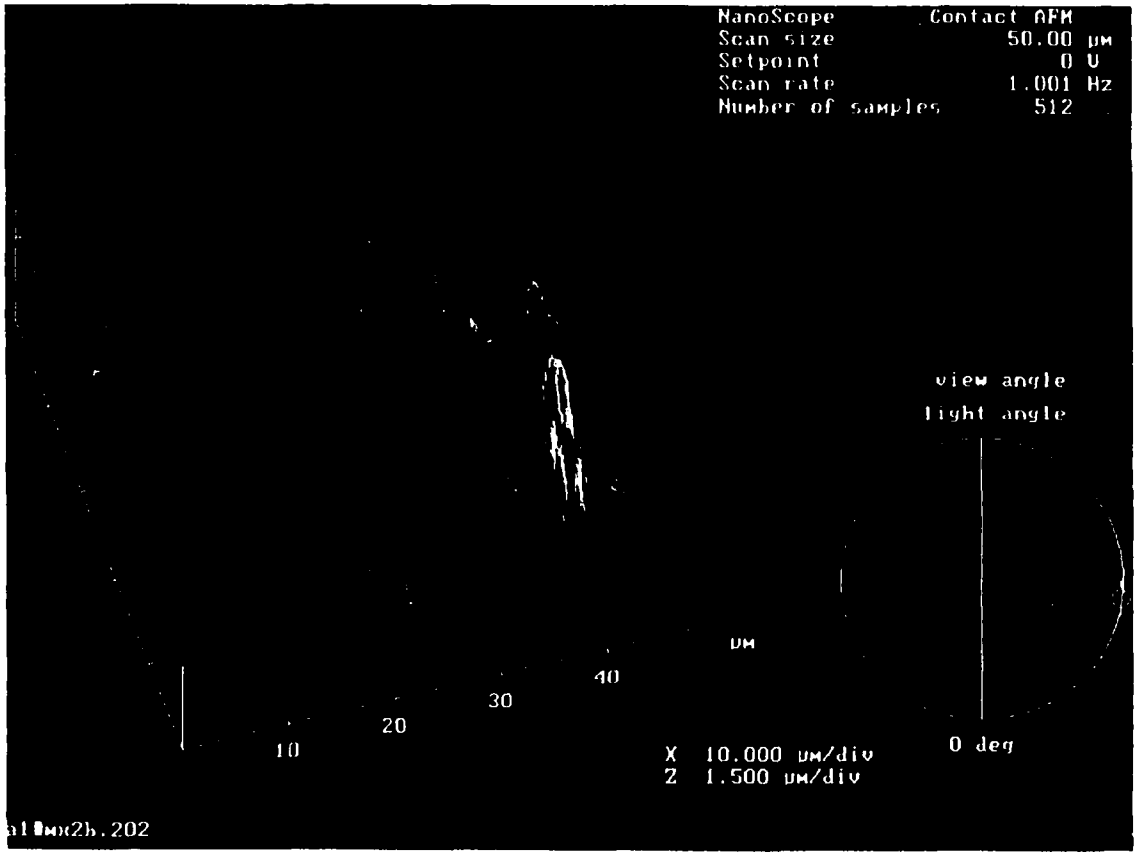


Figure III.31 Top View of $Ca(DS)_2$ CrystalsPrecipitated from a 0.020 M SDS/0.010 M $CaCl_2$ Solution at 30 °C; Taken with Atomic Force Microscope; 50 μm x 50 μm

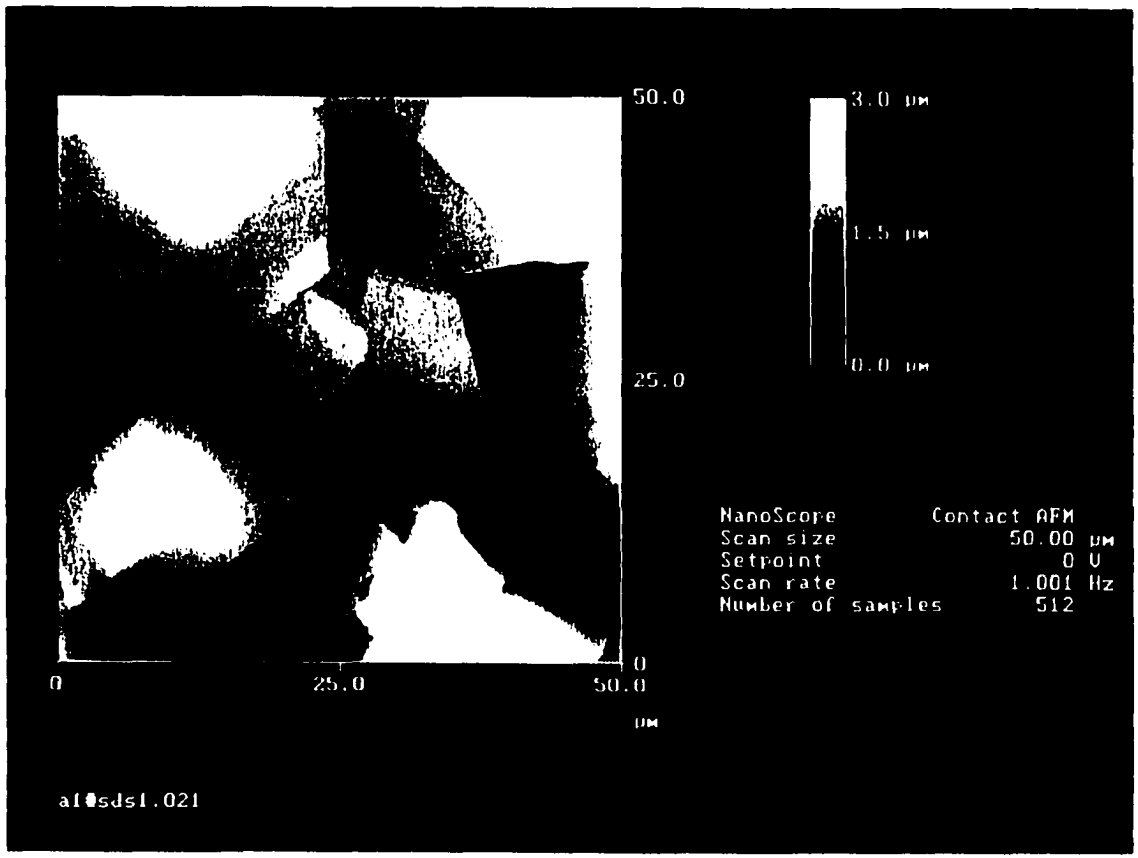


Figure III.32 Top View of $Ca(OBS)_2$ Crystals Precipitated from a 0.020 M SOBS/0.010 M $CaCl_2$ Solution at 30 °C; Taken with Atomic Force Microscope; 50 μm x 50 μm

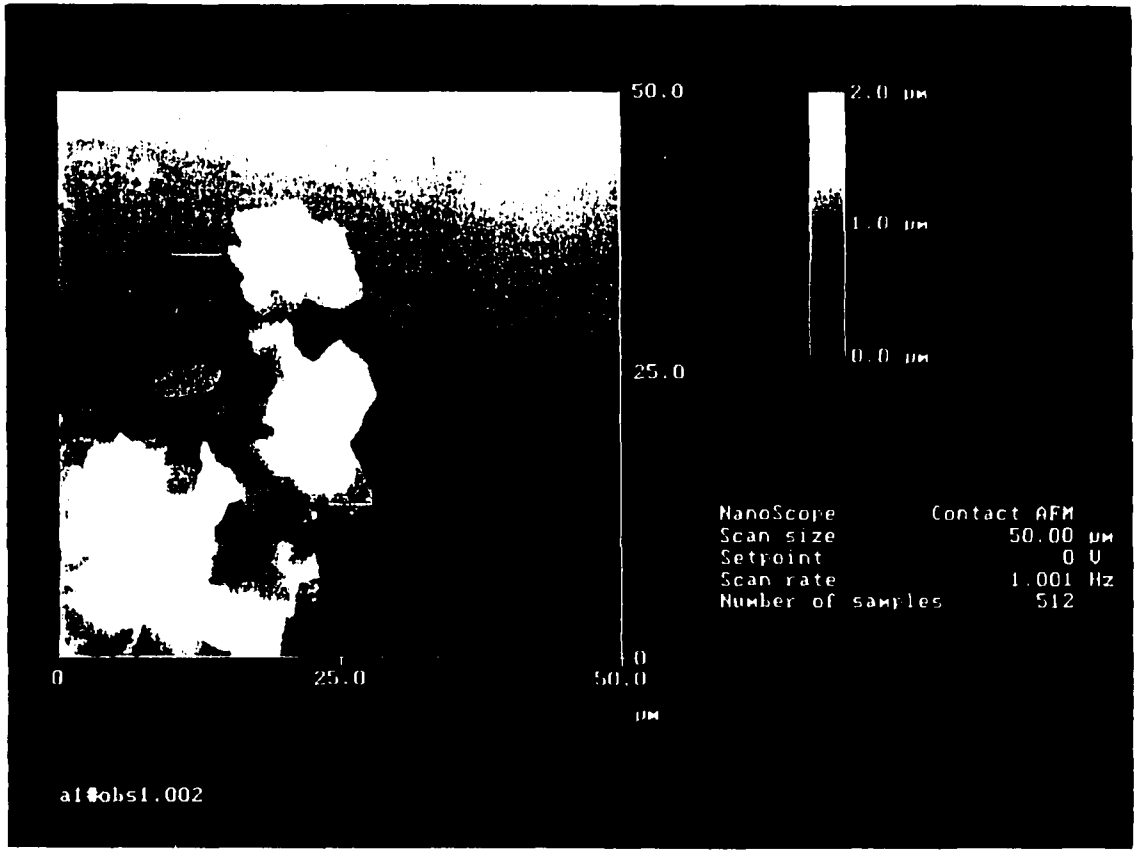


Figure III.33 Top View of Crystals Precipitated from a 0.020 M Surfactant Solution Containing 60/40 SDS/SOBS and 0.010 M $CaCl_2$ at 30 °C; Taken with Atomic Force Microscope; 50 μm x 50 μm

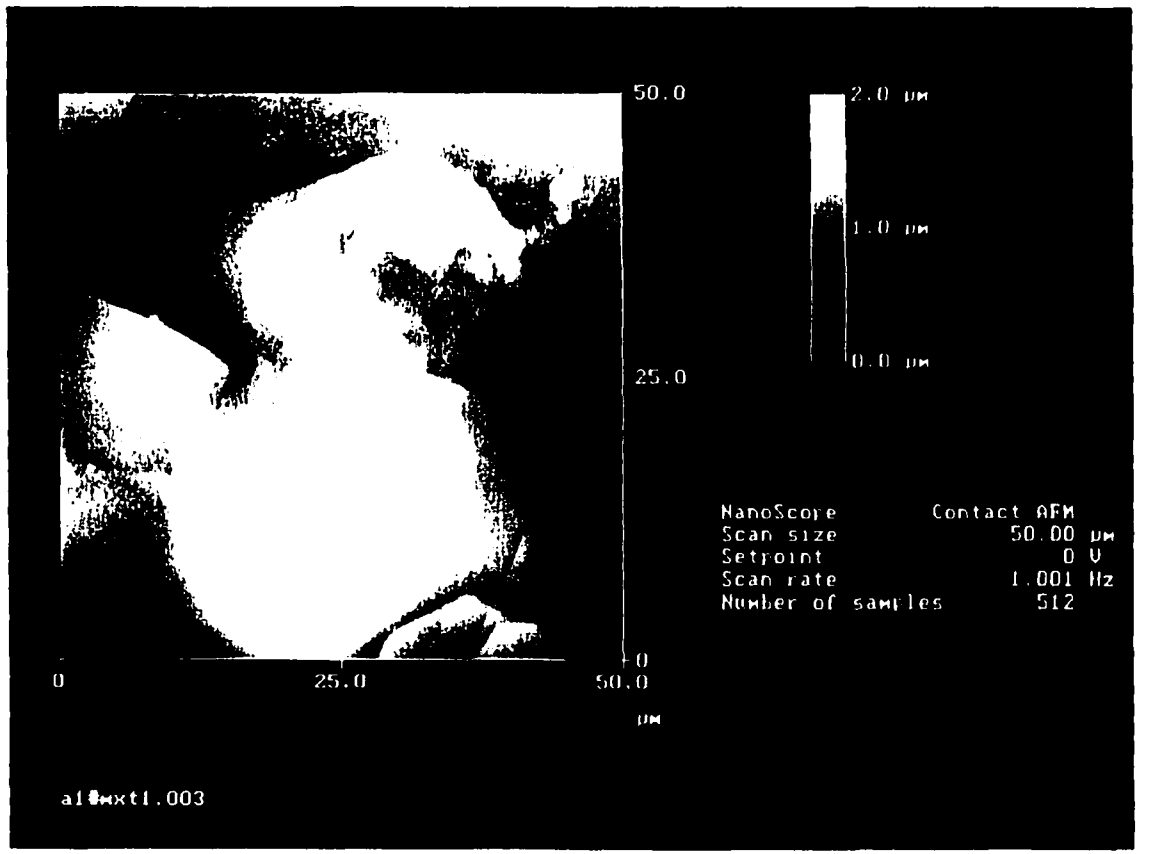


Figure III.34 Top View of Crystals Precipitated from a 0.020 M Surfactant Solution Containing 40/60 SDS/SOBS and 0.010 M $CaCl_2$ at 30 °C; Taken with Atomic Force Microscope; 50 μm x 50 μm

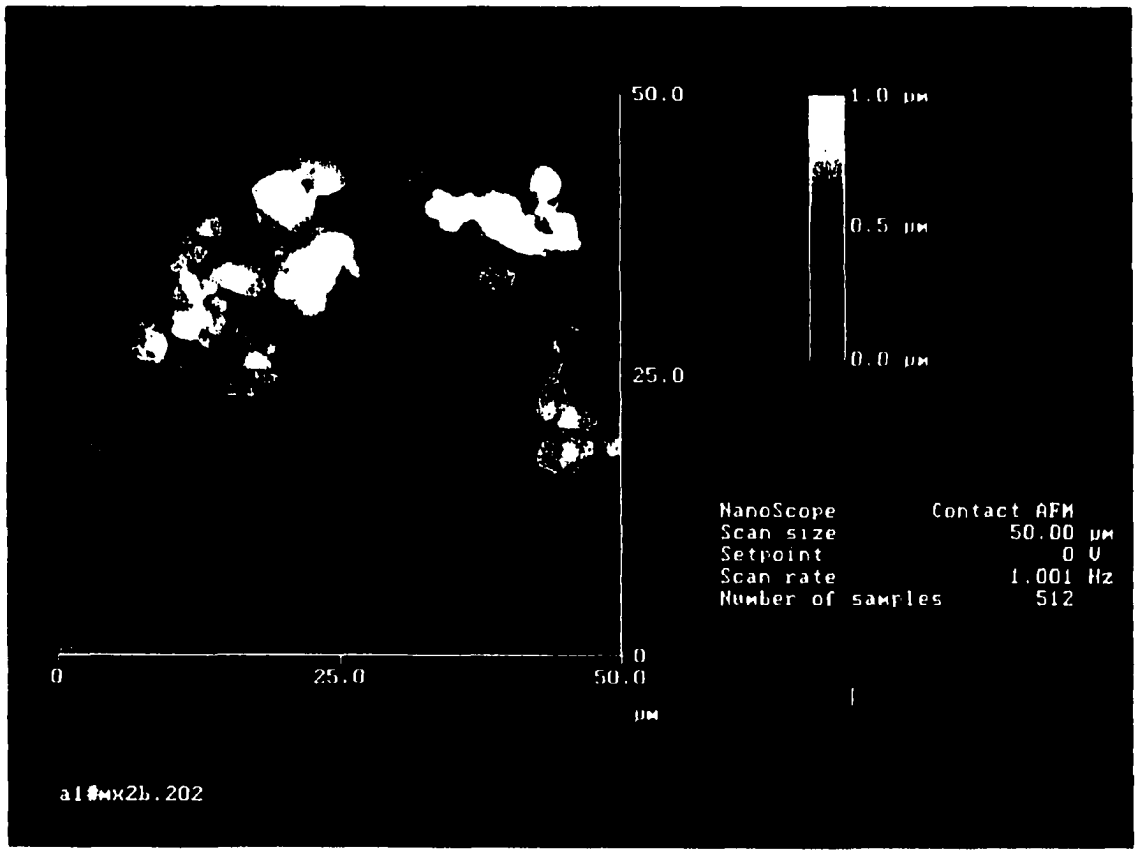


Figure III.35 3-D Atomic Force Microscope Graph of $Ca(DS)_2$ Crystals Precipitated from a 0.020 M SDS/0.010 M $CaCl_2$ Solution at 30 °C; 8 μm x 8 μm

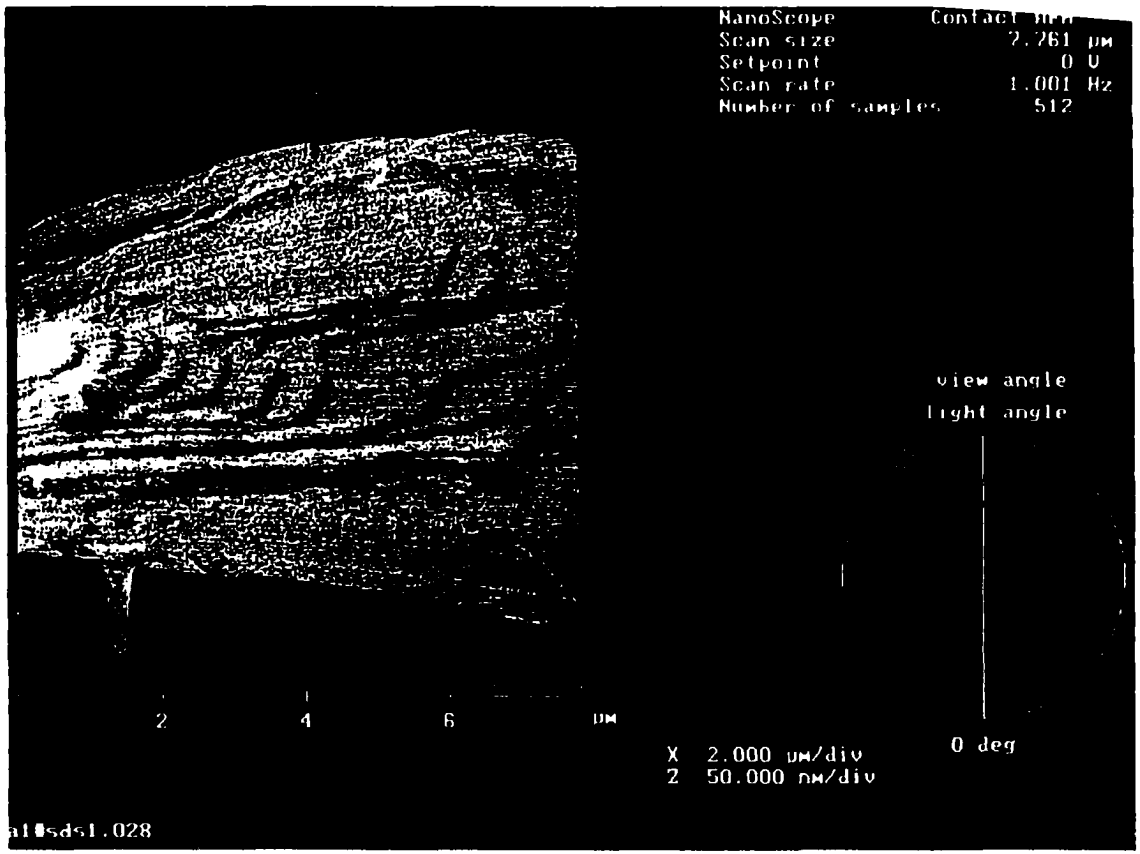


Figure III.36 3-D Atomic Force Microscope Graph of $Ca(OBS)_2$ Crystals Precipitated from a 0.020 M SOBS/0.010 M $CaCl_2$ Solution at 30 °C; 10 μm x 10 μm

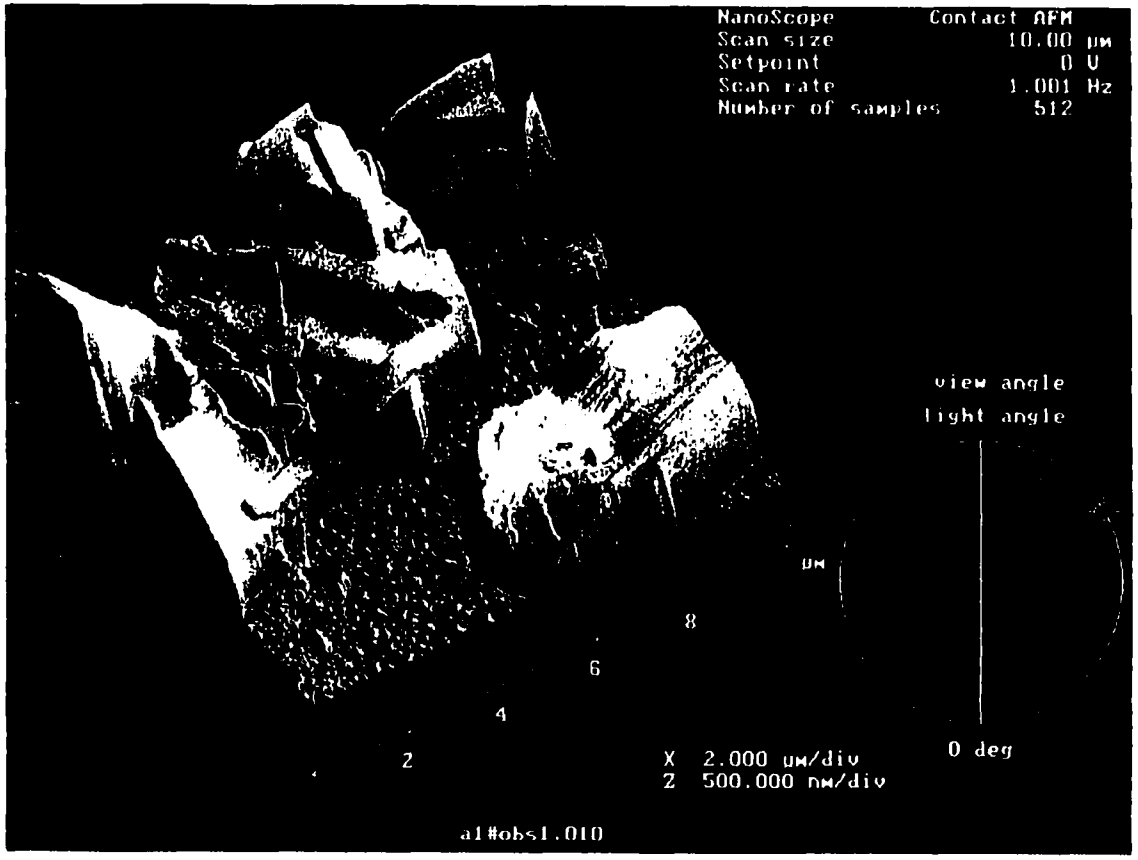


Figure III.37 3-D Atomic Force Microscope Graph of Crystals Precipitated from 0.020 M Total Surfactant Containing 60/40 SDS/SOBS and 0.010 M $CaCl_2$ at 30 °C; 10 μm x 10 μm

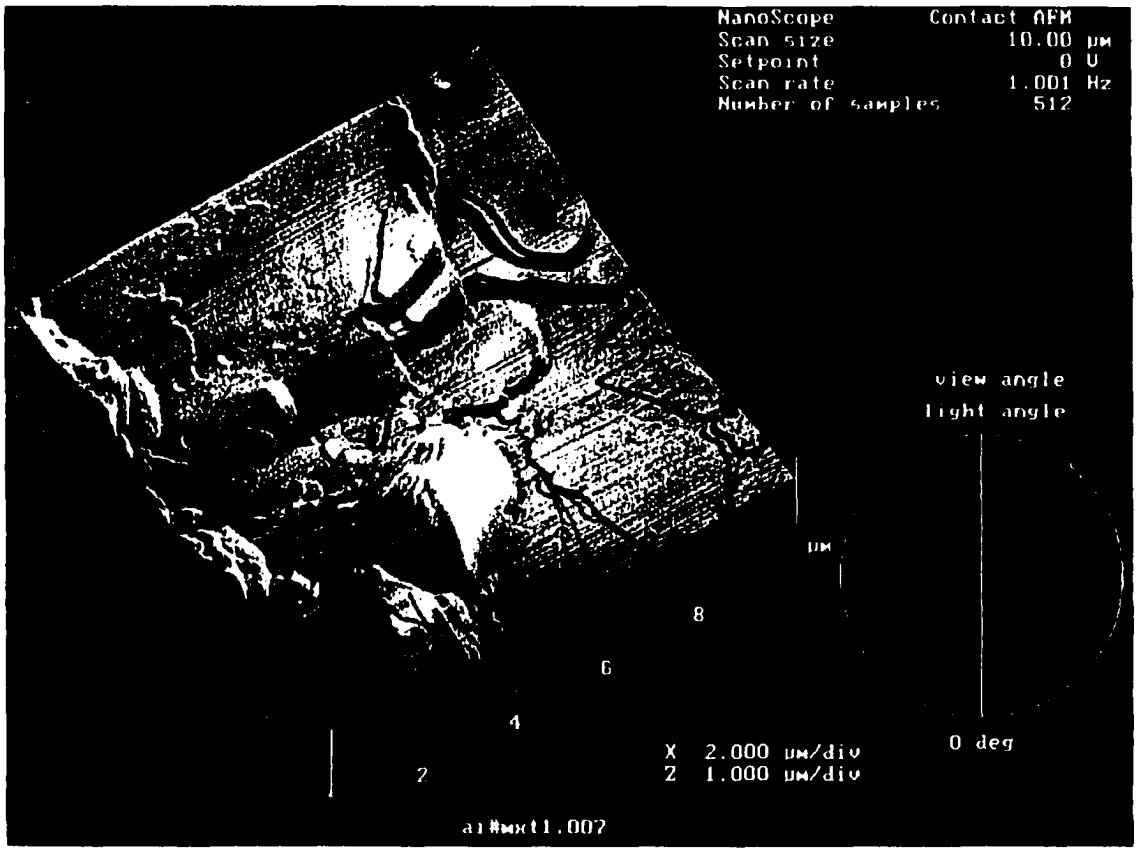


Figure III.38 3-D Atomic Force Microscope Graph of Crystals Precipitated from 0.020 M Total Surfactant Containing 40/60 SDS/SOBS and 0.010 M $CaCl_2$ at 30 °C; 8 μm x 8 μm

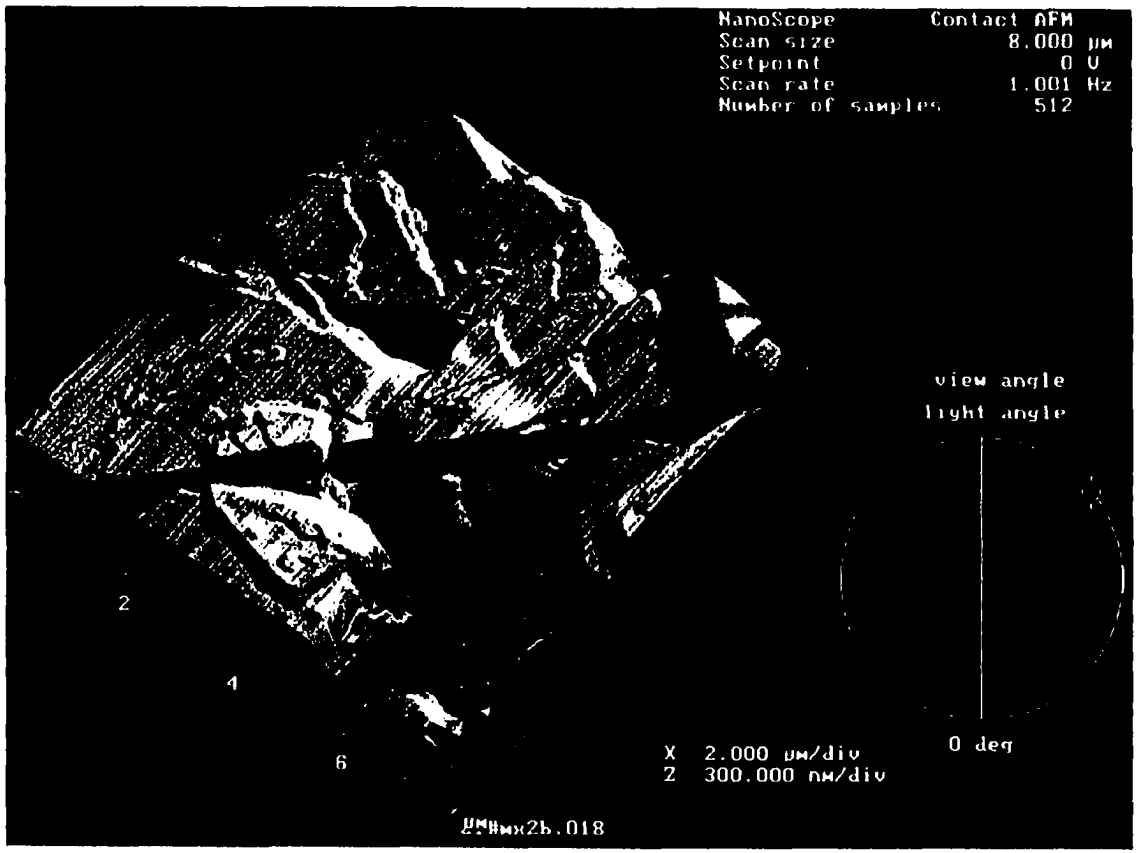


Figure III.39 Top View Atomic Force Microscope Graph of Crystals Precipitated from a 0.020 M Surfactant Solution Containing 40/60 SDS/SOBS and 0.010 M $CaCl_2$ at 30 °C; 5 μm x 5 μm

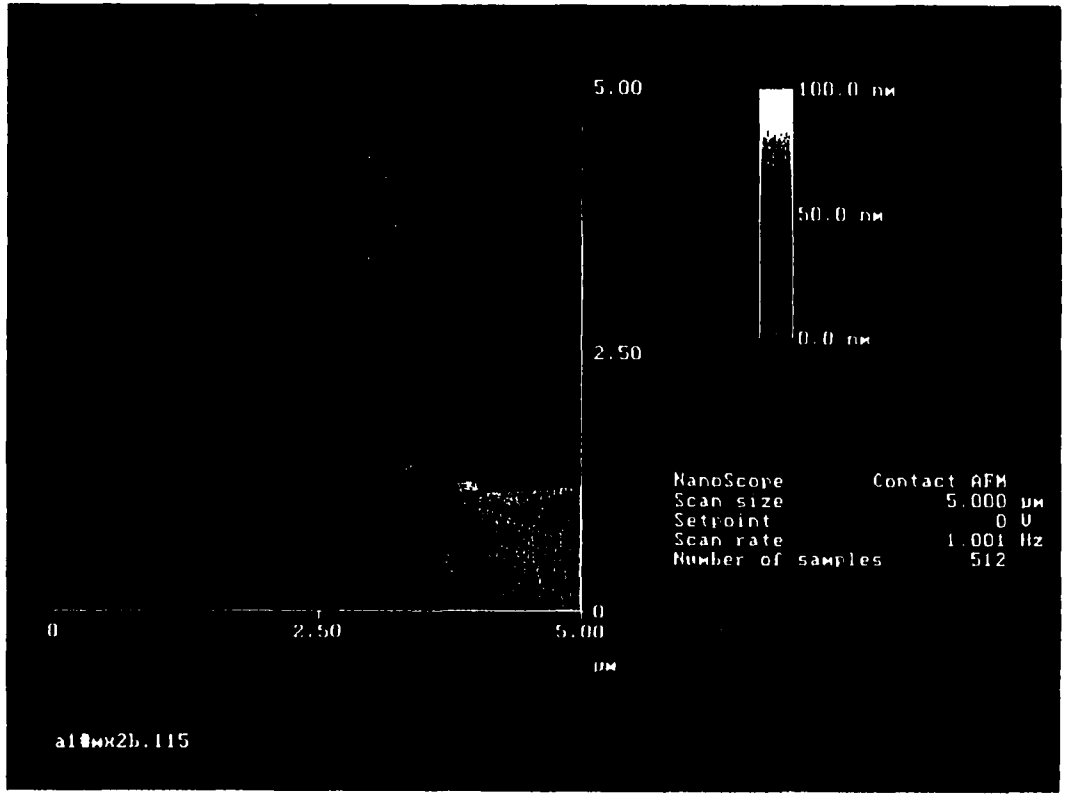


Figure III.40 40X Image Analysis Picture of $Ca(OBS)_2$ Crystals Precipitated from a 0.075 M SOBS/0.010 M $CaCl_2$ Solution; Taken 4 Minutes After Mixing at 30 °C

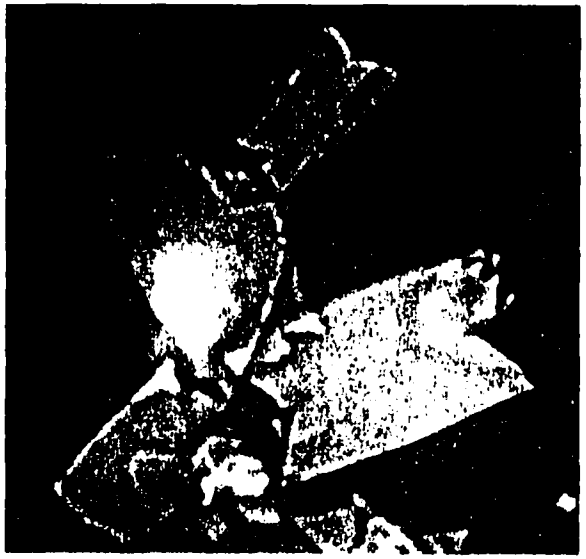


Figure III.41 40X Image Analysis Picture of $Ca(DS)_2$ Crystals Precipitated from a 0.010 M SDS/0.008 M $CaCl_2$ Solution; Taken 4 Minutes After Mixing at 30 °C



Figure III.42 40X Image Analysis Picture of Crystals Precipitated from a 0.012 M Surfactant Solution Containing 83/17 SDS/SOBS and 0.008 M $CaCl_2$; Taken 4 Minutes After Mixing at 30 °C

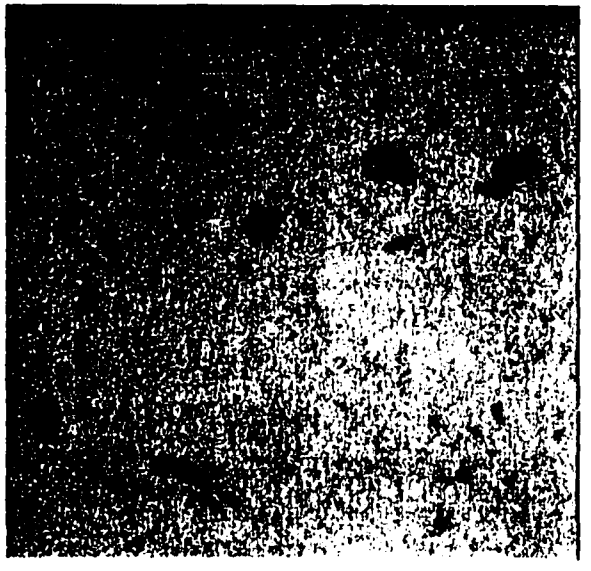


Figure III.43 40X Image Analysis Picture of Crystals Precipitated from a 0.014 M Surfactant Solution Containing 71/29 SDS/SOBS and 0.008 M $CaCl_2$; Taken 4 Minutes After Mixing at 30 °C

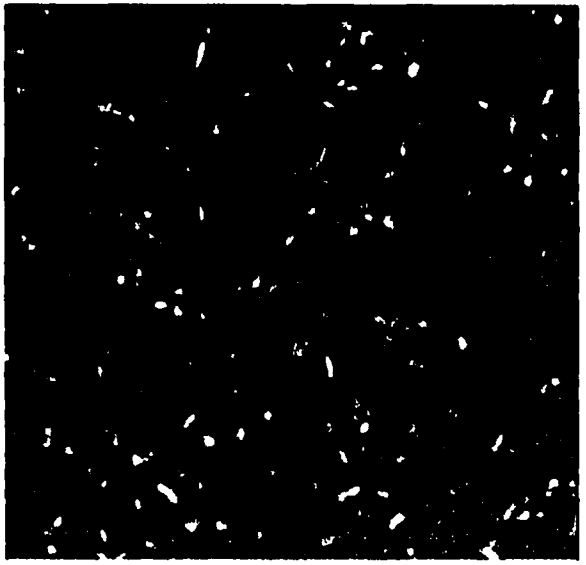


Figure III.44 40X Image Analysis Picture of $Ca(OBS)_2$ Crystals Precipitated from a 0.075 M SOBS/0.010 M $CaCl_2$ Solution; After 1 Week at 30 °C

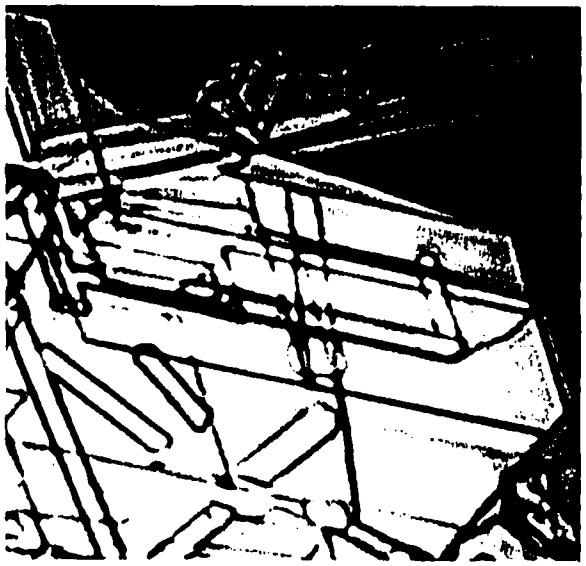


Figure III.45 40X Image Analysis Picture of $Ca(DS)_2$ Crystals Precipitated from a 0.010 M SDS/0.008 M $CaCl_2$ Solution; After 1 Week at 30 °C

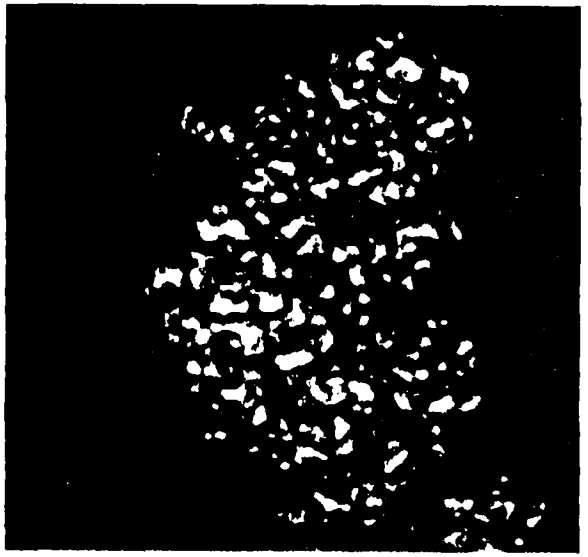


Figure III.46 40X Image Analysis Picture of Crystals Precipitated from a 0.012 M Surfactant Solution Containing 83/17 SDS/SOBS and 0.008 M $CaCl_2$; After 1 Week at 30 °C

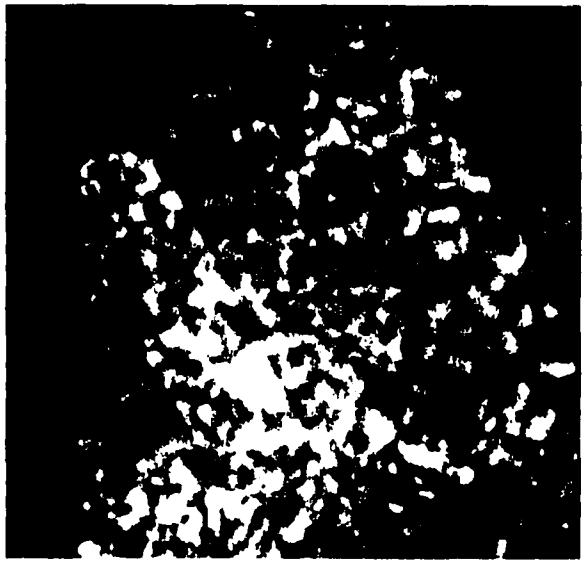
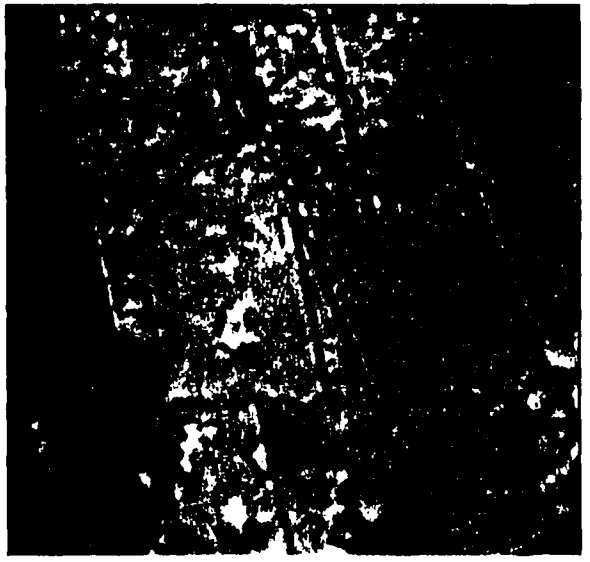


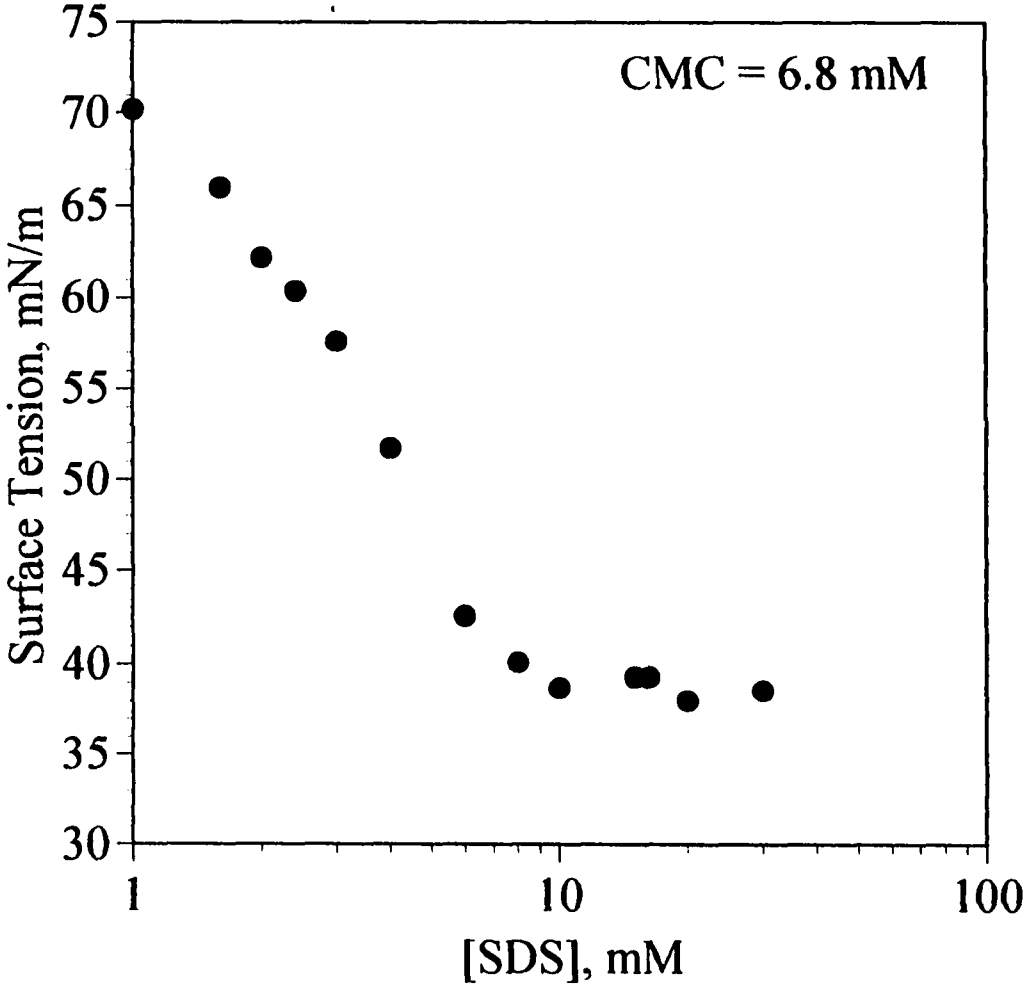
Figure III.47 40X Image Analysis Picture of Crystals Precipitated from a 0.014 M Surfactant Solution Containing 71/29 SDS/SOBS and 0.008 M $CaCl_2$; After 1 Week at 30 °C



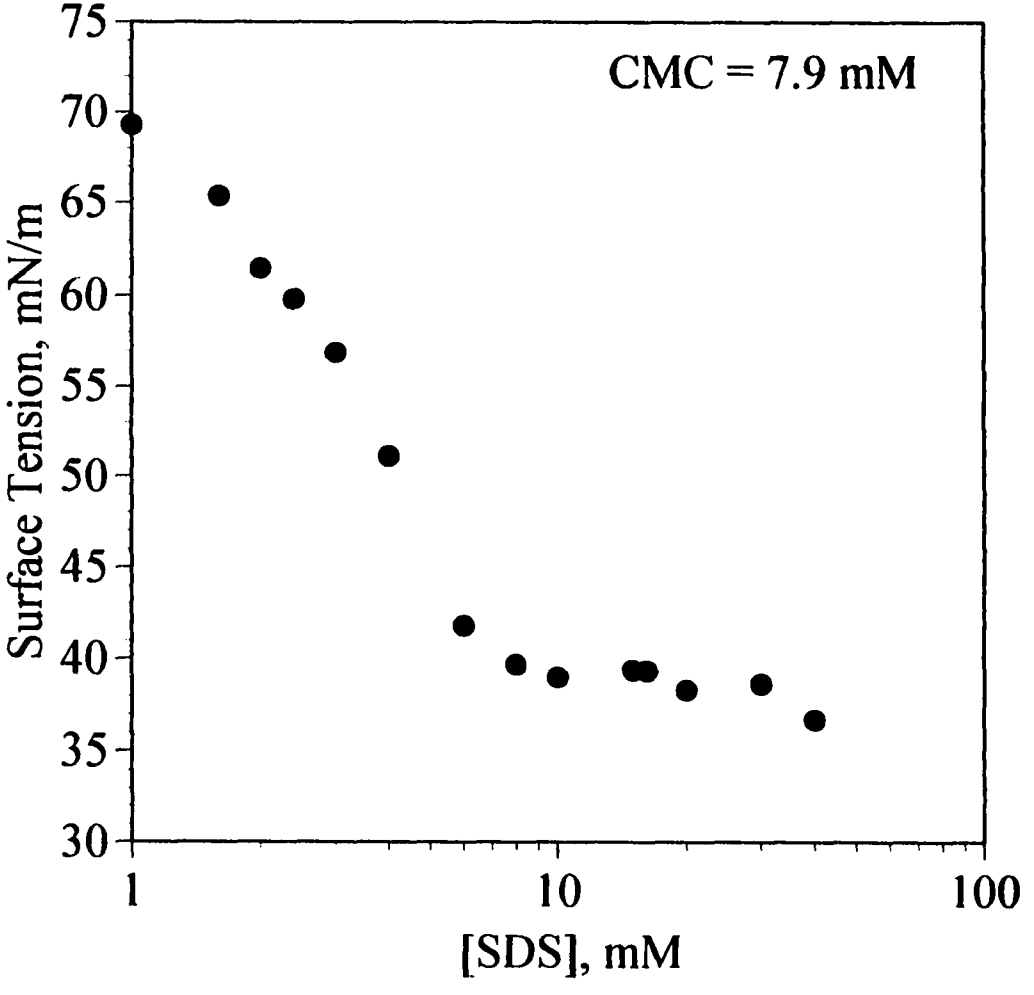
APPENDIX A

Surface Tension versus Log (Concentration)

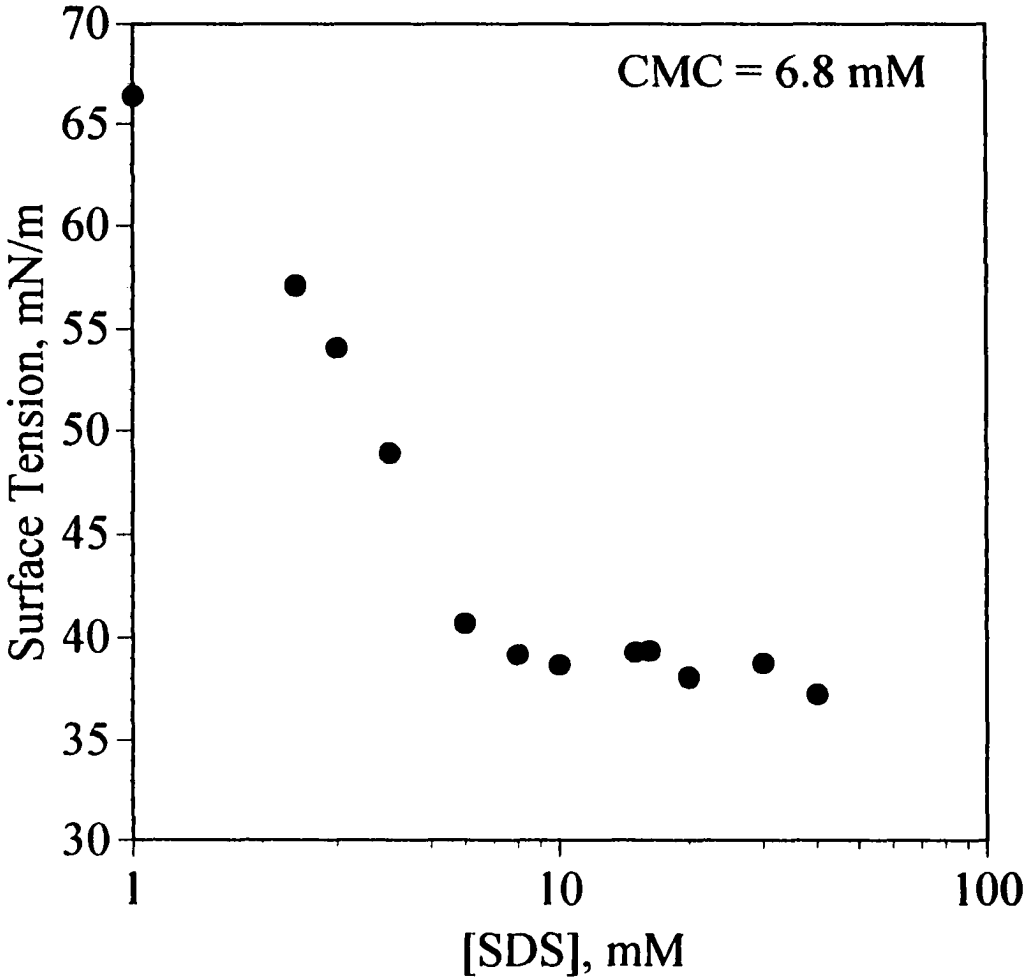
CMC for SDS, 0 M NaCl, 15 ^{o}C Using Maximum Bubble Pressure Method



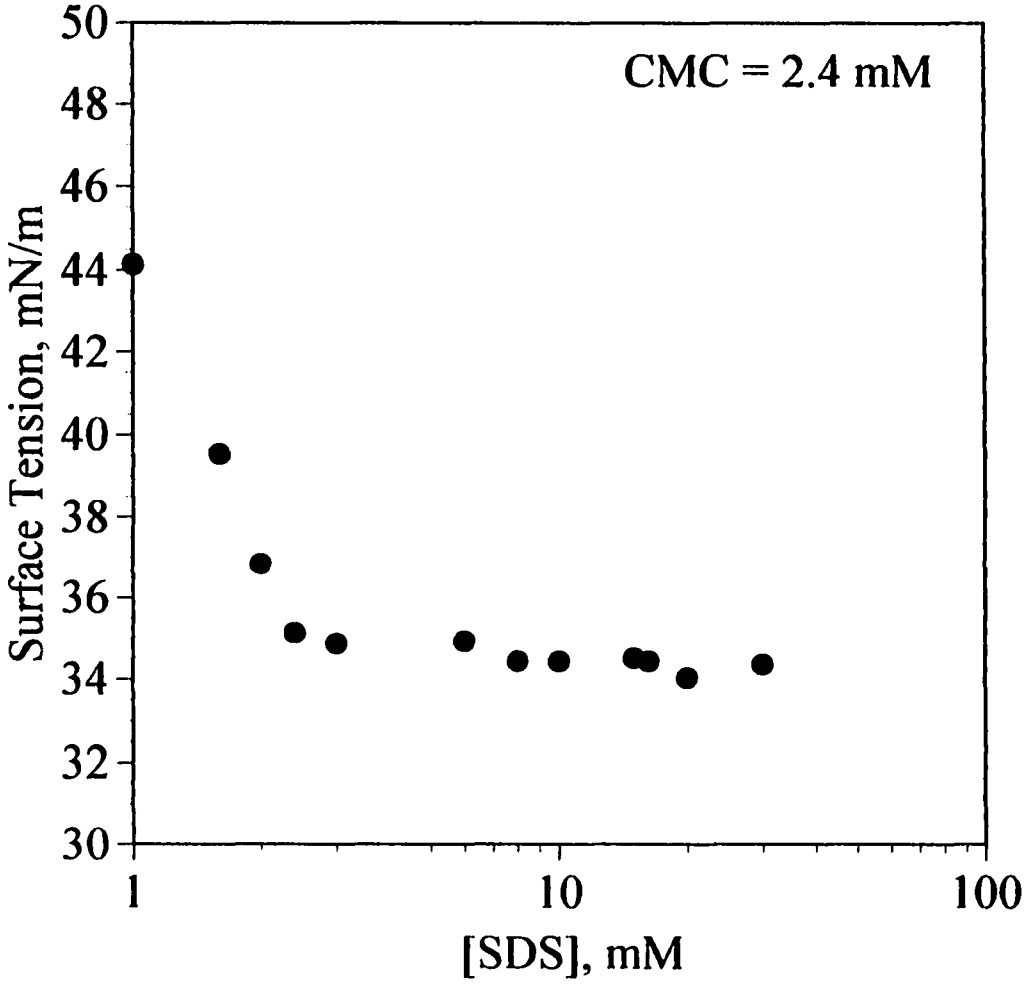
CMC for SDS, 0 M NaCl, 20 ^{o}C Using Maximum Bubble Pressure Method



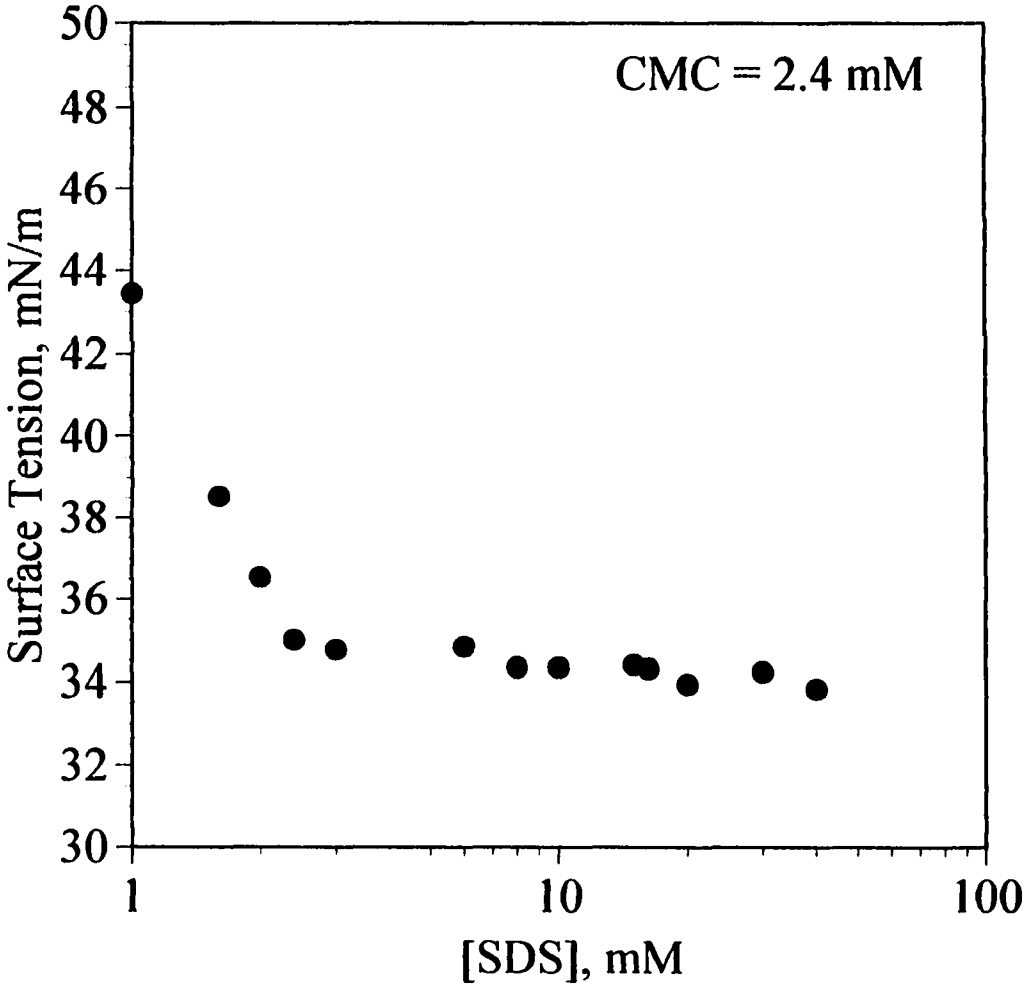
CMC for SDS, 0 M NaCl, 25 ^{o}C Using Maximum Bubble Pressure Method



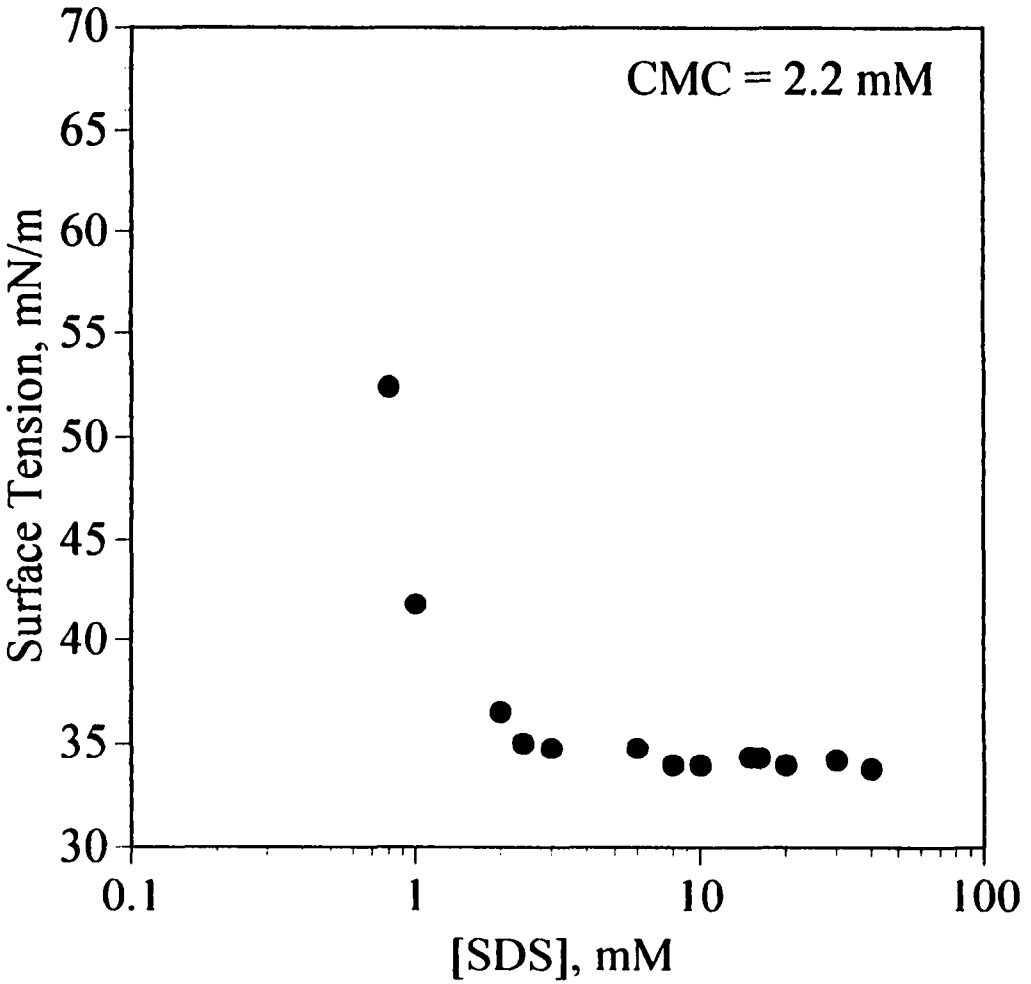
CMC for SDS, 0.1 M NaCl, 15 ^{o}C Using Maximum Bubble Pressure Method



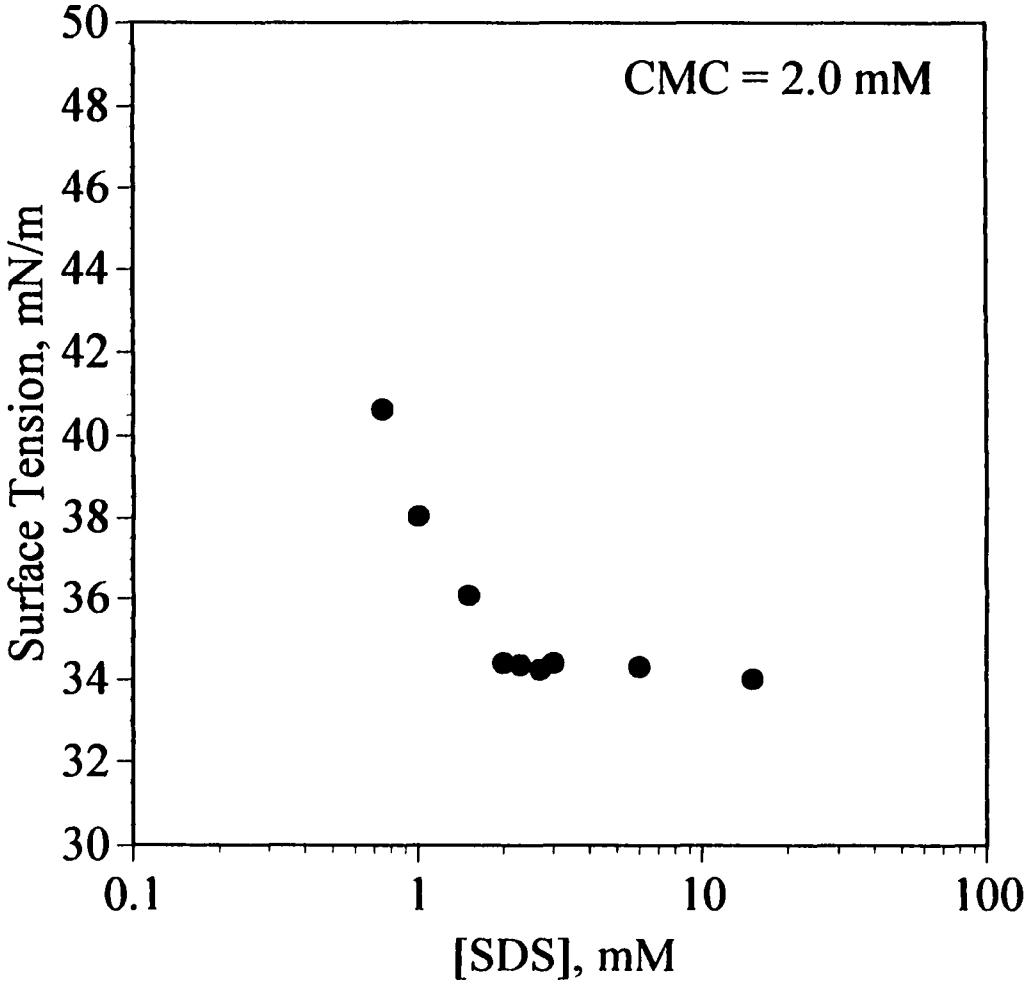
CMC for SDS, 0.1 M NaCl, 20 ^{o}C Using Maximum Bubble Pressure Method



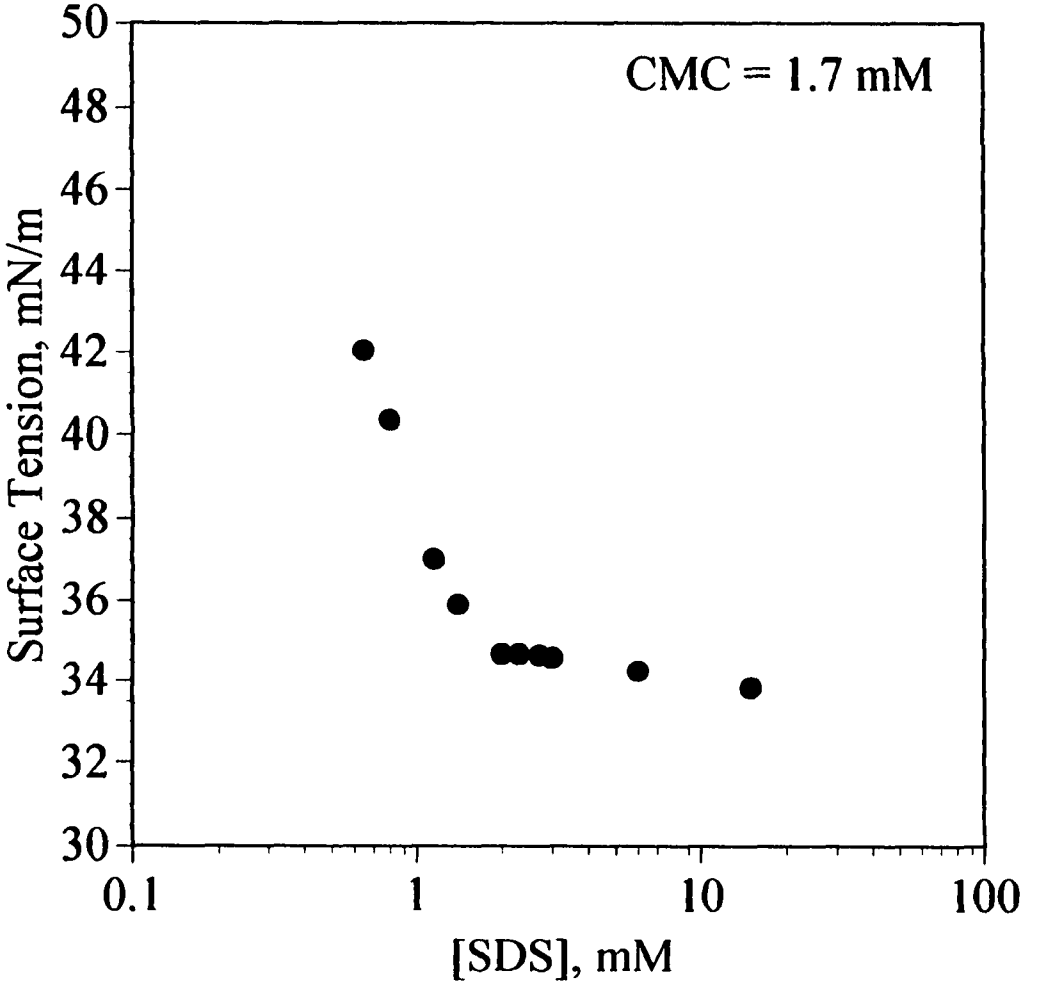
CMC for SDS, 0.1 M NaCl, 25 ^{o}C Using Maximum Bubble Pressure Method



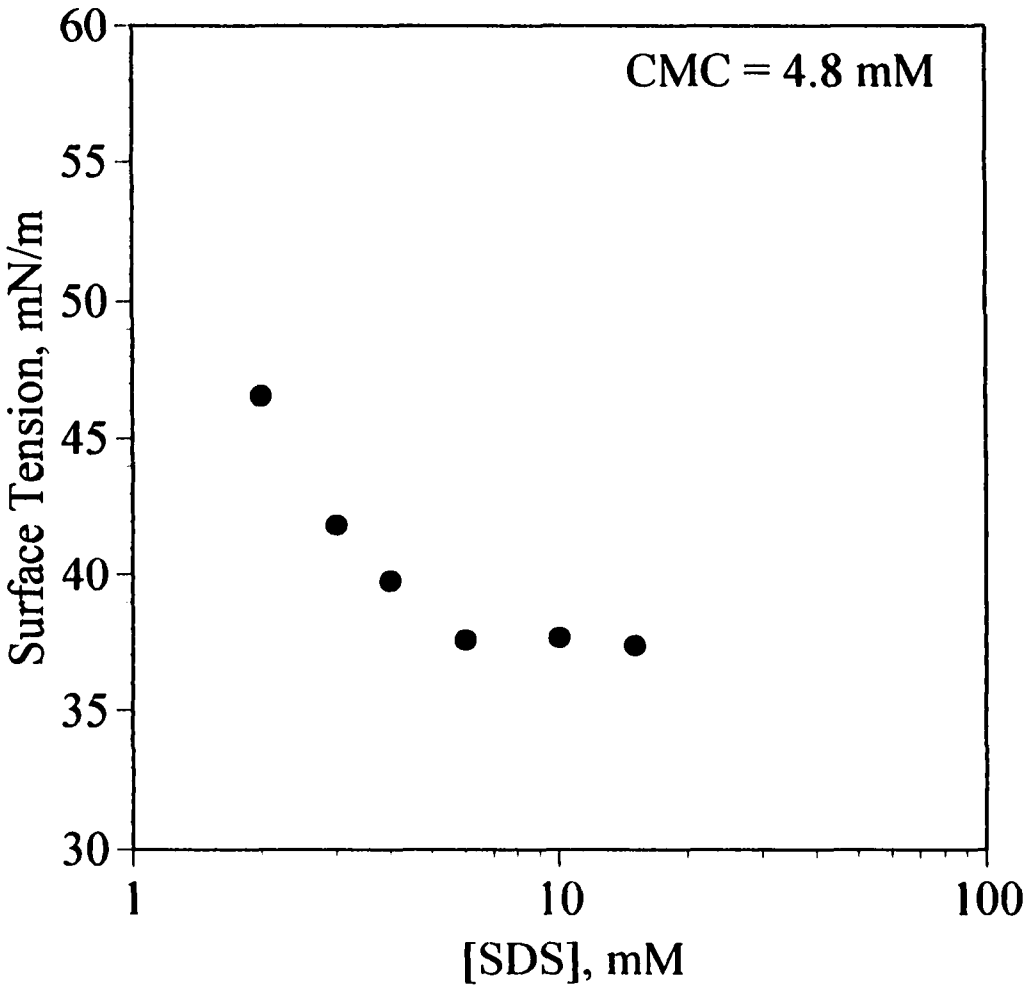
CMC for SDS, 0.15 M NaCl, 20 ^{o}C Using Maximum Bubble Pressure Method



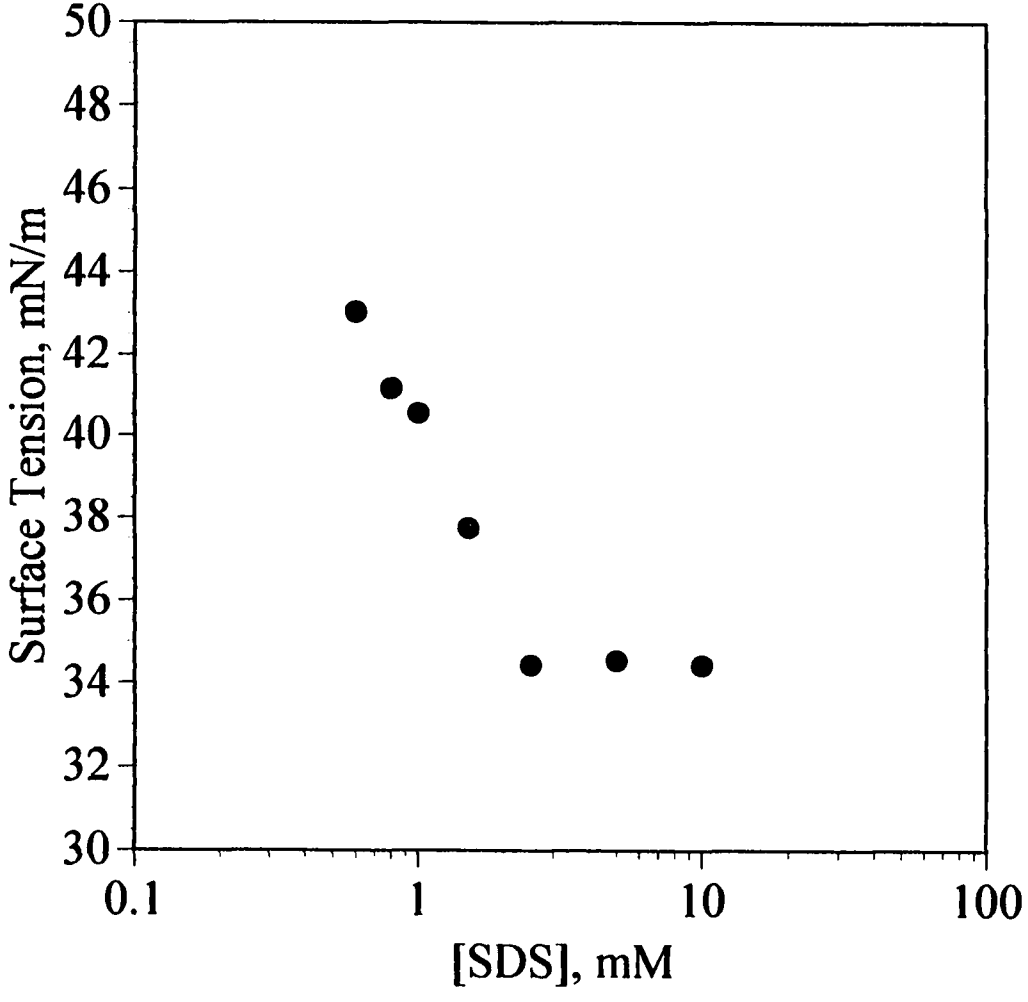
CMC for SDS, 0.15 M NaCl, 25 ^{o}C Using Maximum Bubble Pressure Method



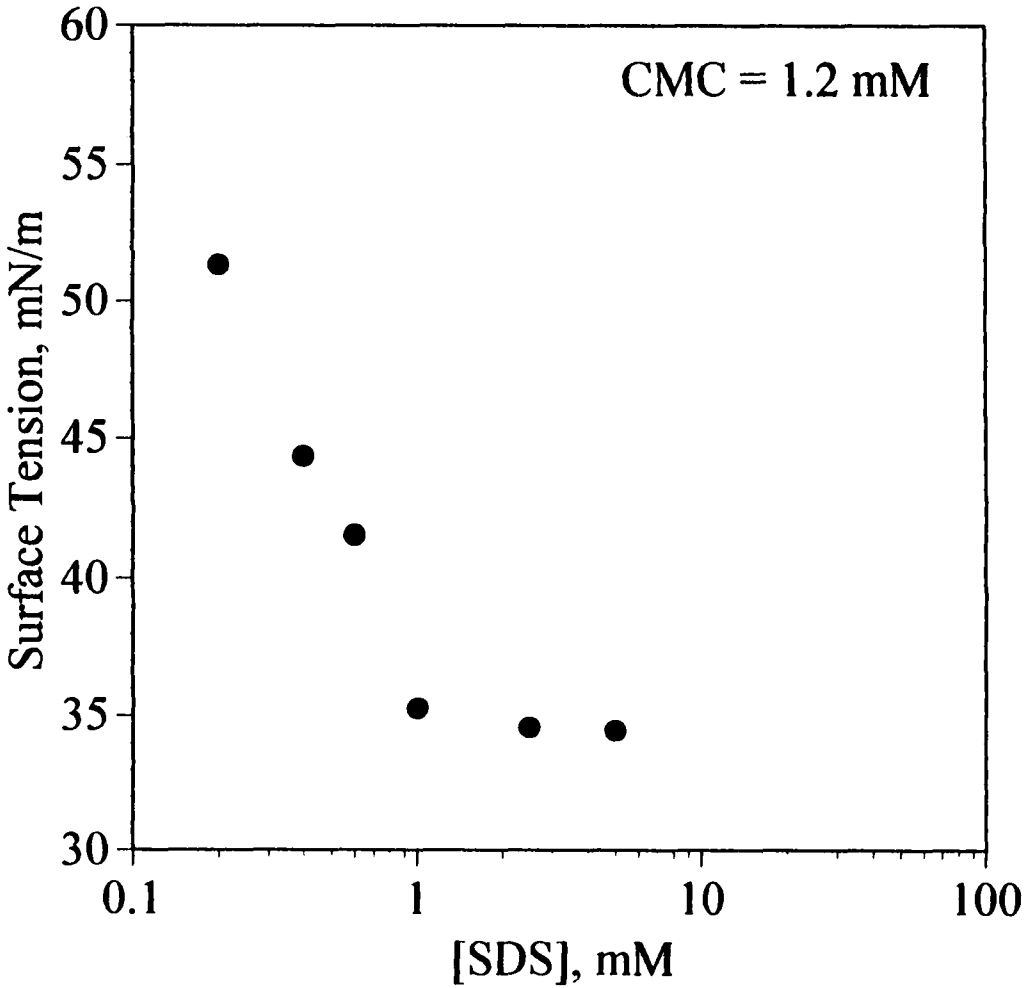
CMC for SDS, 0.01 M NaCl, 25 ^{o}C, Using Du Nouy Ring Tensiometer



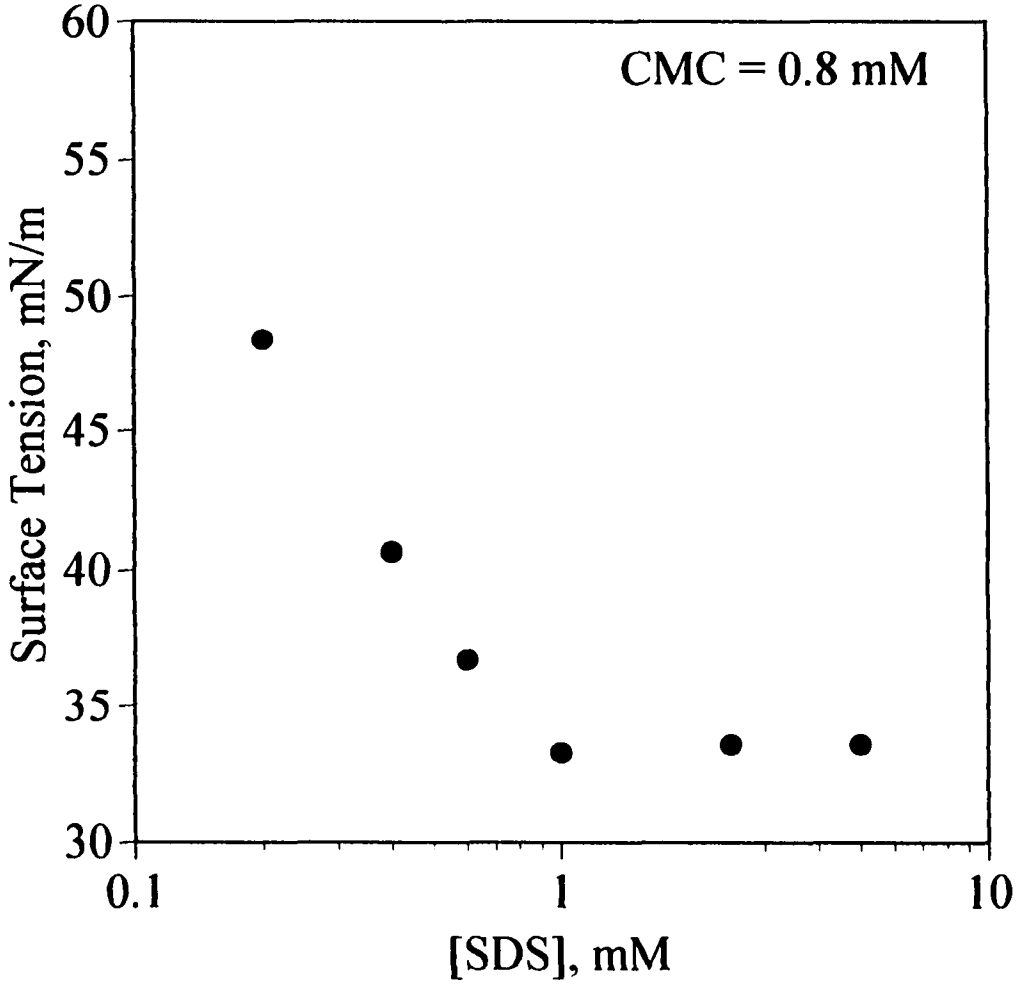
CMC for SDS, 0.05 M NaCl, 25 ^{o}C, Using Du Nouy Ring Tensiometer



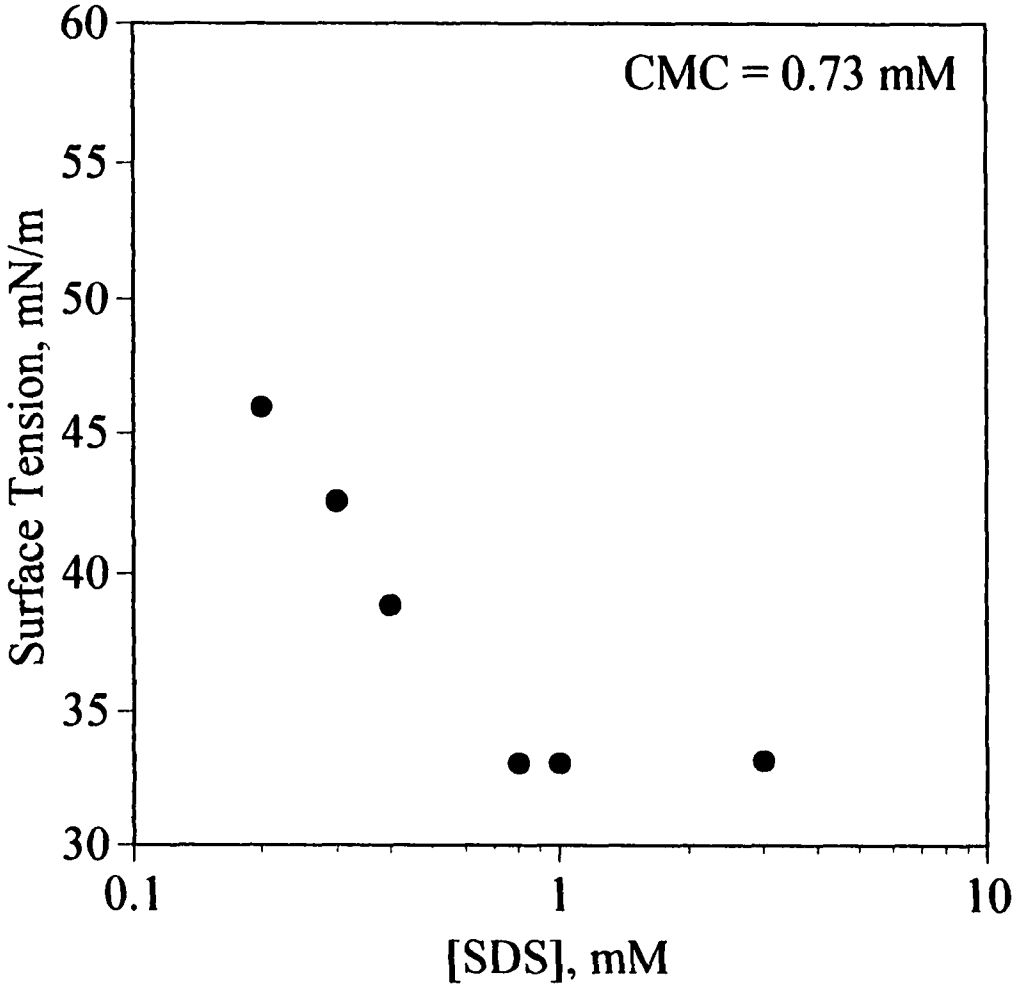
CMC for SDS, 0.1 M NaCl, 25 ^{o}C, Using Du Nouy Ring Tensiometer



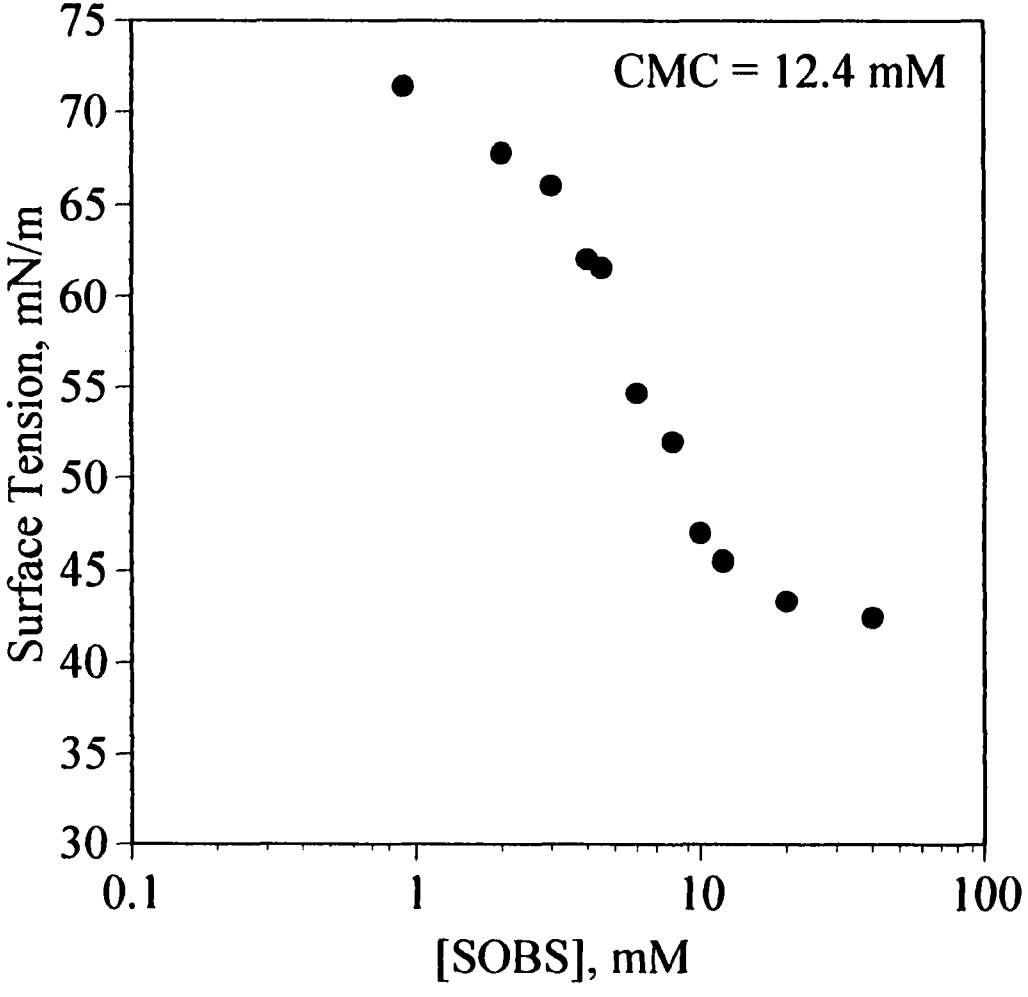
CMC for SDS, 0.15 M NaCl, 25 ^{o}C, Using Du Nouy Ring Tensiometer



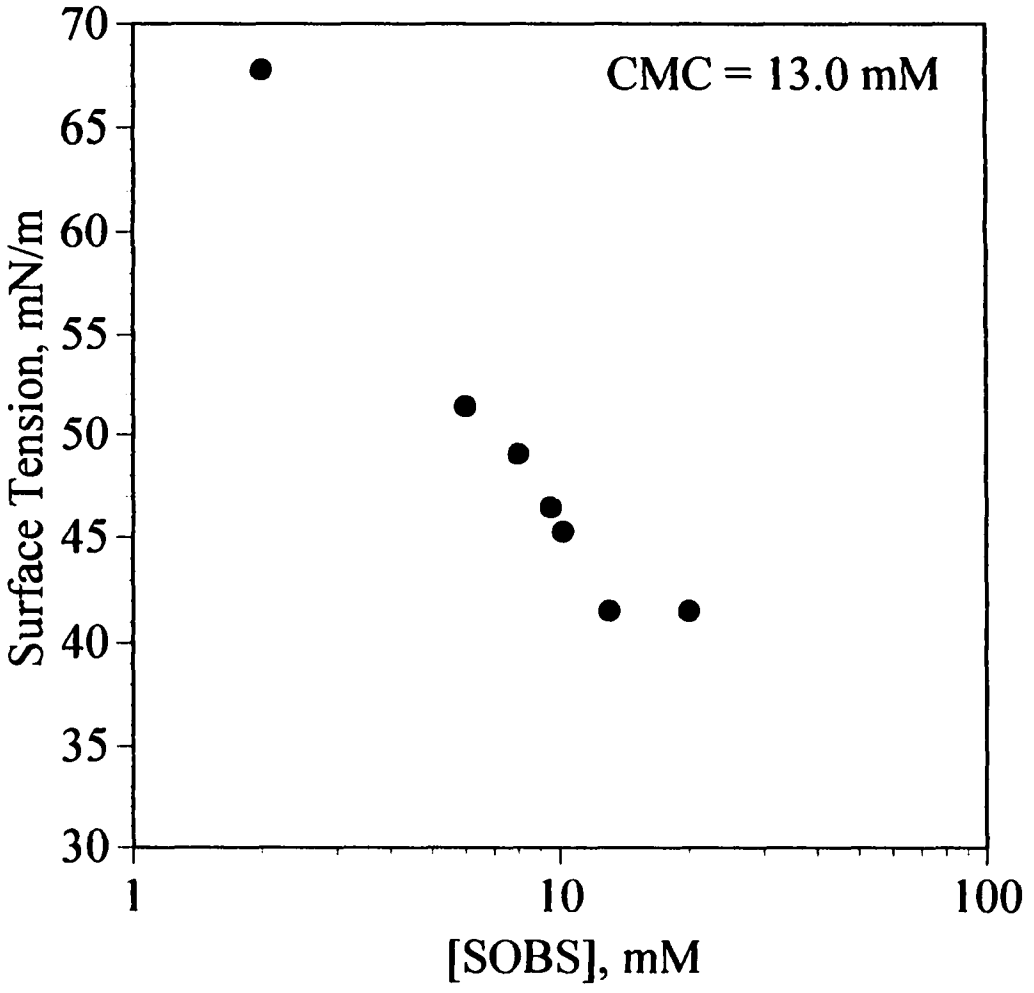
CMC for SDS, 0.2 M NaCl, 25 ^{o}C, Using Du Nouy Ring Tensiometer



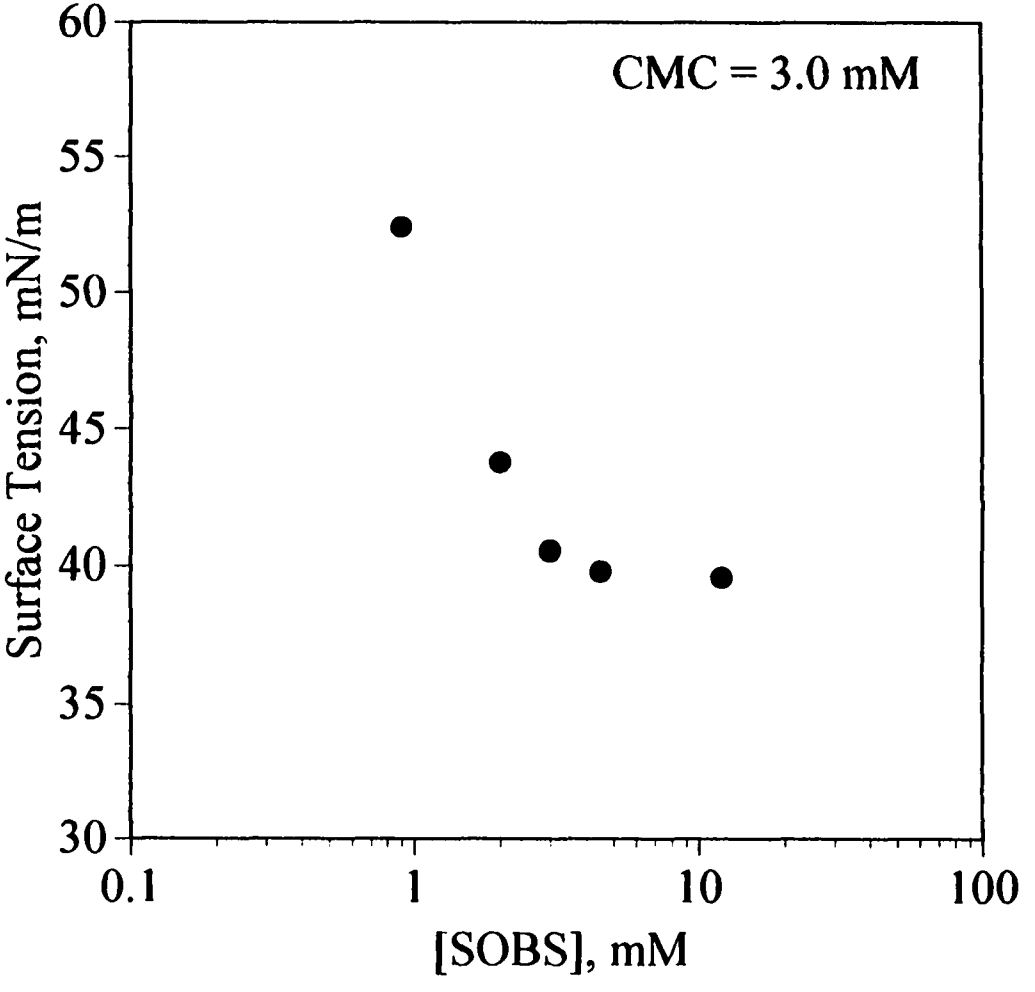
CMC for SOBS, 0 M NaCl, 25 ^{o}C, Using Maximum Bubble Pressure Method



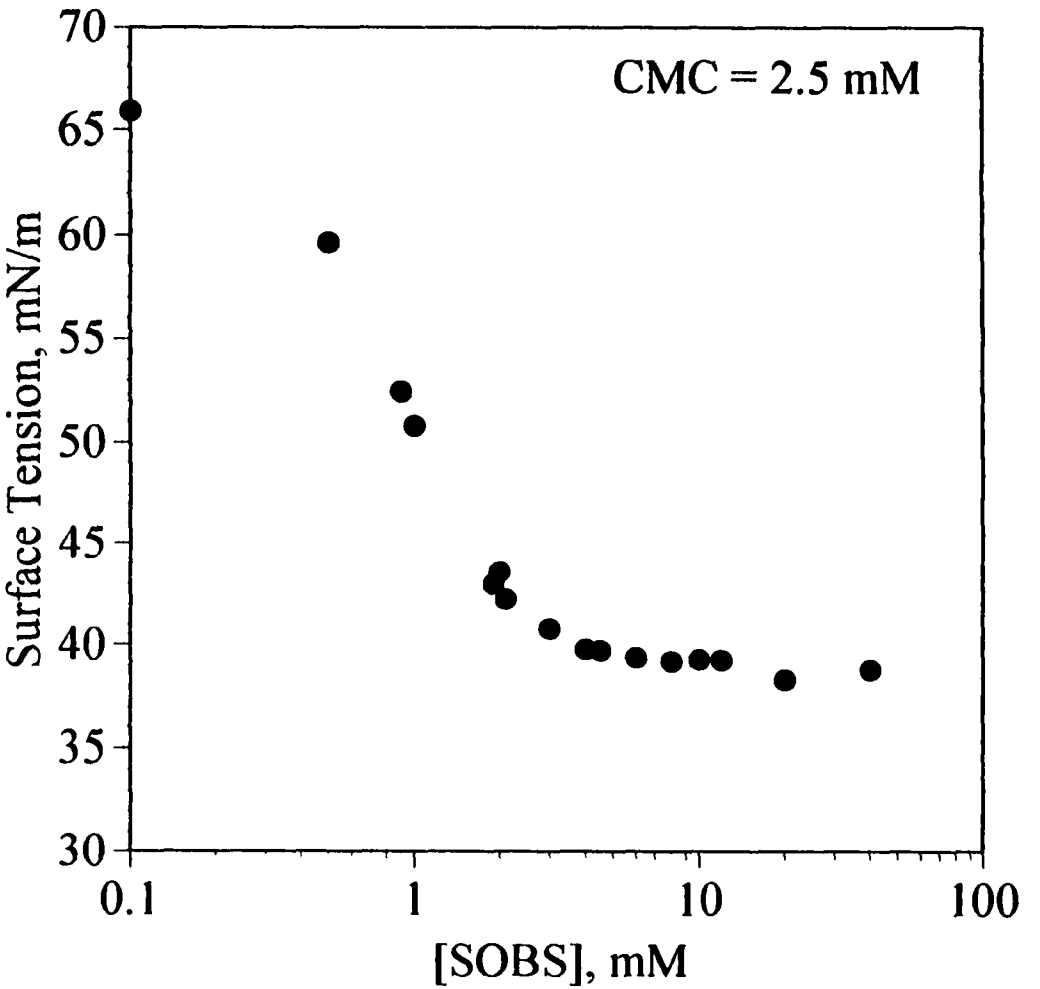
CMC for SOBS, 0 M NaCl, 40 ^{o}C, Using Maximum Bubble Pressure Method



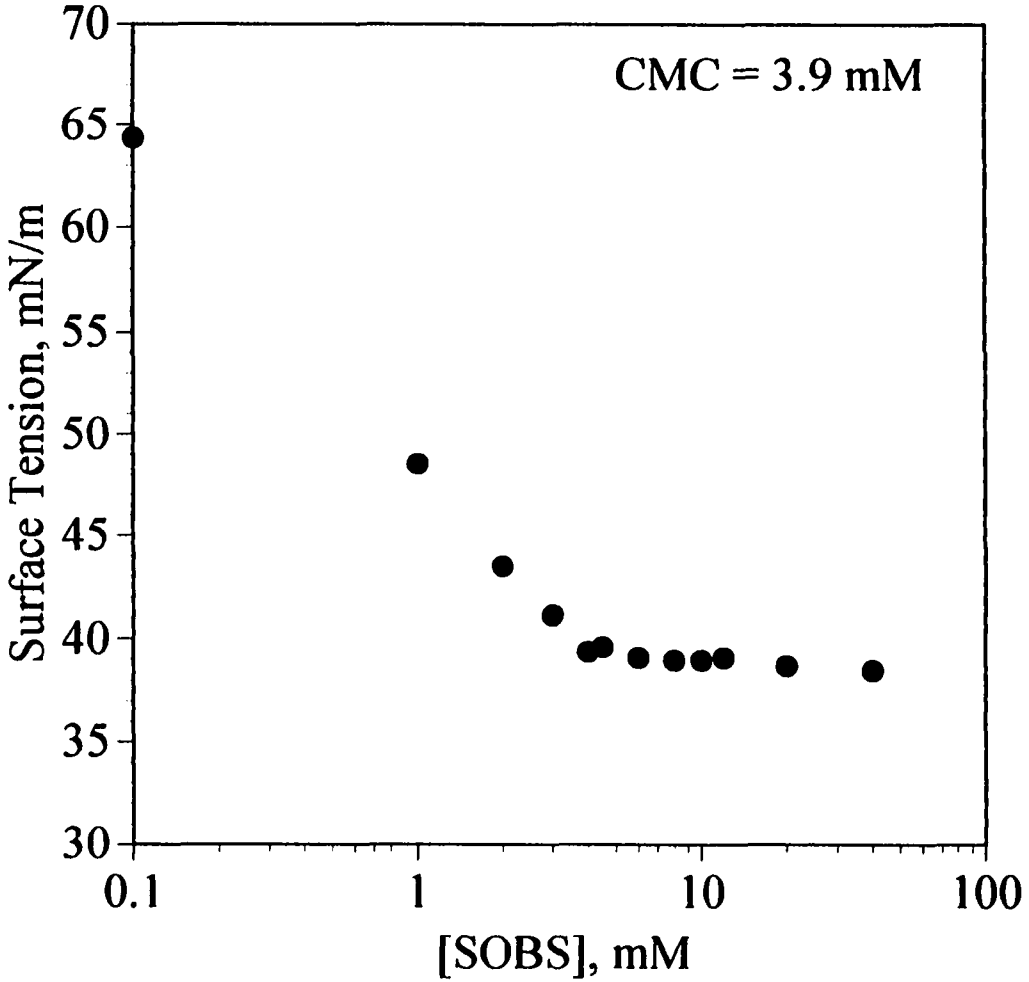
CMC for SOBS, 0.1 M NaCl, 30 ^{o}C, Using Maximum Bubble Pressure Method



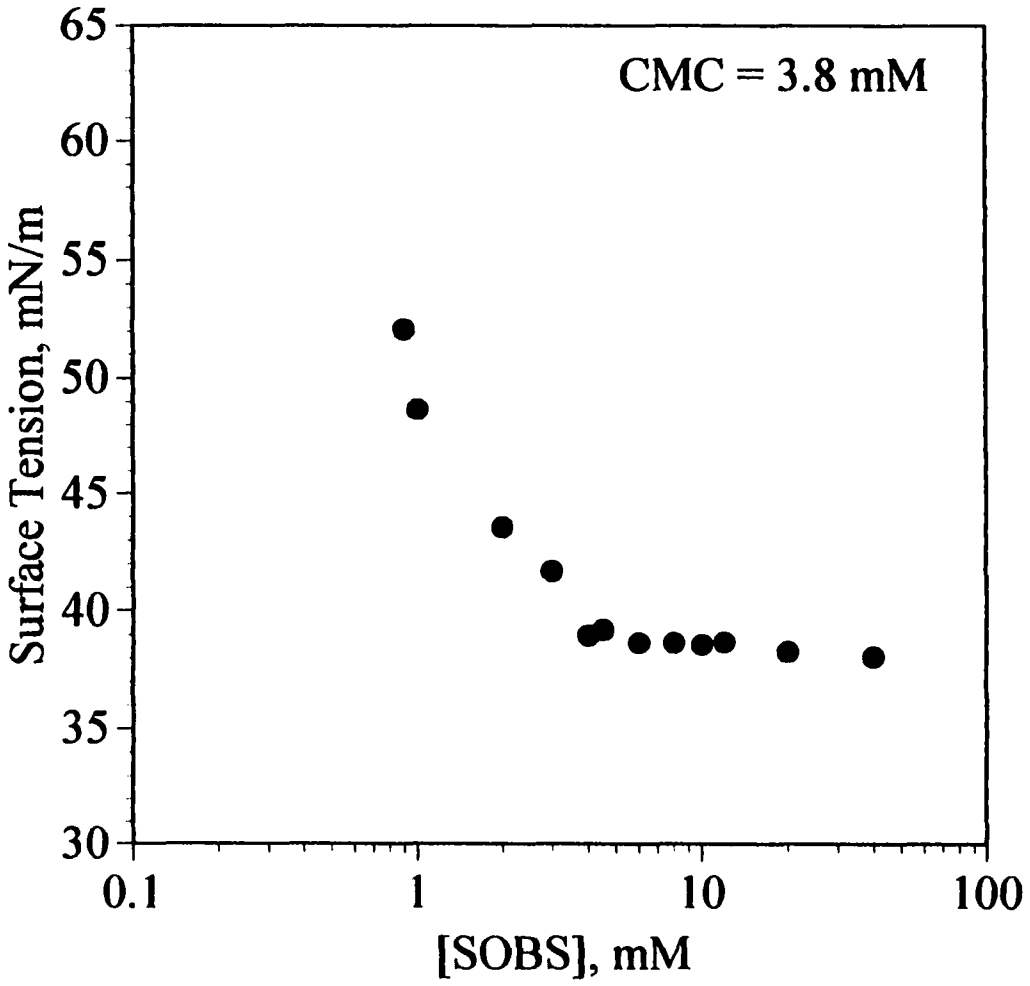
CMC for SOBS, 0.1 M NaCl, 35 ^{o}C, Using Maximum Bubble Pressure Method



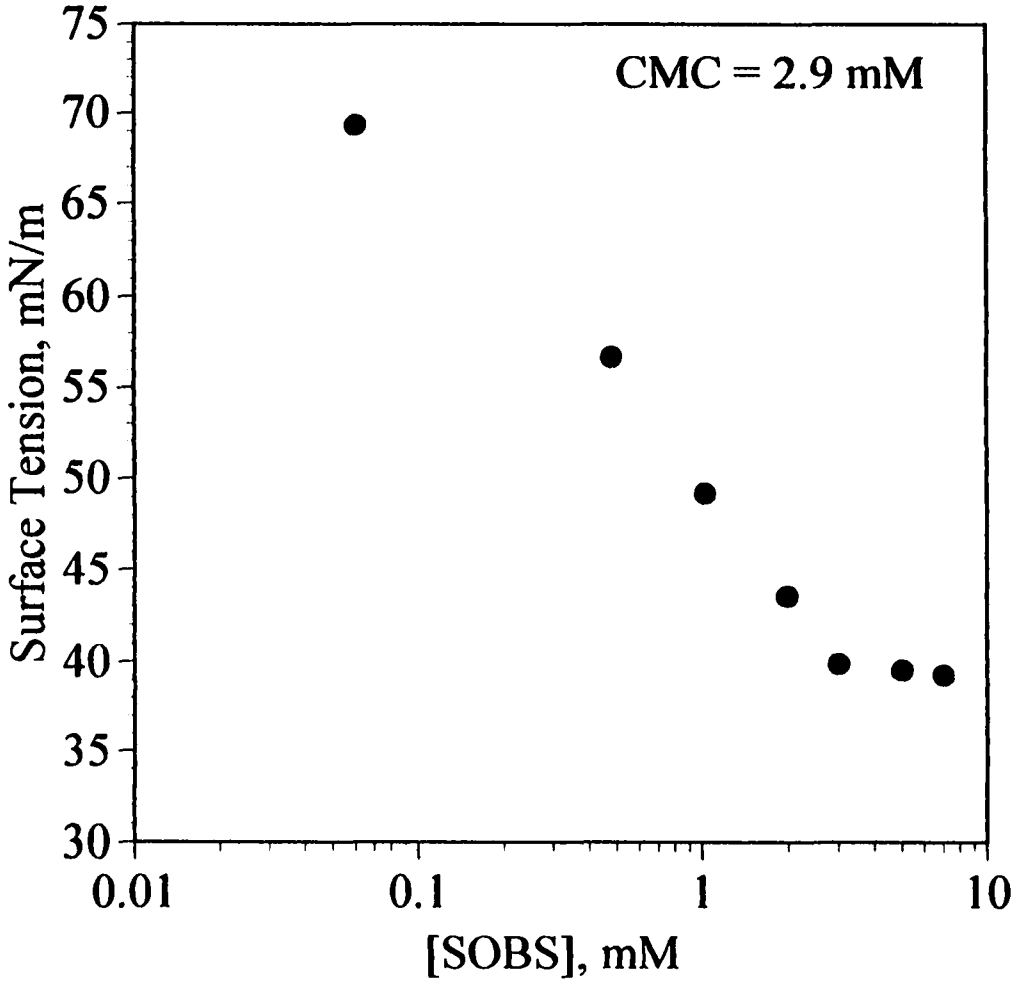
CMC for SOBS, 0.1 M NaCl, 40 ^{o}C, Using Maximum Bubble Pressure Method



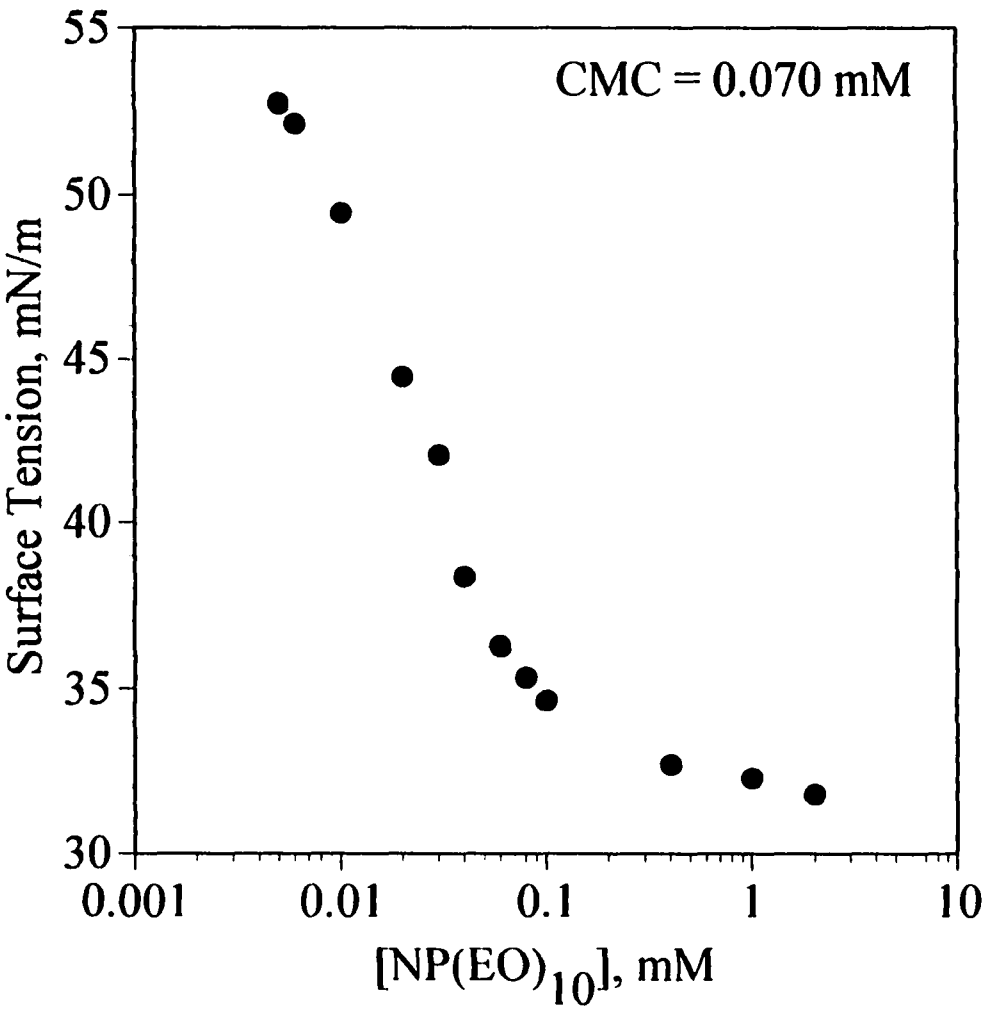
CMC for SOBS, 0.1 M NaCl, 45 ^{o}C, Using Maximum Bubble Pressure Method



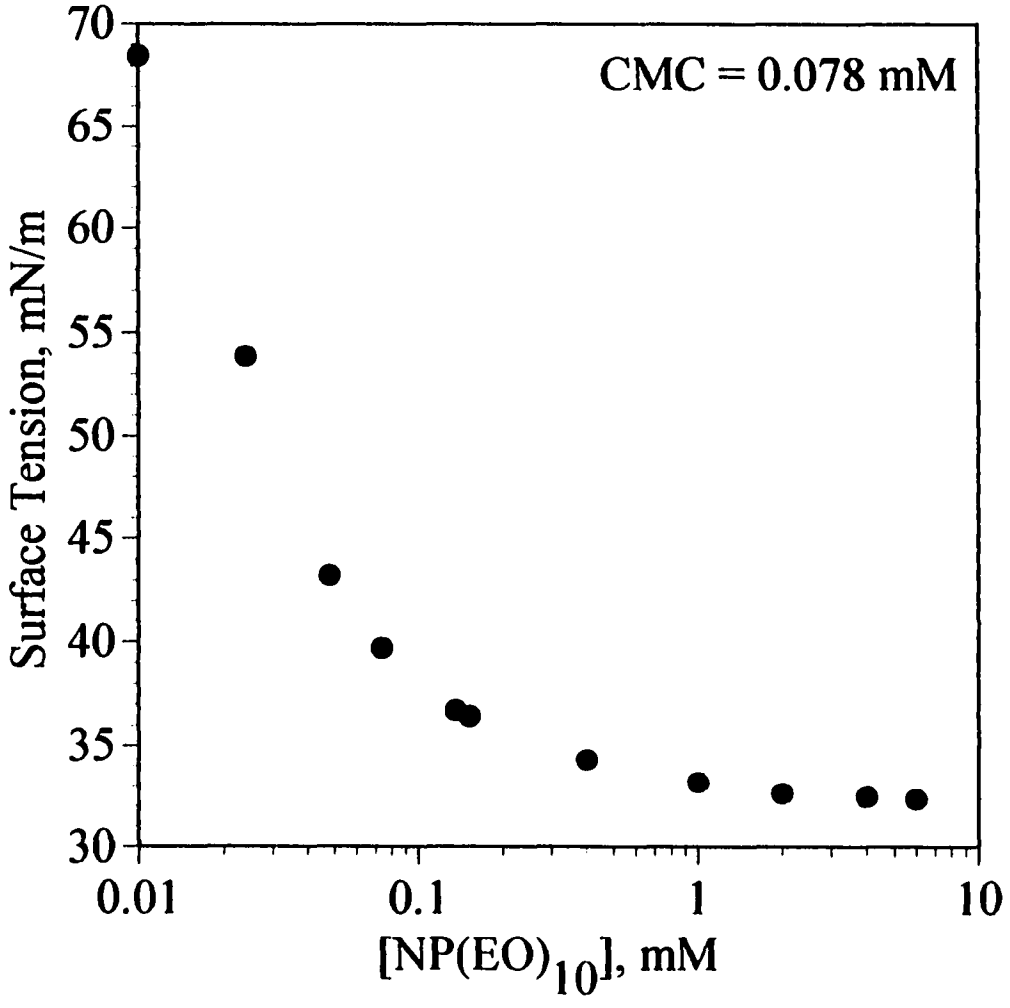
CMC for SOBS, 0.15 M NaCl, 35 ^{o}C, Using Maximum Bubble Pressure Method



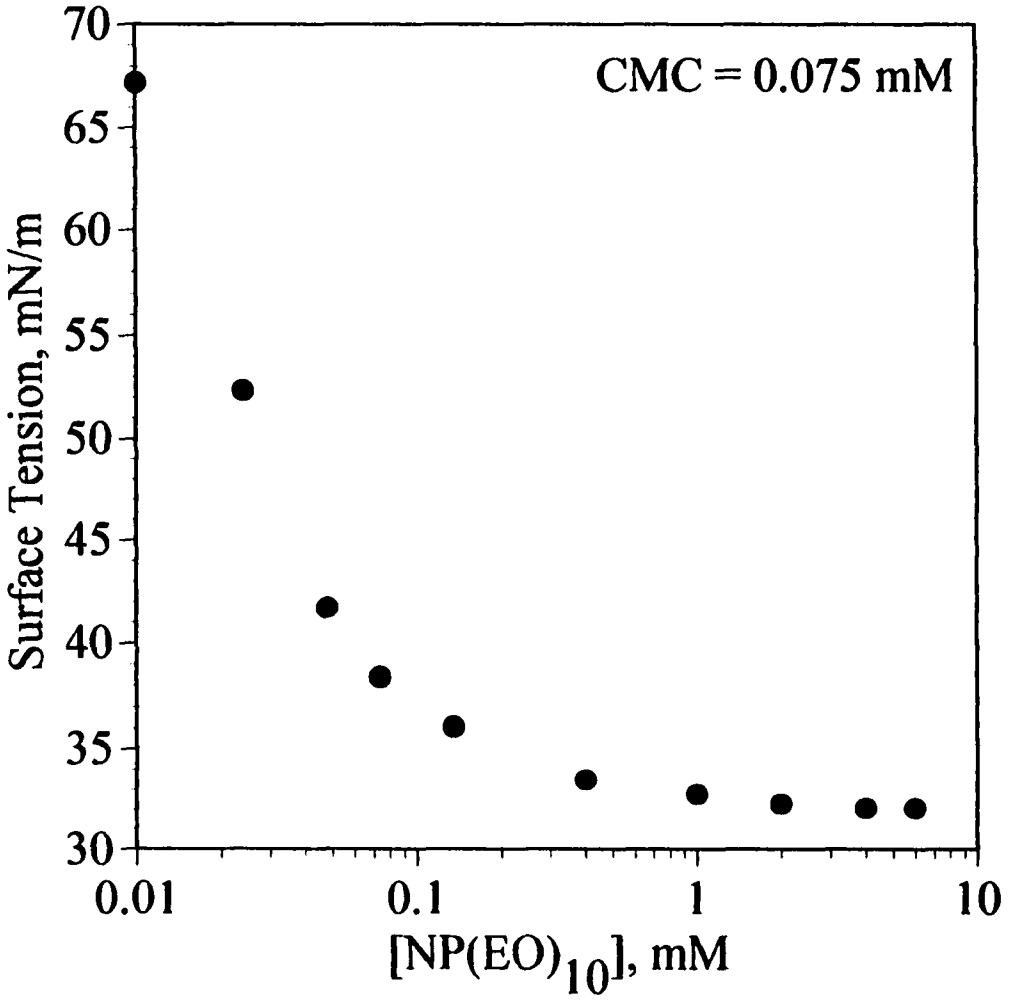
CMC for $NP(EO)_{10}$, 0 M NaCl, 25 ^{o}C Using Du Nouy Ring Tensiometer



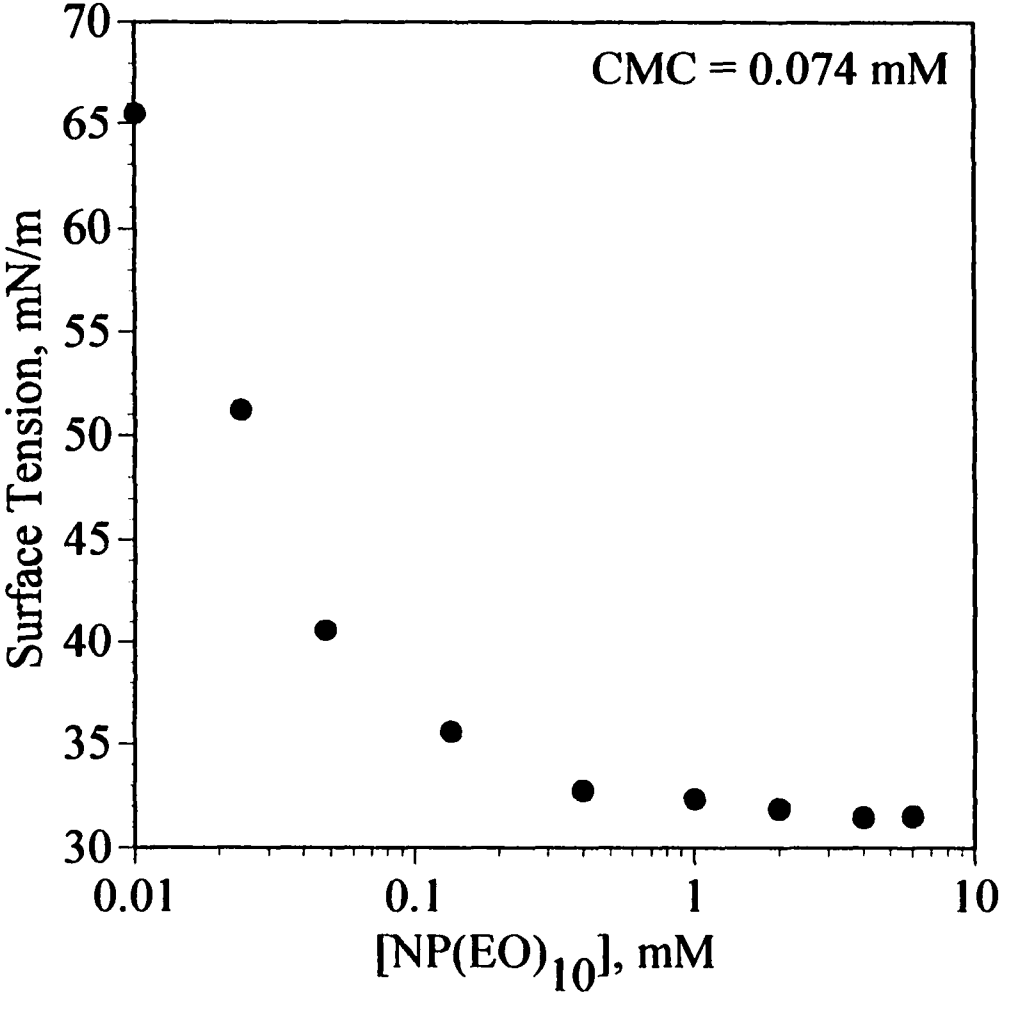
CMC for $NP(EO)_{10}$, 0 M NaCl, 35 ^{o}C Using Du Nouy Ring Tensiometer



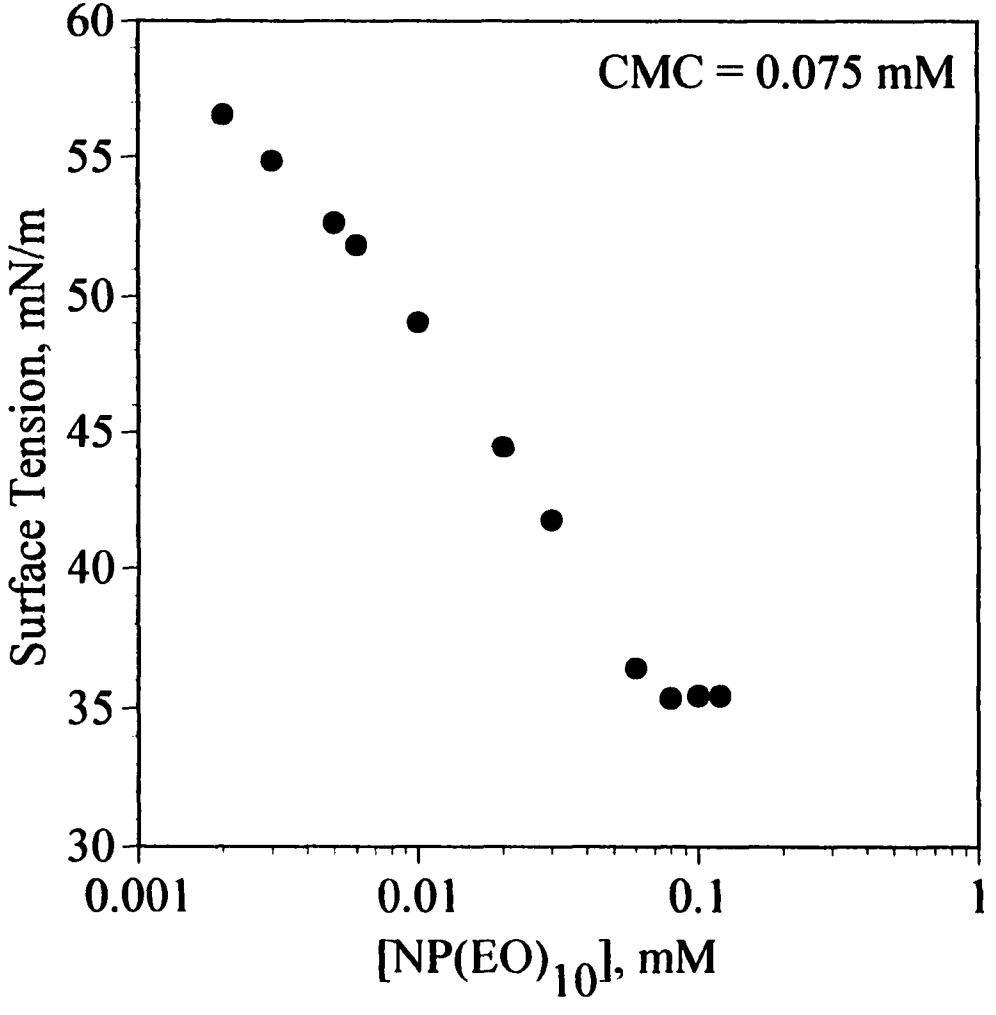
CMC for $NP(EO)_{10}$, 0 M NaCl, 40 ^{o}C Using Du Nouy Ring Tensiometer



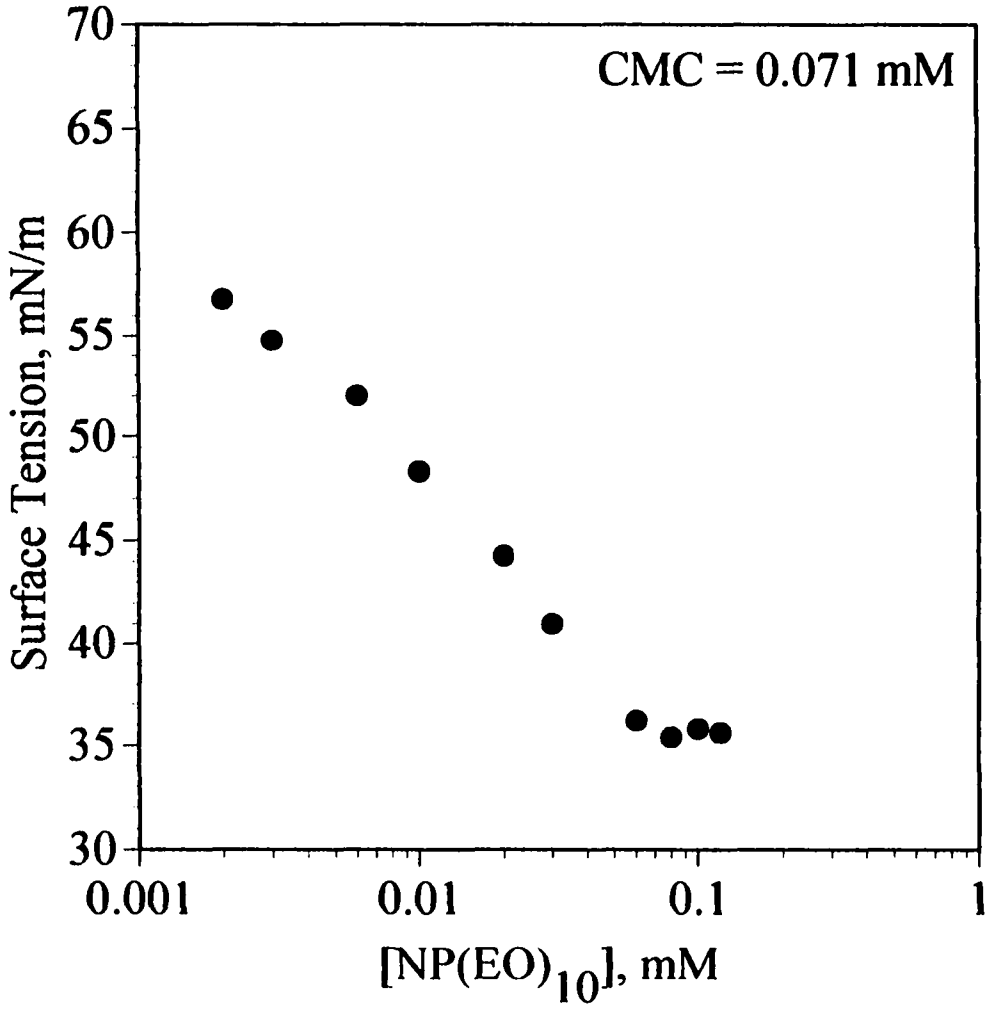
CMC for $NP(EO)_{10}$, 0 M NaCl, 45 ^{o}C Using Du Nouy Ring Tensiometer



CMC for $NP(EO)_{10}$, 0.1 M NaCl, 25 ^{o}C Using Du Nouy Ring Tensiometer

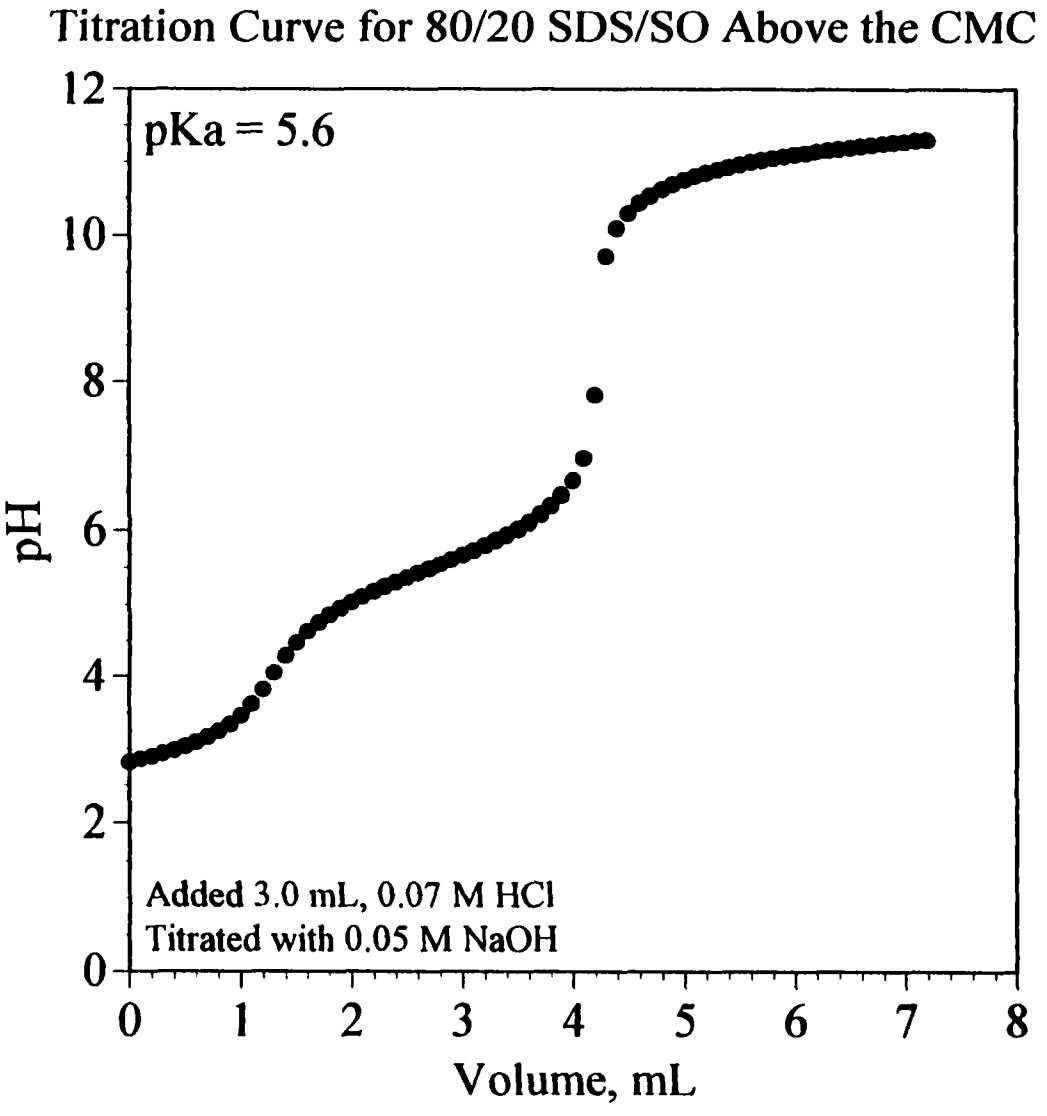


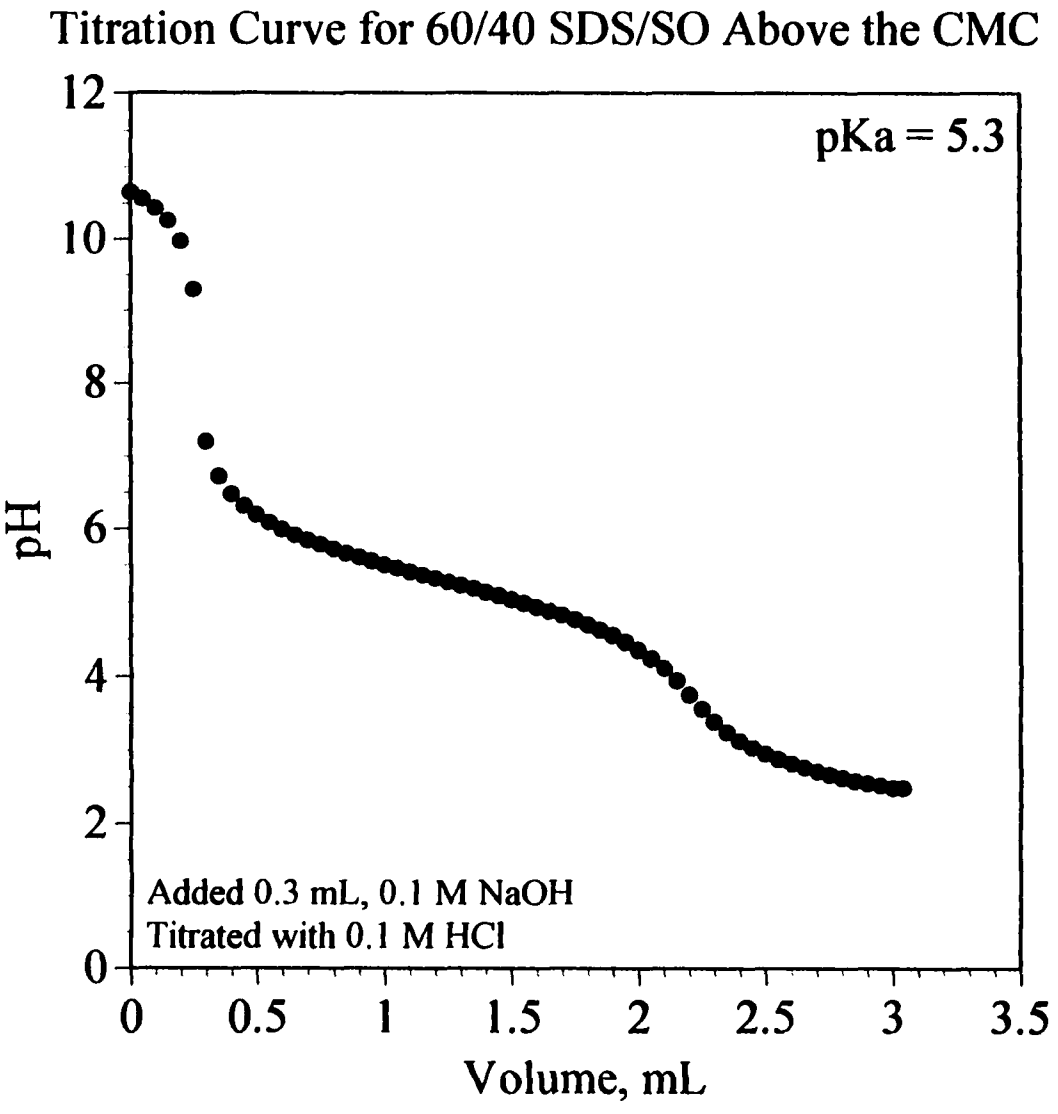
CMC for $NP(EO)_{10}$, 0.15 M NaCl, 25 ^{o}C Using Du Nouy Ring Tensiometer



APPENDIX B

Titrations of SDS/SO Mixtures


Titration Curve for 80/20 SDS/SO Above the CMC
pKa = 5.6
Added 3.0 mL, 0.07 M HCl
Titrated with 0.05 M NaOH
pH
Volume, mL
0
2
4
6
8
10
12
0
1
2
3
4
5
6
7
8


Titration Curve for 60/40 SDS/SO Above the CMC
pKa = 5.3
Added 0.3 mL, 0.1 M NaOH
Titrated with 0.1 M HCl
pH
Volume, mL
0
2
4
6
8
10
12
0
0.5
1
1.5
2
2.5
3
3.5

APENDIX C

Instructions For Isoperibol Set-up for and Control of Tronac Calorimeter

1. The settings for the ISAAC interface system are as follows:

RV Temp	Channel 0	pins 1 and 2	+/- 0.5 V
HTRI	Channel 2	pins 5 and 6	+/- 0.5 V
HTRV	Channel 4	pins 9 and 10	+/- 0.5 V

The differential input S8-2 should be ON

Input voltage settings for range are:

S7/1	ON	+/-5.0 V
S7/2	Off	+/-5.0 V
S7/3	On	+/-5.0 V
S7/4	On	divides range by 10 to get +/- 0.5 V

Channel 2:	SA/D1-3	On
	SA/D2-3	On

Channel 4:	SA/D1-5	On
	SA/D2-5	On

2. The wiring diagrams for connections between the Apple IIe, the ISAAC interface system, and the Tronac Calorimeter in isoperibol mode are shown in Figures C.1 and C.2.

3. Attach a refrigerated bath at 15-20 °C to the calorimeter cooled/heater through the back of the Tronac water bath. Turn on the calorimeter (or place on standby until ready to zero the instrument), temperature controller, digital voltmeter, strip chart, and computer. Bring the Tronac water bath temperature to 30 °C using an accurate thermometer and the temperature controller, set for temperature deviation. The course and fine adjustments on the temperature controller are used for this adjustment. It takes overnight for the temperature to change from room temperature to 30 °C.

4. The timing for the calorimeter runs depends on a timer chip on the 91-A board in the Apple IIe and the time program on the Labsoft Master Disk. The batteries on the back of the computer should keep the timer working in case the computer loses power. To reactivate the timer, run the time program which takes the user through each step. This program requires the user to flip the third dip switch on the 91-A board located near the outer edge of the board (this board has four dip switches).

4. The strip chart should be set to a variable span of about 2 to 10 mV, depending on the amount of heat released in the reaction.

5. Lower the insert assembly into the water bath so that it rests on the metal L-brackets. Use the course, medium, and fine adjustments on the isoperibol side of the calorimeter to set the digital voltage read-out to zero. The bridge voltage (BRV) should be set to about -6.7 V. This value should be set and the dial locked, and only needs to be checked periodically. Run the "Calrun" program. This program will zero the heater voltage and standard resistor voltage at the water bath temperature.

6. Inject approximately 2 grams of a concentrated calcium solution into a 2 mL soft glass ampoule and seal with a Microflame butane torch. Rinse the silver-lined, 50 mL reaction vessel with water and acetone, and dry with nitrogen. Place approximately 48 grams of a surfactant solution into the reaction vessel. Place the O-ring on the top of the reaction vessel with vacuum grease. The total volume of ampoule solution plus reaction vessel solution should not exceed 50 mL.

7. Raise the insert assembly to rest in the highest position and remove the L brackets. Rinse the thermistors and resistor heater with water and acetone, catching the rinse in a beaker, and dry with nitrogen. Gently pull the wires so that they are extended enough to be immersed into the reaction vessel solution. (If needed, extra lengths of wire can be accessed by removing the case over the top of the insert assembly and loosening the screw clamps on the far right side.) Raise the hammer so that it catches in the high position and carefully place the sealed glass ampoule on the stirrer beneath the hammer. Lightly coat the top of the O-ring on the reaction vessel with vacuum grease, and gently

place over the ampoule so that the top of the reaction vessel is touching the metal plate. Clamp the reaction vessel into place tightly enough so that no leaks will occur. Flip on the stirrer motor and listen carefully to make sure the stirrer or ampoule is not hitting the reaction vessel walls. Adjust if necessary.

8. Lower the insert assembly into the water bath. Manually turn on the heater and let the reaction vessel contents warm to about 0.5-0.7 mV. Turn off the heater to allow at least an hour for the reaction vessel and ampoule contents to equilibrate with the water bath temperature (resulting in a temperature voltage reading of approximately zero).

9. When the temperature has equilibrated, press any key on the computer to start the run, and start the strip chart. Alternatively, the calorimeter can be run manually along with the strip chart. The heater power should be set so that temperature rise versus time slope for the calibration run and the precipitation reaction are similar. The entire run should consist of a heater calibration, precipitation reaction, and another heater calibration. To perform a heater calibration, the heater should be turned on (either manually or by the computer) for 5 to 10 minutes, and the heater power, HTRI (voltage across standard resistor in series with calibration heater), and HTRV (voltage across calibration heater) values recorded. Unless recording a value, the knob should be set to "RV Temp". This allows the deviation in temperature between the reaction vessel and the water bath to be monitored as the run proceeds. The precipitation reaction begins when the ampoule is manually broken by releasing the hammer. If "Calrun" is being used, a buzzer will sound and STOP when it

is time to break the ampoule. The hammer should be raised and lowered several times to clear any trapped ampoule glass. The precipitation reaction time depends on the system being studied. A reaction time of 15 or 20 minutes can normally be used, but sometimes much longer times are required. Between each of the segments of the calorimeter run, before the first heater calibration, and after the last heater calibration the contents of the reaction vessel should be allowed to stir for 10 to 15 minutes. These time periods are either called leads or trails, and are important for subtracting out the heat leak from the experimental results. If "Calrun" is being used, a buzzer will sound and then stop when the calorimeter run is complete. If the run is performed manually, each part of the run will have to be timed and the heater turned on and off by the switch on the front of the calorimeter.

Figure C.1 Schematic of Wiring and Board Placement for Operation of Calorimeter in Isoperibol Mode

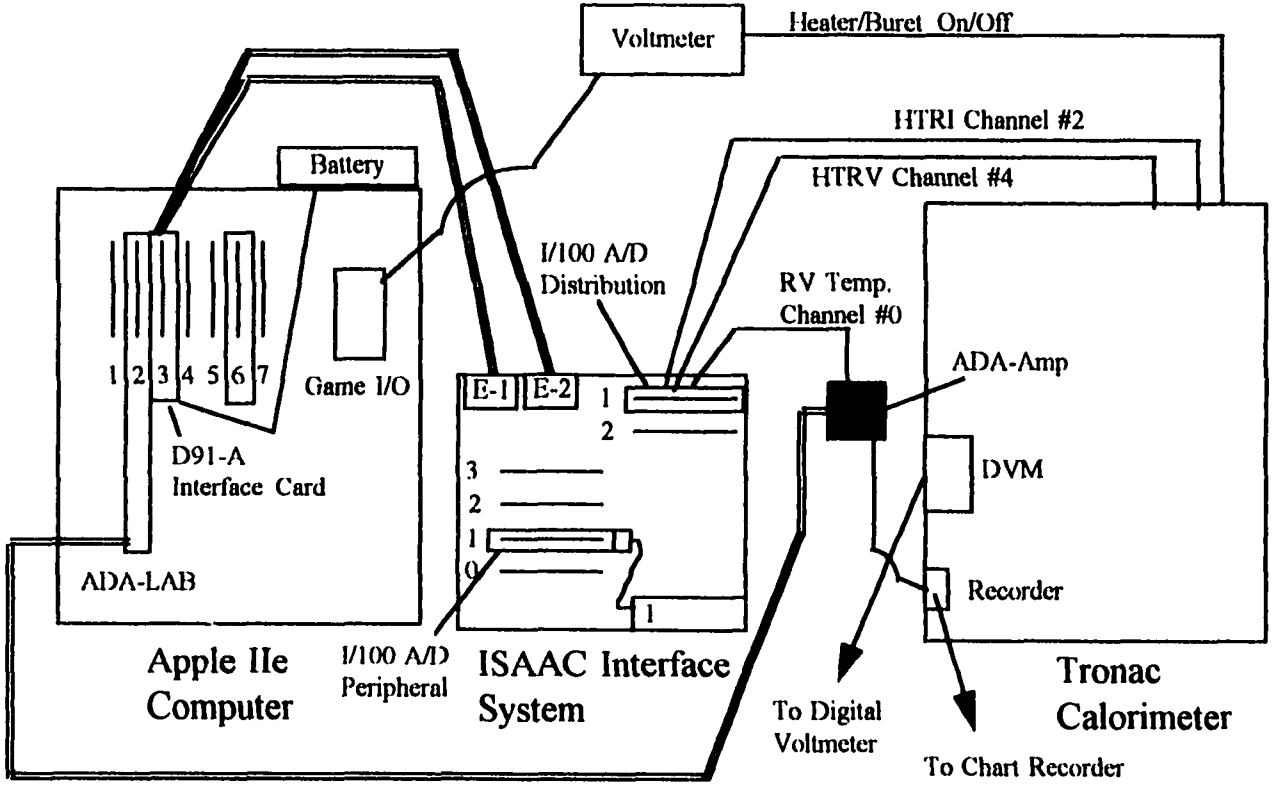
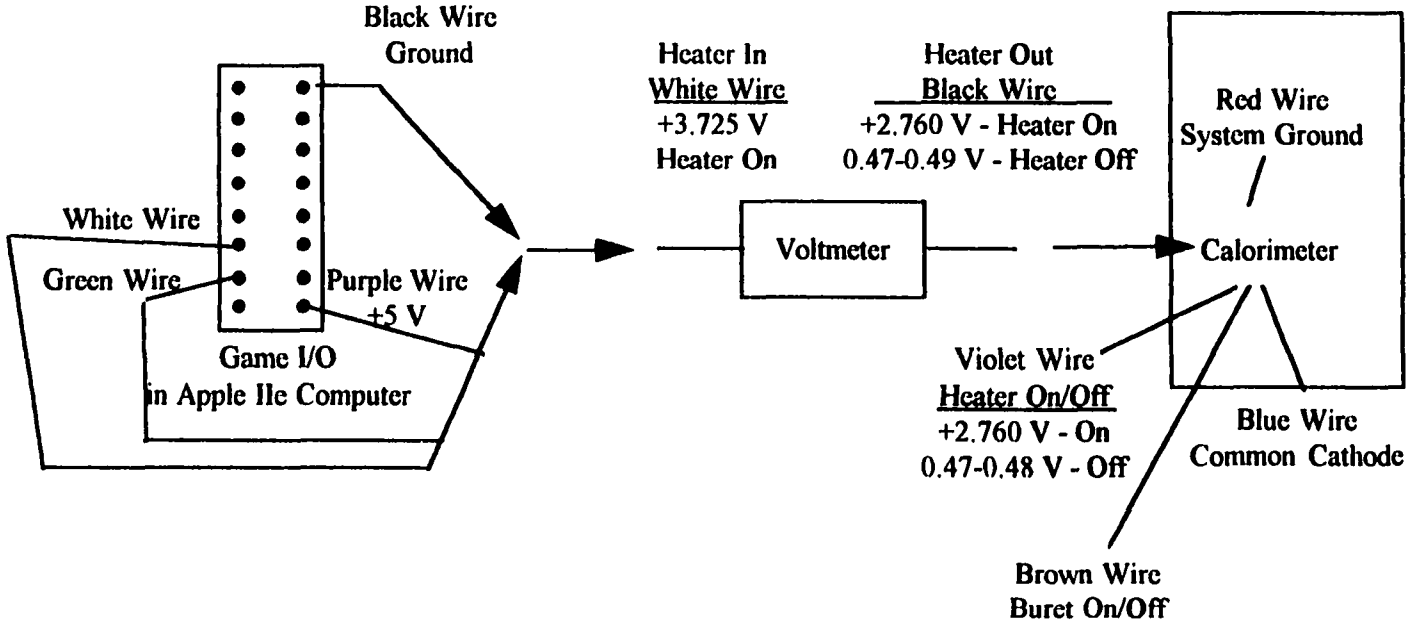


Figure C.2 Wiring for Control of Heater and Buret via Apple IIe Computer with Correct Voltages for Correct Interfacing of Calorimeter with Computer



APPENDIX D

Calculation of Rate of Precipitation of Surfactants with Calcium

1. Calculation of the Total Heat Released During a Precipitation Reaction, Q_T

From the strip chart output of the calorimeter (or the Linres program), the time, T_f, and T_i for each heater calibration run are taken at the middle point as shown in Figure D.1. Also, T_{RXi} and T_{RXf} can be determined in the same manner as shown in Figure D.1. These values, along with HTRI and HTRV for each heater calibration run, are used in the following calculations:

$$Q_{Cp1} = 239.01\ (HTRV_1)\ (HTRI_1) / R_S,\ mcal \qquad (D.1)$$

$$Q_{Cp2} = 239.01\ (HTRV_2)\ (HTRI_2) / R_S,\ mcal \qquad (D.2)$$

$$C_{p1} = Q_{Cp1} / (T_{f1} - T_{i1}),\ mcal/mV \qquad (D.3)$$

$$C_{p2} = Q_{Cp2} / (T_{f2} - T_{i2}),\ mcal/mV \qquad (D.4)$$

$$C_{p,avg} = (C_{p1} + C_{p2}) / 2,\ mcal/mV \qquad (D.5)$$

$$Q_T = (C_{p,avg})\ (T_{RXf} - T_{RXi}) / 1000,\ cal \qquad (D.6)$$

where R_S is the resistance of the standard resistor, and Q_{Cp1} and Q_{Cp2} are the heat added by the calibration heater during the first and second heater calibrations,

respectively. The parameters, Cp_1 and Cp_2, are the apparent heat capacities of the solution calculated during the first and second heater calibrations, respectively, and $C_{p,avg}$ is the average apparent heat capacity of the system. These apparent heat capacities are not only a function of the temperature rise due to the calibration heater, but also of the heat of stirring and the heat required to raise the reaction vessel temperature walls.

2. Calculation of the Heat of Precipitation, Q_{ppt}

The heat of dilution of the ampoule solution when it is added to the reaction vessel solution, Q_{dil}, can be found by breaking an ampoule of calcium into water. The heat of dilution per mole of calcium diluted, q_{dil}, is then:

$$q_{dil} = Q_{dil} / \# \text{ moles } Ca^{2+} \qquad \text{(D.7)}$$

The q_{dil} can then be multiplied by the number of moles of calcium in any precipitation reaction to obtain Q_{dil} for that precipitation reaction. The heat of micellization due to the addition of calcium to a surfactant system, Q_{mic}, can be found by breaking an ampoule of calcium into a surfactant solution that is above its CMC, but outside of the precipitation phase boundary. The heat of dilution is then subtracted from the total heat obtained. The heat of micellization per mole of surfactant forming micelles can be found by calculating the CMC of the solution before and after calcium has been added, taking into account the change in concentrations due to dilution. The model by Stellner and Scamehorn (Stellner, K.L. and J.F. Scamehorn, *Langmuir, 5:*70 (1989)) can be used for these calculations so that:

$$q_{mic} = Q_{mic} / (-\Delta CMC) \qquad (D.8)$$

The Q_{mic} occurring in a precipitation reaction can be obtained by multiplying q_{mic} by the change in number of moles of surfactant in the micelles when calcium is added for the precipitating system. The Q_{ppt} is then found by the following equation:

$$Q_{ppt} = Q_T - Q_{dil} - Q_{mic} \qquad (D.9)$$

If there are no micelles formed during the addition of calcium to the surfactant solution, Q_{mic} equals zero.

3. Calculation of the Heat of Precipitation Per Mole of Surfactant Precipitated, q_{ppt}

The final concentration of each surfactant in solution can be found by determining the precipitation reaction pathway and finding the point where the pathway crosses the appropriate precipitation phase boundary. Since the initial concentrations are known, and the volume, V_{RV}, is known, the number of moles of surfactant precipitated, n_{ppt}, is:

$$n_{ppt} = \{([SDS]_{init} + [SOBS]_{init}) - ([SDS]_{unr} + [SOBS]_{unr})\} V_{RV} \qquad (D.10)$$

where $[SDS]_{init}$ and $[SOBS]_{init}$ are the initial SDS and SOBS concentrations, and $[SDS]_{unr}$ and $[SOBS]_{unr}$ are the unreacted SDS and SOBS concentrations at equilibrium. Then,

$$q_{ppt} = Q_{ppt}/n_{ppt} \qquad (D.11)$$

4. Calculation of the Fraction of Surfactant Precipitated as a Function of Time

For any surfactant concentration beginning above the CMC, the moles of surfactant in the micellar phase can be calculated for each point along the reaction pathways, using the model by Stellner and Scamehorn, and the unreacted surfactant and calcium as the total concentrations in solution. The heat of demicellization for each point during the precipitation reaction can then be subtracted from the heat of precipitation. Points along the strip chart are chosen as shown in Figure D.2, and a proportionality constant is calculated using T_i, T_f, and T_t at each point along the precipitation reaction curve.

$$A = (T_t - T_i) / (T_f - T_i) \qquad (D.12)$$

If there is an initial increase in the rate followed by a plateau before any precipitation begins (as shown occurring in Figure D.2), a new T_i' is used in the calculation of A':

$$T_i' = T_i(t=0 \text{ sec}) + \Delta T_d \qquad (D.13)$$

$$A' = (T_t - T_i') / (T_f - T_i') \qquad (D.14)$$

This new A' keeps the initial temperature rise from affecting the fraction of surfactant precipitated. The final calculations are shown below:

$$q_t = q_{ppt} A \qquad (D.15)$$

$$q_t = (q_{ppt} A' n_{ppt} - q_{demic} \Delta n_{mic}) / n_{ppt} \quad (D.16)$$

$$q_{demic} = -q_{mic} \quad (D.17)$$

$$\text{fraction precipitated} = q_t / q_t(\text{final}) \quad (D.18)$$

For the case where the initial concentration is above the CMC, the calculation of qt is iterative since Δn_{mic} is not known as a function of time:

(1) calculate qt for an initial guess of Δn_{mic}

(2) calculate the fraction precipitated

(3) calculate a new Δn_{mic} for the fraction precipitated

(4) Repeat until the fraction precipitated stops changing